



N7721360

COMBUSTION EFFECTS ON FILM COOLING

AEROJET LIQUID ROCKET CO., SACRAMENTO,
CALIF

24 FEB 1977

1. Report No. NASA CR-135052	2. Government Accession No.	3. Recipient's Catalog No.	
4. Title and Subtitle Combustion Effects on Film Cooling		5. Report Date 11 November 1976	6. Performing Organization Code
7. Author(s) D. C. Rousar and R. L. Ewen		8. Performing Organization Report No.	
9. Performing Organization Name and Address Aerojet Liquid Rocket Company Sacramento, California		10. Work Unit No.	11. Contract or Grant No. NAS 3-17813
12. Sponsoring Agency Name and Address National Aeronautics and Space Administration Washington, C.D. 20546		13. Type of Report and Period Covered Final Report 20 May 1974-31 July 1975	
		14. Sponsoring Agency Code 9521	
15. Supplementary Notes Project Manager, C. A. Aukerman, NASA Lewis Research Center, Cleveland, Ohio			
16. Abstract <p>The effects of: (1) a reactive environment on film cooling effectiveness and (2) film cooling on rocket engine performance were determined experimentally in a rocket thrust chamber assembly operating with hydrogen and oxygen propellants at 300 psia chamber pressure. Tests were conducted using hydrogen, helium, and nitrogen film coolants in an instrumented, thin walled, steel thrust chamber. The film cooling, performance loss, and heat transfer coefficient data were correlated with the ALRC entrainment film cooling model which relates film coolant effectiveness and mixture ratio at the wall to the amount of mainstream gases entrained with the film coolant in a mixing layer. In addition, a comprehensive thermal analysis computer program, HOCOOL, was prepared from previously existing ALRC computer programs and analytical techniques. A computer program user manual was also prepared and the manual and computer program were delivered to NASA for government use. Predictions from the HOCOOL program indicate that the proper application of hydrogen film cooling to a proposed high pressure hydrogen/oxygen thrust chamber will produce a relatively large decrease in wall temperature and a relatively small decrease in performance.</p>			
17. Key Words (Suggested by Author(s)) Film Cooling Heat Transfer Performance Loss Combustion		18. Distribution Statement Unclassified - Unlimited	
19. Security Classif. (of this report) Unclassified	20. Security Classif. (of this page) Unclassified	21. No. of Pages	22. Price*



FOREWORD

The Combustion Effects on Film Cooling Program (Contract NAS 3-17813) was conducted by the Analytical Design Section of the Design and Analysis Department, Aerojet Liquid Rocket Company, for the NASA-Lewis Research Center. The period of performance was 20 May 1974 to 31 July 1975.

C. A. Aukerman was the NASA-Lewis Project Manager. At ALRC the Program Manager was J. D. Sims, the Operations Project Manager was D. L. Kors, the Project Engineer was D. C. Rousar, and the Program Analyst was R. L. Ewen. Significant contributions to this program were also made by the following ALRC personnel:

D. F. Calhoon
E. H. Green
R. S. Gross
R. A. Hewitt
E. V. Hron
D. E. Lemke
P. M. Loyd
S. L. Munger
T. R. Peterson
N. R. Rowett
J. W. Salmon

In addition, D. E. Sokolowski of the NASA-Lewis Research Center made significant contributions toward the design of the program scope and approach.

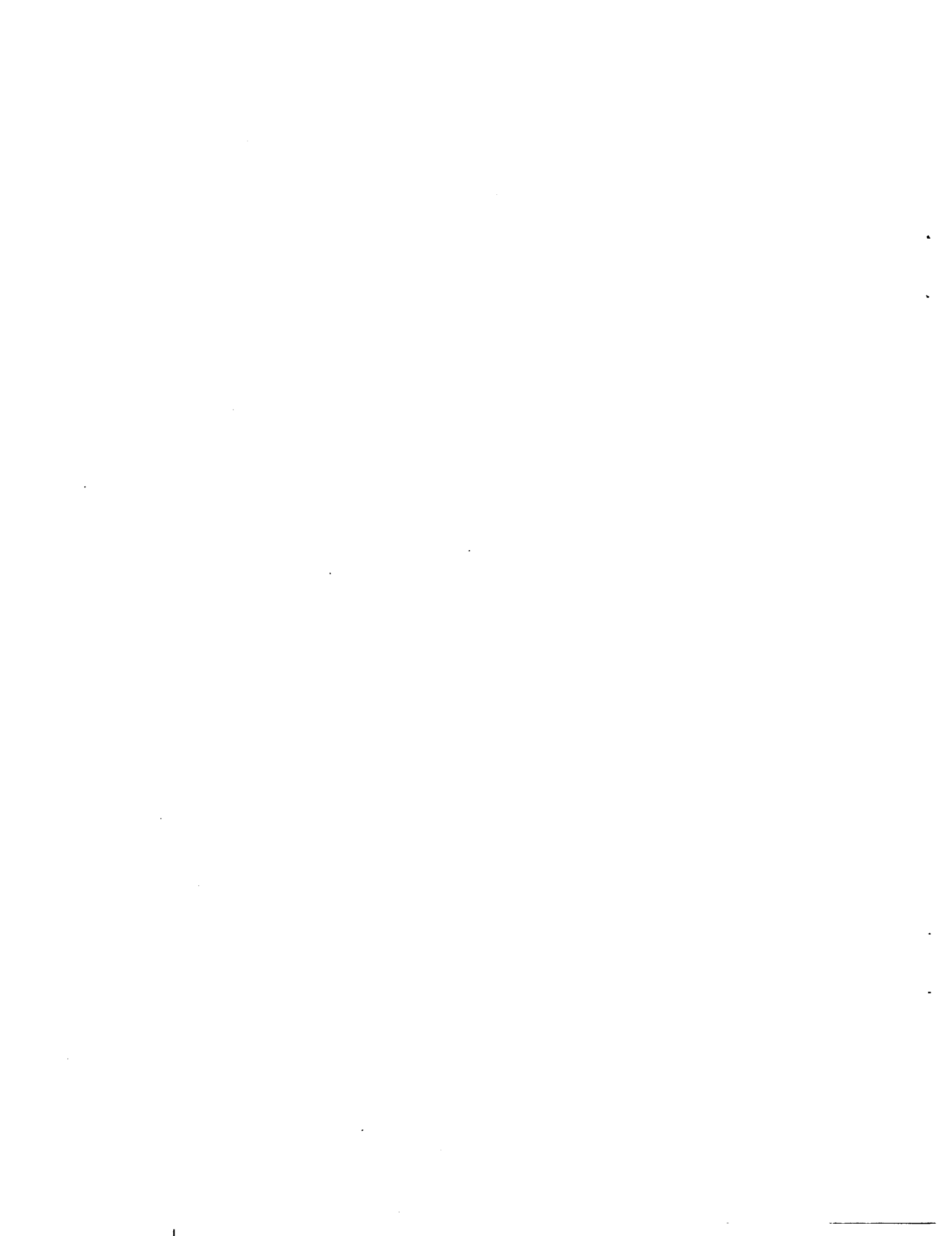


TABLE OF CONTENTS

		<u>Page No.</u>
I	SUMMARY	1
II	INTRODUCTION	4
III	ANALYTICAL MODELS	6
	A. Entrainment Film Cooling Model	6
	B. Film Cooling Performance Loss Model	21
	C. Non-Adiabatic Wall Heat Transfer Model	24
	D. HOCOOL Program	26
IV	EXPERIMENTAL RESULTS AND DATA CORRELATIONS	28
	A. Testing	28
	B. Test Results	34
	C. Film Cooling Data Correlations	43
	D. Correlation of Performance Loss Results	59
	E. Correlation of Heat Transfer Results	63
V	ANALYTICAL PREDICTIONS	65
VI	CONCLUSIONS AND RECOMMENDATIONS	71
	REFERENCES	74
	APPENDIX A - NOMENCLATURE	
	APPENDIX B - TABULATED FILM COOLING TEST DATA	
	APPENDIX C - TEST COMPONENTS AND COLD FLOW DATA	
	APPENDIX D - DISTRIBUTION LIST	



LIST OF TABLES

<u>Table No.</u>	<u>Title</u>	<u>Page</u>
I	Nominal Test Conditions	76
II	Overall Test Conditions	77
III	Entrainment Fraction Results	78
IV	Performance Data Summary	79
V	Film Cooling Heat Transfer Coefficient Data	80
VI	No-Film-Cooling Heat Transfer Coefficient Data	81
VII	HOCOOL $\eta_{I_{sp}}$ Factors	82
VIII	Comparison of Asymptotic Entrainment Fraction Multipliers (k/k_0) for a Velocity Ratio of Unity	83



LIST OF FIGURES

<u>Figure No.</u>	<u>Title</u>	<u>Page</u>
1	Film Cooling Test Assembly (P/N 1182135)	84
2	Entrainment Film Cooling Model Schematic	85
3	Mixing Layer Schematic	86
4	Subsonic Effectiveness vs. W_E/W_C Correlation	87
5	Shape Factor Correlations	88
6	Typical Mixture Ratio Profiles	89
7	Velocity Ratio Correlating Function	90
8	Velocity Decay Function	91
9	HOCOOL Heat Transfer Analysis Options	92
10	Regenerative Coolant Passage Geometries	93
11	Film Cooling Test Assembly Mounted on Test Stand	94
12	Schematic Diagram of Test System	95
13	Thermocouple Locations, Film Cooled Chamber	96
14	O_2/H_2 Core Gas Composition	97
15	Steady State Wall Temperatures Measured with Core Gas O/F = 4	98
16	Steady State Wall Temperature Measured with Core Gas O/F = 6	99
17	Steady State Wall Temperature Measured with Core Gas O/F = 8	100
18	Steady State Wall Temperature Measured with Core Gas O/F = 8 and 2	101
19	Measured Wall Temperatures, Helium Film Coolant	102
20	Measured Wall Temperatures, Nitrogen Film Coolant	103
21A	Circumferential Distribution of Entrainment Fraction, Hydrogen Film Coolant	104
21B	Circumferential Distribution of Entrainment Fraction, Hydrogen, Helium, and Nitrogen Film Coolants	105

List of Figures (cont.)

<u>Figure No.</u>	<u>Title</u>	<u>Page</u>
22	Averaged Entrainment Fractions, Hydrogen Film Coolant	106
23	Averaged Entrainment Fractions, Hydrogen, Helium and Nitrogen Film Coolants	107
24	Effect of Core Mixture Ratio on Entrainment Fraction	108
25	Comparison of Hydrogen and Helium Entrainment Fraction	109
26	Absolute Entrainment Fraction Data	110
27	Effect of Loss Coefficient on Temperature Correction	111
28	Ratio of Maximum To Asymptotic Entrainment Fractions in the Cylindrical Region	111
29	Asymptotic Cylindrical Section Entrainment Fractions	112
30	Average Cylindrical Region Entrainment Fractions	113
31	Effect of Velocity Ratio on Asymptotic Entrainment Fraction Ratio	114
32	Adjusted $f (u_c/u_e)$ Values	115
33	Effect of Velocity Ratio on Asymptotic Entrainment Fraction	116
34	Comparison of Entrainment Fraction Ratios	117
35	Asymptotic Entrainment Fraction Ratio vs. Density Ratio	118
36	Correlation of Convergent Turn Entrainment Fraction with Density Turn Parameter	119
37	Correlation of Convergent Turn Entrainment Fraction with Momentum Turn Parameter	120
38	Attempted Correlation of Throat Turn Entrainment Fraction	121
39	Comparison of Entrainment Model and Boundary Layer Computer Program Results	122
40	Correlation of Convergent Section Rocket Data with Density Difference Parameter	123
41	Correlation of all Available Convergent Region Data with Density Difference Parameter	124
42	Correlation of the Convergent Region Data with Density Turn Parameter	125

List of Figures (cont.)

<u>Figure No.</u>	<u>Title</u>	<u>Page</u>
43	Correlation of the Convergent Region Data with Momentum Turn Parameter	126
44	k_f Factor vs. Injection Velocity Ratio	127
45	Vacuum Specific Impulse Data	128
46	Film Cooling Performance Loss vs. Film Cooling Percentage	129
47	Correlation of Hydrogen Film Cooled Performance Loss Data	130
48	Comparison of Predicted and Measured Film Cooling Performance Loss Values	131
49	Effect of Shape Factor on Predicted Film Cooling Loss	132
50	Comparison of Measured and Predicted Velocity Ratio and Effectiveness Effects on C_g	133
51	Row B C_g Profiles With and Without Film Cooling	134
52	Proposed O_2/H_2 Thrust Chamber Design	135
53	Coolant Passage Geometry and Chamber Contour	136
54	Combustor Wall Temperature Predictions Without Film Cooling	137
55	HOCOOL Predictions of Maximum Wall Temperature In the Film Cooled Region and Performance Loss	138
56	HOCOOL Predictions of Maximum Combustor Temperature and Film Cooling Performance Loss	139



I SUMMARY

The objectives of the Combustion Effects on Film Cooling Program were:

1. To experimentally determine the effects of a reactive environment, and flow turning on the effectiveness of hydrogen film cooling in a hydrogen-oxygen rocket thrust chamber.
2. To experimentally determine the performance loss resulting from the film coolant flow, and
3. To prepare a computer program that integrates a generalized regenerative cooling model, the ALRC entrainment film cooling model, and a film-cooling-performance-loss model.

These objectives were achieved by (1) conducting rocket engine firings with a specially instrumented, thrust chamber test assembly, and (2) by combining previously existing ALRC computer programs for gas film cooling and regenerative cooling with an ALRC analytical technique for calculating film cooling performance loss into one thermal analysis computer program.

The thrust chamber test assembly is shown in Figure 1. It consisted of: (1) a core gas injector which generated O_2/H_2 combustion products, (2) a water cooled mixing length, (3) a gas film coolant injector, and (4) a thin walled stainless steel thrust chamber. The thrust chamber was instrumented with thermocouples for determining adiabatic wall temperature distributions. Tests without film cooling in which a copper heat sink thrust chamber replaced the thin-walled thrust chamber were also performed. A total of 29 firings were performed at the range of test conditions noted below.

Core Gas Mixture Ratio = 0.78 to 8.0
Nominal Chamber Pressure = 207 n/cm² (300 psia)
Film Coolants: hydrogen, helium, nitrogen

I Summary (cont.)

The specific test conditions for each test are listed on Table I.

The thermal analysis computer program created is designated HOCOOL. It was designed for the determination of coolant requirements and associated performance penalties of advanced hydrogen/oxygen rocket thrust chambers. This program can be utilized to perform thermal analyses of film cooled adiabatic wall thrust chamber designs and designs which utilize both film and regenerative cooling. The program and a detailed users manual has been delivered to the NASA-Lewis Research Center. The analytical models contained within the HOCOOL computer program are described in Section III of this report.

Film cooling adiabatic wall temperature data, performance loss data, and heat transfer coefficient data obtained in the film cooled test firings were all correlated with the aid of the ALRC entrainment film cooling model. This model relates film cooling effectiveness and mixture ratio at the wall to the amount of mainstream gases entrained by the film coolant and mixed with it in an annular mixing layer adjacent to the chamber wall. The film cooling data were evaluated in terms of an entrainment fraction which is defined as the ratio of entrained core gas mass flux to the axial core gas mass flux. The entrainment fraction data are summarized in Table II. The two stream tube flow model contained within the entrainment model was used to correlate the performance loss data which are listed on Table III. The heat transfer coefficient data obtained with and without film cooling are listed on Tables IV and V. Discussions on the data reduction techniques and data correlations are presented in Section IV.

It was found that the entrainment fractions in the rocket engine were about twice as high as in previous tests performed with heated nitrogen core gas. This is attributed to a higher free stream turbulence level in the rocket engine. In addition, velocity ratio effects were somewhat different than previously observed. Other significant effects on entrainment fraction noted were: wake effects downstream of the slot lip, flow turning effects, and core gas mixture ratio effects.

I Summary (cont.)

It was found that the experimental entrainment fractions were the same for hydrogen and helium film coolants injected at identical velocity ratio and core gas mixture ratio conditions. Since a potential for combustion between the core gases ($O/F = 8$) and the hydrogen film coolant existed, this agreement of results indicates that either the combustion did not influence the entrainment fraction (i.e., the mixing rate) or that the potential reaction did not occur.

The HOCOOL computer program and the data correlations given in Section IV were used to analyze a proposed high pressure hydrogen/oxygen rocket engine. The results indicate that injecting 10% of the hydrogen as film coolant will reduce the maximum wall temperature 190°K (340°F) and that the corresponding performance loss will be approximately 1% of the no-film-cooling performance.

II INTRODUCTION

The Combustion Effects on Film Cooling Program consisted of two fundamental activities: (1) experimental investigation of film cooling effects in a hydrogen/oxygen thrust chamber, and (2) preparation of a comprehensive thermal analysis computer program.

The experimental portion of the program is the rocket engine equivalent of the two previous experimental programs performed by ALRC using hot nitrogen core gas and reported in References 1 and 2. The testing approach used was similar to that followed during the previous programs except that the hot core gas source was a rocket engine injector operating with hydrogen-oxygen propellants at 300 psia chamber pressure. Heated nitrogen core gas was used previously.

The test hardware assembly is shown in Figure 1. It consisted of a premix-triplet propellant injector, an igniter, a fuel manifold, a water-cooled cylinder, a film coolant injector, and a thin-walled film-cooled nozzle. The propellant injector, fuel manifold and igniter were residual from previous ALRC Contracts (Ref. 3 and 4). The water cooled cylinder, film coolant injector, and film-cooled nozzle were designed and fabricated as part of the Combustion Effects on Film Cooling Program.

The computer program prepared has been designated HOCOOL. It was prepared by combining the ALRC entrainment film cooling model with an ALRC generalized regenerative cooling model, and a film-cooling performance loss model which utilizes the results of the film cooling model analysis. A detailed description of this computer program is given in Reference 5. The HOCOOL computer program has been delivered to NASA for governmental use.¹

During the rocket engine testing, adiabatic wall temperature distributions in the film-cooled nozzle were determined by measuring the outer nozzle wall temperature at appropriate points. These film cooling data were evaluated by

¹The HOCOOL computer program is not to be reproduced, used, or disclosed to anyone without the permission of the Aerojet Liquid Rocket Company, except that the government has the right to reproduce and use, for governmental purposes, any part of the HOCOOL computer program.

II Introduction (cont.)

considering them within the context of the ALRC entrainment film cooling model which relates film cooling effectiveness to the amount of mainstream gases entrained by and mixed with the film coolant in a mixing layer adjacent to the chamber wall. This entrainment flow model, described in Section III.A., appears to be a fundamentally sound approach to the film cooling problem since it has been used to correlate both heat transfer data and performance loss data. The entrainment approach was suggested by boundary layer model work (Ref. 6) and has been applied to rocket engines at ALRC and to jet engines at the NASA Lewis Research Center (Ref. 7).

There are three potential "combustion effects on film cooling" which can be identified. These are:

1. The effect of core gas conditions on the film coolant/core gas mixing process. This effect was evaluated by: (1) comparing data from this program to data obtained previously using heated nitrogen core gas, and (2) documenting core gas mixture ratio effects apparent in the data (See Sections IV.B.1.a, IV.C.1.c, IV.C.1.d, IV.C.1.e, IV.C.4).
2. The effect of chemical reactions within the mixing layer on the film coolant/core gas mixing process. This effect was evaluated by comparing data obtained with hydrogen and helium film coolants at identical core gas mixture ratio and coolant injection velocity ratio. (Sections IV.B.1.a, IV.C.1.b, IV.C.4.)
3. The effect of a chemical reaction between the film coolant and the entrained core gas on the thermodynamic properties of the mixture contained within the mixing layer. This was evaluated by comparing analytical results from a model which considers this reaction to a model which does not. (Section IV.B.2.b).

This report is organized in the following manner: Section I is a brief summary of the work performed and the major findings; Section III contains descriptions of the pertinent analytical models; Section IV contains the experimental results and data correlations; Section V contains analytical predictions for an advanced hydrogen-oxygen thrust chamber; and specific conclusions and recommendations are listed in Section VI. The four appendices provide: nomenclature (Appendix A), test data (Appendix B), description of test components (Appendix C), and distribution list (Appendix D).

III DESCRIPTION OF ANALYTICAL MODELS

A. ENTRAINMENT FILM COOLING MODEL

This section contains a description of the ALRC entrainment film cooling model for gas film cooling of rocket engine thrust chambers operating with oxygen/hydrogen propellants. The general features of the entrainment model are described in Section III.A.1. which presents an overview of the analytical approach. Analytical details are presented in Sections III.A.2. and III.A.3. Section III.A.2. presents the relationships which exist between film cooling effectiveness, enthalpy, and concentration. In Section III.A.3., the relationships between film cooling effectiveness, entrained flow rate and a mixing layer profile shape factor are described.

1. General Features

The ALRC entrainment film cooling model is basically a two stream tube mixing model as illustrated in Figure 2. Core gases or combustion gases emanating from the main propellant injector are considered to be entrained by and to mix with film coolant gases which have been injected onto the chamber wall. The mixing is assumed to occur in an annular mixing layer adjacent to the thrust chamber wall. This mixing layer comprises one of the stream tubes. The other stream tube is the central flow region where the unmixed core gases are located. The rate at which core gases are entrained into the mixing layer is defined in terms of an entrainment fraction, k , as follows:

$$\left(\begin{array}{c} \text{Entrained} \\ \text{Core Gas} \\ \text{Mass Flux} \end{array} \right) = k \left(\begin{array}{c} \text{Axial Flow} \\ \text{Core Gas} \\ \text{Mass Flux} \end{array} \right) \quad \text{Eq. (1)}$$

The k values are model inputs and appropriate values for design calculations are determined from test data.

The Equation 1 approach for describing the mixing which occurs between film coolant and main stream gases is suggested by the boundary layer model analysis of film cooling data presented in Reference 6. This approach has also been used by Marek at NASA-Lewis to model film cooling in jet engine combustors (Ref. 7). Equation 1 defines a bulk mixing process

III Description of Analytical Models (cont.)

between the core gas and film coolant gas. The effects of enthalpy and concentration profiles through the mixing layer are accounted for in the ALRC entrainment model by the use of a profile shape factor which relates bulk mixing layer conditions to adiabatic wall conditions. However, the model does not provide a basis for actually calculating these profiles.

The general analysis approach followed in the ALRC entrainment model is as follows: (1) the total entrained core gas flow rate between the coolant injection point and the point of interest is calculated by integration of Equation 1, (2) the film cooling effectiveness is calculated using previously established correlations between the entrained flow rate and effectiveness, (described in Section III.A.3), (3) adiabatic wall temperature and gas composition at the wall are calculated using appropriate effectiveness definitions.

The fundamental definition of film cooling effectiveness, η , in the ALRC entrainment film cooling model was included in the simplified Reference 6 analysis and is shown as Equation 2.

$$\text{Effectiveness} = \eta = (\gamma)_{\text{at the wall}} = \gamma_w \quad \text{Eq. (2)}$$

Equation 2 states that film cooling effectiveness is always equal to the mass fraction of the injected film coolant gas within the gas mixture directly adjacent to the wall.

Three optional procedures exist within the entrainment model for calculating adiabatic wall temperature from the effectiveness: (1) reactive option, (2) non-reactive option, and (3) core-reaction option. These options are explained in detail in Section III.A.2.

In the reactive option, two independent effectiveness definitions are utilized: one based on total enthalpy and the other based on mass fraction. The mass fraction definition is used to calculate the mixture

III Description of Analytical Models (cont.)

ratio directly adjacent to the wall, $(O/F)_w$, while the enthalpy definition is used to calculate the adiabatic wall enthalpy of this mixture, H_{aw} . Imperfect kinetic energy recovery effects are accounted for with a conventional turbulent flow recovery factor. (The $(O/F)_w$ and H_{aw} values are then used to determine T_{aw} from a thermochemical table relating temperature, enthalpy, and mixture ratio. Equilibrium chemistry is assumed. The reactive option is recommended for analysis of O_2/H_2 engines which are film cooled with hydrogen or low mixture ratio gases.

In the non-reactive model, the film coolant and core gas specific heats are assumed constant. This leads to a direct relationship between effectiveness, adiabatic wall temperature, and recovery factor from which the adiabatic wall temperature is calculated. The non-reactive option is recommended for analysis of rocket engines not operating with O_2/H_2 propellants which are film cooled with inert gases.

Only the film coolant specific heat is assumed constant in the core-reactive option. The non-reactive T_{aw} equation is modified to include core gas enthalpy evaluated at the adiabatic wall temperature from the reactive option thermochemical tables. An iterative solution yields T_{aw} for a given value of effectiveness. The core-reactive option is recommended for O_2/H_2 engines which are film cooled with inert gases.

The two stream tube flow model portion of the entrainment film cooling model has been utilized in constructing an analytical technique for predicting the rocket engine performance loss associated with film cooling. A model in which this technique is applied to the case of hydrogen film cooling in hydrogen/rocket engines is described in Section III.B. and correlated with test data in Section IV.D.

III Description of Analytical Models (cont.)

The fact that both adiabatic wall temperature and gas composition at the wall are obtained from the entrainment model is a very advantageous feature for analyzing non-adiabatic walls such as a regeneratively cooled thrust chamber which is also film cooled. In this case, the adiabatic wall temperature or enthalpy is considered to be the driving potential for heat transfer and the gas composition is used to evaluate the transport properties from which gas-side heat transfer coefficient is calculated. Heat transfer with film cooling is discussed further in Section III.C.

The details of the ALRC entrainment model are described in the remainder of Section III.A. Two film coolant injection cases are mentioned in the following discussions: (1) the subsonic case where film coolant injection is subsonic and the core gas flow is subsonic, and (2) the supersonic case where film coolant injection is supersonic and the core gas flow is supersonic.

2. Effectiveness, Enthalpy and Concentration Relationships

a. Reactive Model

(1) Effectiveness Definitions

Two other effectiveness definitions, which are derived from Equation 2, are used for the reactive version of the entrainment model. One is based on concentration or mass fraction as shown in Equation 3.

$$\eta = \frac{c_e - c_w}{c_e - c_c} \quad \text{Eq. (3)}$$

The c in Equation 3 represents the concentration of any element or species.¹ However, c is generally taken to be the concentration of the film coolant gas. In this case, c differs from γ in that the c mass fraction includes any film coolant gas species present in the entrained core gas. In general,

¹The subscript c indicates film coolant injection conditions. All nomenclature is defined in Appendix A.

III Description of Analytical Models (cont.)

$$c = \gamma c_c + (1-\gamma) c_e \quad \text{Eq. (4A)}$$

At the nozzle wall, this becomes:

$$c_w = \gamma_w c_c + (1 - \gamma_w) c_e \quad \text{Eq. (4B)}$$

which can be combined with Equation (2) to yield the Equation (3) definition of effectiveness.

For thrust chamber applications, the local mixture ratio at the wall is determined by the Equation (3) definition of coolant effectiveness. From Equation 3 with c proportional to $(1 + O/F)^{-1}$ i.e., considering an element in the fuel,

$$(O/F)_w = \frac{1 + (O/F)_e}{\eta \left[\frac{1 + (O/F)_e}{1 + (O/F)_c} - 1 \right] + 1} - 1 \quad \text{Eq. (5)}$$

The other effectiveness definition is the enthalpy definition of Reference 6. It is obtained from Equation 3 by making the following assumptions: (1) molecular diffusion is negligible compared to turbulent diffusion, (2) the viscous sublayer at the wall is thin relative to the mixing layer, and (3) the turbulent Lewis number is unity (experimental evidence indicates it is close to unity). Under these conditions the differential conservation equations for element mass and total enthalpy are the same outside the viscous sublayer, so the effectiveness may also be written in terms of total enthalpies:

$$\eta = \frac{H_{0e} - H_{0v}}{H_{0e} - H_{0c}} \quad \text{Eq. (6)}$$

III Description of Analytical Models (cont.)

(2) High Speed Effects

In Equation (6), the subscript v denotes the edge of the thin viscous sublayer near the wall. Since this sublayer is assumed to be thin, no additional mixing occurs across it. Therefore, the adiabatic wall enthalpy differs from H_{0v} only because of the imperfect recovery of kinetic energy in the viscous sublayer; this high-speed effect is represented in terms of a conventional recovery factor as

$$H_{0v} - H_{aw} = (1 - Pr_w^{1/3}) (H_{0e} - H_e) (\bar{u}/u_e)^2 \quad \text{Eq. (7)}$$

Equation 7 states that the difference between H_{0v} and H_{aw} is proportional to the difference between total core gas enthalpy and static core gas enthalpy ($H_{0e} - H_e$),⁽¹⁾ less the amount recovered in the sublayer. The conventional $Pr^{1/3}$ recovery factor for turbulent flow is assumed.

The proportionality factor in Equation (7) is $(\bar{u}/u_e)^2$ which accounts for the fact that the effective mixing layer velocity, \bar{u} , is not generally equal to the core gas velocity, u_e . The parameter \bar{u} is related to the velocity at the edge of the viscous sublayer in the same way as the freestream velocity for a conventional boundary layer. At the coolant injection point, \bar{u} should equal the film coolant velocity, u_c , while far downstream it becomes u_e since the mixing layer becomes a conventional boundary layer.

In the subsonic case high-speed effects are usually important only after considerable mixing occurs, due to the significant distance between the film coolant injection point and the nozzle throat. Therefore, for the subsonic case it is assumed that $\bar{u} = u_e$, i.e., the mixing layer is fully developed when the high-speed effects are of any significance, and the

⁽¹⁾ H_{0e} and H_e are input values. The TRAN-72 computer program of Reference 8 is recommended for calculating them.

III Description of Analytical Models (cont.)

quantity $(\bar{u}/u_e)^2$ is unity.

In the supersonic case the high-speed effects are important throughout the analysis, so it is necessary to define the axial variation of the effective velocity \bar{u} . This has been accomplished through the use of a velocity mixing function $V (W_E/W_C)$:

$$\bar{u} = u_e + (u_c - u_e) V (W_E/W_C) \quad \text{Eq. (7A)}$$

The function $V (W_E/W_C)$ was developed at ALRC on Contract NAS 3-15844 (Ref. 2) and is shown on Figure 16 of Reference 5. It ranges from 1.0 for $W_E/W_C < 0.5$ to .05 at $W_E/W_C = 3.38$.

Combining Equations (6) and (7) gives the adiabatic wall enthalpy as

$$H_{aw} = H_{o_e} - \eta(H_{o_e} - H_{o_c}) - (1 - Pr_w^{1/3}) (H_{o_e} - H_e) (\bar{u}/u_e)^2 \quad \text{Eq. (8)}$$

(3) Calculation of T_{aw} and O/F at the Wall

When the effectiveness is known, Equation 5 gives the mixture ratio at the nozzle wall and Equation 8 gives the adiabatic wall enthalpy. The Prandtl number in Equation 8 is evaluated at the wall mixture ratio. Adiabatic wall temperature, T_{aw} , is obtained using both (O/F) wall and H_{aw} in an equilibrium chemistry model.

The specific steps followed in calculating adiabatic wall temperature with the reactive model are:

1. The entrained flow rate, W_E , is calculated from Equation 27 (See Section III.A.3.e).
2. η is determined from the basic mixing layer equation, Equation 17 (See Section III.A.3.a.).

III Description of Analytical Models (cont.)

3. $(O/F)_w$ is calculated from Equation 5.
4. H_{aw} is calculated from Equation 8.
5. T_{aw} is interpolated from a table which relates enthalpy, temperature, pressure and mixture ratio (equilibrium chemistry assumed).

b. Non-Reactive Model

The non-reactive model is a constant specific heat version of the entrainment model. As indicated in Equation 2, the effectiveness always equals the mass fraction of the injected film coolant at the wall and consequently the enthalpy of the mixture at the wall is

$$H_{aw} = \eta (H_c)_{aw} + (1 - \eta) (H_e)_{aw} \quad \text{Eq. (9)}$$

$$H_{aw} = [\eta C_{p_c} + (1-\eta) C_{p_e}] T_{aw} \quad \text{Eq. (10)}$$

High speed effects are accounted for in the same manner as the reactive model. Using constant specific heats in Equation (8) and combining Eqns. 8 and 10 yields

$$\eta = \frac{C_{p_e} (T_{o_e} - T_{aw}) - (1-Pr_w^{1/3}) (H_{o_e} - H_e) (\bar{u}/u_e)^2}{C_{p_e} (T_{o_e} - T_{aw}) + C_{p_c} (T_{aw} - T_{o_c})} \quad \text{Eq. (11)}$$

Adiabatic wall temperature is determined in the following way for the non-reactive model:

1. W_F is calculated from Equation 27. (Section III.A.3.e).
2. η is determined from Equation 17 (Section III.A.3.a)
3. $(O/F)_w$ is calculated from Equation (5) but is used solely to evaluate Pr_w .

NOTE: For the inert film coolant case, W_c can be considered as a fuel in the $(O/F)_w$ definition.

4. T_{aw} is determined from Equation (11), where H_{o_e} is input and H_e is interpolated from an input enthalpy vs. area ratio table.

III Description of Analytical Models (cont.)

The core-reactive model discussed in Section III.A.2.c. can be simulated with the non-reactive model by using the correct core specific heat (Equation 12) in the non-reactive model.

$$\bar{C}_{p_e} = \frac{H_{o_e} - H_e(T_{aw})}{T_{o_e} - T_{aw}} \quad \text{Eq. (12)}$$

This equivalent specific heat is exact at any one point and provides a general approximation when the T_{aw} variation is fairly small relative to T_{o_e} .

c. Core-Reactive Model

This model is similar to the non-reactive model described above, except the core is not restricted to a constant specific heat. Therefore the enthalpy of the mixture at the wall is

$$H_{aw} = n C_{p_c} T_{aw} + (1 - n) (H_e)_{aw} \quad \text{Eq. (13)}$$

combining this with Equation (7) to eliminate H_{aw} gives

$$\begin{aligned} n C_{p_c} (T_{aw} - T_{o_c}) &= (1 - n) [H_{o_e} - (H_e)_{aw}] - (1 - Pr_w^{1/3}) \\ &\quad (H_{o_e} - H_e) (\bar{u}/u_e)^2 \end{aligned} \quad \text{Eq. (14)}$$

in which $(H_e)_{aw}$ is evaluated at the adiabatic wall temperature and core mixture ratio using the thermochemical table of the reactive option. Values of T_{aw} are calculated from Equation (14).

3. Effectiveness, Entrained Flow Rate, and Shape Factor Relationships

a. Basic Mixing Layer Equation

The cooling effectiveness η is related to the

III Description of Analytical Models (cont.)

entrained flow W_E into the mixing layer, the coolant flow injected W_C , and a shape factor θ which relates bulk mass fraction to concentration at the wall. The basic mixing layer equation is derived from an element mass balance on the mixing layer,

$$\left[\begin{array}{l} \text{Injected Element} \\ \text{Mass Flow from} \\ \text{The Film Coolant} \end{array} \right] + \left[\begin{array}{l} \text{Element Mass} \\ \text{Flow Entrained} \\ \text{From the Core} \end{array} \right] = \left[\begin{array}{l} \text{Element Mass} \\ \text{Flow in the} \\ \text{Mixing Layer} \end{array} \right]$$

or

$$W_C c_C + W_E c_e = (W_C + W_E) c_b \quad \text{Eq. (15)}$$

The element mass fraction at the wall is related to the bulk value c_b through a mixing layer profile shape factor θ , defined as⁽¹⁾

$$\theta = \frac{c_e - c_b}{c_e - c_w} = \frac{\int_0^s \rho u (c_e - c) dy}{(c_e - c_w) \int_0^s \rho u dy} \quad \text{Eq. (16)}$$

Substituting Equations 3 and 16 into Equation 15 in order to eliminate c_b and c_w gives the basic mixing layer equation, Equation 17, which defines the effectiveness n in terms of the entrainment flow ratio W_E/W_C , and the shape factor θ . Equation 17A is derived from Equation 16 and relates bulk mixing layer mixture ratio to the shape factor and the mixture ratio at the wall.

$$n = \frac{1}{\theta \left(1 + \frac{W_E}{W_C} \right)} \quad \text{Eq. (17)}$$

$$(O/F)_b = \theta \left[\frac{1 + (O/F)_e}{1 + (O/F)_w} - 1 \right] + 1 \quad \text{Eq. (17A)}$$

b. Effectiveness Regimes

The present entrainment model is characterized by a correlation among effectiveness n , entrained flow ratio W_E/W_C , and shape factor

⁽¹⁾ Integral Definition shown is for a film cooled flat plate.

III Description of Analytical Models (cont.)

θ , which relates Equation 17 to three effectiveness regimes: (1) the initial free jet regime, (2) the transition regime, and (3) the fully developed or asymptotic regime. This three-regime correlation was initially developed for the subsonic case by correlating plane unaccelerated flow data as reported in Reference 1 and indicated on Figure 4. The corresponding θ vs W_E/W_C correlation is shown on Figure 5 along with the supersonic θ vs W_E/W_C correlation from Reference 2. The η vs. W_E/W_C correlation of Figure 4 is considered general for all cases where the film coolant is injected subsonically and the core gas flow is subsonic. The η vs. W_E/W_C correlation for supersonic injection and supersonic core flow is somewhat different as indicated by the different θ vs W_E/W_C correlation on Figure 5. The supersonic case is discussed further in Reference 2.

In the initial free jet regime, the mixing effects have not penetrated to the wall, and as a result the effectiveness is unity. The shape factor decreases in this regime according to Equation (18), derived from Equation (17), for both the subsonic and supersonic cases.

$$\theta = \left(1 + \frac{W_E}{W_C}\right)^{-1} \quad \text{Eq. (18)}$$

The initial free jet regime is defined as $W_E/W_C \leq 0.06$ for the subsonic case, $W_E/W_C \leq 0.5$, and for the supersonic case (See Figure 5).

In the transition regime, both the effectiveness and shape factor decrease with W_E/W_C . This regime is defined as $0.06 \leq W_E/W_C \leq 1.4$ for the subsonic case and $0.5 \leq W_E/W_C \leq 2.2$ for the supersonic case (See Figure 4). A curve fit of the effectiveness data in this region and Equation 18 defined the subsonic θ curve in Figure 5 for the transition regime. Analytical results were used in a similar manner to generate the supersonic θ curve.

III Description of Analytical Models (cont.)

In the fully developed or asymptotic regime, the shape factor is constant and η continues to decrease as W_E/W_C increases. For the subsonic case, the asymptotic regime is defined as $W_E/W_C \geq 1.4$. A curve fit of the plane unaccelerated flow data in this regime yielded the following equation.

$$\eta = \frac{1.32}{1 + \frac{W_E}{W_C}} \quad \text{Eq. (19)}$$

Comparison of Equations 17 and 19 indicates that this constant or asymptotic shape factor is $1/1.32 = 0.758$ for the subsonic case. For the supersonic case, the asymptotic region is $W_E/W_C \geq 2.2$ and the asymptotic shape factor is 0.485.

c. Shape Factor Physical Significance

The magnitude of the shape factor θ is indicative of the mixture ratio (O/F) distribution within the mixing layer as indicated schematically on Figure 6. As indicated by curve 1 of Figure 6, a shape factor near 1.0 indicates a nearly constant mixing layer O/F and the wall O/F value characterizes almost the entire mixing layer. This is typical of the mixing layer very near the film coolant injection point. When $\theta \approx 1.0$, the wall mixture ratio is about the same as the bulk mixing layer mixture ratio (See Eq. 17A).

Curve 2 of Figure 6 is typical of the O/F distribution implied by the asymptotic θ values of Figure 5. The change in O/F across the mixing layer is quite regular.

Curve 3 of Figure 6 indicates the case where θ becomes small and most of the mixing layer is characterized by the core gas mixture ratio. This case represents a very well mixed mixing layer and implies the highest entrainment flow rates.

III Description of Analytical Models (cont.)

d. Entrainment Fraction for Plane Unaccelerated Flow

The entrainment fraction for the case of plane-unaccelerated flow is designated k_0 . This parameter is a convenient reference value for experimental subsonic region entrainment fractions since it accounts for the effects of velocity ratio, u_c/u_e , density ratio, ρ_c/ρ_e , and coolant slot Reynolds number, Re_c which are known to exist in the plane unaccelerated flow data.

A correlation for the entrainment fraction in plane unaccelerated flow, k_0 , was derived from the Figure 4 effectiveness correlation assuming that k_0 is constant with x (Ref 1.) This assumption yields Equation 20 which applies only to plane unaccelerated flow.

$$\frac{W_E}{W_C} = \frac{k_0 x}{\left(\frac{\rho_c}{\rho_e}\right) \left(\frac{u_c}{u_e}\right) h} \quad \text{Eq. (20)}$$

Comparison of Equations 17 and 20 to the asymptotic region data curve fit equation on Figure 4, leads to the k_0 correlation, Equation 21.

$$k_0 = \frac{0.1 (u_c/u_e)}{\left(\frac{\rho_c}{\rho_e}\right)^{0.15} f\left(\frac{u_c}{u_e}\right) Re_c^{0.25}} \quad \text{Eq. (21)}$$

The velocity ratio function $f(u_c/u_e)$ is plotted on Figure 7 along with the data from which it was derived.

III Description of Analytical Models (cont.)

e. Determination of Entrained Flow Rate

As indicated in Figure 3, the entrained mass velocity is represented as a fraction k of the axial mass velocity of the mainstream. Thus, the total entrained flow up to any contour position is

$$W_E = \int k (\rho_e u_e) dA$$
$$W_E = \int_0^x 2 \pi (r - s \cos \alpha) k \rho_e u_e dx \quad \text{Eq. (22)}$$

The subsonic entrainment fraction is assumed to be of the Equation 23 form.

$$k = k_o k_m(x) \left(\frac{\rho_e u_e}{(\rho_e u_e)_o} \right)^{-m} \quad \text{Eq. (23)}$$

The multiplier $k_m(x)$ accounts for increased freestream turbulence, flow turning, and other "real world" effects associated with rocket engines such as propellant injector effects and discontinuous coolant slot effects. The bracketed term accounts for subsonic flow acceleration and was suggested by the work of Deissler relative to the effect of acceleration on transverse turbulent transport in a homogeneous fluid. For subsonic region injection, the exponent m was found to be 0.65 in tests performed at ALRC (Ref. 2). Entrainment fractions for supersonic injection into a supersonic region are discussed in References 2 and 5.

A momentum balance on the total nozzle flow should be used to account for the effect of the mixing layer on the freestream mass velocity $\rho_e u_e$. However, for the sake of simplicity the model assumes the mainstream accelerates as if there were no film cooling,

III Description of Analytical Models (cont.)

$$\rho_e u_e = (\rho_e u_e)_o \left(\frac{r_o^2}{r^2} \right) \frac{\emptyset}{\emptyset_o} \quad \text{Eq. (24)}$$

in which subscript o refers to the injection point. (The factor \emptyset is used to account for 2-dimensional flow effects). A nozzle mass balance (integral continuity equation) then gives the mixing layer thickness from

$$\left(1 - \frac{s}{r} \cos \alpha\right)^2 = \left(1 - \frac{s_o}{r_o}\right)^2 \left(1 - \frac{W_E}{W - W_C}\right) \quad \text{Eq. (25)}$$

Substituting equations 23, 24 and 25 in Equation 22 gives

$$W_E = 2\pi (r_o - s_o) k_o (\rho_e u_e)_o \int_0^x \left(1 - \frac{W_E}{W - W_C}\right)^{1-2m} \left(\frac{r_o}{r}\right)^{1-m} \left(\frac{\emptyset}{\emptyset_o}\right) k_m dx \quad \text{Eq. (26)}$$

Solving this integral equation and relation $(\rho_e u_e)_o$ to s_o and the flow rates yields

$$\frac{W_E}{W - W_C} = \frac{W_E/W_C}{W/W_C - 1} = 2 \frac{k_o \emptyset_o \bar{x}}{r_o - s_o} - \left[\frac{k_o \emptyset_o \bar{x}}{r_o - s_o} \right]^2 \quad \text{Eq. (27)}$$

in which

$$\bar{x} = \int_0^x \left(\frac{r_o}{r}\right)^{1-2m} \left(\frac{\emptyset}{\emptyset_o}\right)^{1-m} k_m dx \quad \text{Eq. (28)}$$

Thus Equation 27 gives the entrained flow ratio, W_E/W_C , and Equation 17 then determines the film cooling effectiveness. Note that \bar{x} is an equivalent cylindrical section length for use with the reference entrainment fraction k_o .

III Description of Analytical Models (cont.)

B. FILM COOLING PERFORMANCE LOSS MODEL

The two stream tube entrainment flow model described in the previous section provided the analytical basis for development of a film-cooling performance loss model. This performance loss model was correlated with test data (See Section IV.D.) and subsequently combined with the entrainment film cooling model, and a generalized regenerative cooling model to form the computer program designated HOCOOL which is described in the Section III.C. and in Reference 5.

The specific film-cooling performance loss model incorporated within HOCOOL is applicable only to thrust chambers which are film cooled with either gaseous hydrogen or hydrogen-oxygen combustion products. However; the fundamental approach followed appears to be applicable to any combination of propellant systems provided that the film coolant is a gas by the time it reaches the nozzle throat. The HOCOOL performance loss model calculates the vacuum specific impulse loss associated with cooling a GO_2/GH_2 combustion chamber with a GH_2 fuel film or low mixture ratio barrier gas. The model formulation is based on the entrainment flow model format and the empirical observation that the film coolant loss is best correlated as a function of the engine overall mixture ratio.

The film cooling loss is defined as the difference between uncooled and cooled engine delivered vacuum specific impulse (with both impulse values defined at the same overall mixture ratio, chamber pressure, and nozzle area ratio).

III Description of Analytical Models (cont.)

$$\Delta I_{sp \text{ FCL}} = I_{sp \text{ uncooled @ O/F overall}} - I_{sp \text{ cooled @ O/F overall}} \quad \text{Eq. (29)}$$

Uncooled engine performance is reduced from the theoretical one dimensional equilibrium (ODE) maximum by several real engine performance losses as indicated by Equation 30.

$$I_{sp \text{ uncooled @ O/F overall}} = I_{sp \text{ ODE @ O/F overall}} - \sum I_{sp \text{ Losses}} \quad \text{Eq. (30)}$$

The losses that should be considered for a GO_2/GH_2 engine are reaction kinetics, boundary layer friction and heat transfer, nozzle throat and exit two dimensional flow, and thrust chamber core mixture ratio maldistribution. For simplicity an uncooled engine efficiency factor was defined to account for the real engine losses.

$$\eta_{I_{sp \text{ @ O/F overall}}} = 1 - \frac{\sum I_{sp \text{ losses @ O/F overall}}}{I_{sp \text{ ODE @ O/F overall}}} \quad \text{Eq. (31)}$$

It follows that engine uncooled vacuum specific impulse can be defined as shown in Equation 32.

$$I_{sp \text{ uncooled @ O/F overall}} = \eta_{I_{sp \text{ @ O/F overall}}} \times I_{sp \text{ ODE @ O/F overall}} \quad \text{Eq. (32)}$$

Cooled engine delivered vacuum performance is defined as the mass weighted average of the engine core and mixing layer streamtubes at the thrust chamber throat plane. This is stated mathematically in Equation 33.

$$I_{sp \text{ cooled @ O/F overall}} = \left(\frac{W_{\text{core}}}{W} \right) I_{sp \text{ core @ O/F core}} + \left(\frac{W_{\text{ML}}}{W} \right) I_{sp \text{ ML @ O/F ML}} \quad \text{Eq. (33)}$$

III Description of Analytical Models (cont.)

The core stream tube flow rate, W_{core} , and the mixing layer flow rate, W_{ML} , at the throat plane are calculated by the entrainment film cooling model.

Specific impulse of the core is evaluated at the core mixture ratio in the same manner as overall specific impulse for the uncooled engine.

$$I_{sp \text{ core}} @ O/F \text{ core} = \eta_{I_{sp}} @ O/F \text{ core} \times I_{sp \text{ ODE}} @ O/F \text{ core} \quad \text{Eq. (34)}$$

The specific impulse of the mixing layer is determined using the mixing layer throat plane mixture ratio which is also calculated by the entrainment film cooling model.

$$I_{sp \text{ ML}} @ O/F \text{ ML} = \eta_{I_{sp}} @ O/F \text{ ML} \times I_{sp \text{ ODE}} @ O/F \text{ ML} \quad \text{Eq. (35)}$$

Correlation of hot test data during the Combustion Effects Program (See Section IV.E.) has shown that the Equation 36 definition of the mixing layer performance efficiency factor yields the most accurate model predictions. The Equation 36 definition assumes an isentropic one-dimensional expansion of the film coolant gases (i.e., $\eta_{I_{sp}} = 1.0$ for the film coolant gases).

$$\eta_{I_{sp}} @ O/F \text{ ML} = \eta_{I_{sp}} @ O/F \text{ core} \times \frac{W_E}{W_{ML}} + \frac{W_C}{W_{ML}} \quad \text{Eq. (36)}$$

From Equations 33, 34, and 35 the film cooled engine vacuum specific impulse is defined as:

$$I_{sp \text{ cooled}} @ O/F \text{ overall} = \eta_{I_{sp}} @ O/F \text{ core} \times I_{sp \text{ ODE}} @ O/F \text{ core} \times \frac{W_{core}}{W} + \eta_{I_{sp}} @ O/F \text{ ML} \times I_{sp \text{ ODE}} @ O/F \text{ ML} \times \frac{W_{ML}}{W} \quad \text{Eq. (37)}$$

III Description of Analytical Models (cont.)

Substituting Equations 32 and 37 into Equation 29 yields the equation for the predicted film coolant performance loss.

$$\Delta I_{sp FCL} = \eta_{I_{sp}} @ O/F \text{ overall} \times I_{sp ODE} @ O/F \text{ overall} - \left[\eta_{I_{sp} \text{ core}} @ O/F \text{ core} \times I_{sp ODE} @ O/F \text{ core} \times \frac{W_{core}}{W} + \eta_{I_{sp} \text{ ML}} \times I_{sp ODE} @ O/F \text{ ML} \times \frac{W_{ML}}{W} \right] \quad \text{Eq. (38)}$$

In Equation 38 the performance loss is based on one dimensional equilibrium specific impulse for the two flow field stream tubes. Theoretically, one dimensional kinetic specific impulse is more correct but is impractical in the general case because kinetic impulse depends on many engine design variables such as nozzle length, nozzle shape, throat inlet and outlet radius, area ratio, chamber pressure and thrust level. These effects are more easily handled in the $\eta_{I_{sp}}$ term which includes the effects of all real engine performance losses.

C. NON-ADIABATIC WALL HEAT TRANSFER MODEL

The ALRC approach for calculating heat transfer rates to film-cooled non-adiabatic walls is to utilize conventional heat transfer correlations but with the gas-side boundary conditions specified by the entrainment film cooling model. Two general heat transfer models can be considered: (1) a reactive model, based on enthalpy driving potential; and (2) a non-reactive model, based on temperature driving potential. In both of these models, the following correlation is used to predict heat transfer coefficient.

$$St = .026 C_g(x) Re_D^{-0.2} Pr_{ref}^{-0.6} \quad \text{Eq. (39)}$$

III Description of Analytical Models (cont.)

St	=	Stanton Number
	=	$h_g/G (\rho_{ref}/\rho_e)$, for the reactive heat transfer model
	=	$h_g/G (\rho_{ref}/\rho_e) C_{p_{ref}}$ for the non-reactive heat transfer model.
$C_g(x)$	=	Position dependent correlation coefficient (Eq. 40)
Re_D	=	Reynolds number based on G and chamber diameter = $\rho_{ref} GD/\mu_{ref}$
G	=	Axial mass velocity based on the total gas-side flow rate and flow area.

During previous work (Reference 1), it was found that injection velocity effects influence the C_g parameter. Equation 40 is designed to account for these effects.

$$(C_g)_{u_c/u_e \neq 1.0} = (C_g)_{u_c/u_e = 1.0} \left(\frac{u}{u_e} \right)^{0.8} \quad \text{Eq. 40}$$

where:

u = local film coolant velocity

The u/u_e ratio was correlated in terms of a g parameter defined by Eq. 41.

$$g = \frac{u_e - u}{u_e - u_c} = \frac{1 - u/u_e}{1 - u_c/u_e} \quad \text{Eq. 41}$$

The g parameter is analogous to an effectiveness and correlates with W_E/W_C in a manner similar to effectiveness as shown in Figure 8.

Equation 39 is a convenient analytical tool for analyzing non-adiabatic film cooled walls because it allows the calculation of h_g values with film cooling if the C_g value without film cooling is known. This is a case encountered very often in the rocket engine industry. In evaluating Equation 39, the physical properties are determined using the hot-gas mixture ratio at the wall predicted by the entrainment model. The reference temperatures usually considered are: (1) the average "film" or arithmetic mean temperature, defined as the average between T_{aw} and T_{wg} ; and (2) the adiabatic wall temperature, T_{aw} .

III Description of Analytical Models (cont.)

Heat flux on the gas-side is defined by Equations 42 and 43 respectively for the reactive and non-reactive heat transfer models.

$$Q/A = h_g (H_{aw} - H_w), \text{ (reactive)} \quad \text{Eq. 42}$$

$$Q/A = h_g (T_{aw} - T_{wg}), \text{ (non-reactive)} \quad \text{Eq. 43}$$

D. HOCOOL COMPUTER PROGRAM

The HOCOOL computer program is an analytical tool for determining coolant requirements and performance penalties for advanced rocket thrust chambers using various combinations of gas film cooling, and hydrogen or oxygen regenerative (convective) cooling. The program is designed for the thermal analysis of regeneratively-cooled thrust chambers, film-cooled adiabatic wall chambers, and chambers in which film cooling supplements regenerative cooling. This section contains a discussion of the HOCOOL computer program features. A detailed description of the program including explanation of the input and output is given in Reference 5. The program was delivered to the NASA Lewis Research Center during July of 1975.

There are three basic analytical models in the HOCOOL program: (1) a generalized regenerative cooling model, (2) the ALRC entrainment film cooling model, and (3) a two stream tube model for predicting performance loss due to the use of hydrogen film coolant in a hydrogen-oxygen engine. The entrainment film cooling model and the film cooling performance loss model are described in Section III.A and III.B. The generalized regenerative cooling model has resulted from numerous regenerative studies conducted at ALRC during the past 15 years on government and company sponsored R and D programs. This model provides several options for describing gas-side and coolant-side heat transfer, and a variety of coolant passage geometries can be considered. The coolant flow path is completely flexible. Either hydrogen or oxygen may be considered as regenerative coolants in the HOCOOL version of this regenerative cooling model.

III Description of Analytical Models (cont.)

The HOCOOL computer program was designed to provide a heat transfer analysis of the thrust chamber design concepts indicated on Figure 9. As shown on this Figure, 3 basic cooling options can be analyzed: (1) the film or regenerative cooling options, for analyzing chambers which are either all film cooled (adiabatic wall) or all regeneratively cooled; (2) the complementary cooling option, whereby film and regenerative cooling are operated in parallel down the axial length of the chamber; and (3) the segmented cooling option, whereby film or regenerative or both types of cooling are used in a given section of the chamber and a different individual or combination is used in the remaining section. The diagrams on Figure 9 indicate the specific configurations which can be analyzed with HOCOOL. Five regenerative coolant channel geometries may be considered: rectangular channels, truncated tube, round or flattened tube, u-tube, or convoluted tube. These geometries are illustrated on Figure 10.

The HOCOOL program provides two options for the $\eta_{I_{sp}}$ parameter of Equation 38. One option provides for the use of factors which are built into the program and the other allows for internal calculation of $\eta_{I_{sp}}$ based on input no-film-cooling performance data. The built-in values are listed on Table VII. They were derived from the test data generated on this program and are recommended for estimating the performance loss due to film cooling. If the no-film-cooling performance characteristics of an injector-chamber combination are known, a better estimate of the film-cooling performance loss will probably be obtained using the option in which the no-film-cooling performance data is input as a function of mixture ratio. A table of $\eta_{I_{sp}}$ vs mixture ratio is generated internally using the input data and Equation 31.

IV EXPERIMENTAL RESULTS AND DATA CORRELATION

A. TESTING

1. Test Apparatus

The film cooling test assembly is shown mounted on the test stand on Figure 11. The film cooled chamber was wrapped with aluminum foil insulation prior to testing to create a nearly adiabatic wall for the combustor. A schematic diagram of the test system prepared especially for this program, is shown on Figure 12. Details of the film cooling test assembly are provided on Figure 1 and in Appendix C. Five of the no-film-cooling performance tests were conducted using a copper heat sink thrust chamber in place of the film cooled chamber shown on Figure 1 (copper chamber described in Appendix C).

The following measurements were made during all of the test firings; thrust, core injector flow rates, chamber pressure, water flow rate and outlet temperature, fuel and oxidizer manifold pressures, miscellaneous test system temperatures and pressures. Additional measurements recorded during the film cooling tests were: film coolant flow rate, film coolant injection temperature, and film cooled chamber wall temperature. Thermocouple locations for the film cooled chamber are indicated on Figure 13. Film coolant injection temperature was measured with thermocouples installed in the injection slot between thermocouple rows.

2. Test Conditions

A total of 29 rocket engine test firings were performed. Film coolant was injected onto the thrust chamber walls in 23 of these tests, and 6 tests were performed without any film cooling. The overall range of test conditions is summarized below.

Propellants:	hydrogen/oxygen
Mixture Ratio:	0.78 to 8.0
Chamber Pressure:	207 N/cm^2 (300 psia) nominal
Film Coolants:	hydrogen, helium, nitrogen

IV Experimental Results and Data Correlation (cont.)

An overview of the test program approach is obtained by examination of Table I. which shows the nominal conditions for each of the 29 test firings. The 16 hydrogen film cooling tests were performed over the ranges of core mixture ratio and film coolant velocity ratio, u_c/u_e , which can be expected to occur in a hydrogen film cooled oxygen/hydrogen thrust chamber. The nominal core mixture ratio values tested were 2, 4, 6 and 8. The velocity ratio range was 1.25 to 0.8 for each of these mixture ratios and additional data were obtained at $u_c/u_e = 1.5$ and a core mixture ratio of 8.

Five helium film cooled tests were performed at approximately the same velocity ratio range. The purpose of these tests was to allow an evaluation of "combustion effects", i.e., the effect of film coolant/core gas reactions on entrainment fraction. Such an evaluation was obtained by comparing experimental entrainment fractions with the reactive hydrogen and inert helium film coolants. A core mixture ratio of 8 was chosen for the helium cooled tests because, for the range of core O/F tested, this is where the oxidizer mole fraction is a maximum (see Figure 14).

The purpose of the nitrogen film cooling tests was to obtain additional data on flow turning effects with a relatively heavy film coolant. The lower mixture ratio, 2, was necessary for the nitrogen cooling tests because of film-coolant-injector cooling limits. Previous data relative to flow turning effects on film cooling were published in References 1 and 2.

The specific test conditions for each test firing are listed on Table II. The entrainment fraction test results are summarized in Table III. Specific impulse performance data for each test are given in Table IV. Heat transfer coefficient data are tabulated in Tables V and VI. Steady state wall temperatures measured during the film cooling tests are plotted on Figures 15 through 20, and the experimental entrainment fractions are plotted on Figures 21A through 26. Cold flow test data for the core gas injector and the film coolant injector are presented in Appendix C.

IV Experimental Results and Data Correlation (cont.)

3. Test Summaries

(a) Hydrogen Film Cooling Tests with Core O/F = 4

In the initial series of tests, three tests were conducted with a nominal core gas mixture ratio of 4: Tests: 2K-B6-12-102, 103, and 104. The film-coolant-to-core-gas velocity ratio ranged from 1.21 to 0.77.

The measured steady state wall temperatures are shown on Figure 15. These data indicate that the core gases were not completely uniform in the film cooled chamber since the wall temperatures recorded along thermocouple row B (directly in line with a core gas injector element) were consistently higher than those along row D (centered between 2 core gas injector elements). This slight "streaking" behavior did not impede the study of combustion effects and turning effects on film cooling and is probably representative of the circumferential variation which can be expected in actual rocket engines.

Test 117 was conducted as a repeat of test 104. The data repeatability is considered acceptable even though the throat region wall temperatures were somewhat higher in test 117. These higher temperatures appear to be due to a higher core mixture ratio, and slightly lower H₂ film cooling flow rate in Test 117.

IV Experimental Results and Data Correlation (cont.)

The data from Tests 102, 103 and 117 were used in subsequent data correlation work (one test at each velocity ratio).

(b) Hydrogen Film Cooling Tests with Core O/F = 6

Three film cooling tests were also conducted with a core mixture ratio of 6 in the initial series of tests: Tests 105, 106, and 107. The velocity ratios were 1.25, 1.0, and 0.75.

Steady state wall temperature measurements from these tests are plotted on Figure 16. The data obtained during Tests 105 and 106 are similar to the mixture ratio = 4 data discussed previously. Severe streaking is evident in the test 107 data where throat temperatures range from 617 to 1033°K (650 to 1400°F).

During subsequent film cooling tests at core O/F = 8, it was found that a mis-alignment between the film coolant injector and the film cooled chamber caused the test 107 streaking. The mis-alignment occurred during reassembly of the test hardware after an inspection performed between Tests 106 and 107. The Test 107 conditions were retested during Test 114 and the severe streaking was eliminated as shown by the data plotted on Figure 16. The conditions of test 106 were repeated in Test 115 and good repeatability was obtained. This indicates that no significant mis-alignment existed prior to Test 107.

Data from the following tests were used for determination of entrainment fractions: 105, 115, and 114.

(c) Hydrogen Film Cooling Tests with Core O/F = 8

Five tests were performed with an 8.0 nominal core gas mixture ratio: tests 108, 109, 110, 111, and 116. The wall temperatures measured in these tests are plotted on Figures 17 and 18.

IV Experimental Results and Data Correlation (cont.)

As a result of the severe test 107 streaking, the film coolant flow rate for the first 8.0 mixture ratio test, test 108, was increased so that the film-coolant-to-core-gas velocity ratio, u_c/u_e , was 1.5 instead of the 1.25 originally planned. Severe streaking also occurred in test 108. The top graph of Figure 17 shows that the throat wall temperature ranged from 567°K to over 1030°K (560°F to over 1400°F). Subsequent inspection of the test hardware revealed that a mis-alignment between the film coolant injector and the film cooled chamber had caused the streaking which occurred in both tests 107 and 108.

The film coolant injector and the film cooled chamber were realigned and the test 108 conditions were retested in test 109. The top graph of Figure 17 shows that the realignment removed the severe streaking and that the throat wall temperatures were reduced to the 670 to 755°K (750 to 900°F) range. This smaller amount of "streaking" appears to be due to core injector effects. Similar data were subsequently obtained during tests 110, 111, and 116 which were successfully conducted at velocity ratios of 1.29, 1.07, and 0.84. Before each of these tests and before every subsequent test, the alignment between film coolant injector and film cooled chamber was visually checked and the alignment was adjusted if necessary. No adjustment more than about .05 mm was ever necessary.

Data from tests 109, 110, 111, and 116 were used to determine entrainment fractions with core O/F = 8.

(d) Hydrogen Film Cooling Tests with Core O/F = 2

Two tests were performed at the 2.0 core mixture ratio condition: tests 112 and 113. These two tests were conducted successfully and the measured wall temperatures are shown on Figure 18.

Additional testing with core O/F = 2 was deleted in favor of conducting three repeat tests at O/F = 4 and 6 and the 0.84 velocity ratio test at O/F = 8 (for comparison to the helium data).

IV Experimental Results and Data Correlation (cont.)

(e) Helium Film Cooling Tests

Five tests were conducted with helium film coolant: tests 118, 119, 120, 121, and 122. The velocity ratio range tested was 0.82 and 1.25 and the nominal core mixture ratio was 8.0. The wall temperature data are plotted on Figure 19. Tests 119, 120, and 122 were successful tests. The test 118 data was invalid due to unsteady film coolant flow. In test 121 (a repeat of test 118), the film coolant flow rate was steady but a data acquisition system malfunction occurred and consequently it was necessary to repeat the test conditions again in test 122.

(f) Nitrogen Film Cooling Tests

Tests 123 and 124 were performed with nitrogen film coolant at velocity ratios of 0.32 and 0.27 and with a 2.0 nominal core gas mixture ratio. The tests were completed successfully and the wall temperature data are shown on Figure 20. A third test at 0.2 velocity ratio was planned; however, it was cancelled because the test 123 and 124 wall temperature data indicated that chamber damage would probably occur if the film coolant flow rate was reduced any further.

(g) No-Film-Cooling Performance Tests

Performance data without film cooling effects were obtained in tests 003, 125, 126, 127, 128, 129. Test 129 was run at low O/F in the sheet metal "film cooled" chamber and the other 5 tests were run with a copper heat sink chamber in place of the sheet metal chamber. All performance data are summarized on Table IV. In test 003, wall temperature transients were also recorded from which heat transfer coefficients without film cooling were inferred (See Section IV.D.).

IV Experimental Results and Data Correlation (cont.)

B. TEST RESULTS

This section presents the direct film cooling (heat transfer related) test results and explains the film cooling data reduction procedure. The entrainment fraction and heat transfer coefficient results are discussed in Section IV.B.1. and the film cooling data reduction procedure is discussed in Section IV.B.2. Correlation of these data are presented in Sections IV.C. (entrainment fraction data) and IV.E. (heat transfer coefficient data). The performance results and their correlation are discussed in Section IV.D.

1. Direct Film Cooling Results

(a) Entrainment Fraction Results

The film cooling test wall temperature data were reduced and evaluated in terms of the entrainment film cooling model described in Section III.A. The specific parameter used to characterize the data is the entrainment fraction, k , which relates the entrained core gas mass flux to the axial flow core gas mass flux (See Equation 1).

Initial data reduction consisted of calculating adiabatic wall temperature by correcting the measured wall temperature for heat loss effects. Then the experimental entrainment fraction values between thermocouple pairs were calculated from a specially constructed data reduction version of the entrainment model. The specific procedures used to calculate adiabatic wall temperatures and entrainment fraction are described in the next section of this report, Section III.B.2. Tabulations of each measured wall temperature, calculated adiabatic wall temperature, and corresponding entrainment fraction ratio, k/k_0' , are provided in Appendix B for each film cooling test. The parameter k_0' is a reference entrainment fraction value given by Equation 44. The entrainment fraction data are summarized in Table III.

$$k_0' = k_0 \left[\frac{\rho_e u_e}{(\rho_e u_e)_0} \right]^{-.65} \quad \text{Eq. 44}$$

IV Experimental Results and Data Correlation (cont.)

where:

k_0 = is defined by Equation 21

More specifically, k_0' is the plane unaccelerated flow entrainment fraction modified to account for known acceleration effects (subsonic region only).

The experimental entrainment fractions for the unity velocity ratio tests with hydrogen and helium film coolant and for one of the nitrogen film cooling tests are plotted as a function of axial position on Figures 21A and 21B. These data indicate that circumferential variations in entrainment fraction exist. This circumferential variation in k is significant in some cases (e.g., test 103 between thermocouples 3 and 4). This circumferential k variation is the result of the mild "streaking evident in all of the wall temperature data, which is apparently related to core gas injector effects. The B row k values are generally higher than the row D values and the B and D row data represent the data extremes reasonably well. They are, however, not consistently the highest or lowest values. This circumferential k variation is probably indicative of a real rocket engine environment since core injectors are known to yield less than perfect circumferential mixture ratio and mass flux distributions.

In addition, there were some differences noted between the k values indicated for the upstream and downstream portions of the convergent turn and the conical convergent nozzle section. Since the entrainment rates were generally low in the convergent region, this was believed due to either experimental error or core injector effects.

In the interest of establishing design entrainment fraction correlations, it was decided to circumferentially average the entrainment fraction data, and to correlate the overall entrainment fraction for the convergent turn and the conical section. The averaged k values for each test

IV Experimental Results and Data Correlation (cont.)

are tabulated on Table III. These averaged data are plotted as a function of axial position and velocity ratio on Figures 22 through 23, (all 3 film coolants) and as a function of axial position and core mixture ratio on Figure 24 (hydrogen data only). The hydrogen and helium entrainment fraction data are compared directly on Figure 25.

The following trends are evident in the averaged data plotted on Figures 22 through 23:

(1) In the cylindrical chamber region, the entrainment fraction is initially quite high then decreases to about the level that had been anticipated ($k/k_o' \approx 3$) based on the inert core gas data reported in References 1 and 2.

(2) The hydrogen and helium film coolant data exhibit a tendency toward decreasing k/k_o' in the convergent region of the thrust chamber and very low entrainment fractions (near zero) are indicated in the nozzle throat region. This indicates that turns and a convergent region can be beneficial when the film coolant is relatively light. The negative k values indicated near the throat are the result of either experimental error or core injector effects (i.e., a non-uniform core gas O/F distribution near the wall) combined with flow turning effects (See Section IV.C.2.b.).

(3) The nitrogen k values increase dramatically by almost an order of magnitude in the convergent region. The k/k_o' values near the throat are on the order of 40. This indicates that the convergent region is detrimental for relatively heavy film coolants.

(4) The limited data obtained in the supersonic region all indicate that the entrainment fraction increases downstream of the nozzle throat. For hydrogen and helium film cooling, this increase is not very large and the k/k_o' values are about the same as in the convergent conical region. For nitrogen film cooling, the rapid mixing noted in the

IV Experimental Results and Data Correlation (cont.)

convergent region upstream of the throat continues to increase downstream of the throat where a k/ko value of 63 was indicated.

(5) With hydrogen and helium film cooling, the k/ko' ratio tends to decrease as the velocity ratio decreases, thus indicating more efficient film cooling (reduced mixing rate) at the lower velocity ratio. However, absolute k values must be considered here since ko' contains velocity ratio effects (See Equation 21). Figure 26 contains plots of absolute k vs axial position for core O/F = 4, 6, and 8. The top graph on Figure 26 compares to the top graph in Figure 23. The lower two graphs on Figure 26 compares to the lower two graphs on Figure 22. These Figure 26 plots show that absolute k also tends to be lowest for the lowest velocity ratio and therefore film cooling appears to be more efficient at $u_c/u_e = 0.8$ than at $u_c/u_e = 1.0$ as previously believed. Future testing with hydrogen film coolant at $u_c/u_e < .8$ is recommended to determine the possible existence of an optimum velocity ratio where the entrainment fraction is a minimum.

(6) Plotting the entrainment fraction data with core mixture ratio as a parameter reveals that there is a certain effect of core mixture ratio on entrainment fraction. The data is plotted in this manner for nominal velocity ratios of 1.25, 1.0, and 0.8 on Figure 24. There is clearly a trend toward higher entrainment fraction at the lower mixture ratio. This is believed due to increased turbulence level at the lower mixture ratio. The individual elements of the core gas injector used (premix triplet elements) are conducive to higher turbulence levels at lower mixture ratios because the fuel (gaseous hydrogen) is injected in two opposing, radially oriented streams while the oxidizer (gaseous oxygen) is injected in a single axially oriented stream.

IV Experimental Results and Data Correlation (cont.)

(b) Heat Transfer Results

Heat transfer coefficients were calculated from most of the wall temperature transients recorded during the hydrogen film cooling tests. These coefficients were evaluated in terms of the ALRC analytical model for non-adiabatic wall heat transfer described in Section III.B. The specific parameter calculated from the data was the C_g factor of Equation 39. The reactive heat transfer model and film reference temperature were used.

The calculated C_g values are listed on Table V. Similar data obtained without any film cooling in the copper heat sink chamber are listed on Table VI.

2. Film Cooling Data Reduction Procedure

Reduction of the film cooling test data consisted of three parts:

- (1) Obtaining heat transfer coefficients (h_g) and corresponding correlation coefficients (C_g) from wall temperature transients using the wall as a calorimeter.
- (2) Using these coefficients to correct steady-state wall temperatures for external heat losses to obtain adiabatic wall temperatures, then calculating the corresponding film cooling effectiveness values.
- (3) Calculating from these effectiveness values an average entrainment fraction between successive pairs of thermocouples in each axial row.

IV Experimental Results and Data Correlation (cont.)

Each of these areas is reviewed in the following paragraphs, with the emphasis on changes from the previous work (Ref. 1 and 2). Details of the wall temperature transient analysis and of the heat loss correction are given in Appendix B of Reference (1). The measured wall temperature and calculated adiabatic wall temperature differed by about 2°K at 400°K measured temperature and by 16°K at 800°K measured temperature.

A data reduction computer program was prepared by integrating previous transient and steady state data programs with the basic ALRC film cooling program and selected subroutines from the regenerative-cooling program developed in Task IV. This integration of programs provided all the thermodynamic and transport properties required for data reduction with hydrogen film cooling in the present tests (the previous data reduction programs were restricted to hydrogen-nitrogen systems). Since transport properties were not included for the helium and nitrogen film cooling cases, heat transfer correlation coefficients were not calculated for those tests. Because of this computer program integration, data reduction was accomplished in one step; previously, it was necessary to run a data reduction program followed by the film cooling program.

a. Heat Transfer Coefficient Analysis

Wall temperature responses were used to infer internal heat transfer coefficients and, in the case of hydrogen film cooling, correlation coefficients. The correlation equation used is shown as Equation 45 (a rearranged version of Equation 39).

$$h_g = 0.026 C_g G \left[\frac{MW_w}{MW_e} \cdot \frac{T_e}{T_f} \right]^{0.8} \frac{H_{aw} - H_w}{T_{aw} - T_{wg}} Re_D^{-0.2} Pr^{-0.6} \quad \text{Eq. 45}$$

with all properties evaluated at the wall mixture ratio and the film temperature, T_f , defined by

$$T_f = 0.5 (T_{aw} + T_{wg})$$

The mass velocity in the Reynolds number was based on total flow and total flow area.

IV Experimental Results and Data Correlation (cont.)

Since correlation coefficients were not calculated for helium and nitrogen film cooling, the transient analysis option was used for all such tests. For those hydrogen film cooling tests where the transient analysis was not run, heat transfer coefficients were calculated from the above equation using the following correlation coefficient:

$$C_g = C_{g_1} \left[\frac{1 + g(\eta) \left(\frac{u_c}{u_e} - 1 \right)}{1 + g(\eta_1) \left(\frac{u_c}{u_e} - 1 \right)} \right]^{0.8} \quad \text{Eq. 46}$$

in which subscript 1 refers to a test in the same series for which the transient analysis was run. The function $g(\eta)$ is defined by Figure 8.

b. Evaluation of the Adiabatic Wall Temperature

In References (1) and (2) external heat loss coefficients were determined by running tests without film cooling and measuring both the hot gas temperature and the wall temperature. This concept was not feasible for this program, consequently it was necessary to assume an external loss coefficient based on previous results; a uniform value based on the cylindrical chamber data in Table VII of Reference (1) was used.

A study of the effect of this external loss and its uncertainty was made for the test 103 Row B data. Figure 27 shows the wall temperature correction required to obtain the adiabatic wall temperature as a function of the external heat loss coefficient; this curve applies at the end of the cylindrical section, at the throat and for most of the convergent section. A correction of 10°K (18°F) results for the assumed coefficient. However, the magnitude of the wall temperature correction is of less interest than its spatial variation. Local entrainment fraction multiplier calculations are not affected significantly by a uniform loss coefficient, but can be sensitive to spatial variations in the coefficient. Therefore, a thermocouple-to-thermocouple variations of the loss coefficient from -50% to +50% of the nominal value was studied; this is the approximate range of coefficients in Reference (1).

IV Experimental Results and Data Correlation (cont.)

Entrainment fraction multipliers between adjacent thermocouples in the cylindrical section differed by 1-18 percent between the uniform and variable loss coefficient cases. The overall turn, and overall cone entrainment fractions (used to correlate the convergent region data) were not particularly sensitive to uncertainties in the loss coefficient variation, as shown in the following table.

<u>Region</u>	<u>k/k₀' Change Due to Loss Coeff. Variation</u>
Asymptotic part of Cylindrical Section (2-5)	5.4%
Convergent Turn (5-7)	12.1%
Convergent Section (5-10)	12.4%

c. Entrainment Fraction Multipliers

Entrainment fraction results are normalized herein by the value k_0' , which accounts for injection parameter and acceleration effects and is defined by Equation 44.

An average value of k/k_0' is calculated between adjacent thermocouples in each row. For example, between thermocouples i and j

$$(k/k_0')_{i-j} = \frac{\bar{y}_j - \bar{y}_i}{\bar{x}_j - \bar{x}_i} \quad \text{Eq. 47}$$

with \bar{y} calculated by replacing \bar{x} with \bar{y} in Equation 27 and using the entrainment flow ratio W_E/W_C as calculated by Equation 17 and by Equation 6. Note that \bar{y} is merely the value of \bar{x} required to match the test data.

Entrainment fraction results presented herein are based on the reactive model for hydrogen film cooling and on the core-reactive model for nitrogen and helium film cooling (See Section III.A). However, one hydrogen test (No. 116 with a core O/F of 7.6) was also analyzed using the core-reactive model. This was done to evaluate the analytical significance of chemical reactions between the core gases and the hydrogen film coolant on the thermodynamic properties of the mixing layer. The reactive model accounts

IV Experimental Results and Data Correlation (cont.)

for reactions by relating H_{aw} to T_{aw} through a temperature-enthalpy-O/F table. This table was generated using the Reference 8 computer program assuming equilibrium chemistry. The core reactive model relates H_{aw} and T_{aw} by treating the mixing layer as a two component mixture (core gas and film coolant gas). Reactions between the core and film coolant gases are ignored; however, core gas composition changes with temperature are accounted for by using the equilibrium chemistry table to evaluate core gas enthalpy (the film coolant C_p is assumed constant).

The values of k/k_0' calculated with the two models were virtually identical as shown in the following tabulation:

<u>Region</u>	<u>k/k_0' Reactive Model</u>	<u>k/k_0' Non-Reactive Model</u>
Cylindrical	2.50	2.51
Convergent	1.19	1.18

This agreement of results indicates that the effect of chemical reactions on the thermodynamic properties of the mixing layer is not analytically significant for the Test 116 conditions.

Comparisons of the core-reactive and non-reactive models were also made for Test 120, which had a core mixture ratio of 7.5. Using an equivalent core specific heat (defined by Eq. 12) evaluated at an adiabatic wall temperature of 833°K (1500°R) in the non-reactive cases, yields the following comparison of axially-averaged entrainment fraction multipliers for Row B:

	<u>Core Reactive Model</u>	<u>Non-Reactive Model</u>
Cylindrical Section	2.79	2.82
Convergent Section	1.13	1.25

Agreement is excellent in the cylindrical section, where adiabatic wall temperatures ranged from 570 to 1140°K (570 to 1600°F). In the convergent section, where adiabatic wall temperatures ranged from 1140 - 1230°K (1600-1760°F), the non-reactive model results indicate an entrainment fraction 10 percent higher

IV Experimental Results and Data Correlation (cont.)

than the core reactive model. Therefore, use of the non-reactive model with a core specific heat defined by Equation 12 appears to be justified when the adiabatic wall temperatures are low relative to the core combustion temperature. The non-reactive model was also run for test 120 using the frozen core specific heat evaluated at the core total enthalpy; in this case entrainment fractions were 40 percent higher than those from the core-reactive model.

C. FILM COOLING DATA CORRELATIONS

For film cooling analysis purposes, it is convenient to characterize the entrainment fraction, k , as shown in Equations 23 and 48.

$$k = k_m k_o' \quad \text{Eq. 48}$$

Equation 48 partitions k into two parts: (1) k_o' , a reference entrainment fraction, defined by Equation (44), predicted by the flat plate correlation of Ref. 1 and the acceleration effect correlation of Ref. 2; (2) k_m , an empirical entrainment fraction multiplier used to reconcile differences between Equation 44 and measured k data. The entrainment fraction data in Figures 20 through 25 have been presented in the form of k/k_o' which, by Equation 48, is equivalent to k_m .

The purpose of this section is to interpret the entrainment fraction results of Figures 22, 23, and 24 and correlate them with pertinent physical parameters using the Equation 48 approach. Comparisons with the heated nitrogen laboratory tests of References 1 and 2 are made whenever possible, and design recommendations are presented based on all results. This discussion is divided into four parts: (1) Cylindrical section data are presented first; here the primary interest is in combustion effects resulting from film coolant composition and core mixture ratio changes and in injection velocity ratio effects. (2) The second part reviews all data from the turns at the start of convergence and at the throat. (3) The third part considers the average entrainment fraction over the entire convergent section. (4) Finally, design recommendations are presented.

IV Experimental Results and Data Correlation (cont.)

1. Cylindrical Section Data

a. Injection Slot Lip Effect

Figures 22 and 23 indicate the entrainment fractions are high immediately downstream of the film coolant injection slot and then decrease to an asymptotic value between thermocouples 2 and 5. Similar results were seen in some of the tests of References 1 and 2. The increased entrainment fractions near the slot are probably caused by the wake formed downstream of the slot lip as the lip thickness was significant relative to the slot height (nominal sizes: .05 cm lip, .15 cm slot).

Figure 28 gives the ratio of the maximum to the asymptotic entrainment fractions for the hydrogen and helium coolant tests. The asymptotic value is defined as the average entrainment fraction between thermocouples 2 and 5. The maximum-to-asymptotic ratio decreases with increasing injection velocity ratio, which is opposite to the trend observed in the data of References 1 and 2. In the latter tests the ratio was near unity for a velocity ratio of 0.8 and increased for higher velocity ratios. The nitrogen film coolant data were omitted from Figure 28 due to the potential error in entrainment fraction near the slot in these tests. This error is related to the large change in entrainment flow associated with a small change in coolant effectiveness when the latter is near unity, so that any experimental or model errors result in large errors in entrainment flow. (See η vs W_E/W_C shown on Figure 4).

The asymptotic entrainment fraction data are summarized on Figure 29. These data are circumferential averages using all rows which included thermocouples 2 and 5 and are directly applicable to other designs, at least for the type of core injector used herein, consequently they are discussed in detail in the following paragraphs. Average entrainment fraction data over the entire cylindrical section are shown on Figure 30; these results are applicable only for the cylindrical section length and injection slot geometry used herein.

IV Experimental Results and Data Correlation (cont.)

b. Effect of Film Coolant Composition

One of the primary objectives of this program was to investigate combustion effects on entrainment fractions, with the combustion effects resulting from film coolant composition and core mixture ratio changes. It is postulated that if the turbulent mixing mechanism is constant (constant k) these effects are accounted for explicitly in the various reactive options of the present entrainment model. The model studies discussed in Section IV.B.2 indicate that chemical reactions between the hydrogen film coolant and core combustion products are not significant with regard to calculation of thermodynamic properties. However, changing the film coolant or core mixture can conceivably influence the entrainment fraction if the core gas reactions or reactions within the mixing layer affect the turbulent mixing mechanism.

Figure 29 shows excellent agreement between the hydrogen and helium asymptotic entrainment fraction multipliers for all three common injection velocity ratios. Figure 25 compares the local entrainment fraction multipliers for each velocity ratio; agreement between the hydrogen and helium values is very good throughout the test section. These data indicate that either: (1) combustion of the film coolant within the mixing layer did not increase the rate of film coolant and core gas mixing, or (2) no combustion occurred within the mixing layer.

The hydrogen and helium film coolant data plotted on Figure 25 were obtained at a core mixture ratio of approximately 8.0 where the total mole fraction of oxidizer (OH , O_2 , O) is about 18% (See Figure 14). This is not a highly oxidizing environment but it represents the most severe practical case since significantly higher mixture ratios are not likely to exist in most hydrogen/oxygen rocket engines. However, certain small thruster designs have been considered which operate with core O/F in the 50/1 range. At 50/1 mixture ratio the mole fraction of O_2 is approximately 0.7 and it is possible that some effect of core gas/film coolant gas combustion may exist at this extreme condition. The 50/1 mixture ratio case

IV Experimental Results and Data Correlation (cont.)

would be difficult to test in the larger scale hardware required for experimental accuracy. However, the Figure 1 test components could be used to evaluate an equally extreme case: oxygen film cooling with core O/F = 2 (H_2 mole fraction = 0.75). This oxygen film cooling test is recommended for future work.

Figure 29 also indicates the same entrainment fraction multipliers for nitrogen at velocity ratios of 0.27 - 0.32 and hydrogen at a velocity ratio of 1.0. The hydrogen data at 0.8 velocity ratio lie below these data, consequently there appears to be an optimum injection velocity somewhere between 1.0 and 0.3.

c. Effect of Core Mixture Ratio

Figures 29 and 30 show the effect of core mixture ratio on asymptotic and average cylindrical section entrainment fraction multipliers, respectively, for three hydrogen injection velocity ratios. In each case, increasing the core mixture ratio decreases the entrainment fraction. This general trend was noted previously in the entrainment fraction profiles of Figure 24.

A number of possible explanation of this mixture ratio effect can be postulated.

1. It is likely that the freestream turbulence level increased as the core mixture ratio decreased. Increasing turbulence intensity is known to reduce film coolant effectiveness, i.e., to increase entrainment fractions, as noted in Reference 7. In the APS core injector used in the present tests, oxidizer is injected axially while the fuel is injected perpendicular to the oxidizer flow in two impinging streams. Therefore, at low mixture ratios a significant part of the core flow is associated with these

IV Experimental Results and Data Correlation (cont.)

transverse impinging jets, which should promote turbulence.

2. The entrainment fraction may depend on the core Reynolds number, which decreases by a factor of almost two due to viscosity changes as the core mixture ratio increases from 2 to 8. In Reference 1 a similar reduction in core Reynolds number was accomplished by reducing the chamber pressure in one test series. Entrainment fraction multipliers were reduced in this case as well, but the relative reduction was about half that observed in the rocket engine tests.
3. The assumption of equilibrium core chemistry used to calculate experimental entrainment fraction could be in error. Species concentration changes predicted at the higher mixture ratios due to cooling in the mixing layer may be limited by kinetic effects.
4. If the core reactions noted above do occur, they may affect the turbulent mixing process; e.g., there could be a coupling between the energy absorption associated with these reactions and the decay of turbulent kinetic energy. (This explanation is considered the least likely of the four presented here).

It should be noted that the changes in entrainment fraction multiplier with core mixture ratio are not caused by the corresponding changes in injection density ratio. Larger density ratio changes resulted from the use of nitrogen and helium film coolants vs hydrogen, without changes in entrainment fraction multiplier.

IV Experimental Results and Data Correlation (cont.)

d. Effect of Injection Velocity Ratio

The ALRC entrainment model is designed to account for injection velocity ratio effects in the asymptotic part of the cylindrical section through the reference entrainment fraction k_0 derived from plane, unaccelerated flow laboratory data. However, Figure 29 shows a reduction in entrainment fraction multiplier k/k_0' as the velocity ratio is reduced from 1.3 to 0.8. The single data point obtained at a velocity ratio of 1.5 agrees with the 1.3 velocity ratio data. The nitrogen data obtained in the velocity ratio range 0.27 - 0.32 agrees with the corresponding hydrogen data at a ratio of 1.0. These trends may be seen more clearly in Figure 31, which provides a crossplot vs velocity ratio of the entrainment fraction multipliers of Figure 29. Since it is desirable for the ratio k/k_0' to be independent of injection velocity ratio (See Equation 48), changes in the velocity ratio function $f(u_c/u_e)$ contained within k_0' were considered. Figure 32 compares the Figure 7 $f(u_c/u_e)$ values to values calculated from data using Equation 49 which simply adjusts the $f(u_c/u_e)$ function so that the experimental k/k_0' values are independent of velocity ratio and equal to the values measured at $u_c/u_e = 1.0$.

$$f\left(\frac{u_c}{u_e}\right)_{\text{calculated}} = f\left(\frac{u_c}{u_e}\right)_{\text{Figure 7}} \left[\frac{(k/k_0')_{\frac{u_c}{u_e} = 1.0}}{(k/k_0')_{\frac{u_c}{u_e}}} \right] \quad \text{Eq. 49}$$

The open symbols on Figure 32 are the rocket firing data and reflects the velocity ratio effects described previously. A low entrainment fraction gives a high value of f . Data from References 1 and 2 are shaded and fall below the original correlation line for velocity ratios less than unity, but are mostly above the correlation for the higher velocity ratios. This characteristic is just the opposite of the rocket firing data trend.

Injection velocity ratio effects are of great design importance since they establish the optimum slot height. Figures 29 and 30 also give the absolute entrainment fractions values in order to show the total effect of velocity ratio. Figure 33 presents a cross-plot vs velocity ratio of the absolute asymptotic entrainment fractions for core mixture ratios of 2 and 8. However, in order to isolate the effect of velocity

IV Experimental Results and Data Correlation (cont.)

ratio the nitrogen data have been corrected to the hydrogen density and viscosity using the effects in the k_o correlation, Equation 21. The helium data correction is less than 10 percent and has been neglected. It is seen that the optimum injection velocity ratio based on the Combustion Effects Program tests is less than unity and may be less than 0.8. This result compares with the k_o correlation of Eq. 21, which indicates an optimum velocity ratio of 1.05 with constant slot height. The hot nitrogen core flow data from References 1 and 2 indicate an optimum velocity ratio greater than 1.0.

Design recommendations for the velocity ratio effect are listed on page 58.

e. Comparison with Previous Results

Injection slot lip and velocity ratio effects from previous contracts have been compared above with the present data. It remains to compare the asymptotic entrainment fraction multipliers for a velocity ratio of unity; this comparison is given in Table VII. Except for the nitrogen data of Reference (2), which were obtained with a .038 cm slot height and .05 cm lip, all of the laboratory test entrainment fraction multipliers are well below the present firing data. This is also shown in Figure 34 which compares all of the data obtained with .15 cm slot and .05 cm lip. The higher values measured in an actual rocket engine are probably due to the higher turbulence intensity which is thought to be associated with the firing data. The higher multipliers observed with the smaller slot height are probably caused in part by residual effects from the wake behind the slot lip, i.e., the cylindrical section was not long enough to obtain a true asymptotic value. Film coolant injector alignment is more critical for the small slot as well. Although an asymptotic cylindrical section multiplier cannot be inferred from the limited cylindrical region data of Reference 9 (hot air core gas) the data for the short cylindrical section appear to be consistent with the Reference 1 and 2 results ($k/k_o \approx 2$).

Another difference between the present tests and most of those in References (1) and (2) is the injection density ratio. Figure 35 shows the range of density ratios tested and the resultant asymptotic entrainment fraction multipliers. Also shown is the range of density ratios upon which the k_o correlation is founded; this range approximates that of the test data except for the rocket engine nitrogen film coolant tests.

IV Experimental Results and Data Correlation (cont.)

Although the entrainment multiplier variations shown have been attributed herein to turbulence intensity changes associated with the core flow and to slot height effects, Figure 35 indicates that density ratio effects cannot be completely ruled out in the $\rho_c/\rho_e < 2.0$ region.

2. Turning Effects

The effort initiated in References (1) and (2) to correlate the significant effects of flow turning on entrainment fraction has continued under the present contract. These turning effects are considered to result from the difference in centrifugal force across the mixing layer, which makes it easier for either the core gas or the cooler mixture at the wall to turn with the chamber contour. If the cool gas at the wall can turn easier (relatively low wall gas momentum) mixing is increased in the turn at the start of convergence since the cool gas tends to turn into the core gas; conversely, mixing is decreased in the throat turn since the two flows tend to diverge. The opposite effects would be expected when the core gas can turn easier (relatively high wall gas momentum): relatively high momentum near the wall decreases mixing in the first turn and increases it in the throat turn. A turn correlation parameter was proposed in Reference (1) and also used in Reference (2). It is based on the ratio of the centrifugal force differential across the mixing layer to a reference turbulent shear force in the mixing layer. In Reference (1) the centrifugal force differential was based solely on density differences and the turning parameter was defined by Equation 50.

$$\text{DTP} = \text{Density Turn Parameter} = 2 \frac{\rho_e - \rho_w}{(\rho_e + \rho_w)} \frac{s}{R} \quad \text{Eq. 50}$$

The parameters ρ_e , ρ_w and s (mixing layer thickness) are evaluated at the start of the turn and R is the turn radius of curvature. R is taken to be positive at the start of convergence and negative in the throat turn. Use of this parameter was investigated herein. However, a modification which

IV Experimental Results and Data Correlation (cont.)

accounts for the velocity differential across the mixing layer was also used; this parameter is defined by Equation 51.

$$\text{MTP} = \text{Momentum Turn Parameter} = 2 \frac{(\rho_e u_e^2 - \rho_w u_w^2)}{(\rho_e + \rho_w) u_e^2} \frac{s}{R} \quad \text{Eq. 51}$$

In Equation 51, u_w is an effective velocity near the wall. Physically u_w is the velocity at the edge of the wall boundary layer if the latter is thin relative to the mixing layer. In order to evaluate u_w the effective velocity used in the heat transfer correlation (Figure 8) was selected.

$$u_w = u_e + g \left(\frac{W_E}{W_C} \right) (u_c - u_e) \quad \text{Eq. 52}$$

As indicated on Figure 8, the velocity u_w approaches u_e as the effectiveness becomes small.

a. Start of Convergence

All turning data from References (1) and (2) have been reviewed along with the present results in order to present the various data on a consistent basis. For the turn at the start of convergence, results are presented as the ratio of the average entrainment fraction multiplier in the turn to the asymptotic multiplier in the upstream cylindrical section. Using the thermocouple designations of Figure 13, this ratio is given by Equation 53.

$$k_{ct} = \frac{(k/k_0')_{5-7}}{(k/k_0)_{2-5}} = \text{Convergence turn effect factor} \quad \text{Eq. 53}$$

In Reference (1) the thermocouples did not isolate the turn; however, interpolated adiabatic wall temperatures were used to eliminate the small segment of the conical section between thermocouples.

Figure 36 shows all convergent turn data, including a point from Reference 9 as a function of the density turn parameter defined by

IV Experimental Results and Data Correlation (cont.)

Equation 50. Except for the two nitrogen tests of the present contract, this plot shows the expected trend, i.e., k_{ct} increases from unity as the $(\rho_e - \rho_w)$ term becomes positive. In this turn a positive value of the correlation parameter is associated with a smaller centrifugal force at the wall, so that the film coolant tends to turn into the core flow and promote mixing. The two nitrogen film cooling points which are not consistent with the other data represent very low injection velocity ratios (0.27 and 0.32), while most of the other data are in the 0.8 - 1.3 velocity ratio range. This apparent velocity ratio effect resulted in consideration of the momentum turn parameter of Equation 51. Figure 37 shows the same k_{ct} data as a function of the momentum turn parameter. It is seen that the two low-velocity nitrogen points are now consistent with the rest of the data. The curve drawn on Figure 37 is the correlation recommended for the turn at the start of convergence.

b. Throat Turn

In the present testing 18 of the 32 throat turn entrainment fraction multipliers were negative, as were 16 of the 25 multipliers in the second half of the conical section. Negative values in the cone and throat turn were also observed with one test section in Reference (2). Two explanations of these negative values can be postulated. The most likely cause is that entrainment fractions were small and a fundamental accuracy problem was encountered, since the entrainment fraction multiplier in this region was usually inferred from a very small change in adiabatic wall temperature. Converting this measurement to a change in effectiveness depends on the accuracy of the kinetic energy recovery model. Converting the resultant entrainment fraction to k/k_0' depends on the acceleration model. Therefore, measurement and model errors are much more significant in the throat region than in the cylindrical section or in the turn at the start of convergence.

IV Experimental Results and Data Correlation (cont.)

The second explanation of the negative entrainment fractions concerns the mixing layer profile shape factor, θ . It is possible that θ changes due to turning effects (contrary to the present model assumption) or that the basic shape factor correlation is in error. Data from test 115, Row B were selected to study the effect of a change in throat shape factor on the entrainment fraction multiplier (k/k_o') ₈₋₁₀ between the middle of the conical section and the throat. These data were selected because of the large negative multiplier inferred with the present shape factor correlation (-2.01). Two new throat shape factors were calculated, using the experimental effectiveness and Equation 17, which correspond to k/k_o' values of 0. and 3.0 in the thermocouple 8-10 region. The 3.0 value approximates the average value from the start of convergence to the middle of the conical section. The results are listed below.

(k/k_o') ₈₋₁₀	W_E/W_C Calculated	θ Calculated	θ Model (Figure 5)
-2.01	0.960	-	0.784
0	1.033	0.756	0.7785
3.0	1.142	0.717	0.772

It is noted that a very small change in shape factor yields a non-negative entrainment fraction; such a change could be the result of turning effects influencing the velocity and mixture ratio distributions in the mixing layer. An error in the basic shape factor correlation cannot be the sole cause of negative entrainment fractions, since an extremely steep slope is required for the θ vs W_E/W_C correlation if negative values are to be avoided. In Section IV.D. it is shown that acceptable performance loss predictions for Test 115 are obtained for all three of the foregoing θ values. This means that the performance loss data do not rule out the possibility of decreased θ in the convergent region due to turning effects.

Correlation of the throat turn entrainment fraction multipliers was investigated using the momentum turning parameter evaluated

IV Experimental Results and Data Correlation (cont.)

for the throat turn. It was of interest to see if a trend similar to the convergent turn correlation could be observed with the positive values and if the negative entrainment fraction values were grouped in a particular region. The turn multipliers were normalized by the corresponding multipliers in the conical section, so that in terms of the Figure 13 thermocouple notation the resulting ratio is

$$k_{tt} = \frac{(k/k_o')_{9-10}}{(k/k_o')_{7-9}} \quad \text{Eq. 54}$$

Data from Reference (1) were not used since it was not possible to isolate the conical section and the throat turn with sufficient accuracy. Figure 38 is a plot of k_{tt} as a function of the corresponding momentum turn parameter. This correlation attempt was unsuccessful since the negative values occur over a wide range of the momentum parameter and no trend is apparent in the other data.

c. Boundary Layer Studies

A two dimensional finite-difference boundary layer computer program was used in an attempt to define alternate parameters for the correlation of turning effects. NASA Langley Research Center Program D2630, References 10 and 11, was selected for this purpose since the eddy viscosity formulation was developed specifically for film cooling. Although it was found that this program cannot predict observed turning phenomena, an interesting comparison with the ALRC entrainment model in a cylindrical flow region was obtained. Four cases were run with Program D2630, representing air film cooling with a heated air core flow in the Figure (1) test section. The air/air system was chosen for analysis because the computer program cannot consider two gases with unequal molecular weights. Two film coolant temperatures were assumed in order to provide different injection density ratios (ρ_c/ρ_e). For each density ratio two problems were run: one representing the cylindrical section plus the turn at the start of convergence, and the other a cylindrical reference case with the same contour length. The free stream velocity was constant in each problem in order to isolate turning effects.

IV Experimental Results and Data Correlation (cont.)

Figure 39 compares the effectiveness predictions of Program D2630 and the ALRC entrainment model for the cylindrical section. An entrainment fraction multiplier of 1.6 was used for the latter based on the heated nitrogen tests of Reference (1). Although the entrainment model effectiveness curves in Figure 39 drop below unity sooner than the Program D2630 curves, the effectiveness values at the end of the cylindrical section are in reasonable agreement. Better agreement between the effectiveness distributions could be obtained by increasing the initial free jet region in the entrainment model and modifying the first part of the transition regions. However, the amount of such a change which can be justified by test data has not been investigated. Mixing layer concentration and enthalpy profiles from Program D2630 indicate a much lower asymptotic shape factor than used in the entrainment model, approximately 0.41 vs. 0.76.

Program D2630 predicted only a small effect of turning on effectiveness. For both density ratios the effectiveness change along the turn was about 5 percent less than for the corresponding straight case, which indicates a similar reduction in entrainment fractions. The two density ratios give momentum turning parameters of 0.038 and 0.070, for which the turning correlation of Figure 37 indicates entrainment fraction increases of 90 and 170 percent, respectively. In view of the significant discrepancies between predicted and observed results, additional parametric studies with Program D2630 were not run. It is apparent that the limitations of boundary layer theory preclude the analysis of mixing phenomena in turns.

3. Convergent Section

In view of the problems encountered with the throat turn data and in order to provide design guidelines extending to the throat, correlation of the overall entrainment fraction multipliers for the convergent section was investigated. Three correlation parameters were studied, each evaluated for the turn at the start of convergence since this turn usually dominates the convergent section entrainment. Entrainment fraction multipliers were normalized by the asymptotic cylindrical section multiplier, so the data are presented as

IV Experimental Results and Data Correlation (cont.)

$$k_{\text{conv.}} = \frac{(k/k_0')_{5-10}}{(k/k_0')_{2-5}} \quad \text{Eq. 55}$$

Direct correlation of the convergent section multiplier $(k/k_0')_{5-10}$ was also investigated, but this approach was not as good.

The first correlation studied was based on the density difference parameter $(\rho_e - \rho_w)/\bar{\rho}$ and was motivated by the data from the present contract.¹ Since the coolant injection slot and chamber contour were fixed in the present testing, variations in the density turning parameter used above and in References (1) and (2) are due primarily to the density difference parameter. Figure 40 shows the convergent section data obtained during the Combustion Effects tests as a function of this parameter. It indicates the domination of the first turn decreases as the density difference parameter becomes more negative (trend toward relatively heavy film coolant). The nitrogen data are influenced significantly by large entrainment fractions in the throat turn. Note that the hydrogen data with velocity ratios less than unity are not in good agreement with the rest of the data.

Figure 41 adds the data of References (1) and (2) to Figure 40, thereby adding a high entrainment region at positive density differences which is dominated by the turn at start of convergence. Thus, Figure 41 is consistent with our original hypothesis that positive density differences (relatively light film coolant) increase mixing in the convergent turn but decrease it in the throat turn, while negative differences (relatively heavy film coolant) have the opposite effect. The convergent turn dominates except at large negative density differences, where the increased mixing in the throat turn overpowers the greatly decreased mixing in the former.

Figure 41 leads to a useful design rule for ρ_c/ρ_e . The data indicate that the convergent section entrainment fraction multiplier does not exceed the asymptotic cylindrical section value if ρ_w/ρ_e at the end of the cylindrical section is in the following range:

$$0.75 < \rho_w/\rho_e < 2.5$$

$$\bar{\rho} = 1/2 (\rho_e + \rho_w)$$

IV Experimental Results and Data Correlation (cont.)

No increased entrainment occurs in the convergent region if ρ_w/ρ_e at the upstream end is in this range, in fact, the entrainment will be reduced. Mixing effects will always move ρ_w/ρ_e from ρ_c/ρ_e toward 1.0; therefore, for film coolant injected upstream of the start of convergence, the desirable ρ_c/ρ_e range is somewhat larger than 0.75-2.5 depending on the amount of mixing which occurs between the injection point and the start of convergence.

Figure 42 shows the convergent section data as a function of the density turning parameter, i.e., the density difference parameter of Figure 41 is multiplied by the dimensionless mixing layer thickness S/R , where S is the mixing layer thickness at the start of convergence. The primary effect of this modification is to spread the high entrainment data from References (1) and (2) into two groupings corresponding to different radii of curvature.

The final correlation investigated was based on the momentum turning parameter. This approach is shown in Figure 43, which includes the convergent turn correlating line from Figure 37. It is seen that most of the convergent section data with positive momentum turning parameters are slightly higher than the convergent turn line and most of the data with negative parameters are somewhat lower, but the trends are the same. This illustrates the statement made previously that the first turn dominates the entrainment characteristics in the convergent section for almost all of our tests. However, Figure 43 does not adequately correlate those nitrogen tests in which the throat turn is important (half-shaded squares). Therefore, Figure 43 shows two results for momentum turning parameters near zero, depending on which turn is tending to control the convergent section. Evaluation of the momentum turning parameter at the throat turn rather than the start of convergence for the nitrogen tests does not help to solve this problem. It can only be concluded that Figure 43 does not provide a general correlation for heavy film coolants such as nitrogen. It does, however, provide a design correlation for hydrogen film cooled hydrogen-oxygen rocket engines.

4. Design Recommendations

The key results from this section can be summarized in the following design recommendation for the local entrainment fraction multiplier:

$$k/k_o' = k_m = k_{lip} k_f k_\infty k_t \quad \text{Eq. 56}$$

The parameter k_o' is given by Equations 21 and 44, and the four individual factors which comprise k_m are defined below.

- (1) k_{lip} is the slot lip multiplier and accounts for lip wake effects. It is given in Figure 28 for $x \leq 15h$. For $15h < x < 27h$, k_{lip} is the average of unity and the multiplier from Figure 28. For $x > 27h$, k_{lip} is unity. (h = slot height). For t_{lip}/h ratios smaller than tested (1/3), k_{lip} is probably smaller and likewise if t_{lip}/h is greater than 1/3, k_{lip} is probably larger.
- (2) k_f accounts for uncertainties in the function $f(u_c/u_e)$. Three curves for k_f , based on Figure 32, are plotted on Figure 44 as a function of u_c/u_e . The k_f parameter is unity at $u_c/u_e = 1.0$ by definition. If a conservative analysis is desired, the maximum k_f on Figure 44 is recommended. If a "best estimate" analysis for rocket engines is desired, the dashed line on Figure 44, which is based on the Combustion Effects Program rocket engine data, is recommended.
- (3) k_∞ is the asymptotic cylindrical section multiplier for a velocity ratio of unity. Measured values range from 1.6-4.2 (including the Ref. 1 and 2 data) and the magnitude of k_∞ probably depends on turbulence intensity. For most rocket applications k_∞ is probably in the 3.0-4.2 range, the range measured on this program (see k_{2-5}/k_o' for $u_c/u_e = 1.0$ on Figure 29). A

X = contour distance from injection point, h = slot height

IV Experimental Results and Data Correlation (cont.)

value of 3.0 represents the rocket firing data obtained in the present contract for the core mixture ratio range most likely to be encountered in film-cooled hydrogen/oxygen applications. The $k_{\infty} k_f$ products measured during the Combustion Effects Program tests are the k_{2-5}/k_0' values shown on Figures 29 and 31.

- (4) k_t accounts for turning effects in the convergent section. In the turn at the start of convergence the correlation of Figure 37 is recommended. For an overall average in the convergent section, multipliers can be determined from either of the correlations shown on Figures 41, 42, and 43. For a conservative analysis, all three of these correlations should be evaluated and the highest k_t should be used.

D. CORRELATION OF PERFORMANCE LOSS RESULTS

Twelve hydrogen film cooled tests, five inert gas film cooled tests, and five no-film-cooling tests were utilized to calibrate and verify the performance loss model described in Section III.B. The hot fire test performance and film cooling data are summarized in Table IV. The five uncooled engine tests provided no-film-cooling performance data over the overall mixture ratio range from 0.8 to 8. The purpose of these tests was to establish the uncooled delivered performance for the premix triplet injector tested. This characteristic curve is shown on Figure 45 along with all the film cooled specific impulse data. Uncooled engine data for a very similar injector created during Contract NAS 3-14379 was included in the figure to aid in drawing the no-film-cooling performance curve.

The film cooled data plotted on Figure 45 indicate that cooled engine performance is well characterized as a function of overall mixture

IV., Experimental Results and Data Correlation (cont.)

ratio and the coolant injection velocity ratio, u_c/u_e . These data also indicate that the film cooling specific impulse loss can be referenced to an uncooled engine delivered impulse defined as a function of the overall engine mixture ratio.

The influence of the film coolant percentage and the core flow mixture ratio on the film coolant performance loss is shown on Figure 46. This plot indicates that the film cooling loss is a function of the core mixture ratio and the distribution of mass between the core streamtube and the wall mixing layer streamtube.

The primary form of the film coolant loss equation, which was developed after assessing the data shown in Figures 45 and 46, is shown below.

$$\Delta I_{spFCL} = I_{sp \text{ uncooled @ O/F overall}} - I_{sp \text{ cooled @ O/F overall}}$$

$$I_{sp \text{ cooled @ O/F overall}} = \left(\frac{W_{\text{core}}}{W} \right) I_{sp \text{ core @ O/F core}} + \left(\frac{W_{\text{ML}}}{W} \right) I_{sp \text{ ML @ O/F ML}}$$

The exact formulation of the above equations including engine efficiency factors and one dimensional equilibrium specific impulse reference values is detailed in Section III.B. In correlating the film cooled engine data with predictions of the performance loss model, the primary problem became proper definition of the respective efficiency factors ($\eta_{I_{sp}'s}$). Figure 45 indicates that the uncooled engine specific impulse can be referenced to the overall mixture ratio, thus:

$$I_{sp \text{ uncooled @ O/F overall}} = \eta_{I_{sp}} \times I_{sp \text{ ODE @ O/F overall}}$$

This definition was left unchanged for all the model correlation variations. The $\eta_{I_{sp}}$ values calculated from the uncooled tests are listed on Table VII.

IV Experimental Results and Data Correlation (cont.)

The final expression obtained for film cooling performance loss is stated as Equation 38 in Section III.B. In finalizing the form of this equation, four combinations of the definitions for the core and mixing layer efficiency factors were investigated. Each is briefly explained below.

$$\text{Case 1: } \eta_{I_{sp \text{ core}}} = \eta_{I_{sp \text{ ML}}} = \eta_{I_{sp}} \text{ @ O/F overall}$$

This definition assumes the core and mixing layer efficiency factors are equal to the uncooled engine efficiency at the overall mixture ratio. This formulation is lacking in that the efficiency factor is known to be a function of mixture ratio and the core and mixing layers operate at mixture ratios different from the overall.

$$\text{Case 2: } \eta_{I_{sp \text{ core}}} = f(\text{O/F core}) = \eta_{I_{sp \text{ ML}}}$$

In this case, the core efficiency factor is defined from the uncooled engine data at the core mixture ratio. The mixing layer factor is assumed equal to the core value.

$$\text{Case 3: } \eta_{I_{sp \text{ core}}} = f(\text{O/F core}), \quad \eta_{I_{sp \text{ ML}}} = f(\text{O/F}_{\text{ML}})$$

In this case, the core and mixing layer factors are defined at their respective mixture ratios from the uncooled engine delivered impulse versus overall mixture ratio curve. This form tends to underpredict mixing layer performance because injector effects lowered uncooled engine performance at low mixture ratios.

$$\text{Case 4: } \eta_{I_{sp \text{ core}}} = f(\text{O/F core}), \quad \eta_{I_{sp \text{ ML}}} = \eta_{I_{sp \text{ core}}} \times \left(\frac{W_E}{W_{ML}} \right) + \frac{W_C}{W_{ML}}$$

Since the mixing layer streamtube is made up of entrained core gases (\dot{W}_E) and injected film coolant gas (\dot{W}_C), the $\eta_{I_{sp \text{ ML}}}$ can be defined by

IV Experimental Results and Data Correlation (cont.)

mass weighting $\eta_{sp\ core}$ and assuming a coolant efficiency factor of 1.0. The coolant efficiency factor of 1.0 assumes the film coolant gases expand isentropically to the exit nozzle area ratio. This is reasonable since at low mixture ratios (typical of the mixing layer) combustion related performance losses are small.

Performance model predictions are compared with the measured hydrogen film cooling losses on Figure 47. The most consistently accurate correlation was obtained with the Case 4 correlation. The data agree with this prediction within -10%/+25% at low ΔI_s values (< 200 m/sec or 20 lb_f-sec/lb_m) and within ± 5 sec for the 200 to 450 m/sec (25 to 45 sec) ΔI_s range. This is considered a good correlation.

Figure 48 compares the selected correlation predictions to the hydrogen, helium, and nitrogen film coolant data. The helium coolant predictions are within the accuracy of the hydrogen film cooled tests while the film coolant loss is underpredicted by approximately 40 percent for the nitrogen cooled tests.

The underprediction of the nitrogen data has not been explained and does not seem important for practical design cases. The wall temperature data from the nitrogen tests indicate extremely rapid mixing in the convergent region and this could indicate an extremely well mixed mixing layer with a shape factor smaller than predicted by the entrainment model (See Figure 6). This could be responsible for the discrepancy. It is also possible that the Equation 38 formulation is simply not valid for all combinations of O_2 , H_2 , and an inert gas. Some oxygen film cooled data may clarify this area since oxygen is a heavy gas like nitrogen but not inert.

The sensitivity of the predicted film coolant loss to the shape factor, θ , at the nozzle throat was also investigated. Figure 49 shows the film cooling loss predicted for test 115 by making the following assumptions:

IV Experimental Results and Data Correlation (cont.)

- (1) The entrainment model shape factor correlation, θ vs W_E/W_C (Figure 5), and the circumferential average entrainment fractions calculated from the wall temperature data. (This is the procedure used to generate all of the predictions shown on Figures 47 and 48).
- (2) Same as (1) except only the row B k data were used,
- (3) $k/k_0' = \theta$ between thermocouples 8 and 10 (the region between the convergent cone midpoint and the nozzle throat) and the corresponding θ value calculated from Equation 17 (See Section IV.C.2.b. for further discussion).
- (4) Same as (3) except $(k/k_0')_{8-10} = 3.0$ was assumed.

The Figure 49 plot shows that the predicted loss decreases as the shape factor decreases. This occurs because a smaller shape factor corresponds to a larger W_E/W_C which means that the film coolant mixing upstream of the throat is more complete. The most significant aspect of the Figure 49 results is that even for the most extreme case assumed ($k/k_0' = 3.0$) the comparison between measured and predicted loss is acceptable (within 10%). Consequently, the effect of flow turning on shape factor theorized in Section III.C.2.b. is plausible since it does not lead to unreasonable performance loss predictions.

E. CORRELATION OF HEAT TRANSFER RESULTS

Experimental C_g values, defined by Equation 39, were obtained experimentally with and without film cooling effects during the Combustion Effects on Film Cooling Program Tests. In the film cooling test data reduction procedure, h_g values were calculated from the wall temperature transients and used to calculate T_{aw} from the measured wall temperatures. These h_g

IV Experimental Results and Data Correlation (cont)

values were also converted to the C_g values listed on Table V assuming the reactive model and the average film reference temperature. Similar results from a test firing performed without film cooling are listed on Table VI. In the test without film cooling, heat fluxes were calculated from copper heat sink chamber temperature transients assuming one-dimensional radial conduction. The C_g values are based on the theoretical combustion enthalpy and the heat flux and wall temperature indicated at the end of the firing.

Equation 40 is compared to the Row B C_g values on Figure 50. This data plot indicates that the Equation 40 correlation for injection velocity effect on C_g predicts the trend of the data reasonably well.

The Row B C_g values determined without film cooling and with film cooling at $u_c/u_e = 1.0$ are compared on Figure 51 (The copper heat sink chamber thermocouples were located at the Row B circumferential position). The chamber contours tested with and without film cooling were nearly identical, therefore the data can be compared on an axial distribution basis. Better agreement between the two sets of data is obtained using the adiabatic wall reference temperature.

V ANALYTICAL PREDICTIONS

A. Analysis Scope

This section contains analytical predictions of wall temperature and performance loss vs. hydrogen film cooling flow rate which were obtained for a proposed hydrogen/oxygen combustor design using the HOCOOL computer program. The combustor design analyzed is regeneratively cooled with hydrogen flowing in rectangular coolant passages. The design is defined on Figure 86 of Reference 12. Figure 52 shows the combustor attached to a tubular, regeneratively cooled nozzle. The regenerative coolant for the combustor enters the cooling channels downstream of the nozzle throat at an area ratio of about eight and flows toward the main injector through the coolant channels in one pass. Coolant passage geometry and the thrust chamber contour are defined on Figure 53.

The nominal operating conditions for the combustor operating without film cooling are listed below:

Propellants:	O_2/H_2
Overall Mixture Ratio:	6.5
Chamber Pressure:	1310 N/cm^2 (1900 psia)
Nominal Thrust:	88,964N (20,000 lbf)
Hydrogen Inlet Temperature:	50°K (90°R)
Hydrogen Inlet Pressure:	2896 N/cm^2 (4200 psia)
Total Propellant Flow Rate:	20.4 kg/sec (45 lb/sec)
Regenerative Coolant Flow Rate:	1.73 kg/sec (3.808 lb/sec)

Wall temperature and film cooling performance loss predictions were determined for the following four cases:

V Analytical Predictions (cont.)

	<u>Case 1</u>	<u>Case 2</u>	<u>Case 3</u>	<u>Case 4</u>
W_{FC}/W_f	None	.05,.1,.2,.3	.05,.1,.15,.2	.05,.1,.15,.2
Film Coolant Injection Temperature	-	(a) 50°K (90°R) and (b) 273°K (460°R)	273°K	273°K
Film Coolant Injection Point	-	Main Injector	End of Cylindrical Section	Halfway between main injector and throat
$W_{regen}/(W_{regen})_{Case 1}$	1.0	(a) $1.0 - (W_{FC}/W_f)$ (b) 1.0	1.0	1.0

Overall mixture ratio, total propellant flow rate, and regen coolant inlet pressure were assumed constant for the film cooled cases. The results for these four cases are described in Sections V.C.

B. Method of Analysis

In each of the four cases considered, the hot-gas-side heat transfer coefficient values, h_g , were calculated from Equation 39 with adiabatic wall reference temperature. The C_g values were determined so that the no-film-cooling h_g values were exactly the same as given on pages 14-16 of Reference 12. The coolant side coefficient, h_L , was calculated from the Hess and Kunz correlation (Reference 13) adjusted for turning effects with the equation given by Taylor (Reference 14). Some arbitrary adjustment of the h_L correlation was required as explained in the next section.

In the film cooling analyses, the film coolant was assumed either injected at $u_c/u_e = 0.8$ or through a .0625 cm (.025 in.) thick annular slot if the 0.8 velocity ratio corresponded to a slot height less than .0625 cm (.025 in.). The velocity ratio and slot height data used in all the film cooled cases are tabulated below.

V Analytical Predictions (cont.)

% Hydrogen Film Cooling	Core O/F	Injection Temp. = 273°K (460°R)				Injection Temp. = 50°K (90°R)		
		u_c/u_e	h,cm	Momentum Turn Parameter		u_c/u_e	h,cm	Momentum Turn Parameter
				(1)	(2)			(1)
5	6.84	.17	.0625	.0041	(.0006)	.031	.0625	.005
10	7.22	.35	.0625	.0046	(.0005)	.0654	.0625	.0072
15	7.65	.55	.0625	-	(.0003)	-	-	-
20	8.15	.77	.0625	.0017	(-.0007)	.14	.0625	.0071
30	9.29	.8	.159	.0017	-	.23	.0625	.0058

(1) Calculated at the start of convergence for film coolant injection at the main injector.

(2) Calculated at the start of convergence assuming injection at the start of convergence.

Entrainment fractions for the film cooling analyses were evaluated using the Equation 56 approach:

$$k = km ko' = (k_{lip} k_f k_\infty k_t) ko'$$

The individual components of km were evaluated as follows:

k_{lip} - considered to be a function of axial position and velocity ratio ranging from the maximum value given by Figure 28 at the injection point to 1.0 at a distance of 0.69 cm (1.75 inches) downstream of the injection point. For the range of u_c/u_e considered, maximum $k_{lip} = 2.0$.

$k_f k_\infty$ - This product was considered a function of core O/F and velocity ratio. It was assumed to be the same as the data plotted on Figure 29. For the range of u_c/u_e considered, $k_f k_\infty$ ranged from 2.0 ($u_c/u_e = 0.8$) to 3.0 ($u_c/u_e = 0.3$).

k_t - The momentum turning parameter correlation for the entire convergent region (Figure 43) was used. For injection into the cylindrical

V Analytical Predictions (cont.)

region, the momentum turning parameters were calculated using the results of an entrainment model analysis for the cylindrical region. The resulting k_t factors determined from Figure 43 were: 1.05 for film coolant injection at the main injector, 1.0 for film coolant injection at the start of the turn or in the middle of the turn.

C. Analysis Results

1. Case 1: No Film Cooling

Axial distributions of maximum gas-side wall temperature calculated assuming no film cooling are shown on Figure 54 along with the distribution from Figure 79 of Reference 12. The initial wall temperatures calculated (curve (1) of Figure 54) were significantly higher than the Reference 12 values, shown as curve (3). The difference was most significant in the two areas where the step change in channel width occurs. The maximum wall temperature calculated in this initial analysis is 933°K (1220°F) while a value of 745°K (880°F) is reported in Reference 12. A thorough investigation of this discrepancy was beyond the scope of this program; however it is recommended that such an investigation be undertaken in the future. Since the h_g values used are identical to those given in Reference 12, the differences must be associated with the wall conduction model and the coolant side heat transfer coefficient. It was decided to decrease the analysis differences by arbitrarily increasing the h_L values by 30% in the high heat flux regions of the combustor. This was done solely to allow an expedient evaluation of the effect of film cooling on wall temperature. Curve (2) of Figure 54 is the wall temperature distribution obtained with the increased h_L values. This curve was used as a reference in evaluating the effect of film cooling on wall temperature. The maximum temperature predicted with the increased h_L values is 828°K (1030°F).

2. Case 2: Hydrogen Film Coolant Injected at the Main Injector

Two film coolant injection temperatures were considered: 50°K (90°R), the regenerative coolant inlet temperature, and 273°K (460°R),

V Analytical Predictions (cont.)

the regenerative coolant outlet temperature when no film coolant is injected. For the 50°K injection case, the film coolant flow rate was subtracted from the regenerative coolant flow rate. These two injection temperatures represent film cooling with hydrogen upstream of the coolant passages and downstream of the cooling passages. Curves (2a) and (2b) of Figure 55 show maximum combustor wall temperature for these two injection conditions versus the calculated film-cooling performance loss. The Figure 55 graph provides the basis for two conclusions: (1) Maximum cooling effectiveness is obtained by film cooling downstream of the cooling passages using the higher temperature film coolant, and (2) A significant reduction in wall temperature is predicted for a relatively small loss in performance. For example, 10% of the hydrogen flow injected as film coolant at a temperature of 273°K (460°R) is predicted to produce a 190°K (340°F) wall temperature decrease at the cost of approximately 1% in overall specific impulse performance.

3. Case 3: Hydrogen Film Coolant Injected at the End of the Cylindrical Region

Only the higher injection temperature was considered due to the Case 2 findings. The maximum wall temperature in the film cooled region tends to be slightly less than the Case 2 value as shown on Figure 55. However, in this type of configuration one must also consider the wall temperature upstream of the injection point. The two most likely ways of introducing film coolant at this point are: (1) with a sleeve through which the film coolant is injected, and (2) from the OD at an axial position near the injection point. Consideration of a sleeve was beyond the scope of this analysis. It was assumed that the film coolant is introduced from the OD, the axial length of the injection device is negligible, and that the coolant channel geometry downstream (coolant wise) of the injection point was unchanged.

The maximum combustor wall temperature corresponding to the above assumptions is plotted on Figure 56. It was found that the region upstream of the injection point is limiting for Case 3 if more than 10% fuel film cooling is used. At lower film cooling percentages, the wall temperature versus performance loss curve is about the same as for Case 2b.

V Analytical Predictions (cont.)

Consequently, there appears to be no advantage in injecting the film coolant at the end of the cylindrical section in the assumed manner. Consideration of an axially oriented injection sleeve is recommended for future work.

4. Case 4: Hydrogen Film Coolant Injected Midway Between The Main Injector and Throat

The results of this case are also plotted on Figures 55 and 56. The wall temperature versus ΔI_S curve on Figure 55 for the film cooled region yields the lowest wall temperatures for a given ΔI_S ; however, Figure 56 shows that the region upstream of the injection point is limiting even at the 5% film cooling condition. Consequently, the conclusion is the same as for Case 3; there appears to be no advantage in injecting film coolant at this point in the assumed manner, but consideration of a sleeve is recommended.

VI CONCLUSIONS AND RECOMMENDATIONS

A. CONCLUSIONS

1. The ALRC entrainment film cooling model, which relates film cooling effectiveness to the amount of mainstream or core flow gases entrained by and mixed with film coolant gases, can be used to predict adiabatic wall temperature, film cooling performance loss, and gas-side heat transfer coefficient in gas film cooled rocket engines.

2. The 2-streamtube entrainment flow model has provided a valid analytical basis for a film cooling performance loss prediction model. The performance loss prediction equation developed for hydrogen/oxygen rocket engines is:

$$\Delta I_{sp} = \eta_{I_{sp}} \times I_{sp \text{ ODE}} - \left[\eta_{I_{sp \text{ core}}} \times I_{sp \text{ ODE}} \right. \\ \left. \times \frac{w_{\text{core}}}{W} + \eta_{I_{sp \text{ ML}}} \times I_{sp \text{ ODE}} \times \frac{w_{\text{ML}}}{W} \right] \quad \text{Eq. (38)}$$

where:

$$\eta_{I_{sp}} = \text{engine efficiency factor} = f(O/F)$$

$$\eta_{I_{sp \text{ ML}}} = \eta_{I_{sp \text{ core}}} \times \frac{w_E}{w_{\text{ML}}} + \frac{w_C}{w_{\text{ML}}}$$

The above equation can be expected to predict performance loss within $\pm 25\%$ for loss values less than 196 meters/second (20 seconds), and within ± 49 meters/second (± 5 seconds) for loss values greater than 196 meters/second (20 seconds).

VI Conclusions and Recommendations (cont.)

3. The entrainment fraction, k , which relates entrained core gas mass flux to the axial core gas mass flux, can be estimated from the following equation for hydrogen/oxygen rocket engines:

$$k = k_o' k_{lip} k_f k_\infty k_t \quad \text{Eq. (56)}$$

where:

- k_o' = the entrainment fraction for plane unaccelerated flow corrected for known acceleration effects (defined by Equations 44 and 21)
- k_{lip} = a factor which accounts for wake turbulence effects in the region immediately downstream of the injection slot lip,
- k_f = a factor which accounts for velocity ratio effects not predicted by the k_o correlation, Equation 21.
- k_∞ = the asymptotic cylindrical section multiplier (ranges from 3.0 to 4.2 in the rocket engine data),
- k_t = a factor which accounts for the effect of flow turning

The evaluation of each term of Equation 56 is described in Section IV.C.4.

4. No adverse entrainment due to turning effects occurred in the convergent region of the thrust chamber tested when:

$$0.75 < \rho_w / \rho_e < 2.5$$

where:

- ρ_w = density of mixing layer gas adjacent to the nozzle wall at the convergent region inlet
- ρ_e = density of core gases

The above relationship is recommended as a design guideline for convergent geometries similar to the one tested (Figure 13).

VI Conclusions and Recommendations (cont.)

5. Combustion between the film coolant gas and the core gas has no effect on entrainment fraction for the range of core gas mixture ratios likely to be encountered in a hydrogen/oxygen rocket engine. This conclusion is based on the agreement of data obtained with hydrogen and helium film coolants at a core mixture ratio of eight (Figure 25). Either the film coolant combustion did not influence mixing or else no film coolant combustion occurred.

6. A significant reduction in the wall temperature of the hydrogen/oxygen combustor proposed in Reference 12 can be realized with a relatively small film cooling performance loss. Analyses performed with the HOCOOL computer program and the Section IV data correlations (Section V) indicate that if 10% of the hydrogen is injected as film coolant at the main injector, the maximum wall temperature will be reduced 190°K (340°F) and the performance loss will be approximately 1% of the no-film-cooling performance.

B. Recommendations

1. The HOCOOL computer program is recommended for future heat transfer analyses of hydrogen/oxygen rocket engines. The HOCOOL computer program consists of: (1) a version of the ALRC entrainment model prepared specifically for hydrogen film cooled hydrogen/oxygen rocket engines, (2) film cooling performance loss formulations, and (3) a generalized regenerative cooling model.

2. Extension of the HOCOOL computer program to include the case of liquid film cooling, and a series of test firings with liquid film coolants to determine appropriate design inputs (as done on this program for gas film coolants) is recommended for future work.

3. Additional testing with gas film coolants injected at velocity ratio, u_c/u_e , values in the 0.3 to 1.0 range is recommended to determine the "optimum" velocity ratio where the entrainment fraction, indicative of the rate at which the film coolant and core gases mix, is a minimum.

4. In future film cooling tests, oxygen film cooling and a fuel rich core gas mixture ratio are recommended as an extreme case for further evaluating: (a) film coolant/core gas combustion effects, (b) performance loss with heavy film coolants, and (c) turning effects with heavy film coolants.

REFERENCES

1. R. L. Ewen, "Hydrogen Film/Conductive Cooling", ALRC Final Report, Contract NAS 3-14343, NASA CR-120926, November 1972
2. D. C. Rousar, R. L. Ewen, "Hydrogen Film Cooling Investigation", ALRC Final Report, Contract NAS 3-15844, NASA CR 121235, August 1973
3. L. Schoenman, R. J. LaBotz, "Hydrogen-Oxygen Auxiliary Propulsion for the Space Shuttle", Vol. I; High Pressure Thrusters", ALRC Final Report, NAS 3-14354, January 1973.
4. D. F. Calhoun, J. I. Ito, D. L. Kors, "Investigation of Gaseous Propellant Combustion and Associated Injector/Chamber Design Guidelines", ALRC Final Report, NAS 3-14379, July 1973
5. R. L. Ewen, D. C. Rousar, E. H. Green, J. W. Salmon, "HOCOOL Users Manual", Aerojet Liquid Rocket Company, Contract NAS 3-17813, July 1975 (Proprietary)
6. J. L. Stollery, A. A. M. El-Ehmany, "A Note on the Use of a Boundary Layer Model for Correlating Film Cooling Data", Int. J. Heat Mass Transfer, Vol. 8, pp. 55-65, 1965
7. C. J. Marek, R. R. Racina, "Effect of Free-Stream Turbulence on Film Cooling", NASA TND-7958, Lewis Research Center, Cleveland Ohio, June 1975
8. Svehla, R. A., and McBride, B. J., "Fortran IV Computer Program for Calculation of Thermodynamic and Transport Properties of Complex Chemical Systems", NASA TN D-7056, January 1973
9. Williams, J. J., "The Effect of Gaseous Film Cooling on the Recovery Temperature Distribution in Rocket Nozzles", PhD. Thesis, University of California at Davis, May 1969. Also ASME Paper No. 70-HT/SpT-42.
10. I.E. Beckwith, D. M. Bushnell, "Calculation by a Finite-Difference Method of Supersonic Turbulent Boundary Layers with Tangential Slot Injection", NASA TN D-6221, Langley Research Center, Hampton, Va., April 1971
11. B. A. Hixon, I. E. Beckwith, "Computer Program for Compressible Laminar or Turbulent Nonsimilar Boundary Layers", NASA TM X-2140, Langley Research Center, Hampton, Va., April 1971
12. J. M. Shoji, "Advanced Hydrogen/Oxygen Thrust Chamber Design Analysis", NASA CR 121213, Rocketdyne Division of Rockwell International, NAS 3-16774, November, 1973
13. H. L. Hess, H. R. Kunz, "A Study of Forced Convection Heat Transfer to Supercritical Hydrogen", Journal of Heat Transfer, ASME, February 1965, 41-48

References (cont.)

14. M. F. Taylor, "Heat Transfer Predictions in the Cooling Passages of Nuclear Rocket Nozzles", J. Spacecraft, Vol. 5, No. 11, November 1968, 1353-1355.



TABLE I
NOMINAL TEST CONDITIONS

<u>Core O/F</u>	<u>Film Coolant</u>	<u>u_c/u_e</u>	<u>Test Number</u>	<u>Remarks</u>
2	H ₂	1.25	112	Film Cooled Chamber (O/F) _{core} = 2
2	H ₂	1.0	113	
2	N ₂	0.30	123	
2	N ₂	0.25	124	
4	H ₂	1.25	102	Film Cooled Chamber (O/F) _{core} = 4
4	H ₂	1.0	103	
4	H ₂	0.80	104,117	
6	H ₂	1.25	105	Film Cooled Chamber (O/F) _{core} = 6
6	H ₂	1.0	106,115	
6	H ₂	0.80	107,114	
8	H ₂	1.50	108,109	Film Cooled Chamber (O/F) _{core} = 8
8	H ₂	1.25	110	
8	H ₂	1.0	111	
8	H ₂	0.80	116	
8	He	1.25	118,121, 122	
8	He	1.0	119	
8	He	0.80	120	
0.8	none	-	129	
2	none	-	125	Uncooled Chamber, No-Film-Cooling Performance Tests
4	none	-	126	
6	none	-	003,127	
8	none	-	128	

TABLE II
OVERALL TEST CONDITIONS

Test Number	p_c , psia	Core O/F	Film Coolant	u_c/u_e	Remarks
2KB6-12-003	322	5.39	None	-	Checkout test, copper heat sink chamber, no-film-cooling performance data
-102	303	3.89	H ₂	1.21	
-103	286	3.82	H ₂	1.02	
-104*, -117	282,281	3.84, 4.00	H ₂	.77	Data repeatability good
-105	293	5.85	H ₂	1.31	
-106, -115	294,289	6.07, 5.93	H ₂	1.07	Data repeatability good
-107*, -114	282,287	5.98, 6.27	H ₂	.84	Test 107: invalid data
-108*, -109	310, 310	8.0, 7.97	H ₂	1.51	Test 108: invalid data
-110	308	7.71	H ₂	1.29	
-111	298	7.99	H ₂	1.07	
-116	285	7.60	H ₂	.84	
-112	296	2.06	H ₂	1.28	
-113	295	2.07	H ₂	1.01	
-118*	332	7.75	H _e	-	Test 118: invalid data
-121*	332	7.75	H _e	-	Test 121: data system malfunction
-122	332	7.75	H _e	1.25	
-119	317	7.75	H _e	1.02	
-120	307	7.46	H _e	.82	
-123	330	2.11	N ₂	0.32	
-124	318	2.06	N ₂	0.27	
-125*	312	2.14	None	-	Tests 125, 126, 127, 128: No film cooling performance tests with copper heat sink chamber
-126*	299	3.99	None	-	
-127*	308	6.23	None	-	
-128*	314	8.09	None	-	
-129*	138	.782	None	-	

(*) No film cooling data reduction performed for this test.

TABLE III
ENTRAINMENT FRACTION RESULTS

Values Tabulated are k/k_0'
 k_0' Defined by Equation 44

Test	Film Coolant	Core O/F	u_e/u_e	k_0	Thermocouples:				Cylindrical			Conv. Turn 5-7	Subsonic Cone 7-9	Subsonic Throat Turn 9-10	Supersonic Throat Turn 10-11	Supersonic Cone 11-12	Supersonic 12-13
					T _{in-1}	1-2	2-3	3-4	4-5								
112	H ₂	2.06	1.28	.00538	7.84 ⁽¹⁾	9.16	5.79*	4.46*	5.75	3.14	2.78 ⁽²⁾	1.65 ⁽²⁾	-	-	-	-	-
113	H ₂	2.07	1.01	.00486	7.45	8.02	4.71*	3.48*	4.55	1.85	2.83 ⁽²⁾	1.41 ⁽²⁾	-	-	-	-	-
102	H ₂	3.89	1.21	.00523	7.69	7.66	5.74	4.27	3.76	2.72	1.70	0.47	2.09(B)	1.35 (B)	2.8 (B)	-	-
103	H ₂	3.82	1.02	.00508	7.20	6.34	4.56	3.39	2.85	2.58	1.54	0.17	0.87(B)	-	-	-	-
117	H ₂	4.00	0.77	.00637	4.56	4.07	2.65*	2.48*	2.44*	2.25	2.28	1.73	-	1.78 (B)	(11-13)	-	-
105	H ₂	5.75	1.31	.00594	6.55	6.08	5.52	3.89	3.64	3.22	0.92	-1.74	.35 (B)	-	-	-	-
115	H ₂	5.93	1.07	.00537	6.31	5.37	4.19*	3.25*	3.34*	2.25	1.39	-1.45	-	-	-	-	-
114	H ₂	6.27	0.84	.00628	4.26	3.48	2.82*	1.93*	1.95*	1.88	0.99	0.06	-	-	-	-	-
109	H ₂	7.97	1.51	.00752	4.62	4.96	3.72*	3.03*	3.07	2.05 (3)	1.04 ⁽⁴⁾	-1.56	-	-	-	-	-
110	H ₂	7.71	1.29	.00614	5.18	5.09	3.76*	3.24*	3.08	2.25(3)	1.04 ⁽⁴⁾	-1.74	.81 (D)	(10-12)	-	-	-
111	H ₂	7.99	1.07	.00560	5.03	4.40	3.06*	2.66*	2.56	2.03 (3)	1.04 ⁽⁴⁾	-1.15	1.33 (D)	(10-12)	-	-	-
116	H ₂	7.60	0.84	.00657	3.78	3.30	2.21*	1.67*	1.80*	1.78	0.99	0.33	-	-	-	-	-
122	H _e	7.75	1.25	.00524	5.20	4.44	4.19	2.88*	3.47*	1.73	1.15	-0.22	-	-	-	-	-
119	H _e	7.75	1.02	.00523	4.69	4.11	3.62	2.64*	2.93*	1.78	0.76	-0.69	-	-	-	-	-
120	H _e	7.46	0.82	.00617	3.57	3.10	2.50	1.88*	2.12*	1.59	0.42	0.28	-	-	-	-	-
123	N ₂	2.11	0.32	.00480	10.33	2.51	3.68	4.50*	4.77*	4.11	9.32	42.3	-	-	-	-	-
124	N ₂	2.06	0.27	.00549	7.6	2.2	3.66	4.25	4.56	4.80	13.85	44.0	38.8	63	-	-	-

- NOTES: (1) All values are average of Rows B and D except as noted
(2) D Row value based on cone + subsonic throat turn
(3) B row value based on turn + 1/2 of cone
(4) B row, value based on 1/2 turn + cone
(B), (D) Indicates Row B or Row D data
(*) Indicates average of Row B, D, F, G

TABLE IV

PERFORMANCE DATA SUMMARY

Test No.	Meas. F _{vac} (lbf)	\dot{W}_T (lbm/sec)	I _{S vac} (sec)	Overall O/F	Core O/F	% FFC, W _c /W _F	u _c /u _e	$\Delta I_{S FCL}$ (sec)	Film Coolant	Meas. $\eta_{I, sp}$
102	1516	4.165	364.0	2.04	3.89	47.5	1.21	16.9	H ₂	-
103	1427	3.919	364.1	2.19	3.81	42.6	1.02	17.5	H ₂	-
105	1474	4.131	356.9	2.66	5.75	53.7	1.31	25.8	H ₂	-
109	1563	4.638	337.1	3.25	7.90	58.9	1.51	44.5	H ₂	-
110	1534	4.526	338.9	3.46	7.71	55.1	1.29	41.6	H ₂	-
111	1503	4.463	336.7	3.97	7.99	50.2	1.07	40.6	H ₂	-
112	1475	4.069	362.5	1.25	2.06	39.3	1.28	7.6	H ₂	-
113	1467	3.998	367.0	1.35	2.05	34.1	1.01	5.2	H ₂	-
114	1444	4.083	353.7	3.61	6.27	42.4	.84	26.0	H ₂	-
115	1424	4.026	353.8	3.07	5.93	48.3	1.07	28.4	H ₂	-
116	1437	4.222	340.4	4.31	7.60	43.3	.84	33.9	H ₂	-
117	1393	3.764	370.0	2.57	4.00	35.8	.77	12.6	H ₂	-
119	1598	4.873	327.9	2.80	7.76	63.9	1.02	45.7	H _e	-
120	1555	4.657	333.8	3.07	7.46	58.9	.82	37.8	H _e	-
122	1667	5.140	324.3	2.33	7.75	69.9	1.25	52.9	H _e	-
123	1651	5.936	278.1	.642	2.10	69.0	.32	22.0	N ₂	-
124	1595	5.470	291.6	.717	2.05	64.9	.27	17.9	N ₂	-
125	1296	3.398	381.5	2.14	2.14	0	-	-	None	.956
126	1243	3.310	375.5	3.99	3.99	0	-	-	None	.948
127	1291	3.658	352.9	6.23	6.23	0	-	-	None	.952
128	1316	3.971	331.5	8.09	8.09	0	-	-	None	.962
129	711.6	2.074	343.1	.782	.782	0	-	-	None	.948
003	1341	3.785	354.3	5.39	5.39	0	-	-	None	-

TABLE V
FILM COOLING HEAT TRANSFER COEFFICIENT DATA

Values Tabulated are C_g as Defined by Equation 39
Reference Temperature = $1/2 (T_w + T_{aw})$

Test	(θ/F) _{core}	u_c/u_e	Row	T.C. No.	1	2	3	4	5	6	7	8	9	10	11	12	13		
112	2.06	1.28	B		2.20	1.59	1.22	1.06	0.96	1.05	1.09	0.98	0.88	0.49	-	-	-		
			D		1.89	1.53	1.22	1.08	0.90	-	1.12	-	-	-	0.45	-	-	-	
			F		-	1.50	1.16	0.99	-	-	-	-	-	-	-	-	-	-	-
			G		-	1.81	1.18	1.03	-	-	-	-	-	-	-	-	-	-	-
113	2.07	1.01	B		1.90	1.22	1.08	0.97	0.89	-	.96	1.14	0.86	0.46	-	-	-		
			D		1.32	1.36	1.17	1.02	0.89	-	1.03	-	-	-	0.46	-	-	-	
			F		-	1.17	1.08	0.96	-	-	-	-	-	-	-	-	-	-	-
			G		-	1.70	1.13	0.93	-	-	-	-	-	-	-	-	-	-	-
102	3.89	1.21	B		1.75	1.24	1.18	1.17	1.06	1.22	1.29	1.10	0.95	0.54	0.50	0.76	0.89		
			D		1.78	1.40	1.38	1.11	.999	1.13	1.14	1.01	-	-	0.88	0.46	-	-	
103	3.82	1.02	B		1.72	1.39	1.20	1.19	1.04	1.15	1.25	1.12	.98	.54	0.92	-	-		
			D		1.58	1.5]	-	1.20	1.01	1.09	1.13	1.05	-	-	0.94	0.54	-	-	
117	4.00	.77	B		1.50	1.12	1.00	0.96	0.87	-	0.92	0.97	0.93	0.59	-	-	-		
			D		1.25	1.19	1.08	0.97	0.88	1.02	-	-	-	0.94	0.59	-	-	-	
			F		-	1.07	0.94	0.93	0.88	-	-	-	-	-	-	-	-	-	-
			G		-	1.15	1.01	0.92	0.85	-	-	-	-	-	-	-	-	-	-
105	5.75	1.31	B		4.26	1.75	1.57	1.45	1.38	1.40	1.44	1.47	1.08	0.59	0.59	-	-		
			D		2.76	1.72	1.46	0.93	0.88	0.91	0.85	0.69	-	-	0.66	0.39	-	-	
115	5.93	1.07	B		1.89	1.44	1.28	1.18	1.07	-	1.09	1.07	0.95	0.60	-	-	-		
			D		1.66	1.76	1.48	1.24	1.01	-	1.24	-	-	0.94	0.52	-	-	-	
			F		-	1.45	1.18	1.15	1.05	-	-	-	-	-	-	-	-	-	-
			G		-	1.99	1.31	1.11	0.99	-	-	-	-	-	-	-	-	-	-
111	7.99	1.07	B		1.78	1.46	1.39	1.31	1.20	1.27	-	1.15	1.10	0.67	-	-	-		
			D		1.48	1.58	1.43	1.31	1.16	-	1.25	-	-	0.98	0.60	0.89	-	-	
			F		-	1.49	1.93	1.04	-	-	-	-	-	-	-	-	-	-	-
			G		-	1.39	1.28	1.14	-	-	-	-	-	-	-	-	-	-	-
116	7.60	.84	B		1.42	1.24	1.16	1.13	1.01	-	0.99	1.02	1.00	0.68	-	-	-		
			D		1.32	1.40	1.25	1.15	1.02	-	1.12	-	-	0.98	0.62	-	-	-	
			F		-	1.23	1.12	1.09	1.02	-	-	-	-	-	-	-	-	-	-
			G		-	1.31	1.18	1.08	0.96	-	-	-	-	-	-	-	-	-	-

TABLE VI
NO-FILM-COOLING HEAT TRANSFER COEFFICIENT DATA

Test 003 Data

$R_{\text{Throat}} = 2.44 \text{ cm } (.960 \text{ in})$

Copper Heat Sink Thrust Chamber

C_g Values Defined by Equation

<u>Z, cm (in.)</u> (1)	<u>A/A_T</u>	<u>Thermo- couple</u>	<u>(C_g) film</u>	<u>Average (C_g) film</u>	<u>Average (C_g) aw</u>
4.39 (1.73)	-3.36	A9	0.63	0.64	0.93
		B9	0.65		
5.66 (2.23)	-3.36	A8	0.69	0.68	0.99
		B8	0.67		
6.93 (2.73)	-3.36	A7	0.701	0.695	1.01
		B7	0.69		
10.67 (4.2)	-3.36	B5	0.64	0.64	.93
11.94 (4.7)	-3.36	A4	0.58	0.575	.835
14.38 (5.66)	-1.98	A3	0.64	0.62	.90
		B3	0.60		

(1) Z = Axial Distance From Film Coolant Injection Point in the Film Cooled Chamber (Fig. 13)

<u>Row</u>	<u>Circumferential Position</u>
Ox Inlet	0°
A	16° 30'
B	39°

TABLE VII
 HOOCOOL η I_{SP} FACTORS

<u>O/F (O₂/H₂)</u>	<u>η, I_{SP}</u>
.1	.900*
.3	.917*
.6	.938*
.9	.9607**
1.2	.9665**
2	.9570**
3	.9533**
4	.9525**
5	.9523**
7	.9522**
9	.9522**
12	.9522*

*Indicates Extrapolated Values

** Values Calculated from the ODE and No-Film-Cooling Curves
 on Figure 45

TABLE VIII
 COMPARISON OF ASYMPTOTIC ENTRAINMENT FRACTION MULTIPLIERS
 (k/k_0) FOR A VELOCITY RATIO OF UNITY

Source	.15 cm Slot Height	.038 cm Slot Height
Reference (1) - Ambient	1.6-1.9	
- Cold		2.2
Reference (2) - Hydrogen	1.3	
- Nitrogen		3.7-4.0
Present Data	2.8-4.3 (Varies with core O/F)	

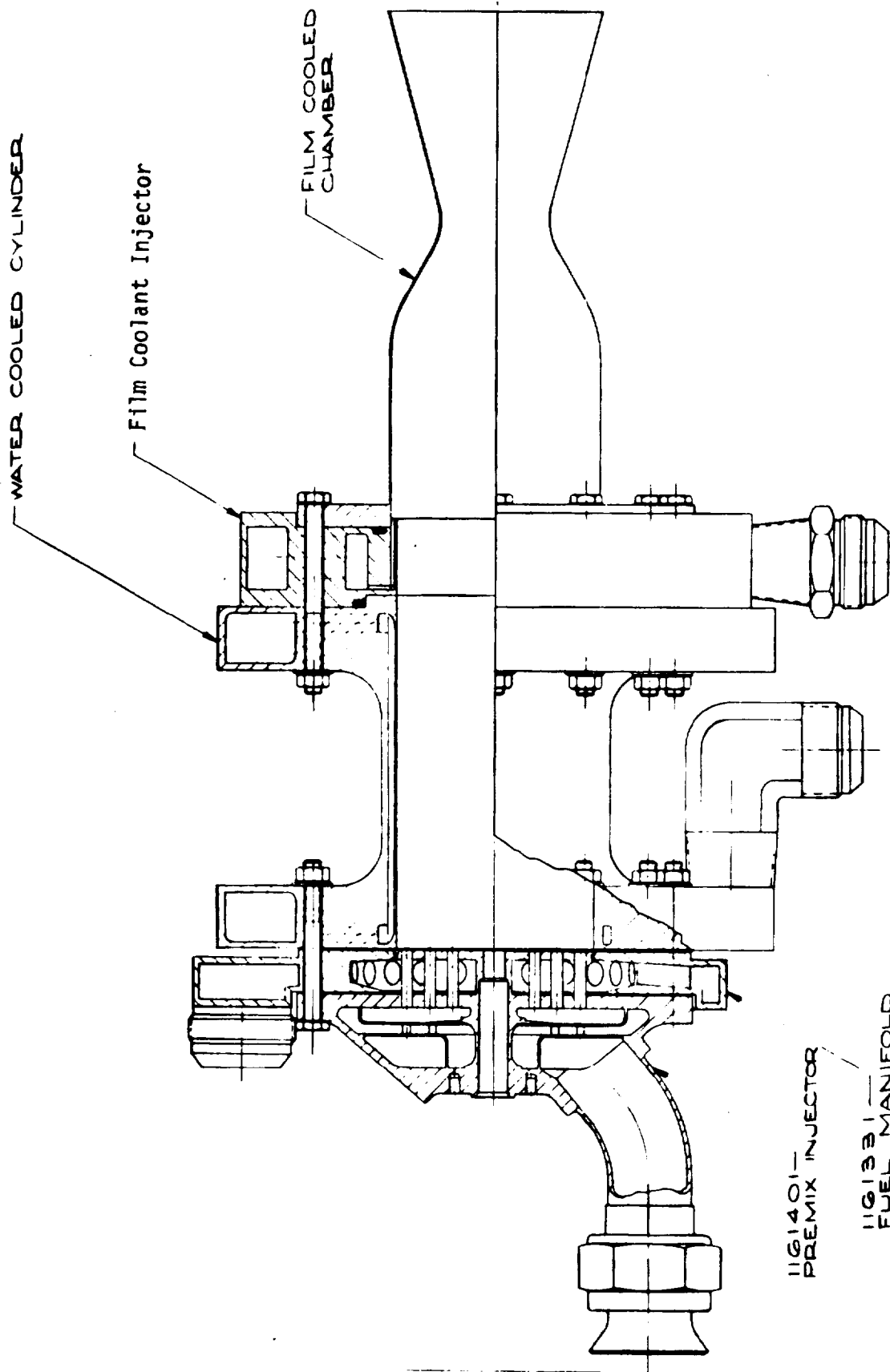


Figure 1. Film Cooling Test Assembly (P/N 1182135)

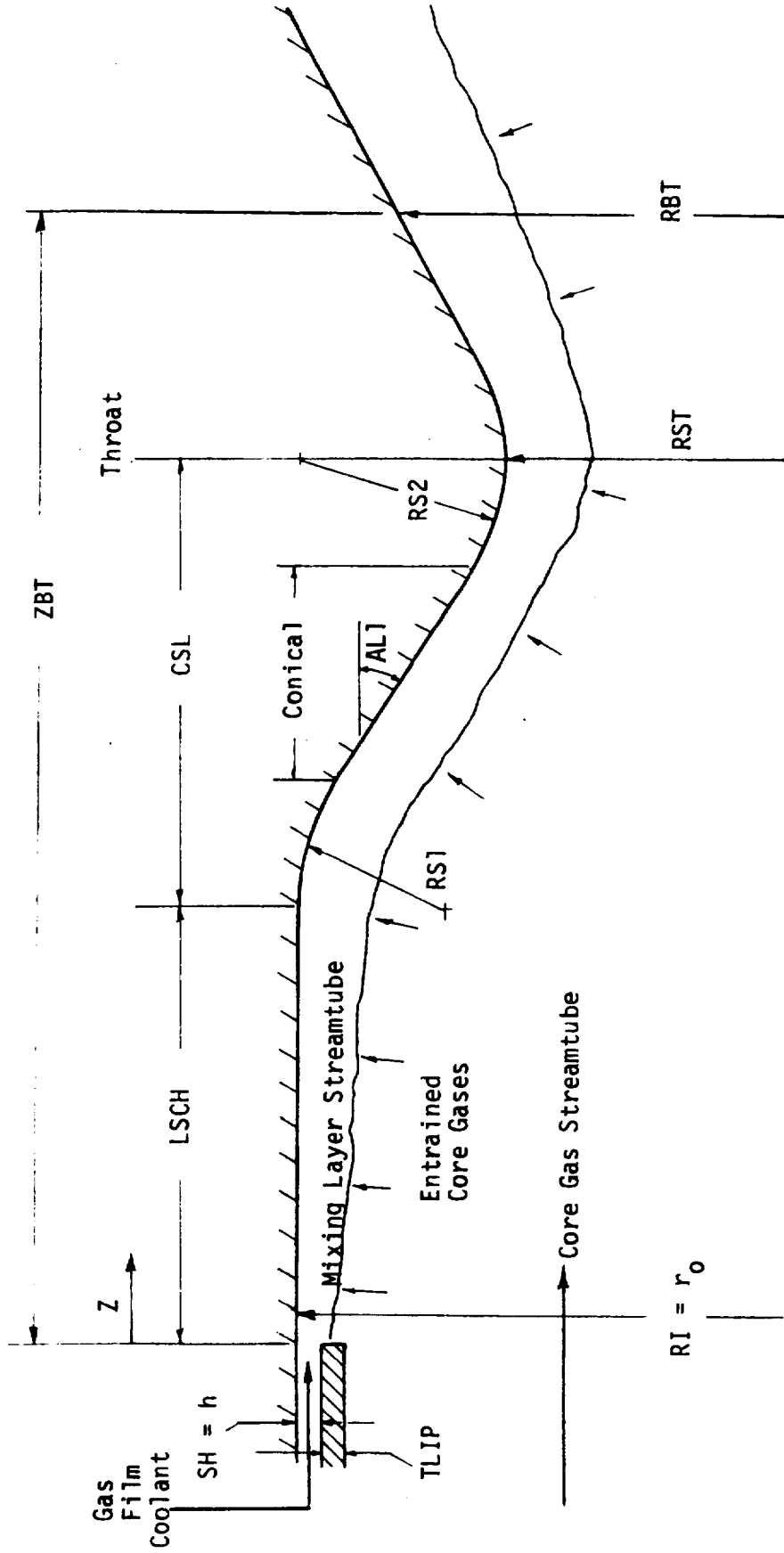


Figure 2. Entrainment Film Cooling Model Schematic

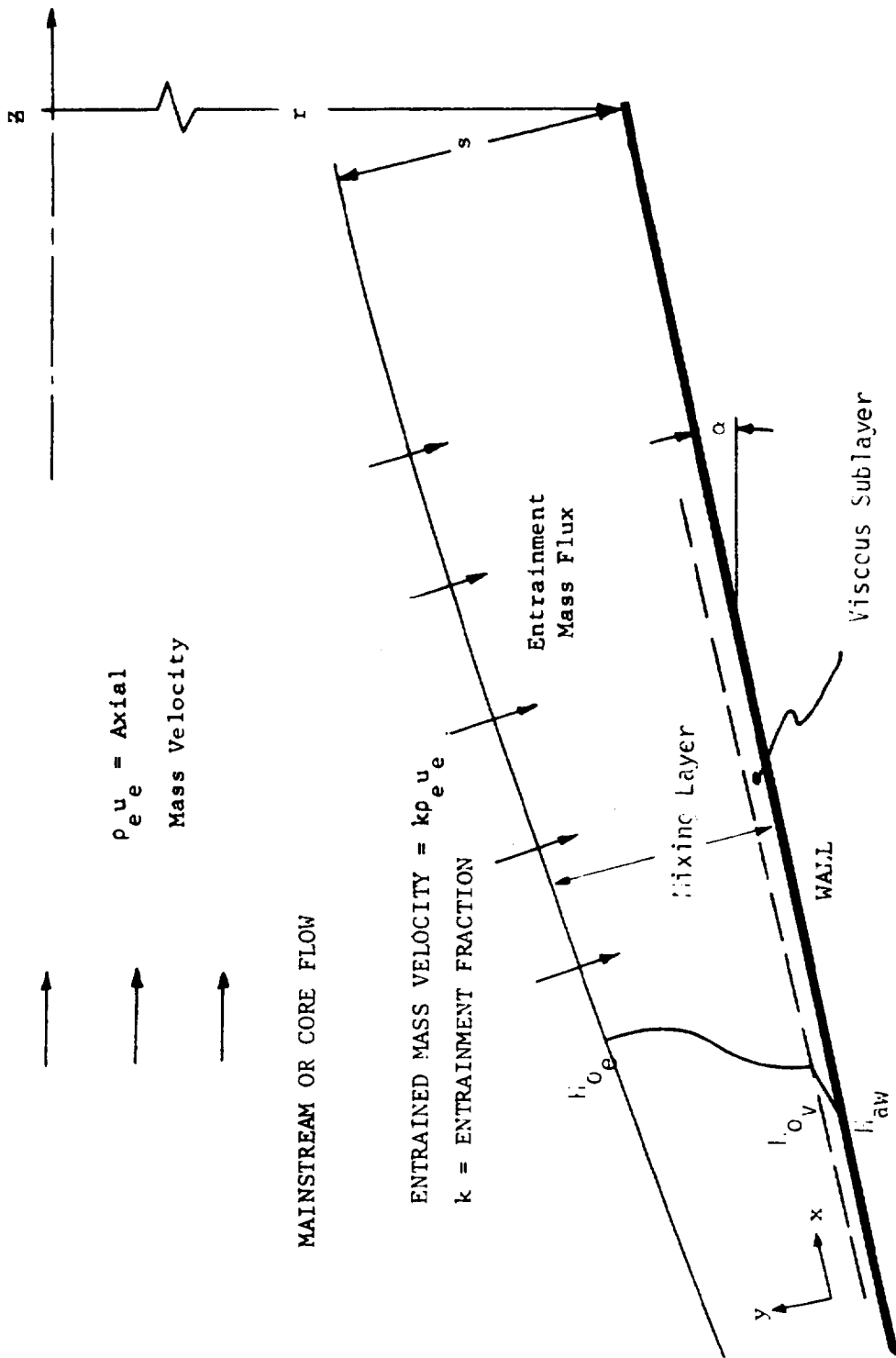


Figure 3. Mixing Layer Schematic

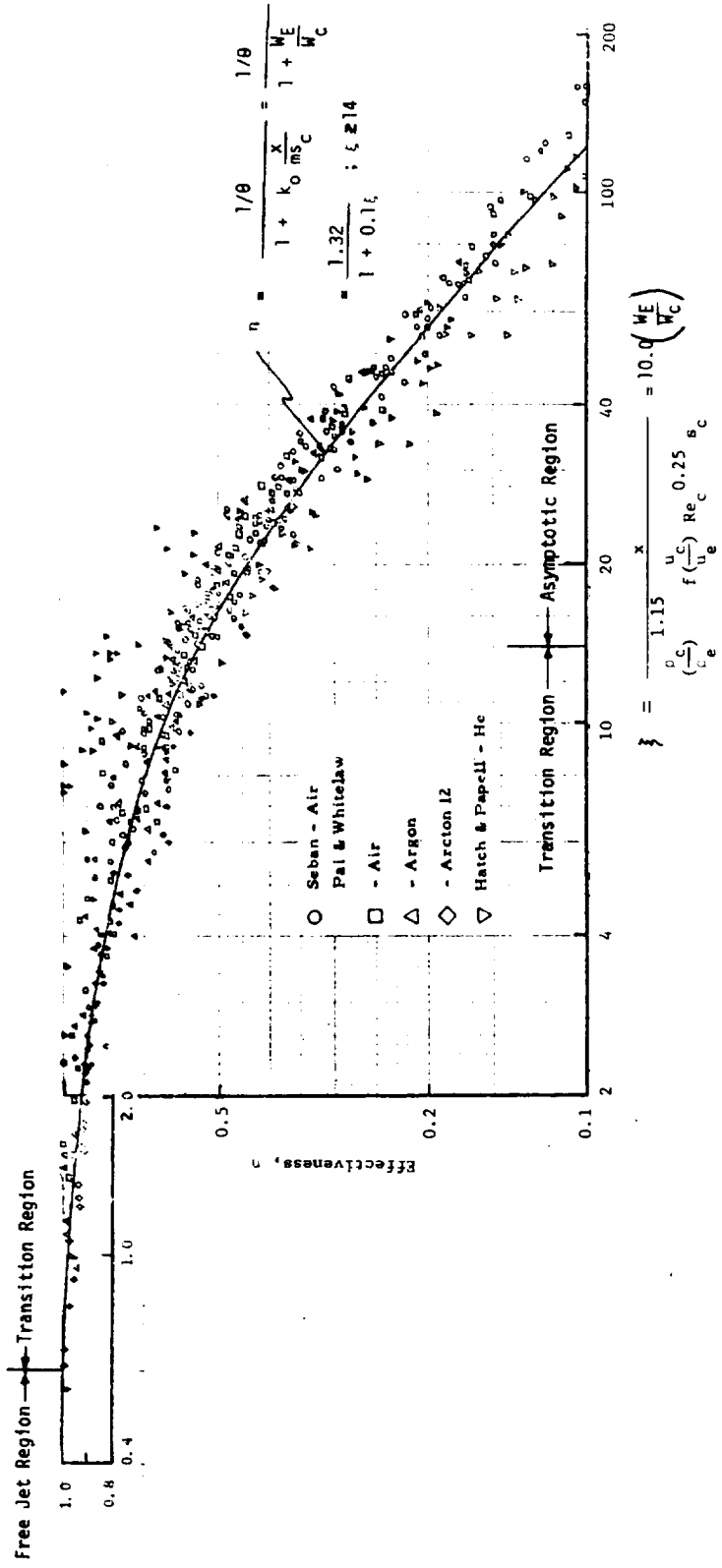


Figure 4. Subsonic Effectiveness vs. M_E/M_C Correlation

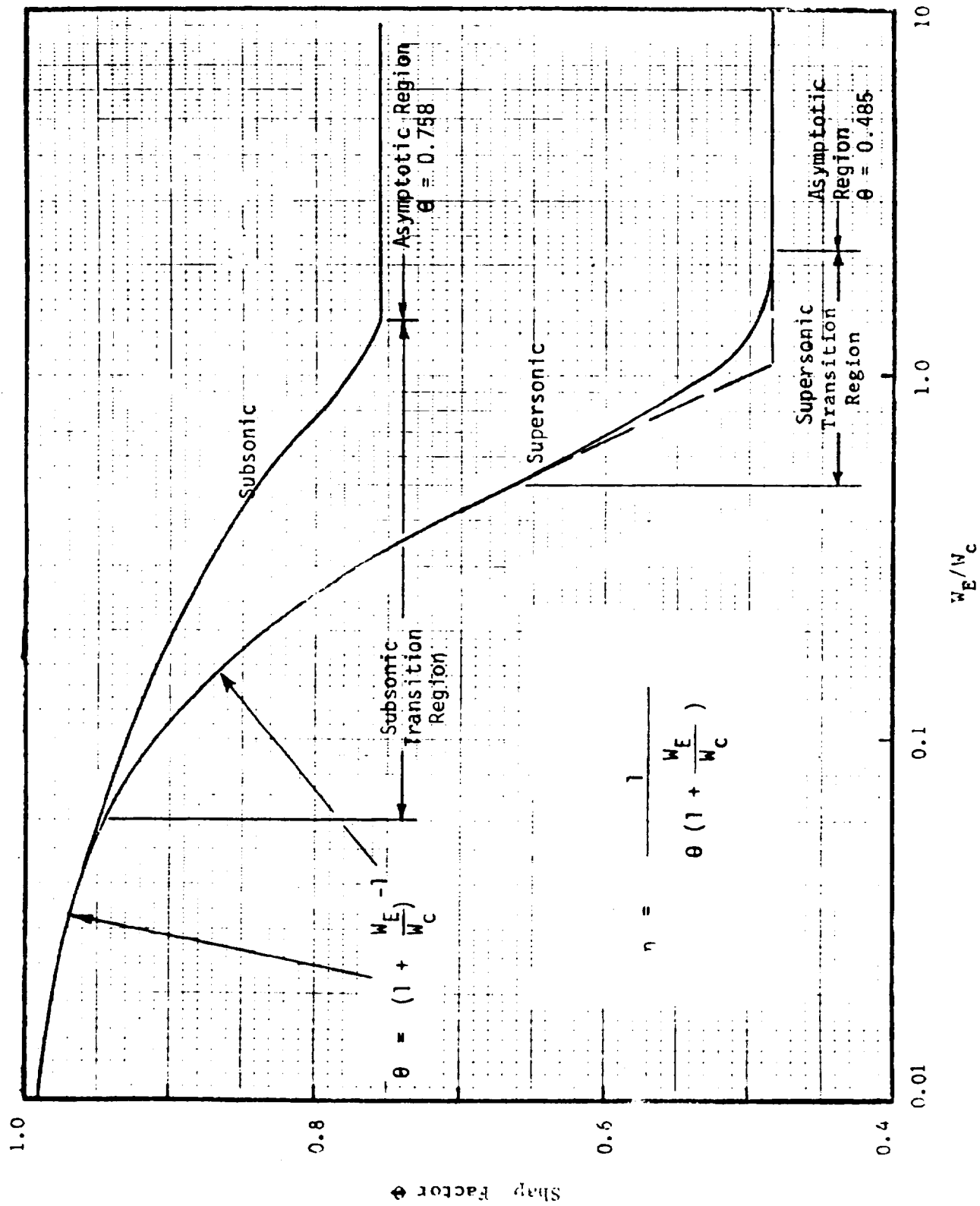


Figure 5. Shape Factor Correlations

$$\theta = \text{Shape Factor} = \frac{c_e - c_b}{c_e - c_w}$$

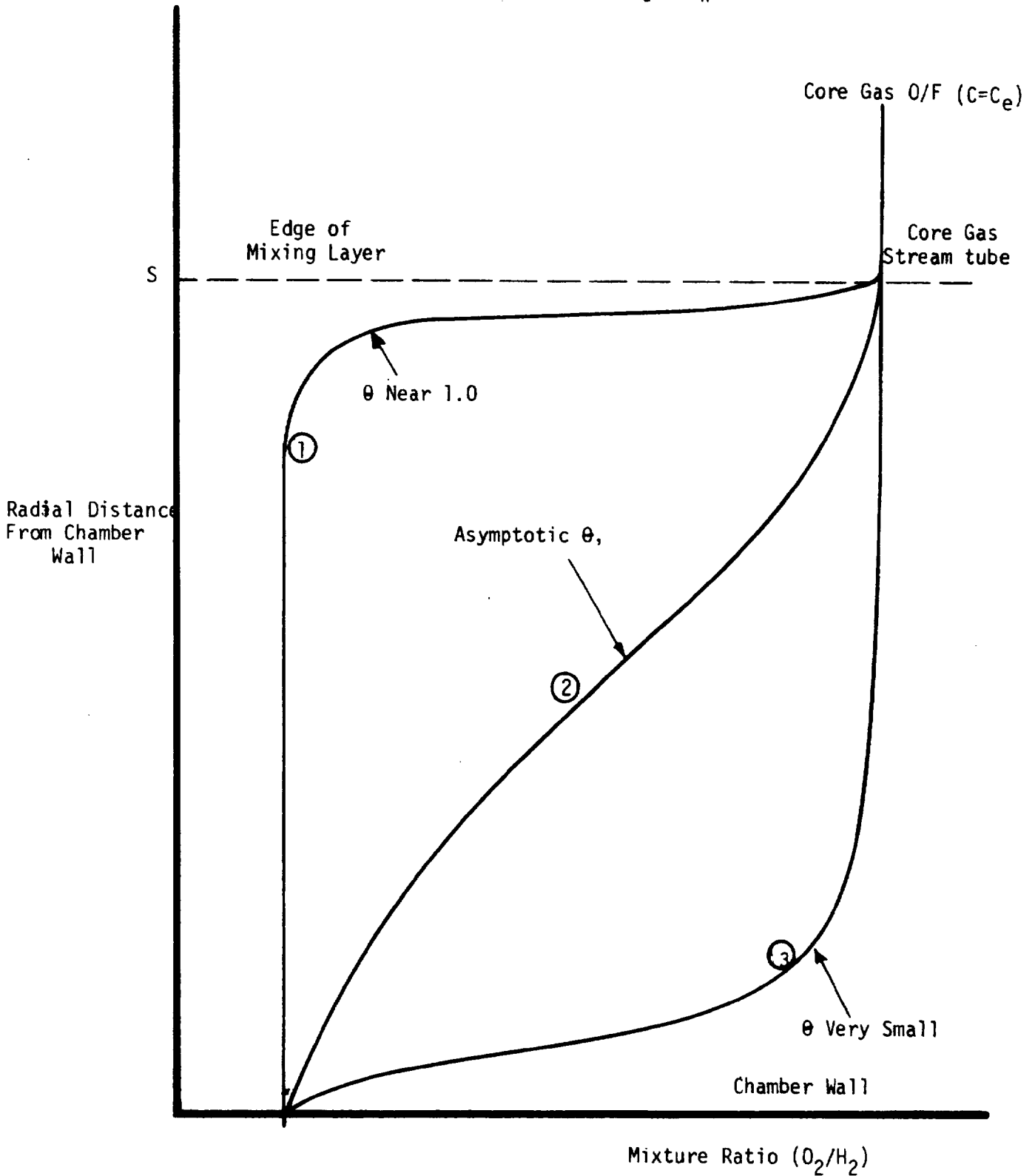


Figure 6. Typical Mixture Ratio Profiles

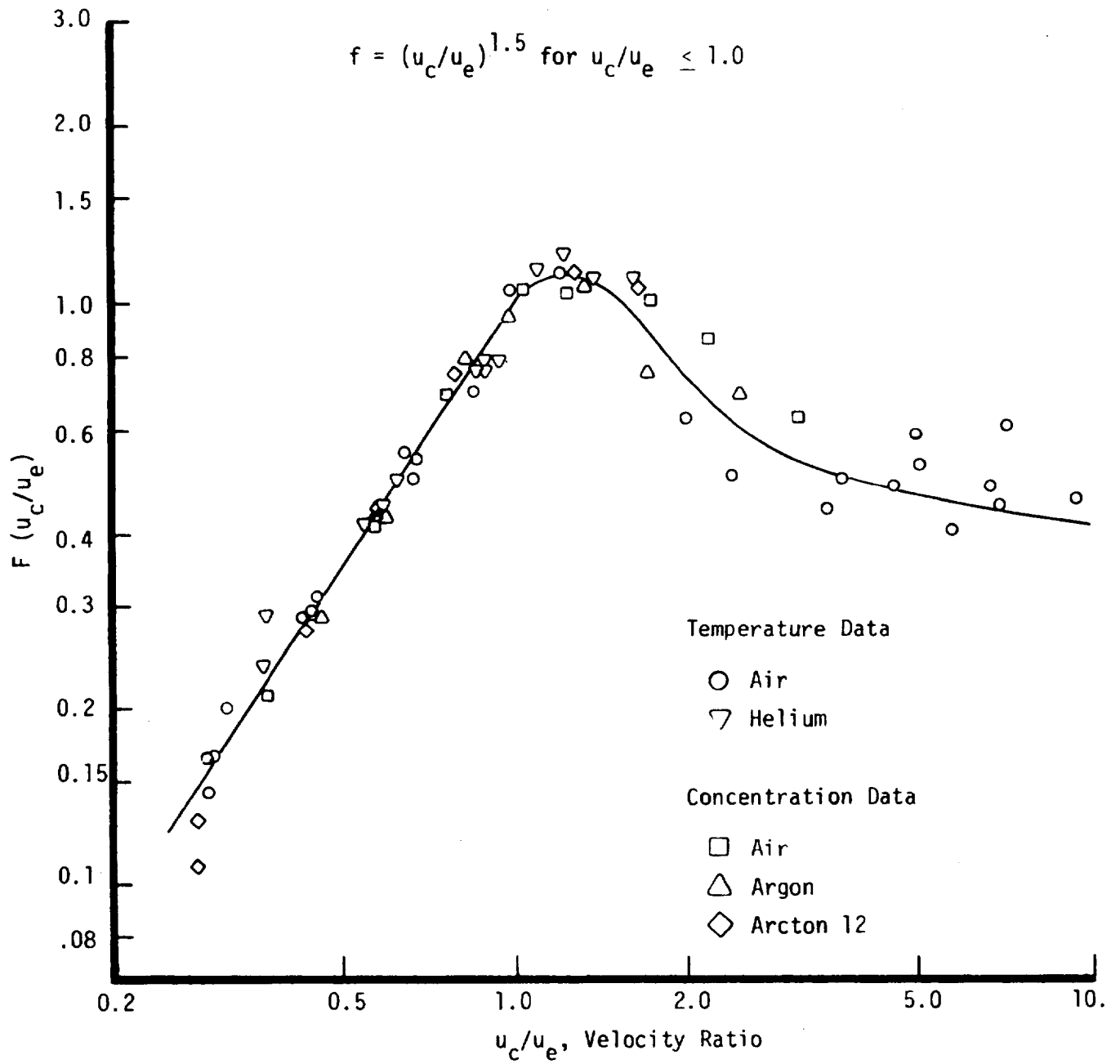


Figure 7. Velocity Ratio Correlating Function

22

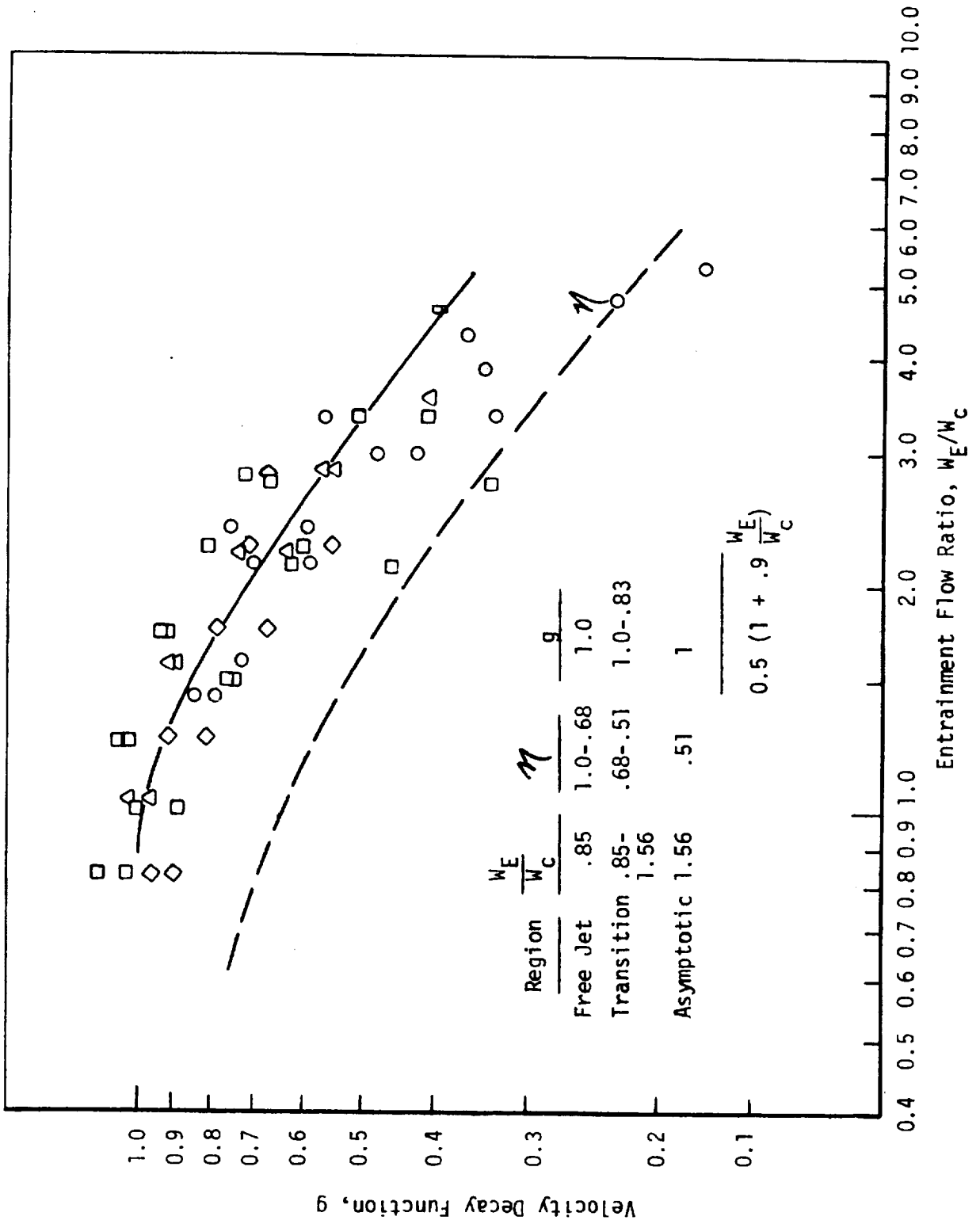


Figure 8. Velocity Decay Function

1. OPTION 1: FILM OR REGENERATIVE COOLING OPTION

(a) Regeneratively Cooled Chamber



1. No Film Cooling
2. Subsonic and/or Supersonic Regions
3. Coolant Flow Path Optional

(b) Film Cooled Chamber



1. No Regenerative Cooling
2. Subsonic Film Coolant Injection
3. Supersonic Region Optional

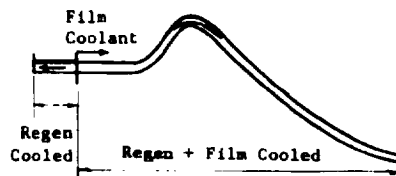
(c) Film Cooled Nozzle



1. No Regenerative Cooling
2. Supersonic Film Coolant Injection into Supersonic Region

2. OPTION 2: COMBINED COOLING OPTION

(a) Film and Regeneratively Cooled Chamber



1. Film Coolant Injection in Subsonic or Supersonic Region.
2. Regenerative Cooling Upstream of Injection Point, Regen + Film Cooling Downstream.
3. Regen Section can be a Film Coolant Injecting Sleeve; However, two Analysis Cases Required:
 - (a) Case 1 - Option 1a (Sleeve)
 - (b) Case 2 - Option 2a (Regen + Film)
4. Regen Coolant Flow Path Optional

(b) Film and Regeneratively Cooled Nozzle



1. Supersonic Injection into Subsonic Region.
2. Regen Coolant Flow Path Optional

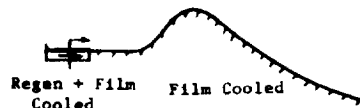
3. OPTION 3: SEGMENTED COOLING OPTION

(a) Regenerative Cooling Upstream



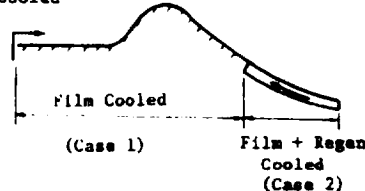
1. Regenerative Cooling Upstream of Injection Point, Film Cooling Downstream.
2. Subsonic or Supersonic Injection
3. Regen Cooled Section can be a Film Coolant Injecting Sleeve (Input TSIN = 0)

(b) Combined Cooling Upstream



1. Similar to Option 3a except Film Coolant Injected in Regen Cooled Section.

(c) Film Cooling Upstream



1. Subsonic or Supersonic Injection
2. Two Analysis Cases Required:
 - (a) Case 1 - Option 1b Analysis for Entire Chamber.
 - (b) Case 2 - Option 2b Analysis for Film + Regen Cooled Region (ISOL = 0, Taw Input)

Figure 9. HOCOOL Heat Transfer Analysis Options

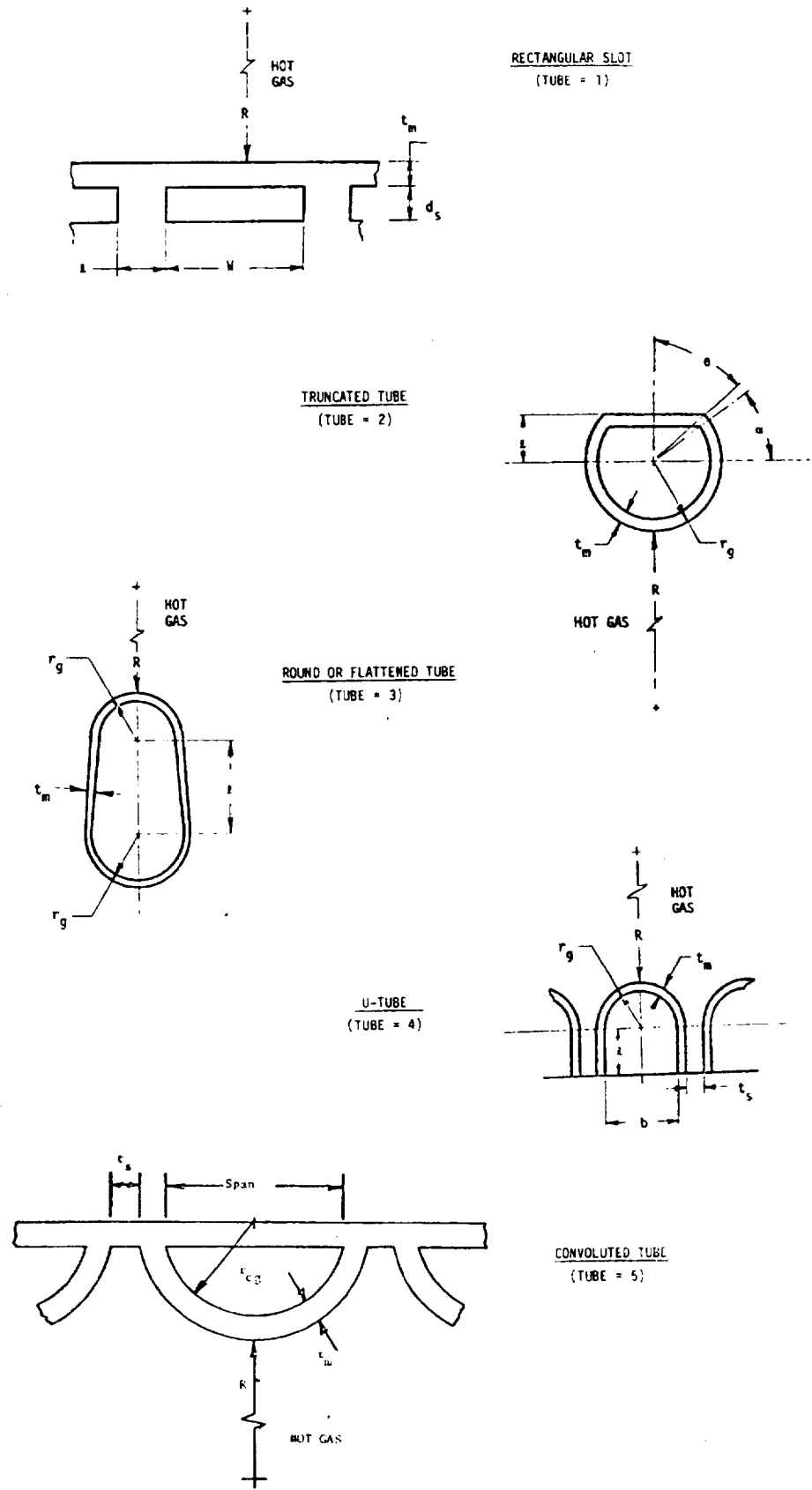


Figure 10. Regenerative Coolant Passage Geometries

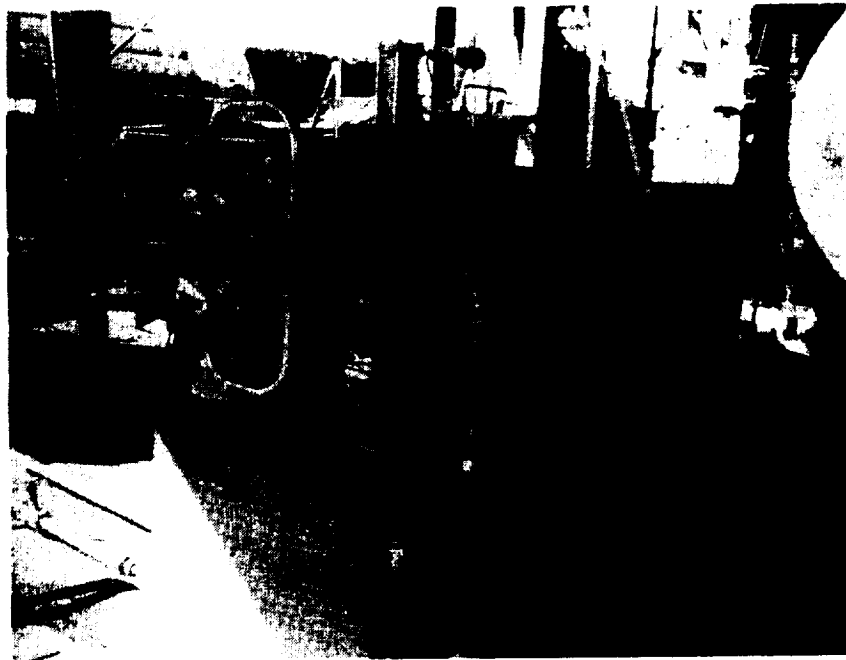
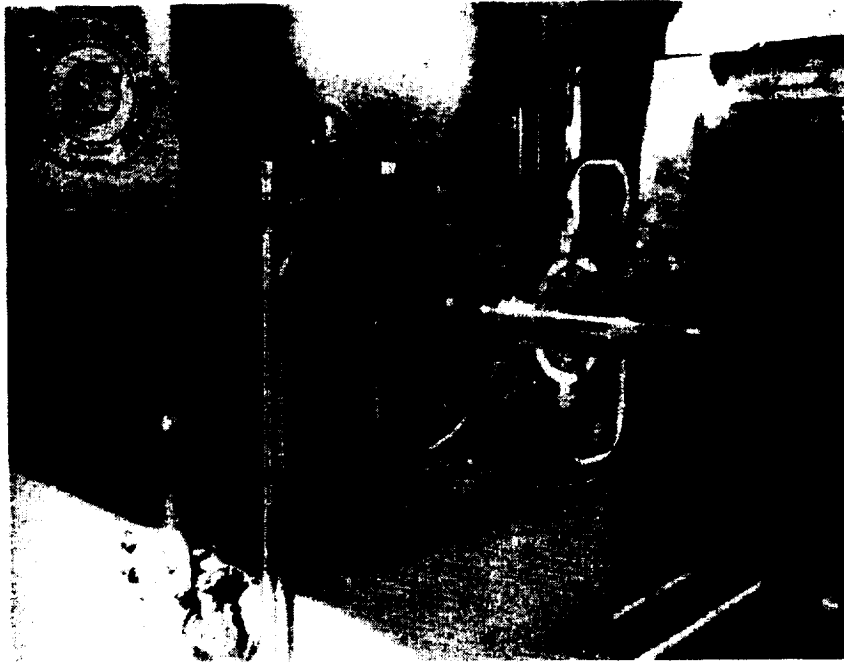


Figure 11. Film Cooling Test Assembly Mounted on Test Stand

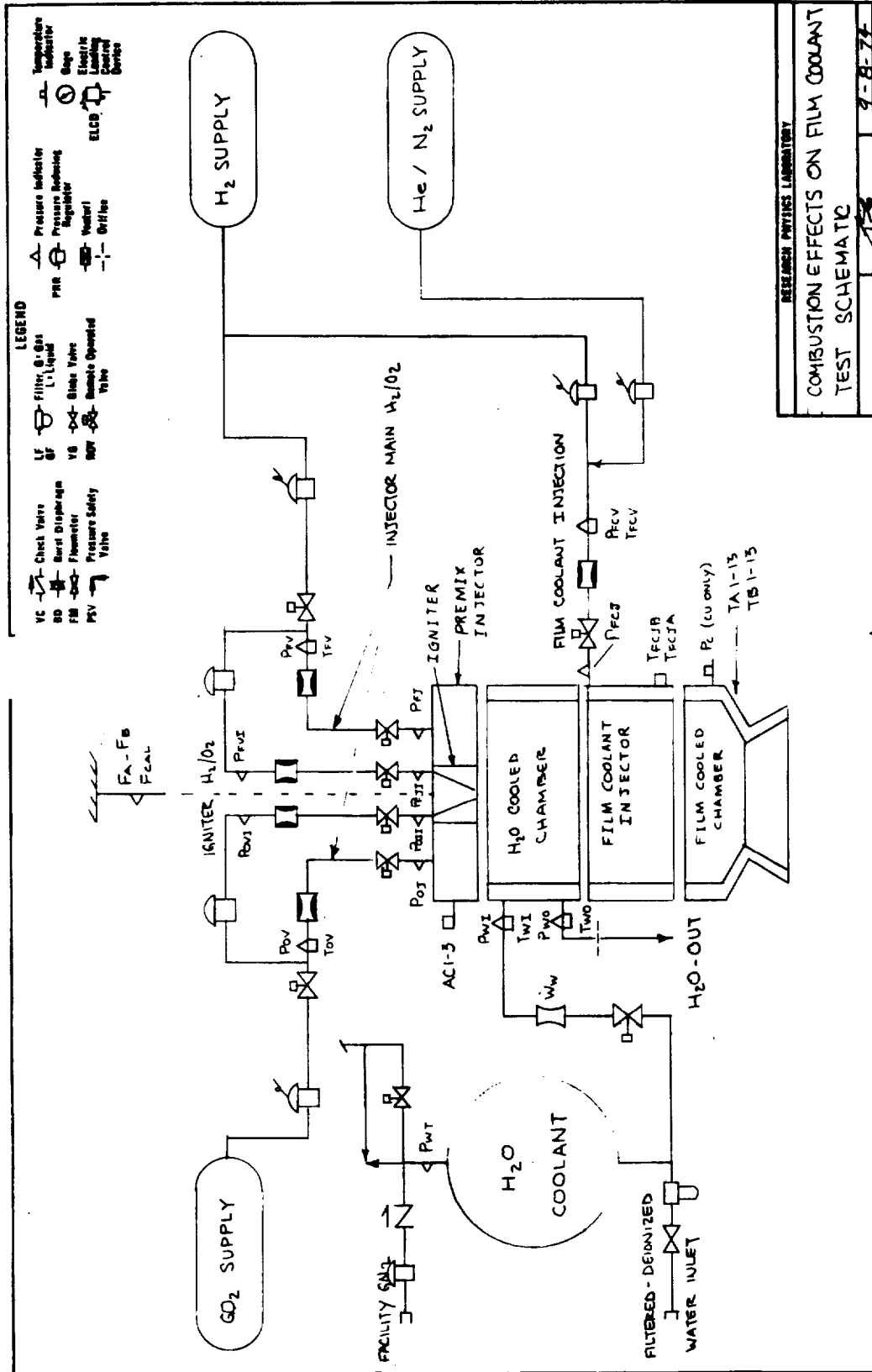


Figure 12. Schematic Diagram of Test System

ODE Computer Program Results
Pc = 300 psia
Ambient Temperature Propellants

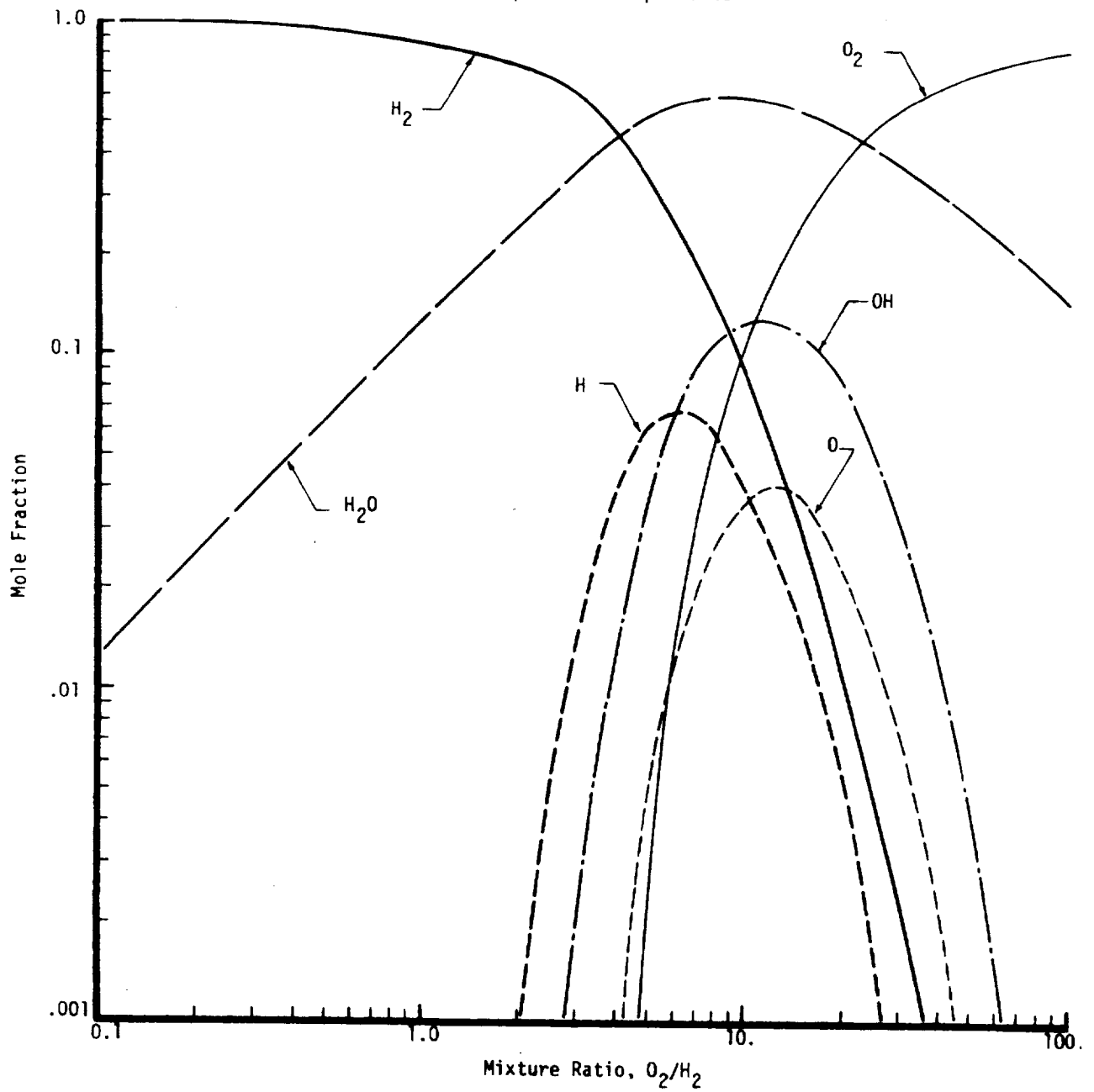


Figure 14. O_2/H_2 Core Gas Composition

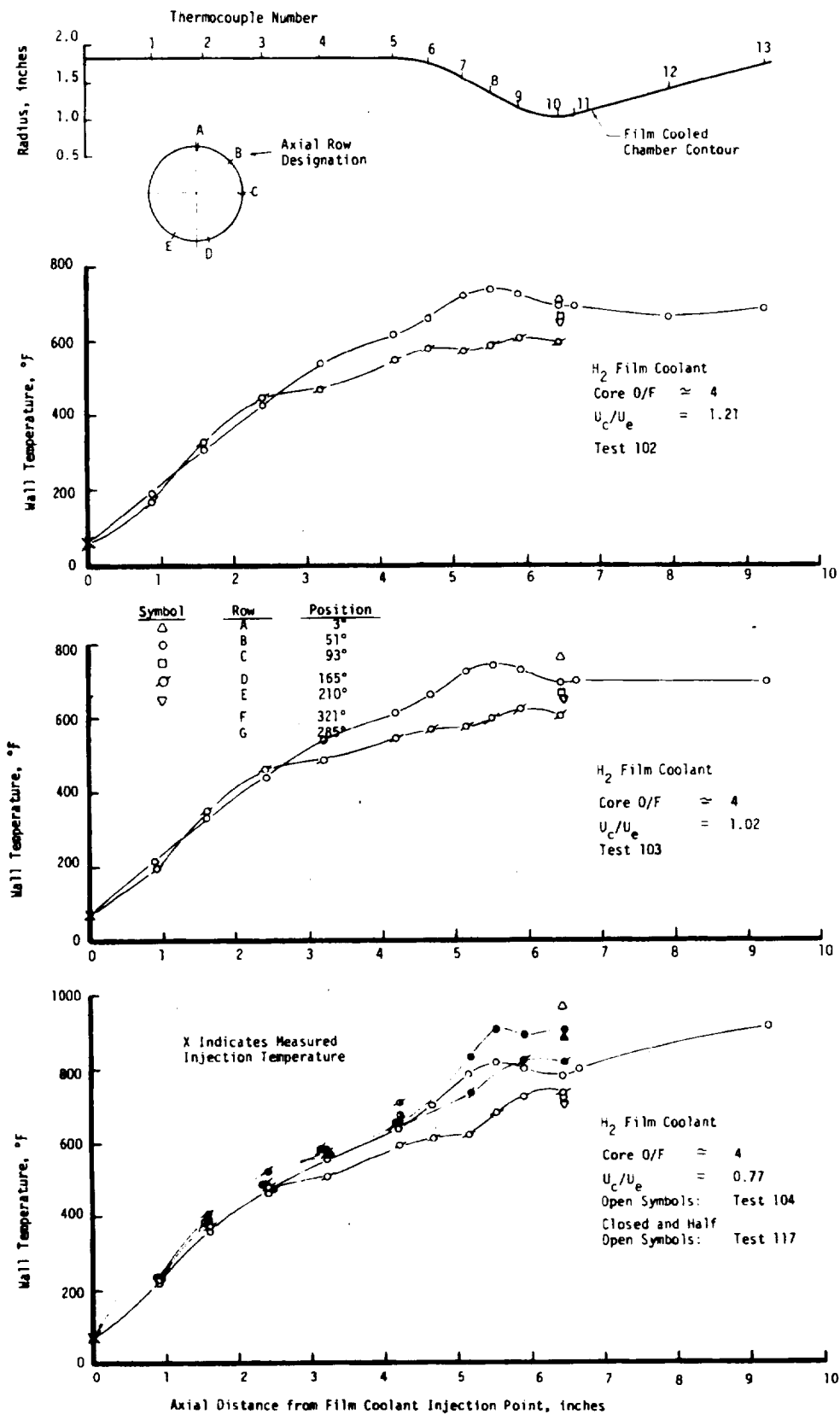


Figure 15. Steady State Wall Temperatures Measured with Core Gas O/F = 4

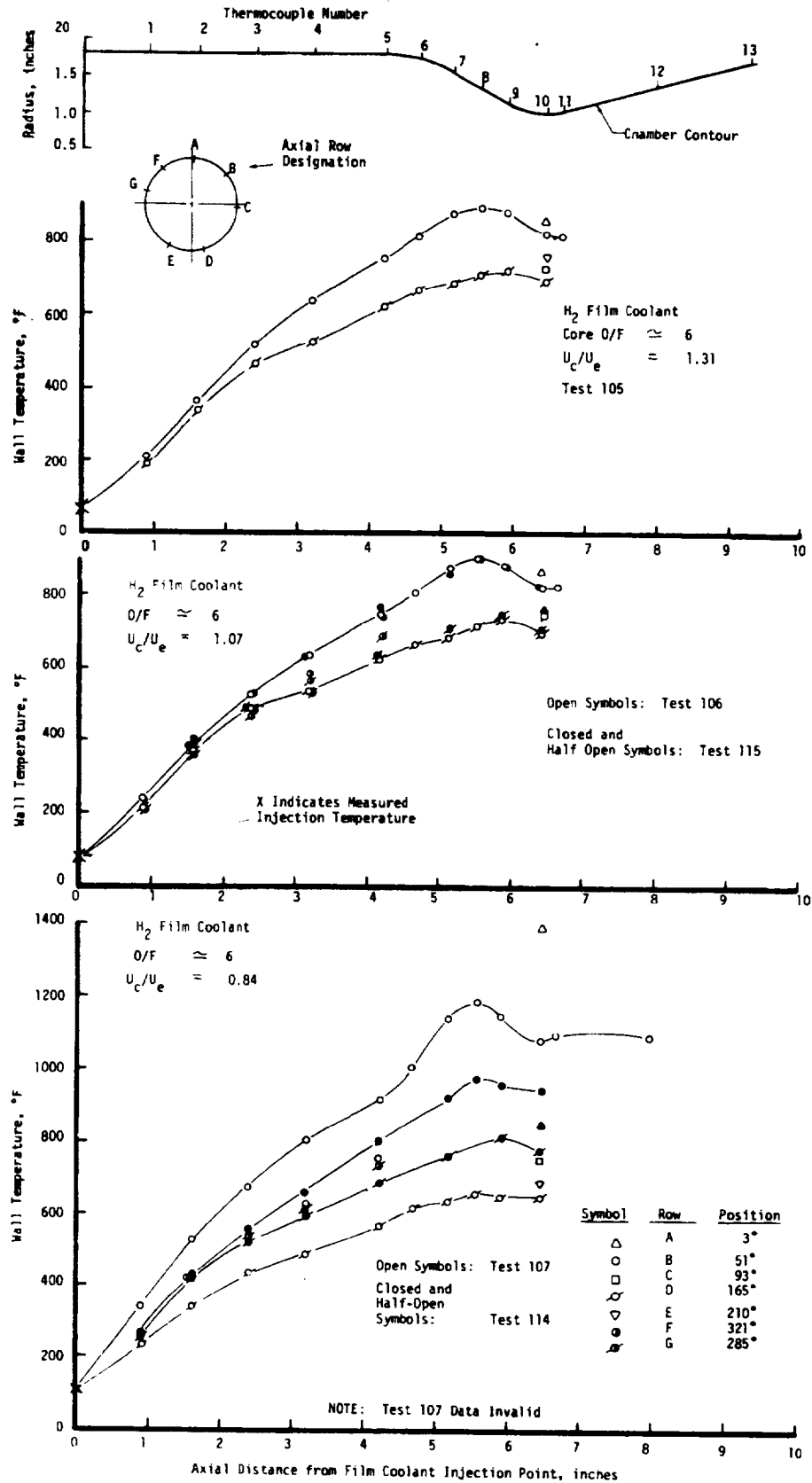


Figure 16. Steady State Wall Temperature Measured with Core Gas O/F = 6

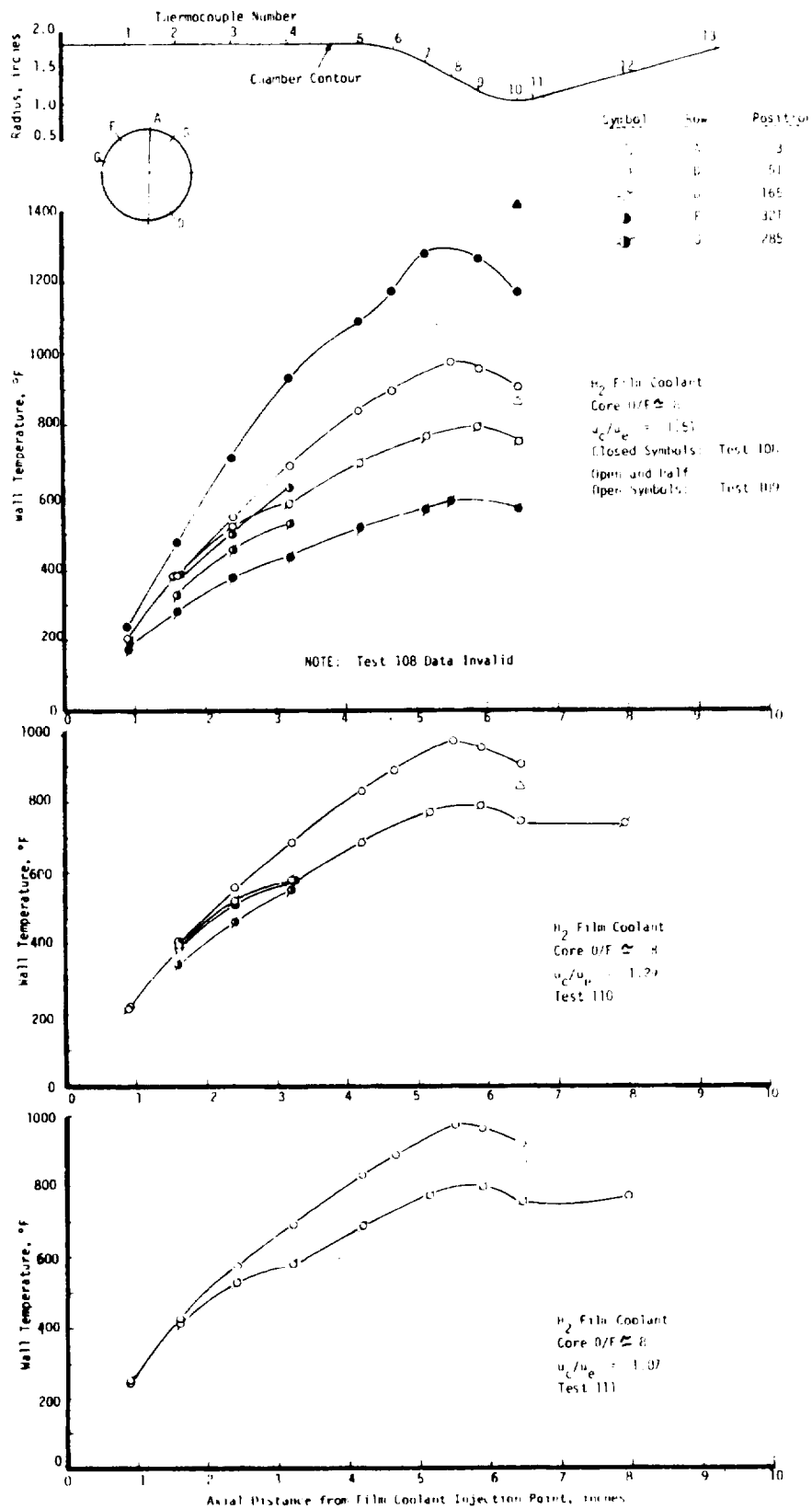


Figure 17. Steady State Wall Temperature Measured with Core Gas O/F = 8

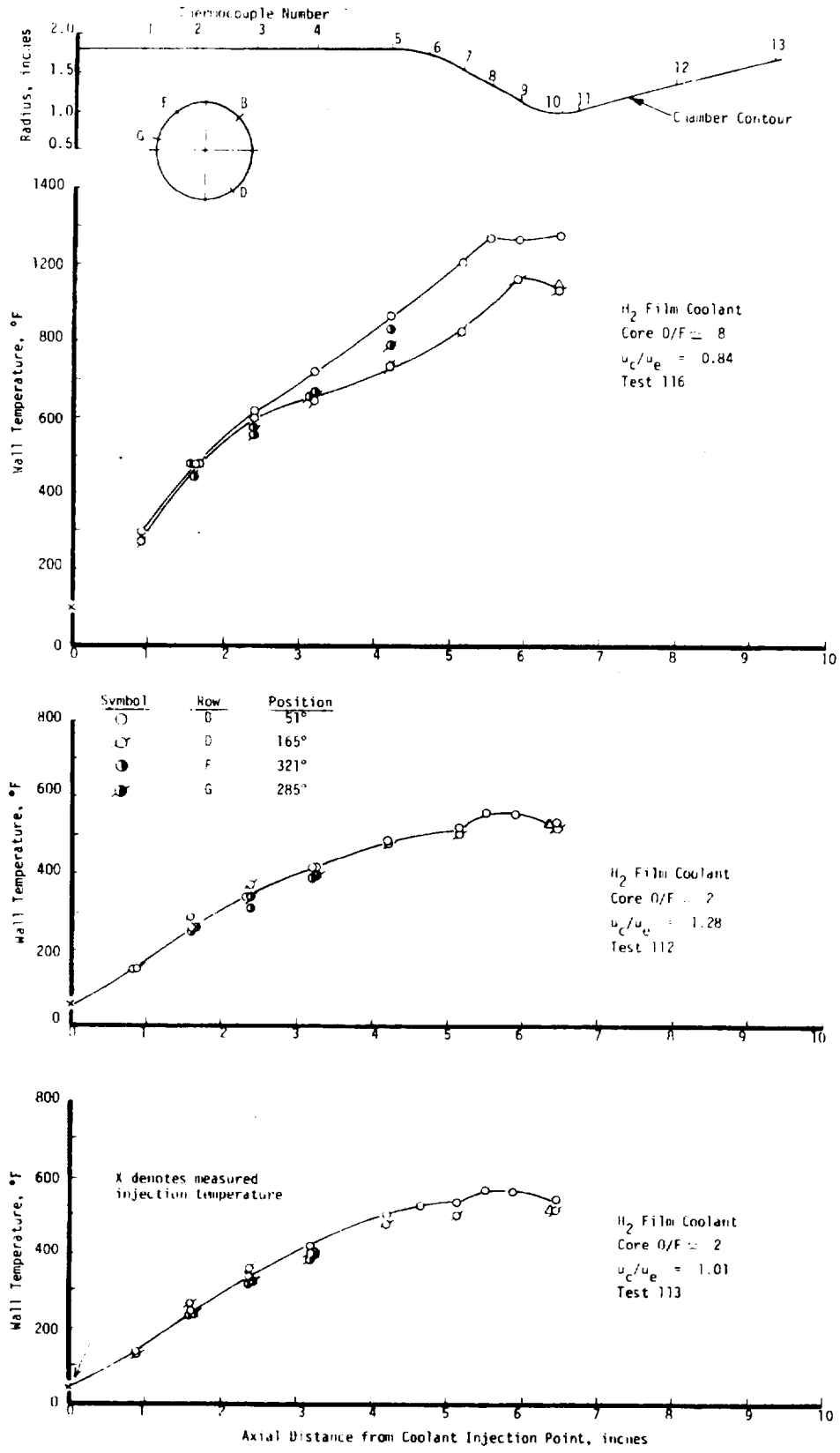


Figure 18. Steady State Wall Temperature Measured with Core Gas O/F = 8 and 2

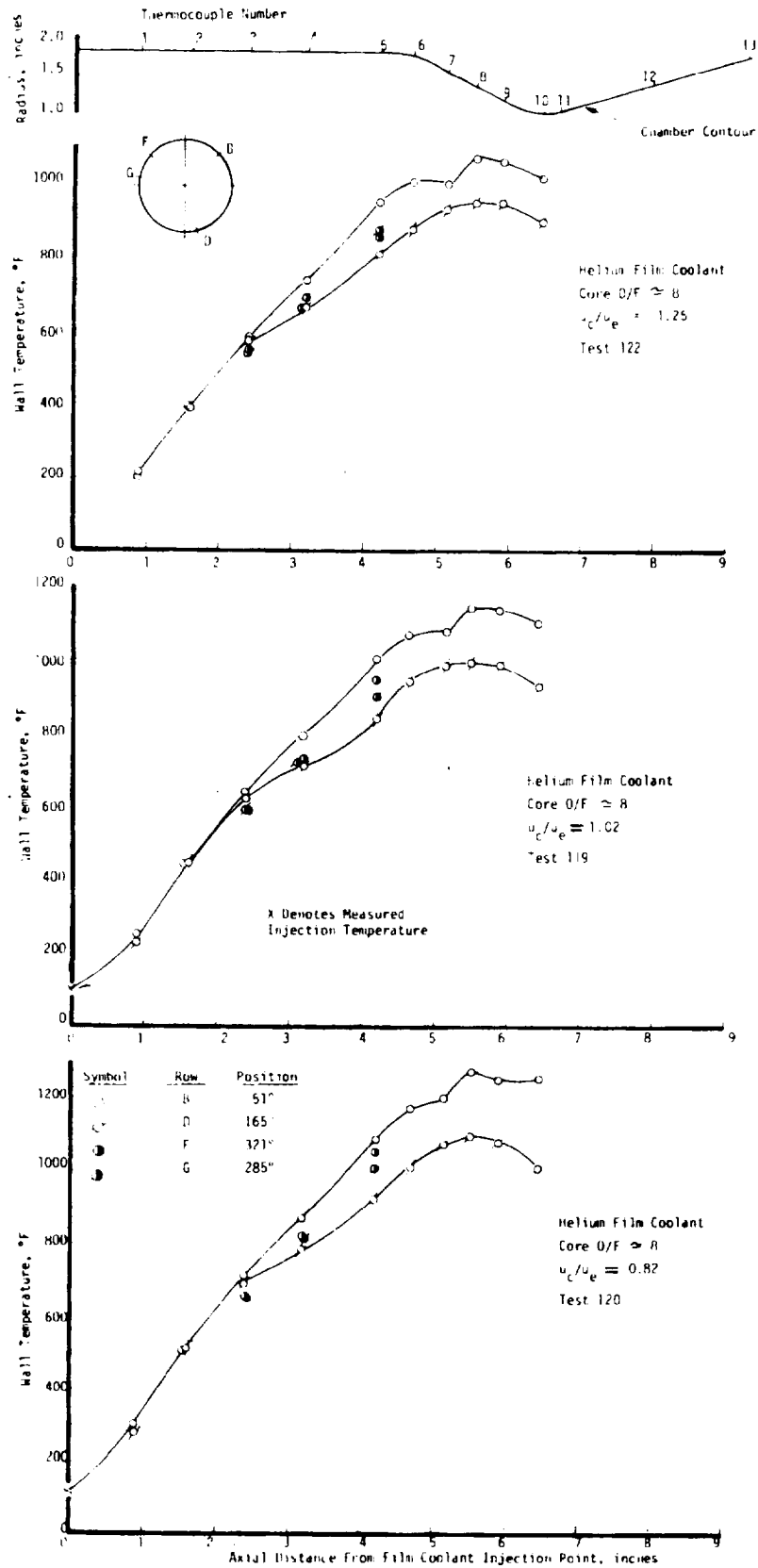


Figure 19. Measured Wall Temperatures, Helium Film Coolant

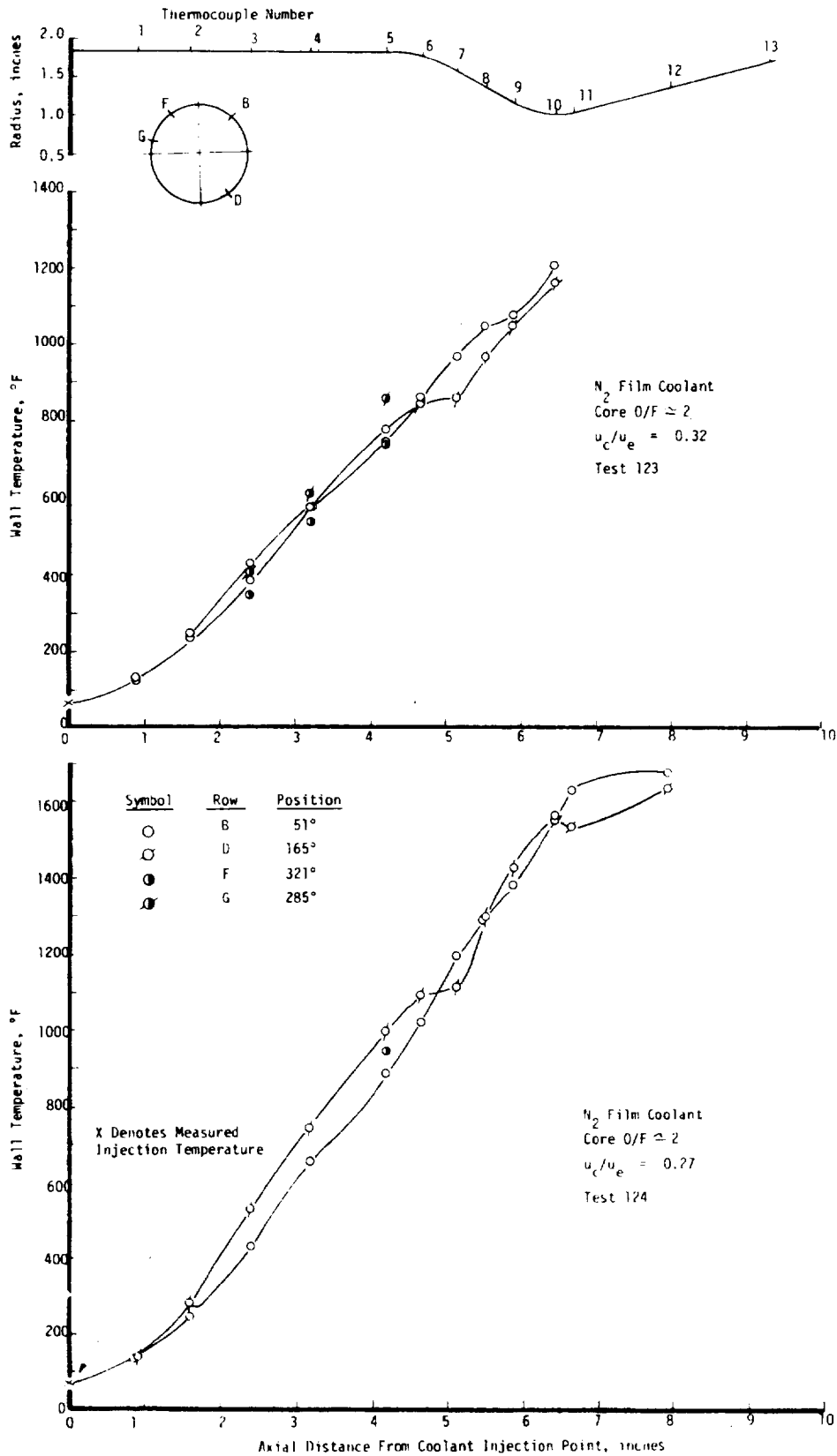


Figure 20. Measured Wall Temperatures, Nitrogen Film Coolant

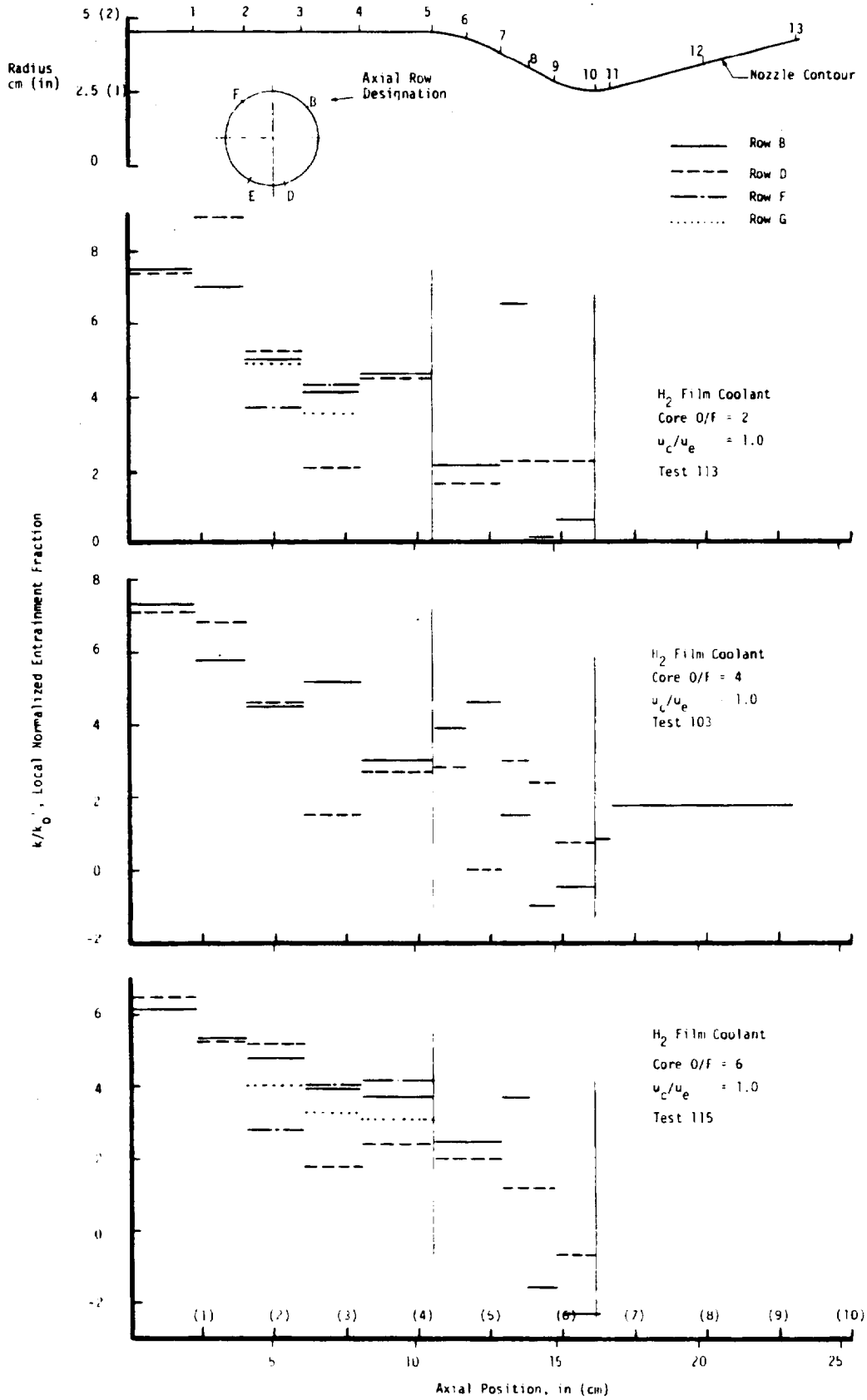


Figure 21A. Circumferential Distribution of Entrainment Fraction, Hydrogen Film Coolant

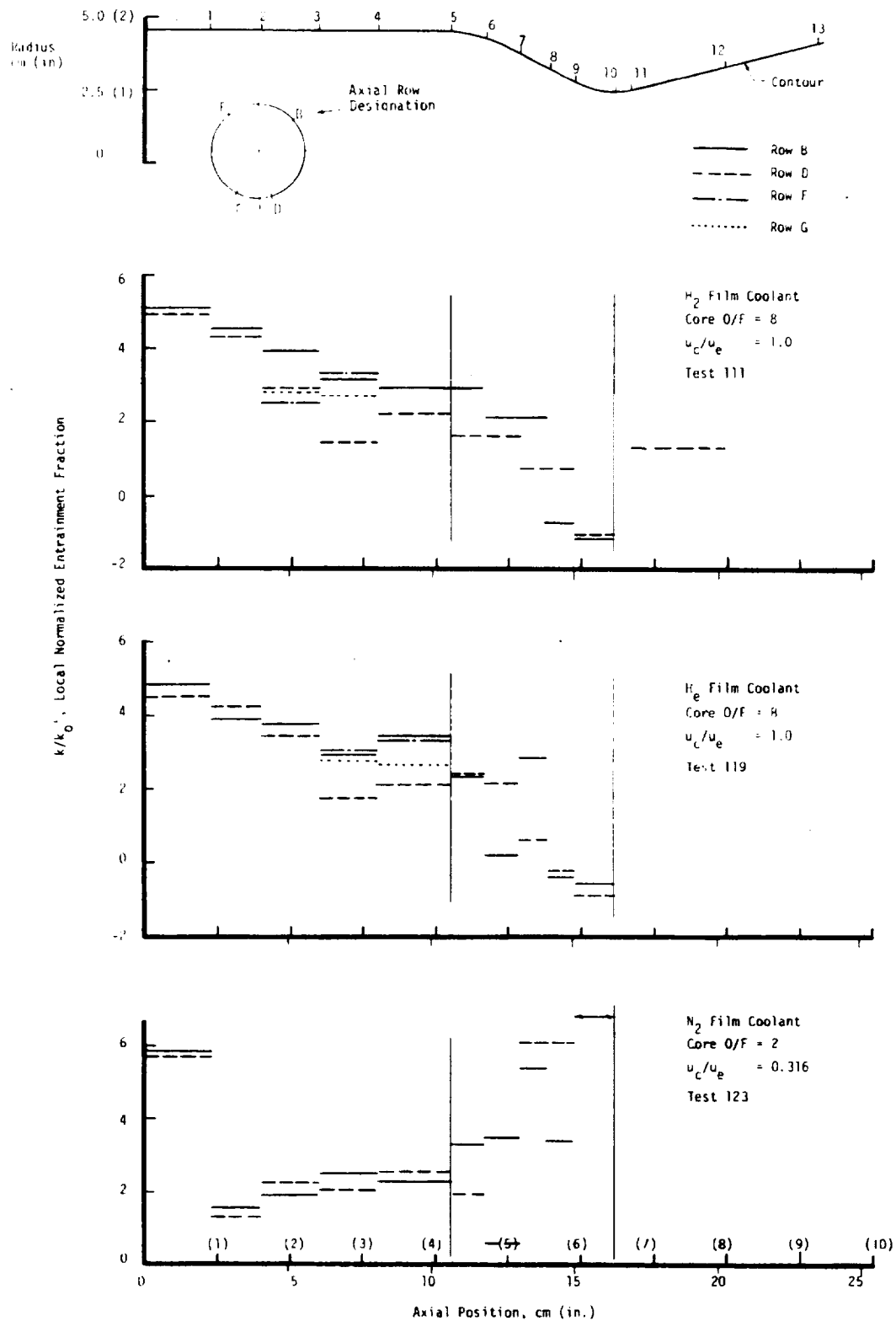


Figure 21B. Circumferential Distribution of Entrainment Fraction, Hydrogen, Helium, and Nitrogen Film Coolants

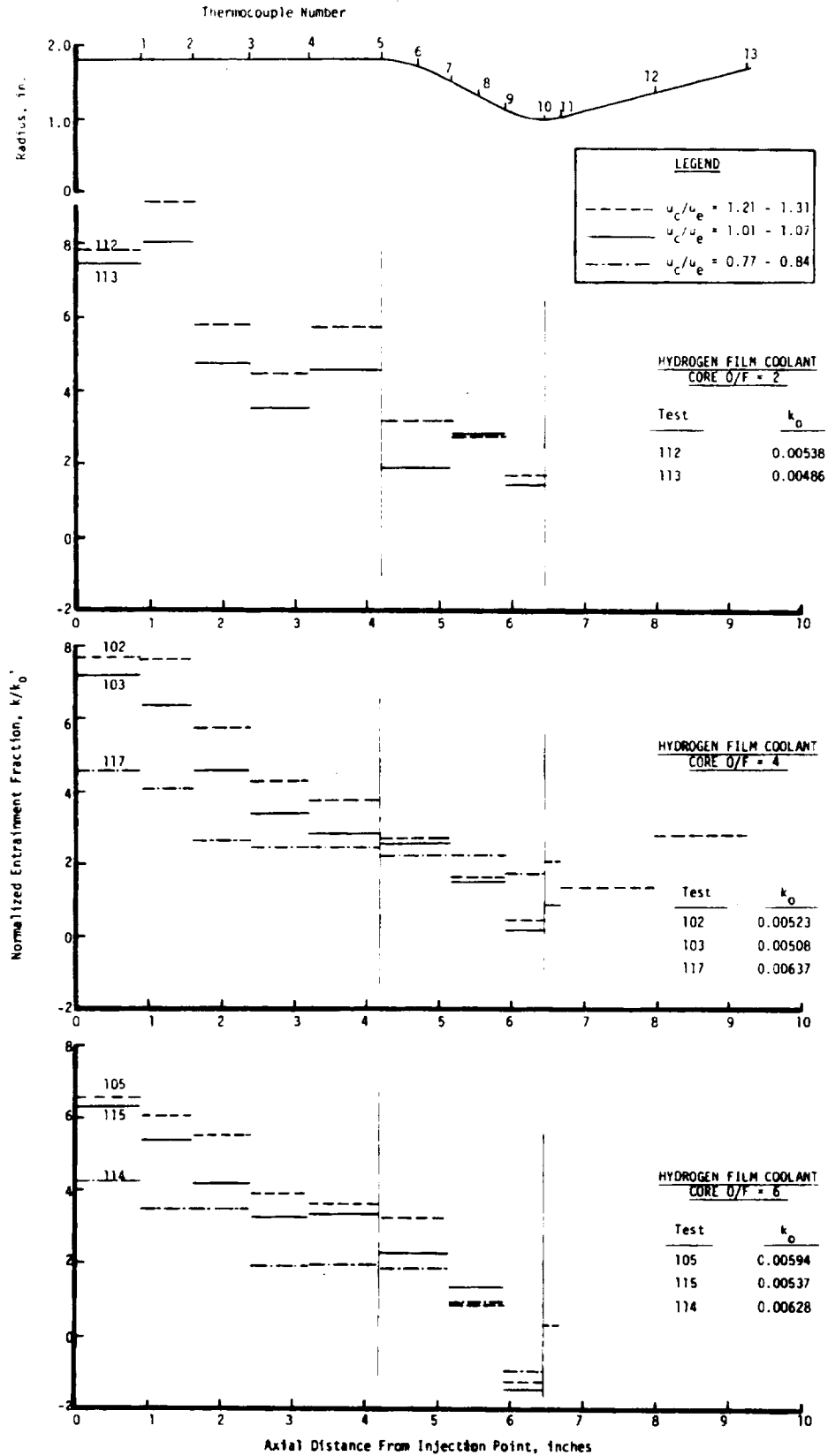


Figure 22. Averaged Entrainment Fractions, Hydrogen Film Coolant

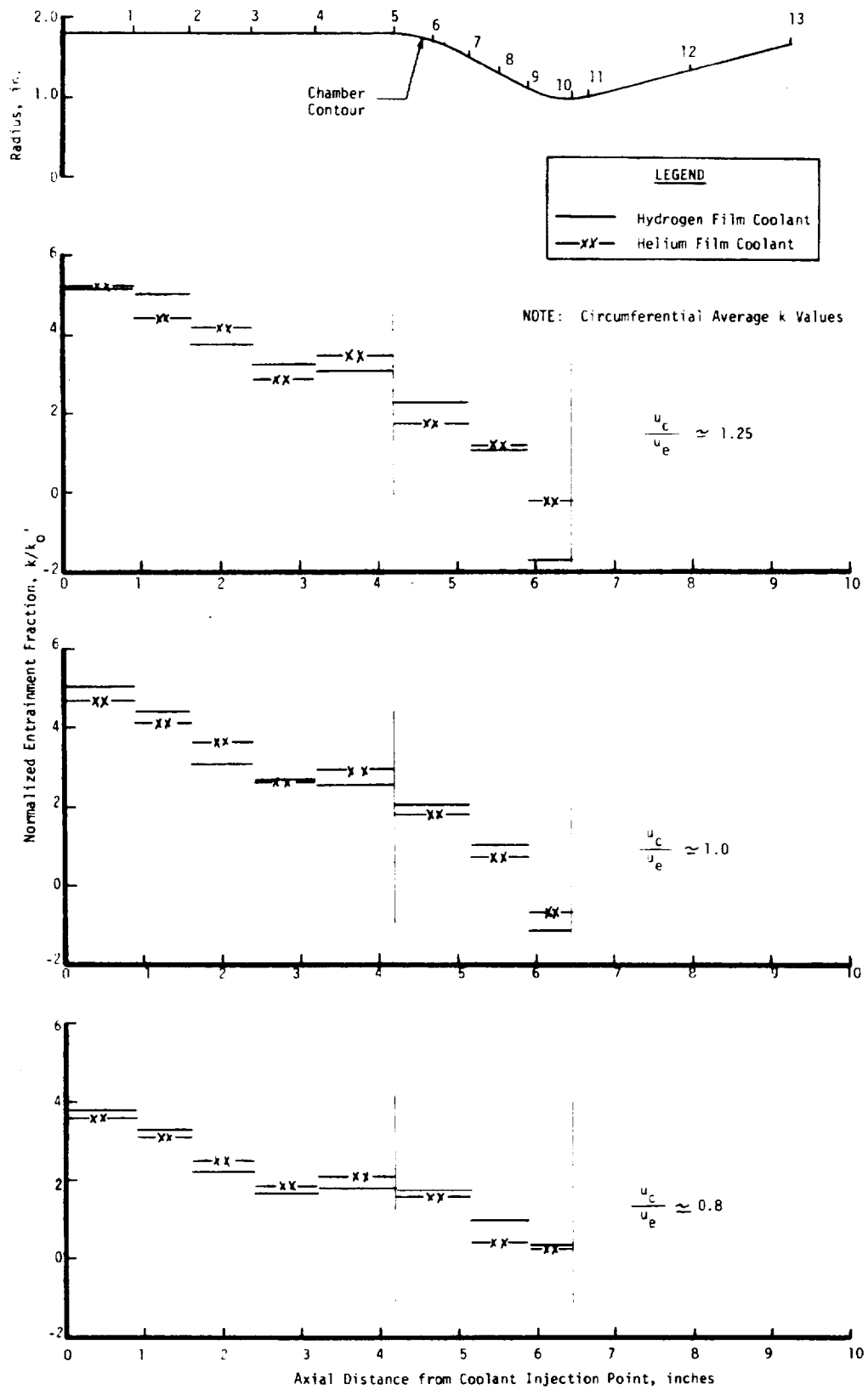


Figure 25. Comparison of Hydrogen and Helium Entrainment Fraction

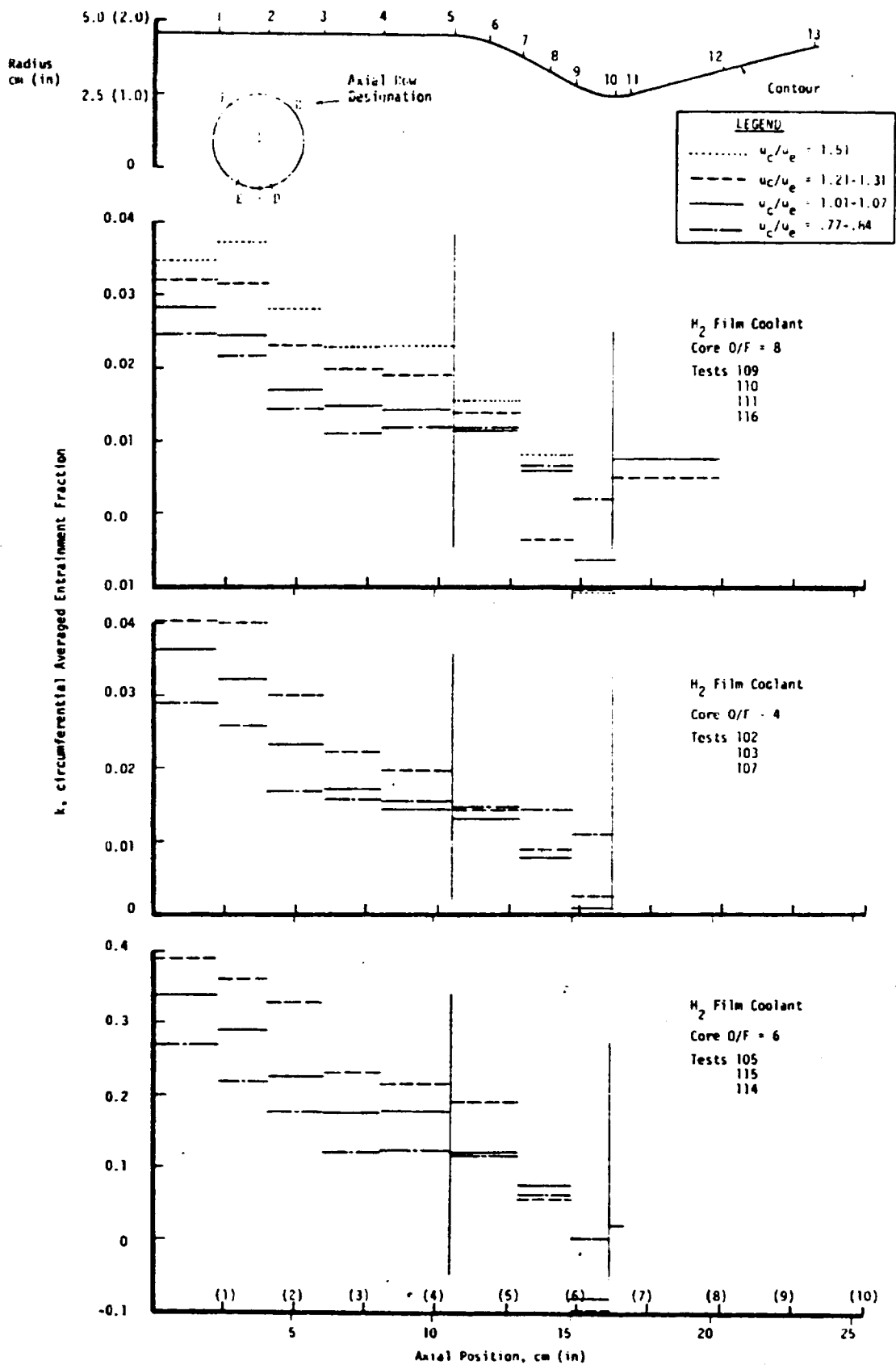


Figure 26. Absolute Entrainment Fraction Data

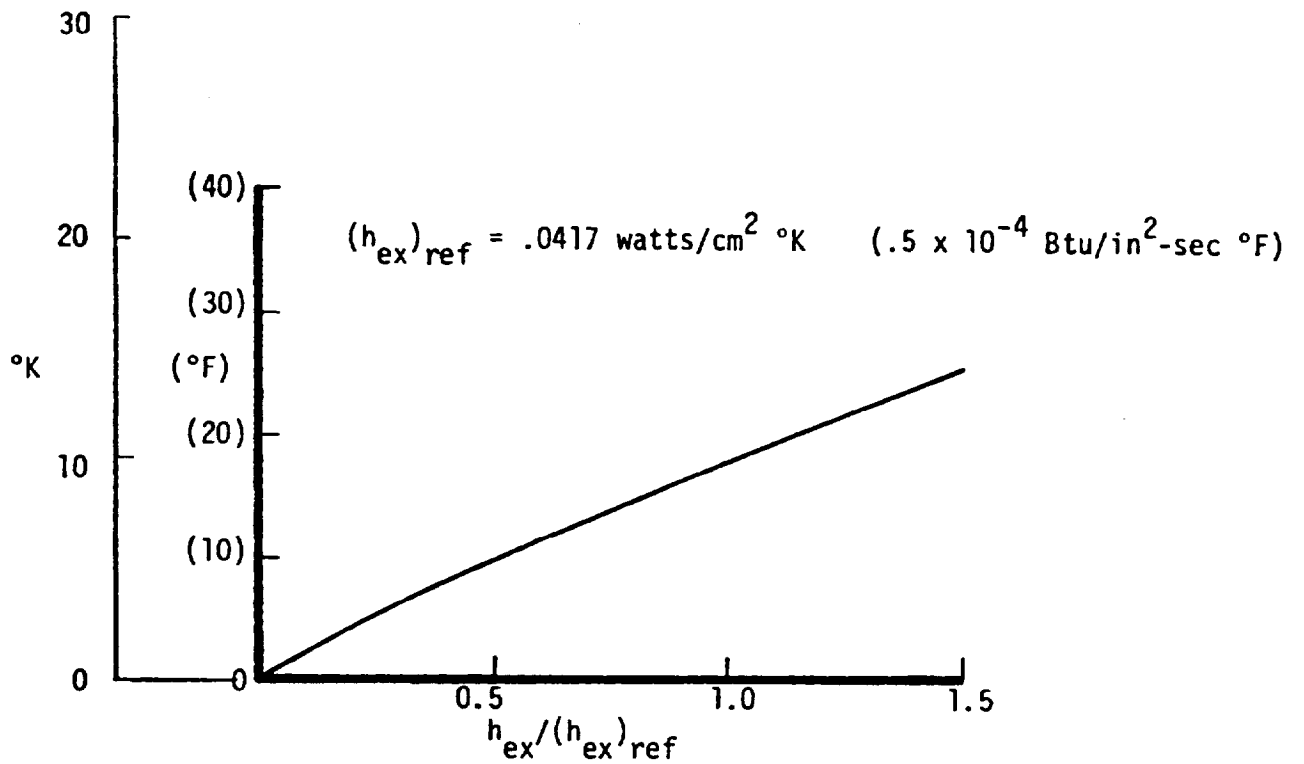


Figure 27. Effect of Loss Coefficient on Temperature Correction

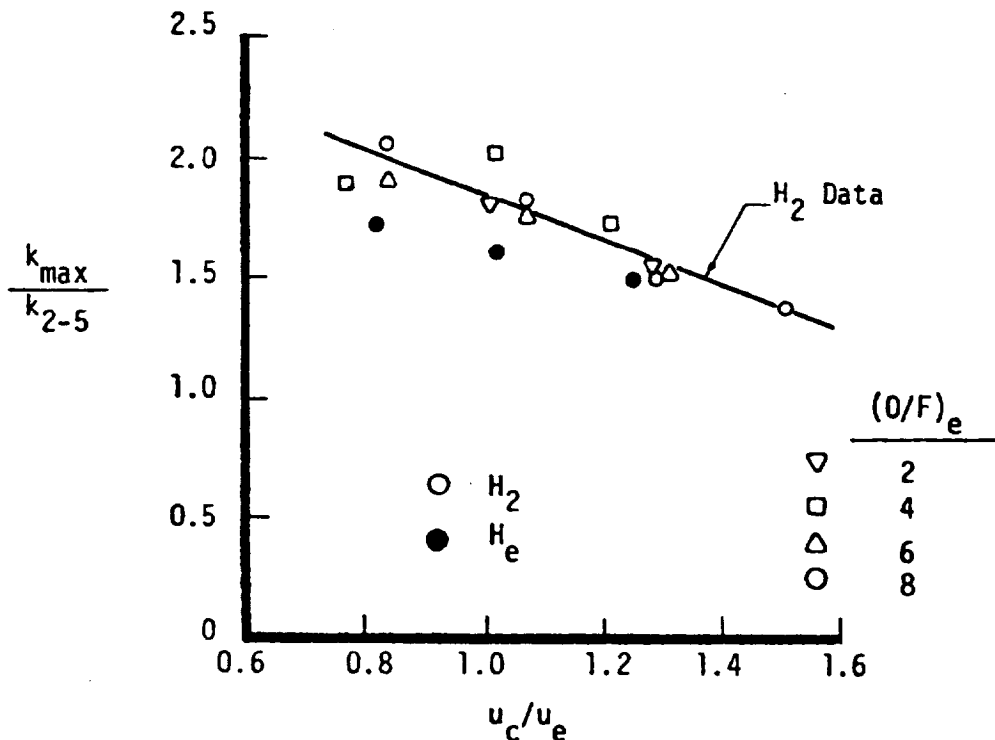


Figure 28. Ratio of Maximum To Asymptotic Entrainment Fractions in the Cylindrical Region

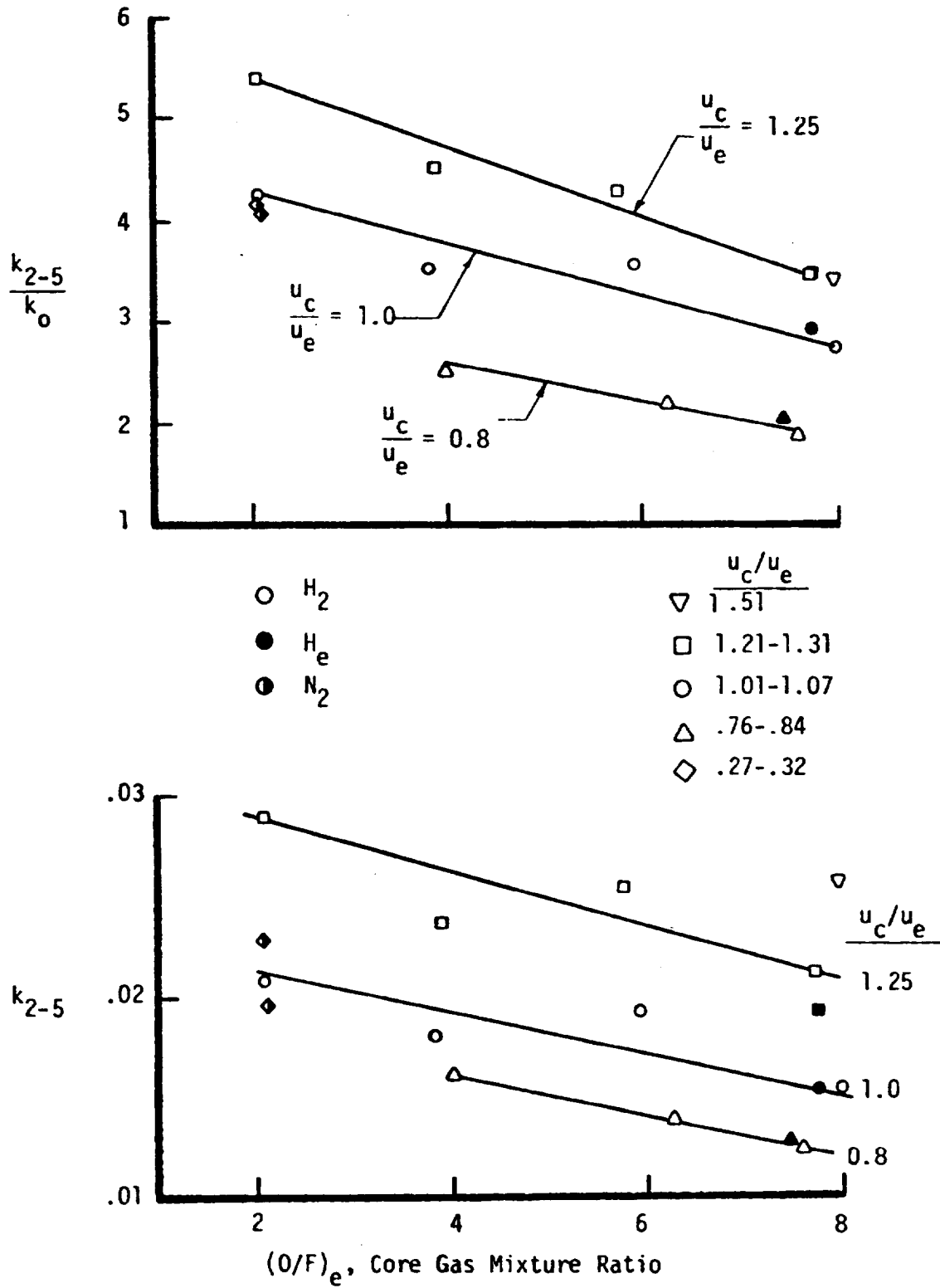
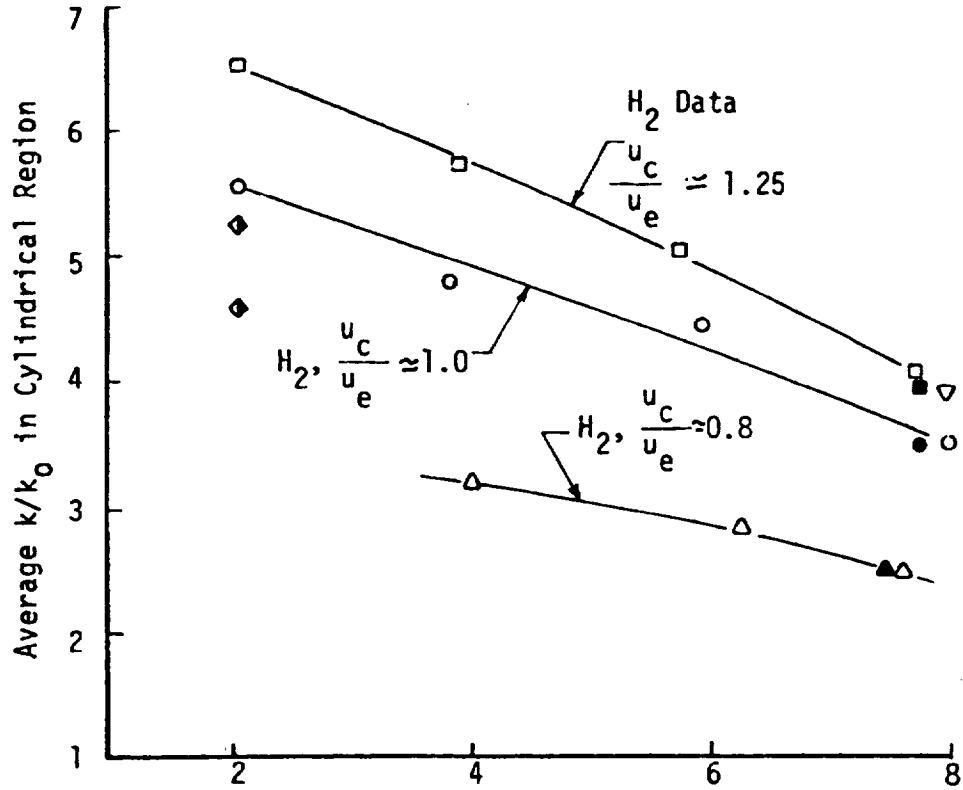


Figure 29. Asymptotic Cylindrical Section Entrainment Fractions



Open: H₂ Film Coolant
 Closed: H_e Film Coolant
 Half-
 Open: H₂ Film Coolant

▽ $u_c/u_e = 1.51$
 □ $u_c/u_e = 1.21 - 1.31$
 ○ $u_c/u_e = 1.01 - 1.07$
 △ $u_c/u_e = 0.76 - 0.84$
 ◇ $u_c/u_e = 0.27 - 0.32$

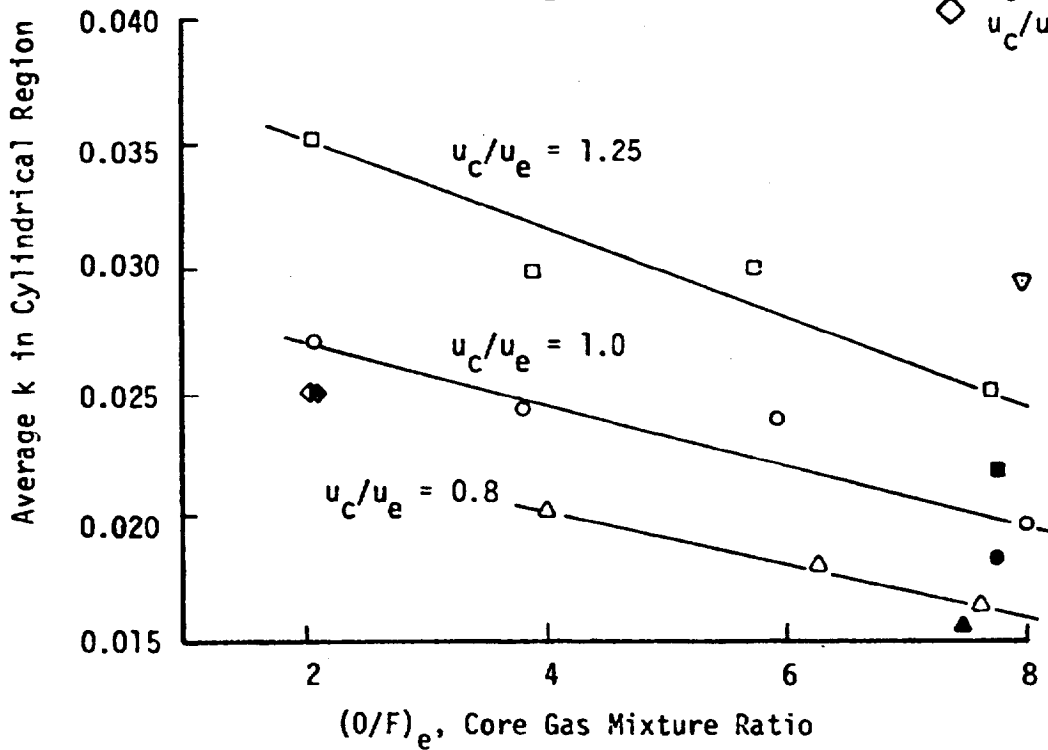


Figure 30. Average Cylindrical Region Entrainment Fractions

- ▽ $u_c/u_e = 1.51$
- $u_c/u_e = 1.21 - 1.31$
- $u_c/u_e = 1.01 - 1.07$
- △ $u_c/u_e = 0.76 - 0.84$
- ◇ $u_c/u_e = 0.27 - 0.32$

Open: H₂ Film Coolant
 Closed: H_e Film Coolant
 Half-Open: N₂ Film Coolant

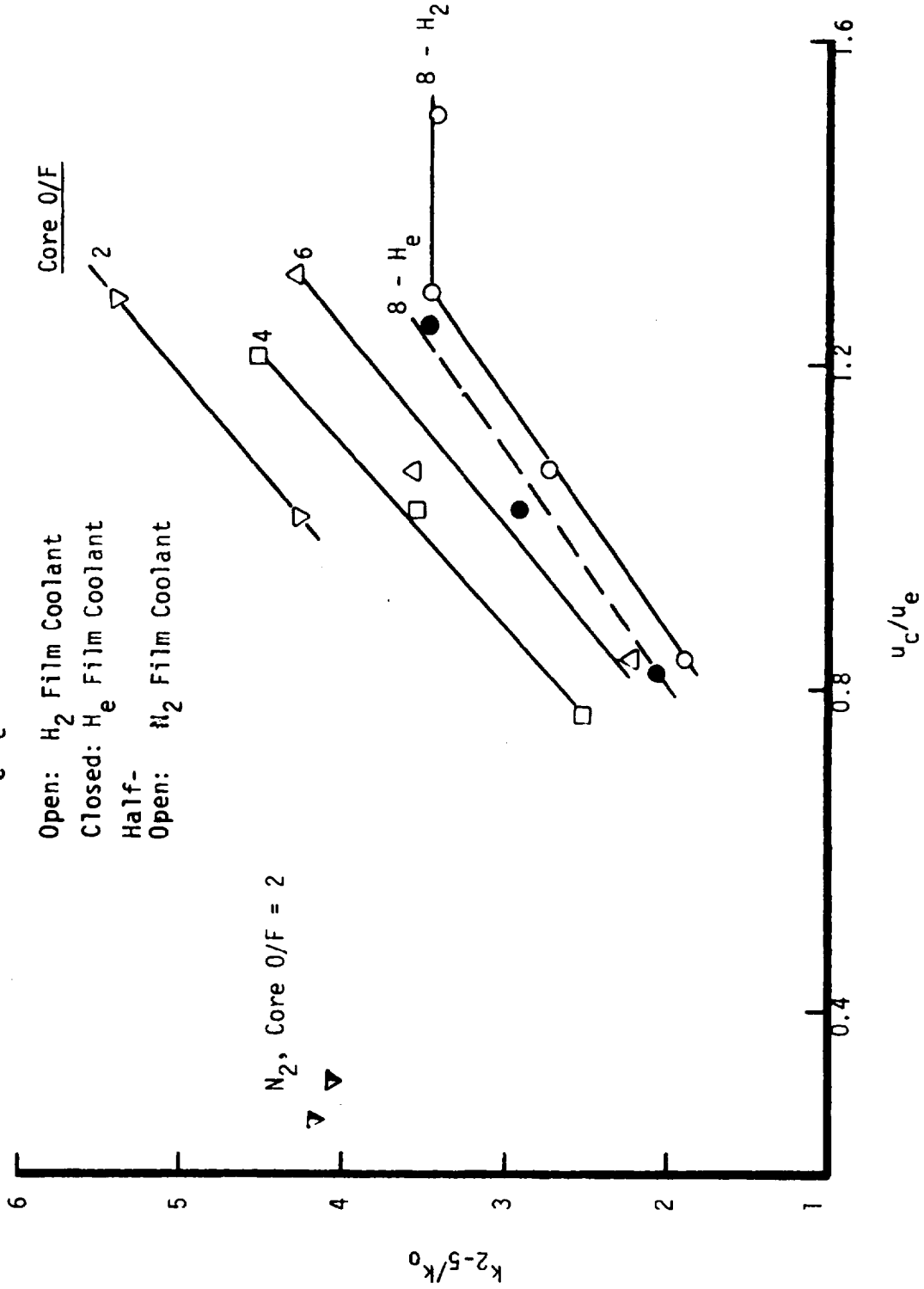


Figure 31. Effect of Velocity Ratio on Asymptotic Entrainment Fraction Ratio

Symbol	Film Coolant	Symbol Shading	Contract	Test Conditions
○	Hydrogen	○	NAS3-17813	O ₂ /H ₂ Rocket Engine
△	Helium	●	NAS3-15844	Hot N ₂ Core Gas
□	Nitrogen	●	NAS3-14343	Hot N ₂ Core Gas

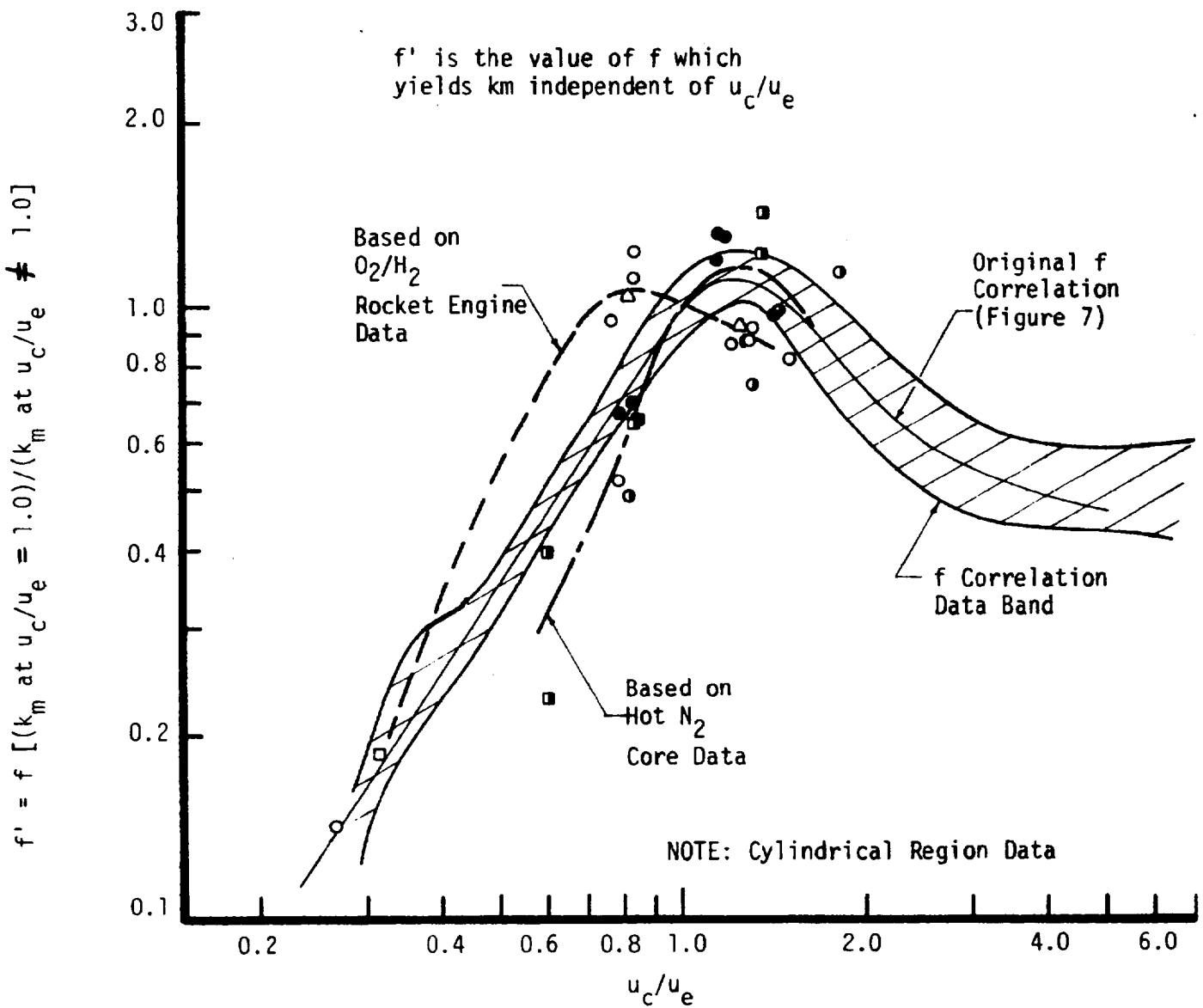


Figure 32. Adjusted $f(u_c/u_e)$ Values

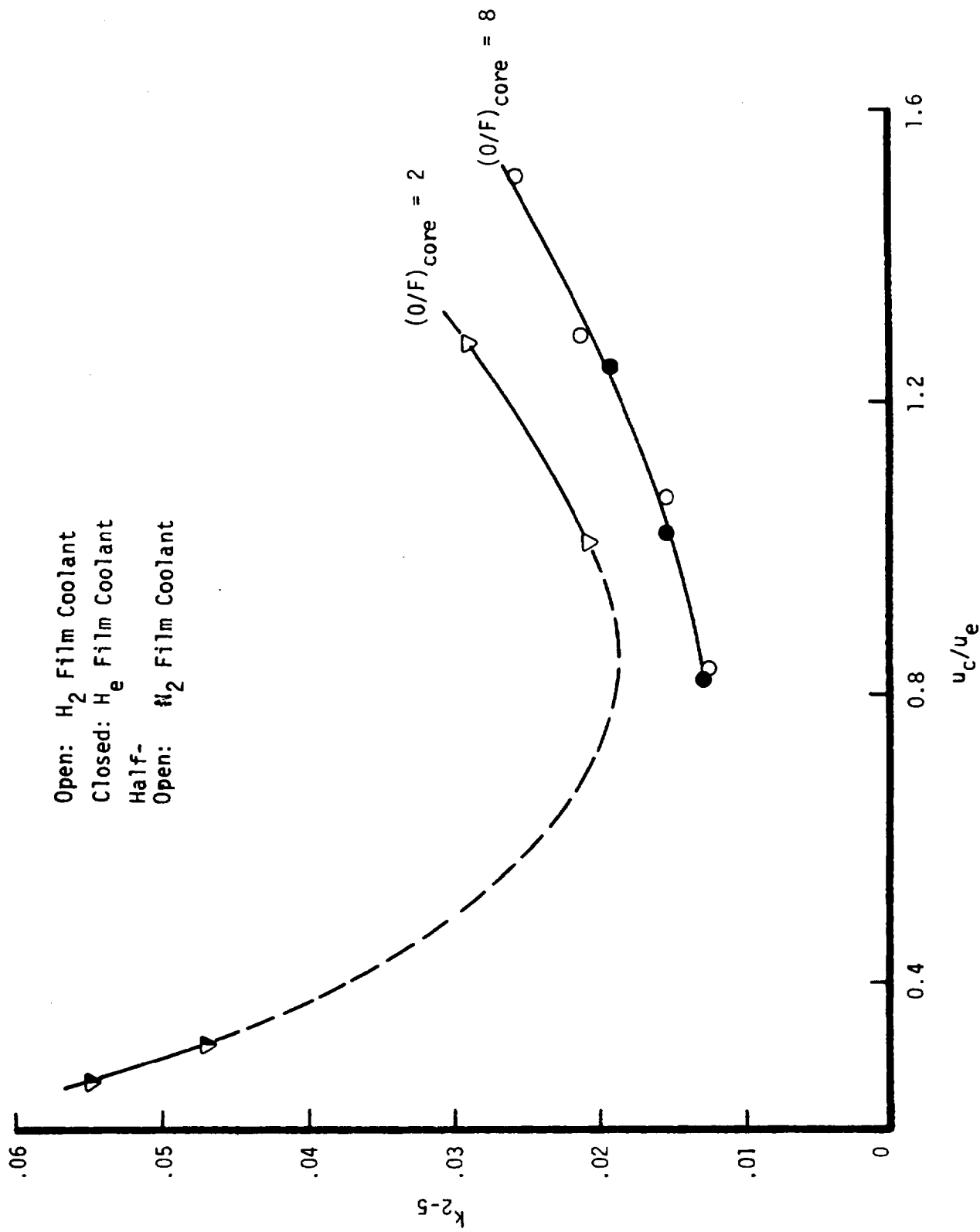




Figure 33. Effect of Velocity Ratio on Asymptotic Entrainment Fraction

	Contract	Core Gas	Film Coolants	$\frac{u_c}{u_e}$	$\frac{\rho_c}{\rho_e}$	Re_c	$(Re)_{core}$	r_o
	NAS3-17813 (Tests 102-124)	O ₂ /H ₂ O/F=2-8	H ₂ , H _e , N ₂	.31-1.5	1.5-33	.5-2 x10 ⁵	2-4x10 ⁵	1.83
	NAS3-14343 (Tests 3,4,5)							
	NAS3-15844 (Tests 102,103A)	N ₂ T=1000°F	H ₂	.79-1.83	.2	2.4 x10 ⁵	5.6x10 ⁵	0.63

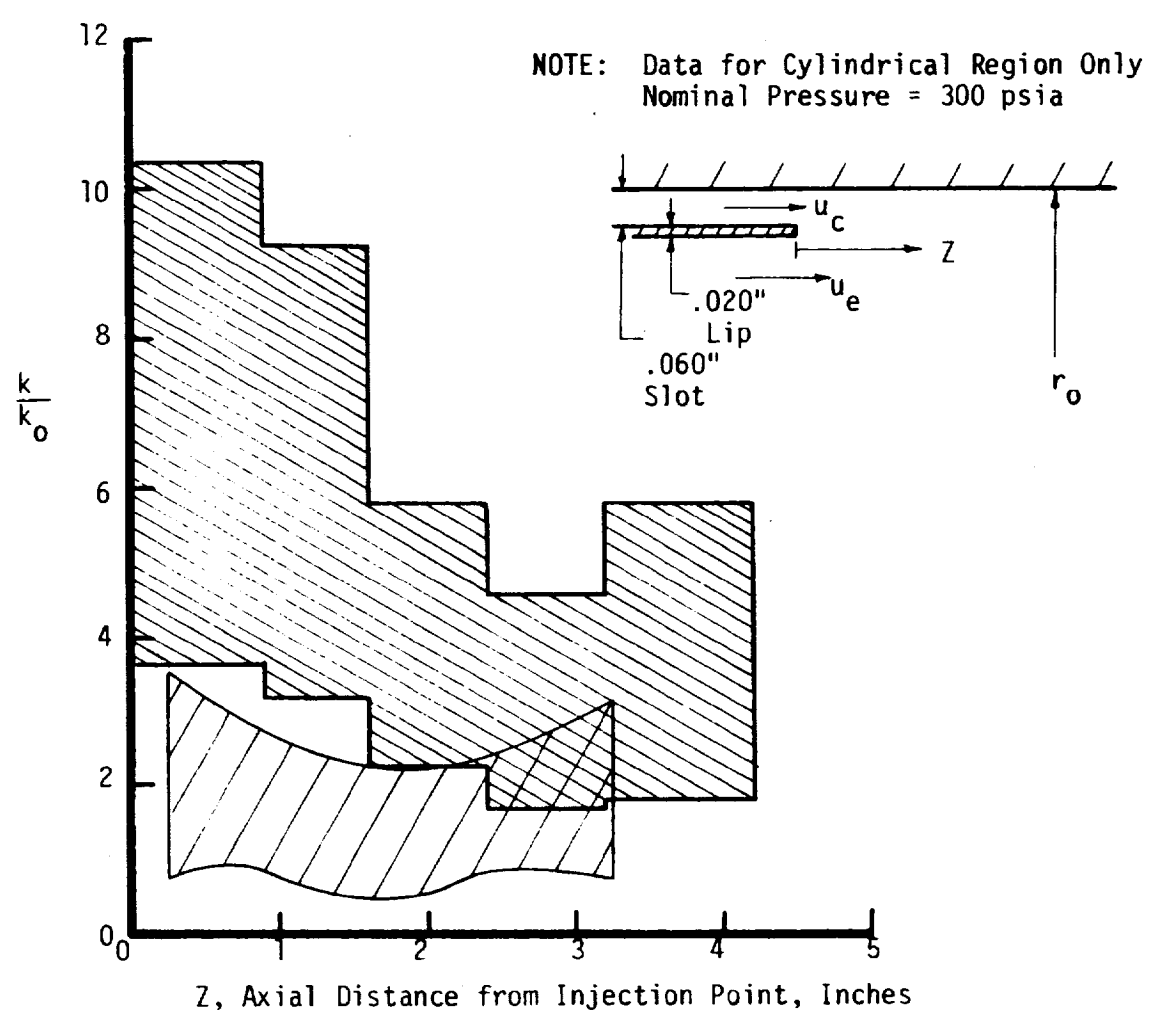


Figure 34. Comparison of Entrainment Fraction Ratios

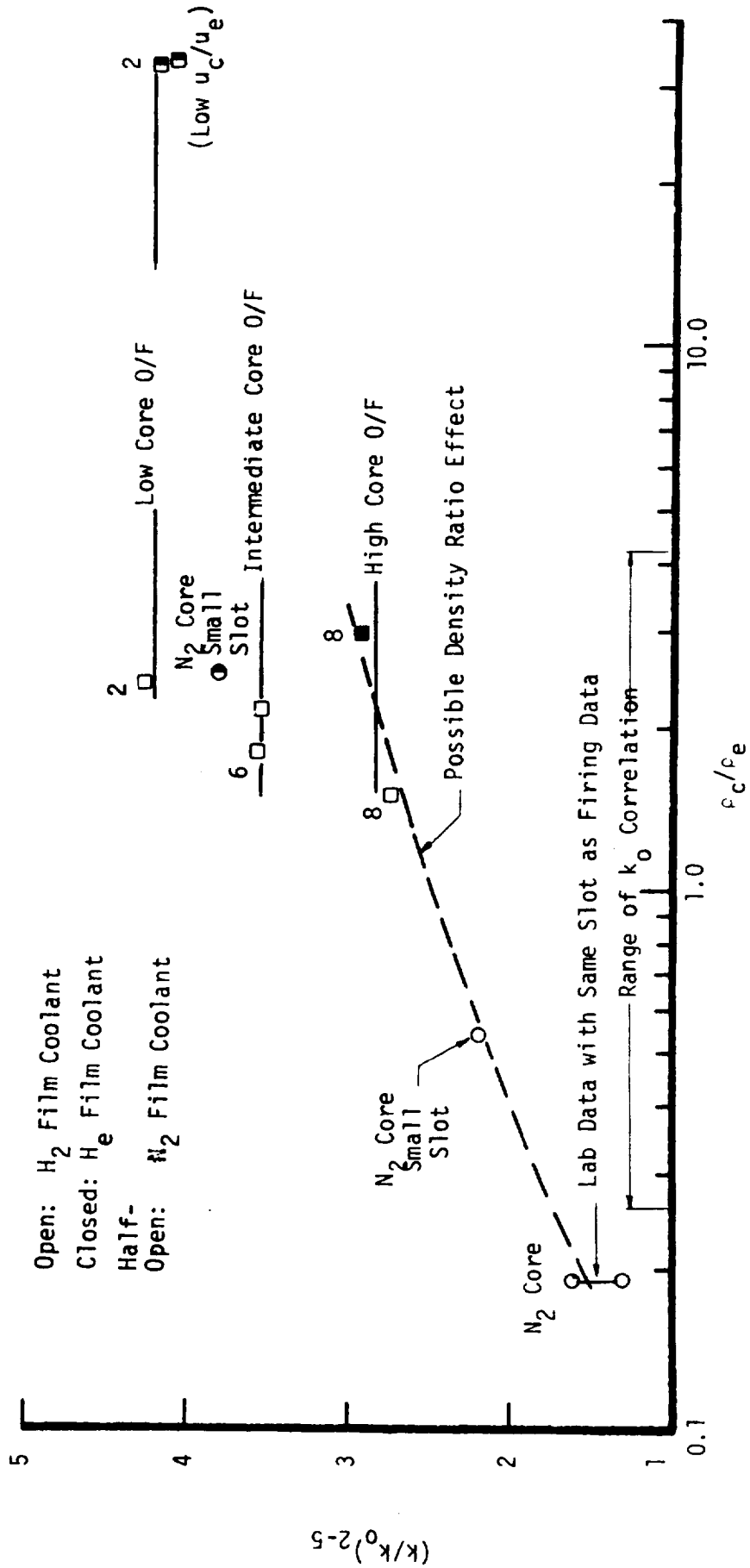


Figure 35. Asymptotic Entrainment Fraction Ratio vs. Density Ratio

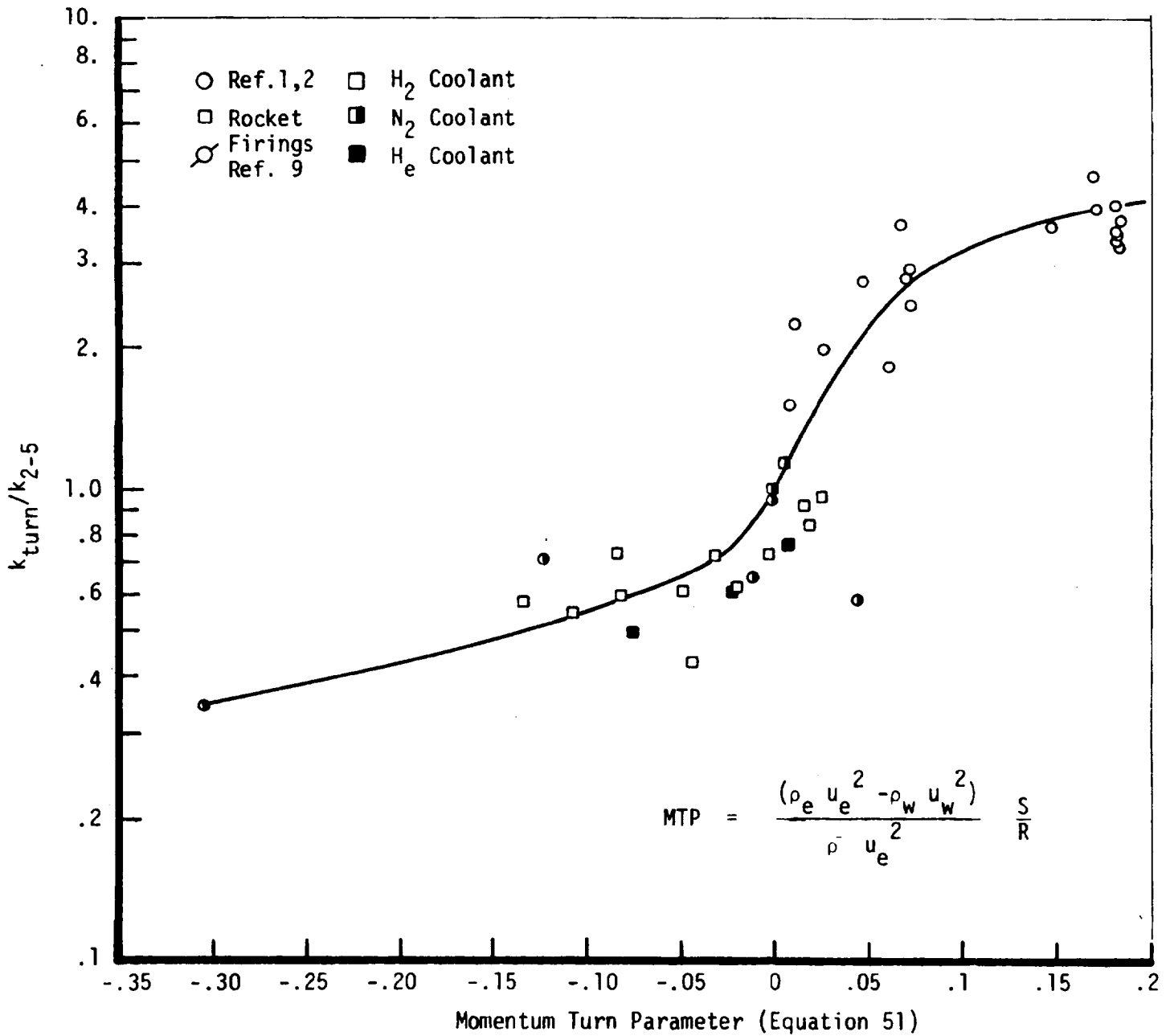


Figure 37. Correlation of Convergent Turn Entrainment Fraction with Momentum Turn Parameter

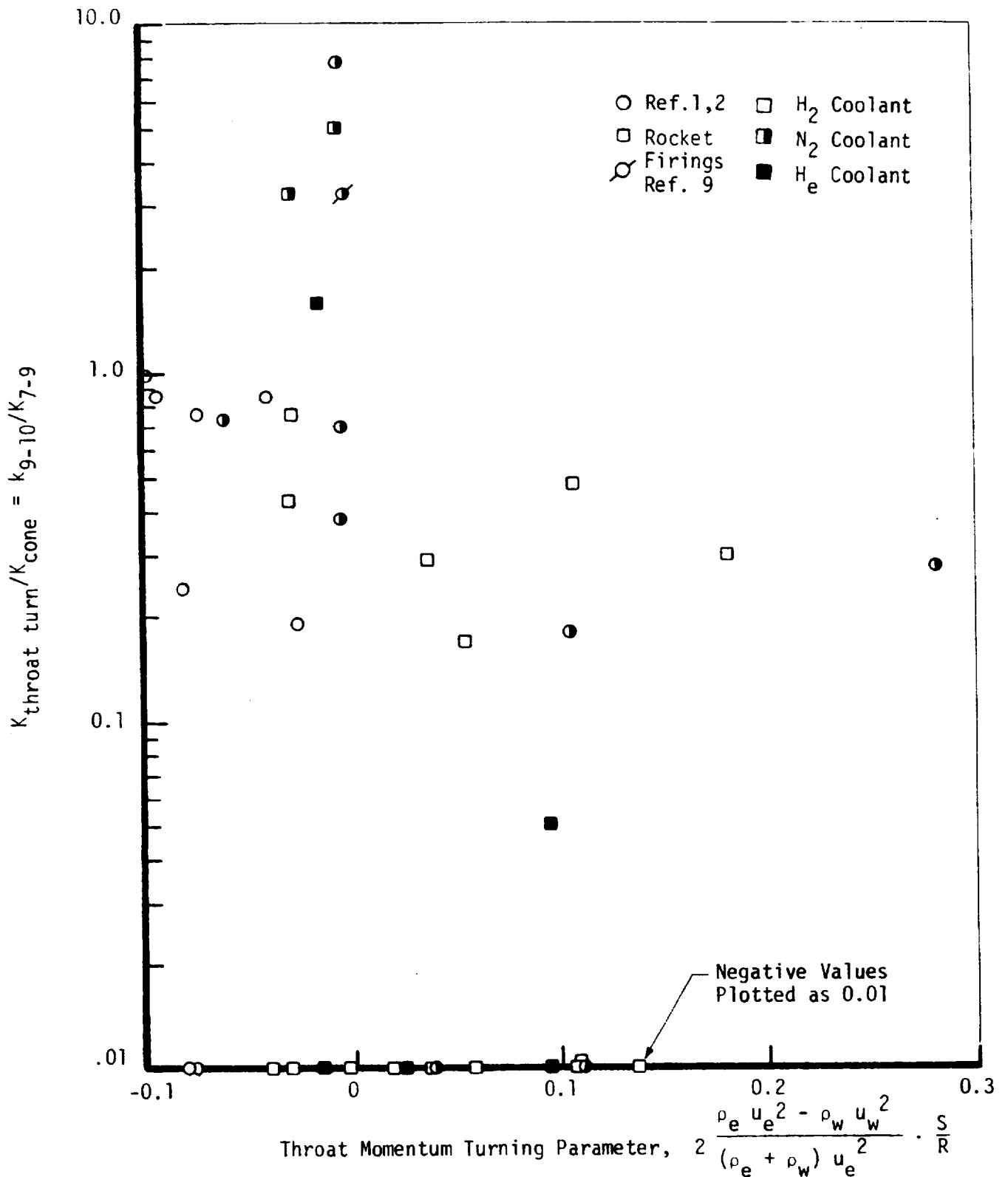


Figure 38. Attempted Correlation of Throat Turn Entrainment Fraction

Core Gas: Hot Air
 Film Coolant: Cold Air

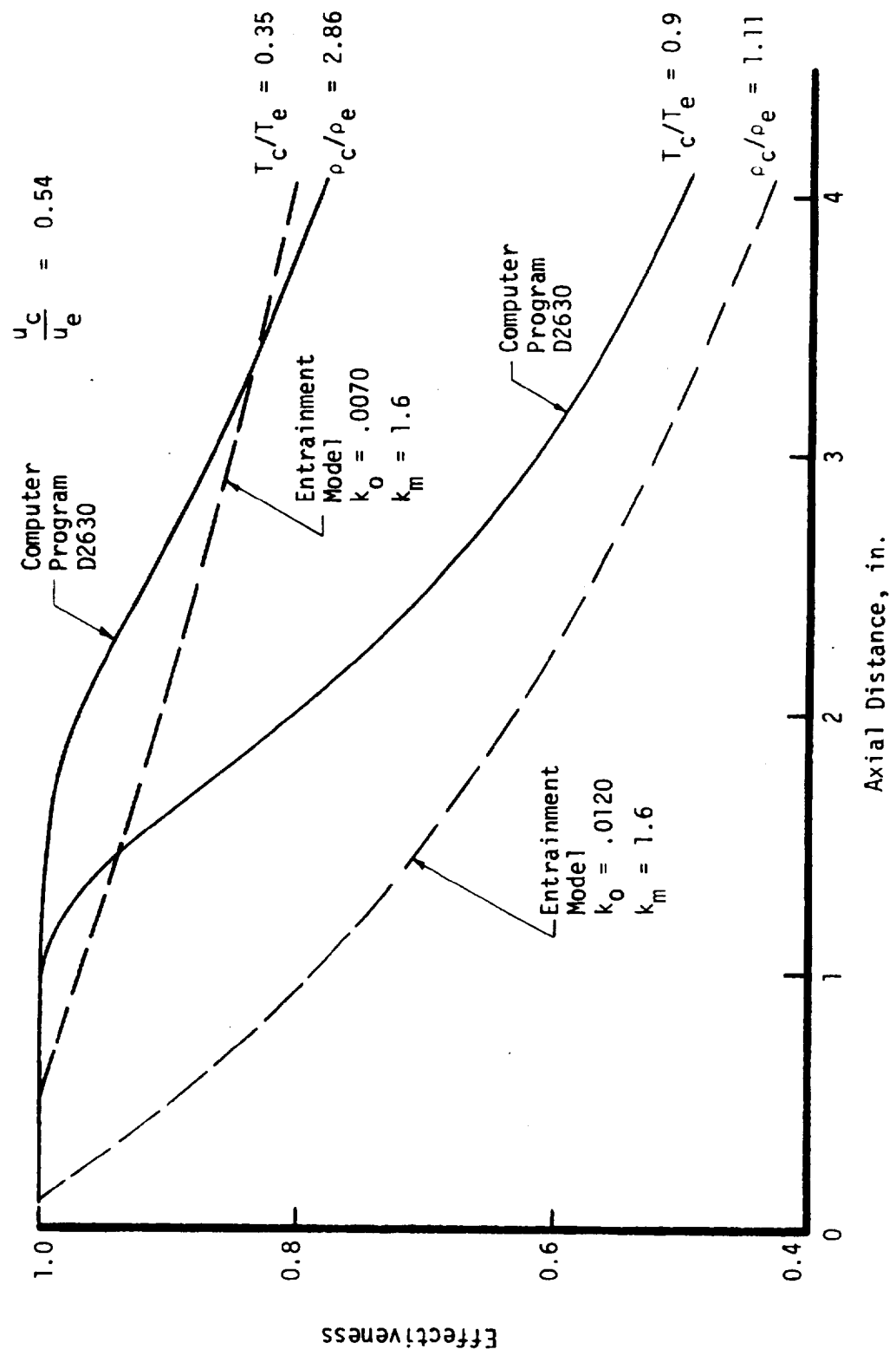


Figure 39. Comparison of Entrainment Model and Boundary Layer Computer Program Results

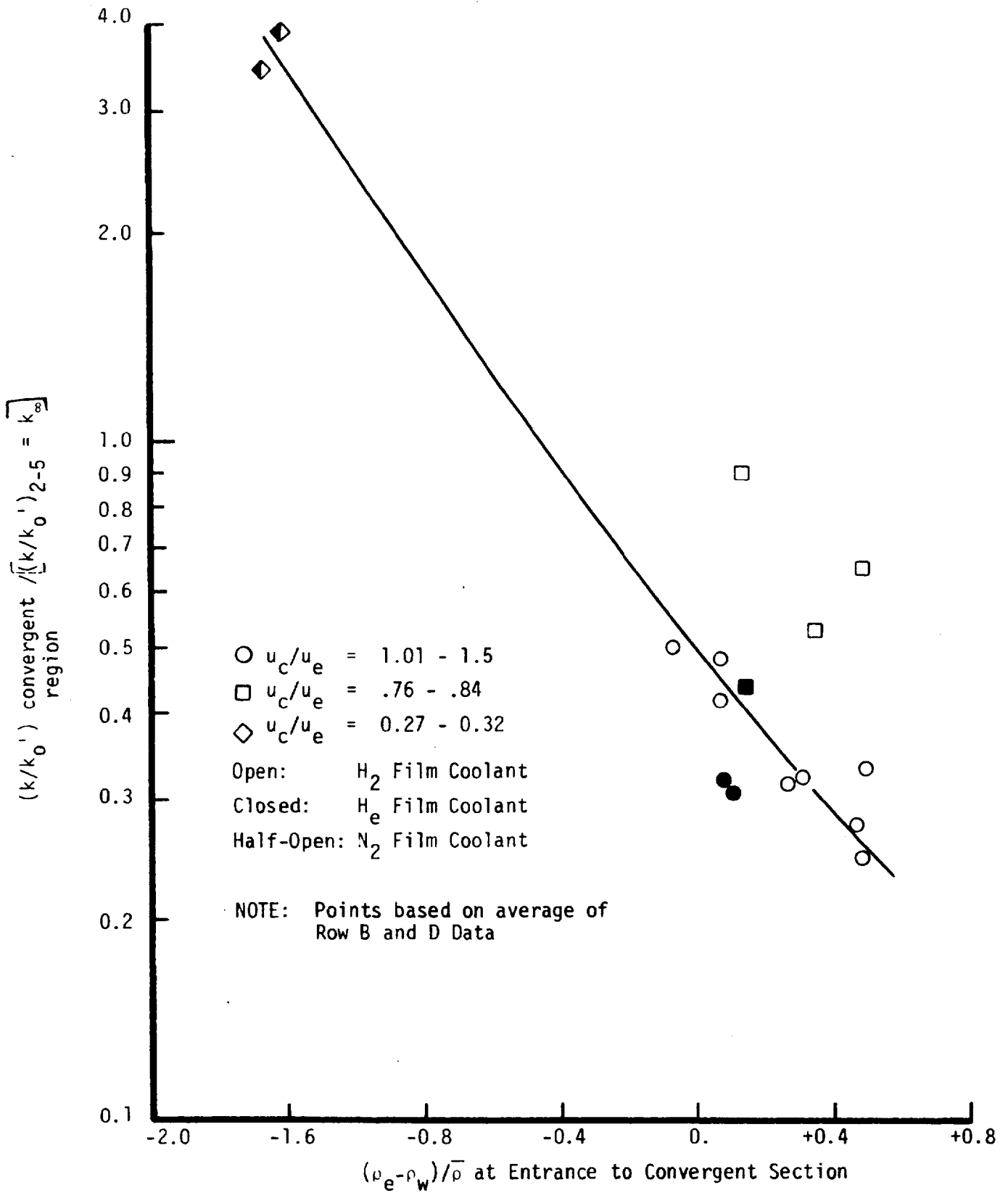


Figure 40. Correlation of Convergent Section Rocket Data with Density Difference Parameter

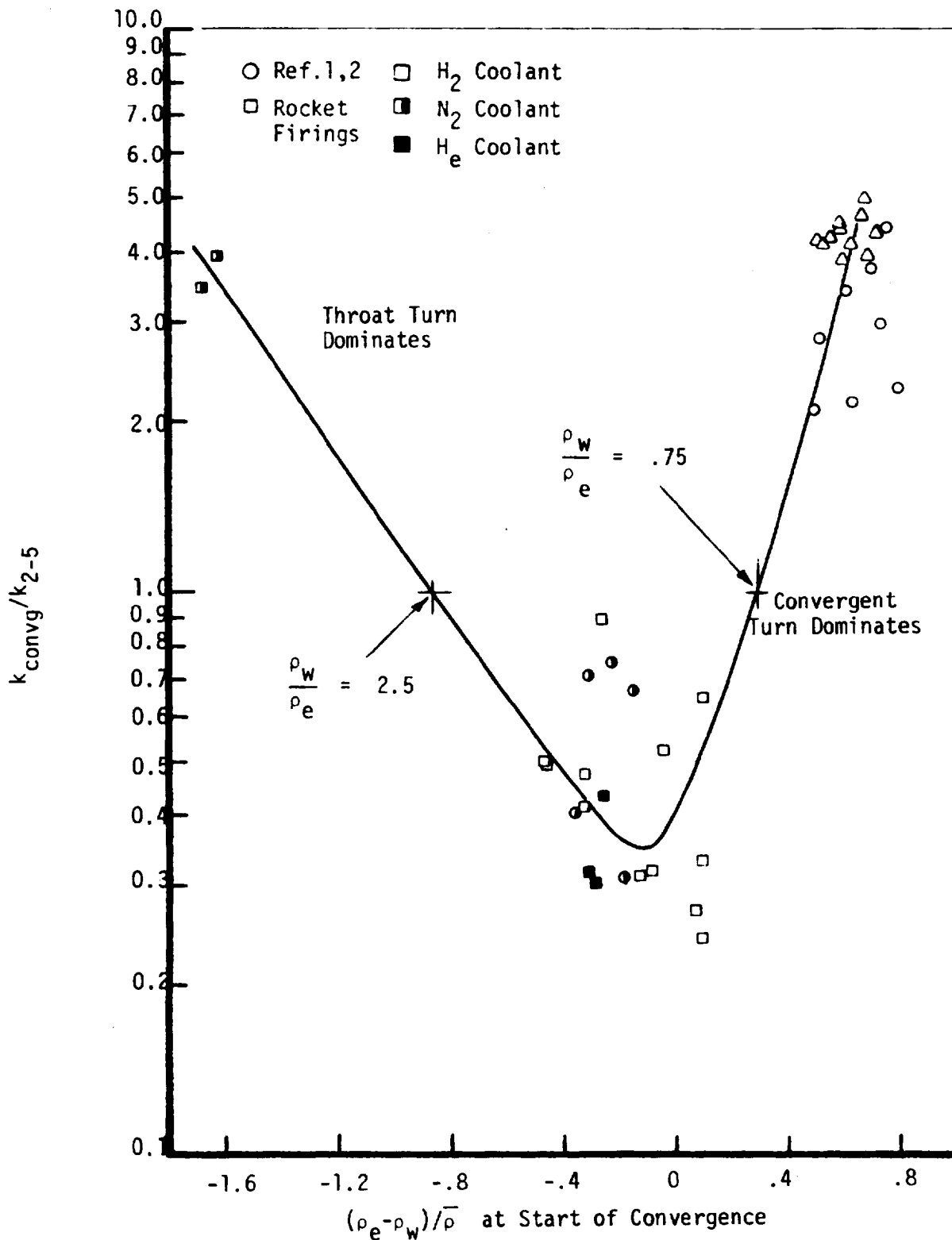


Figure 41. Correlation of all Available Convergent Region Data with Density Difference Parameter

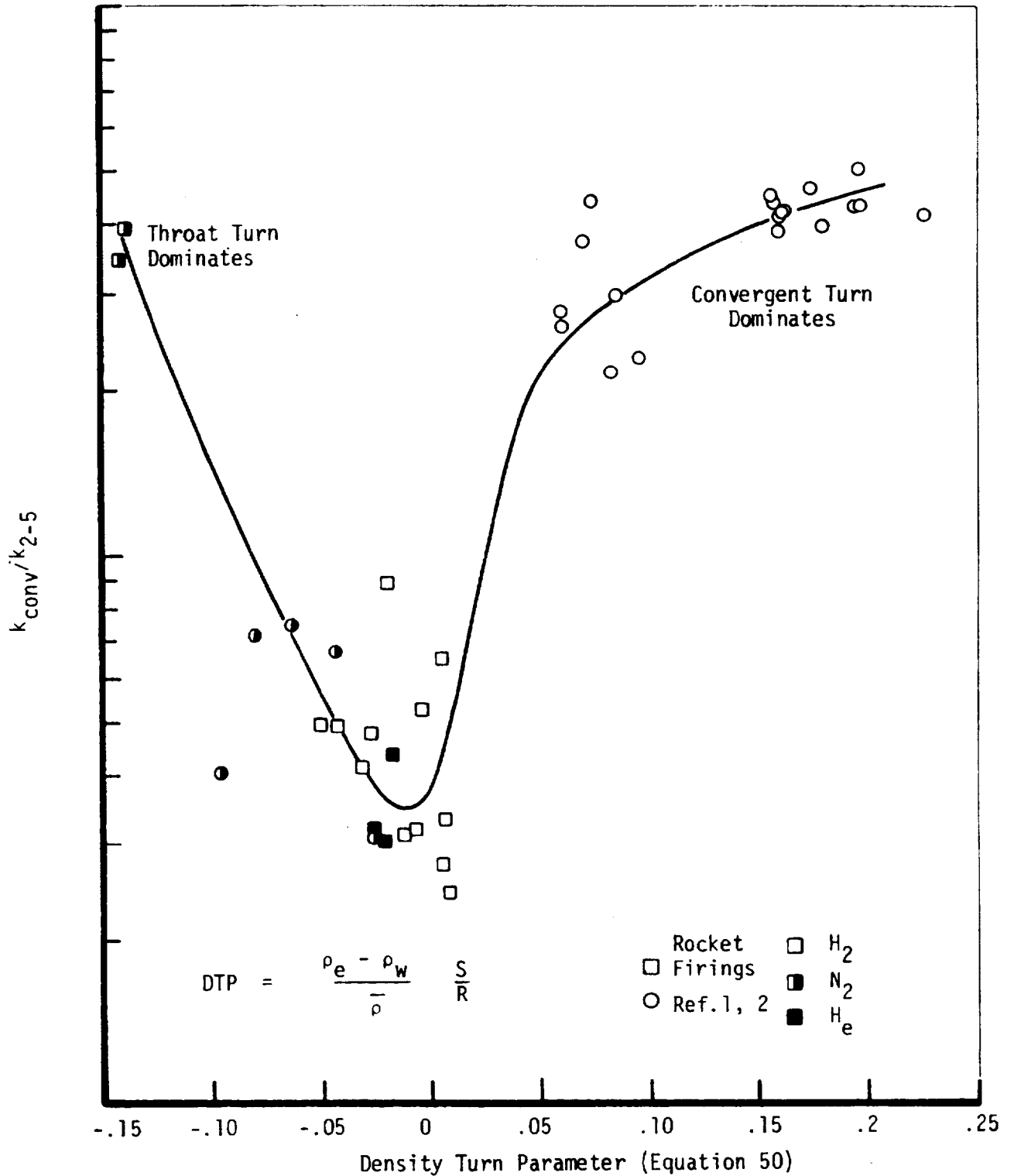


Figure 42. Correlation of the Convergent Region Data with Density Turn Parameter

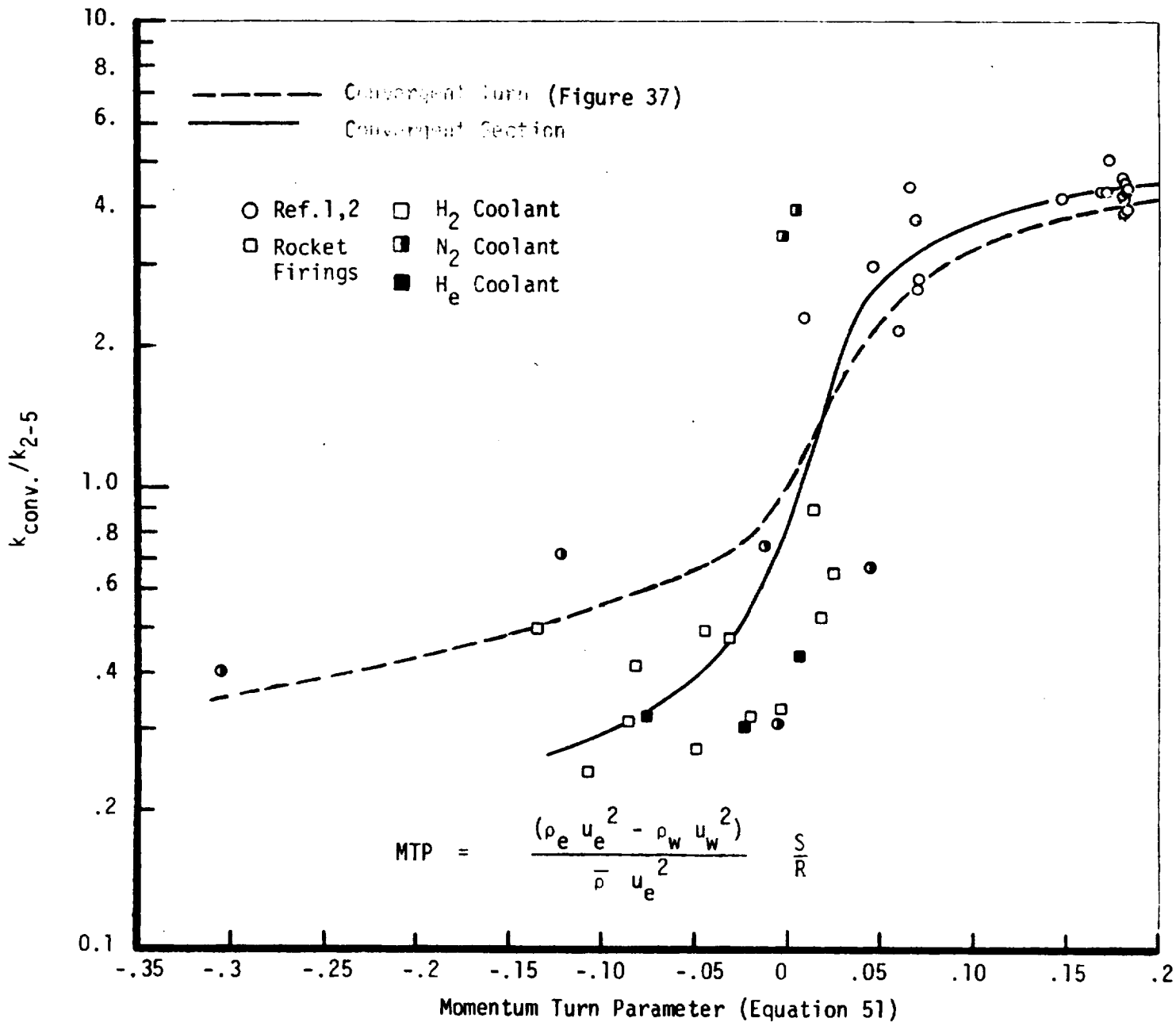


Figure 43. Correlation of the Convergent Region Data with Momentum Turn Parameter

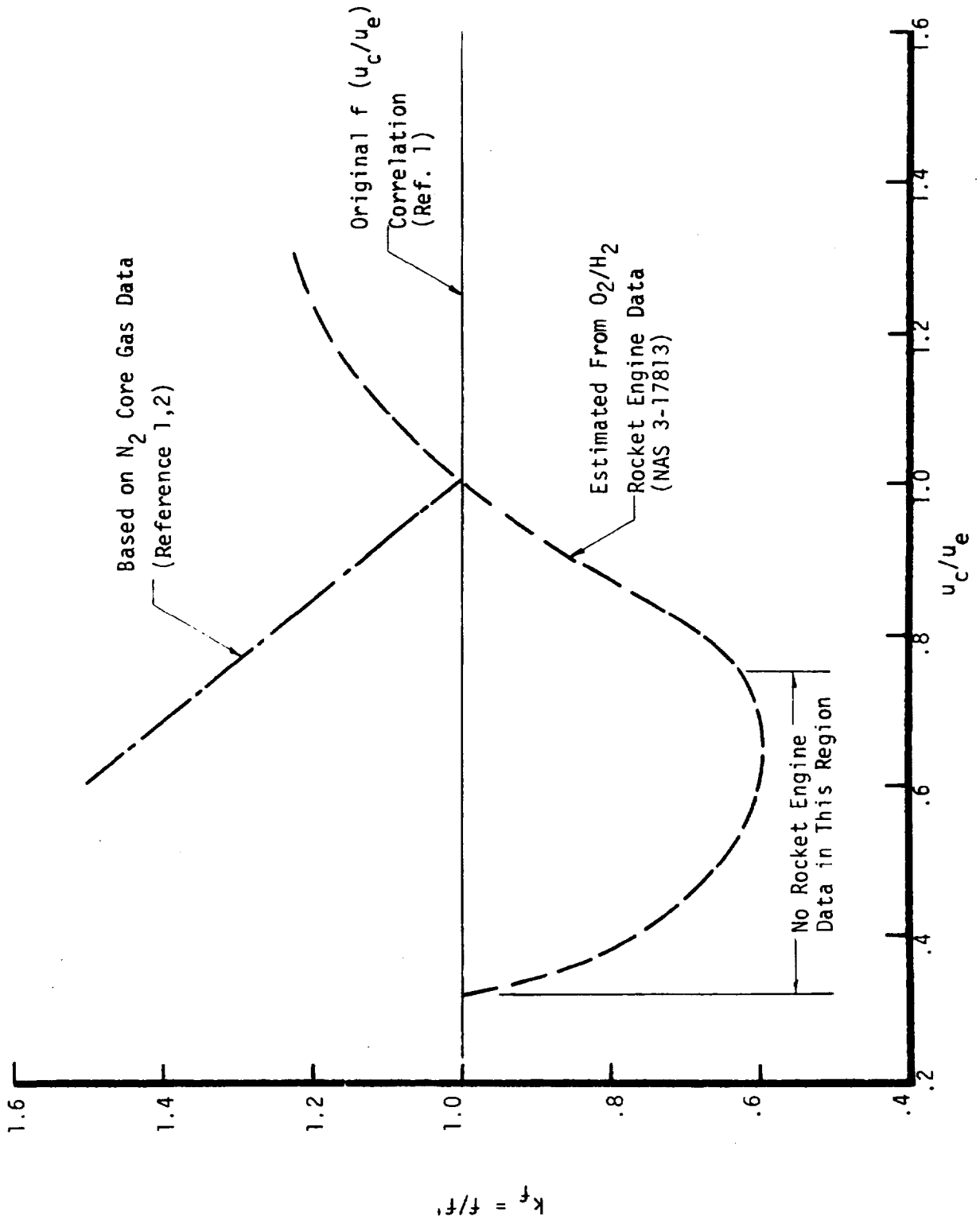


Figure 44. k_f Factor vs. Injection Velocity Ratio

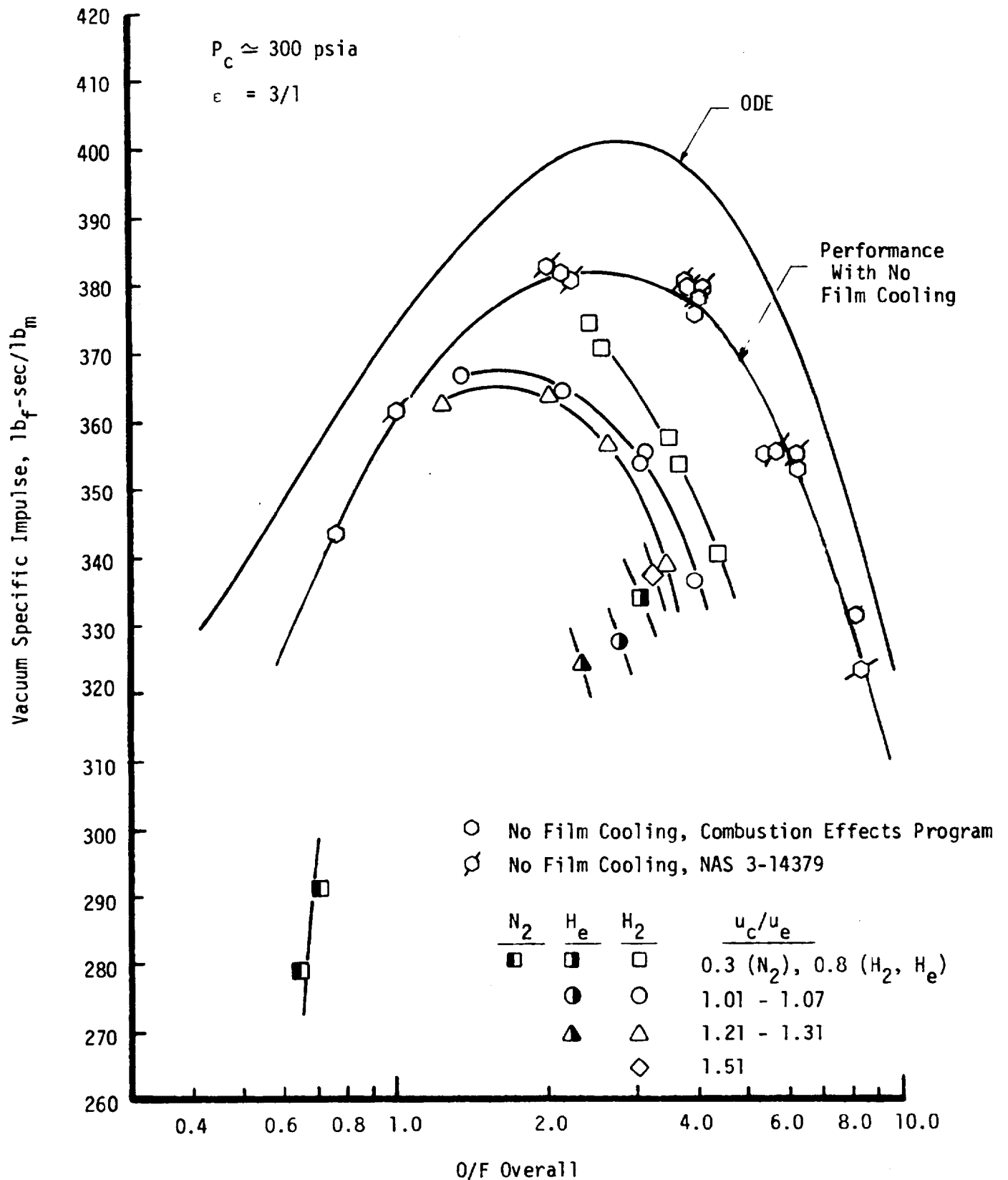


Figure 45. Vacuum Specific Impulse Data

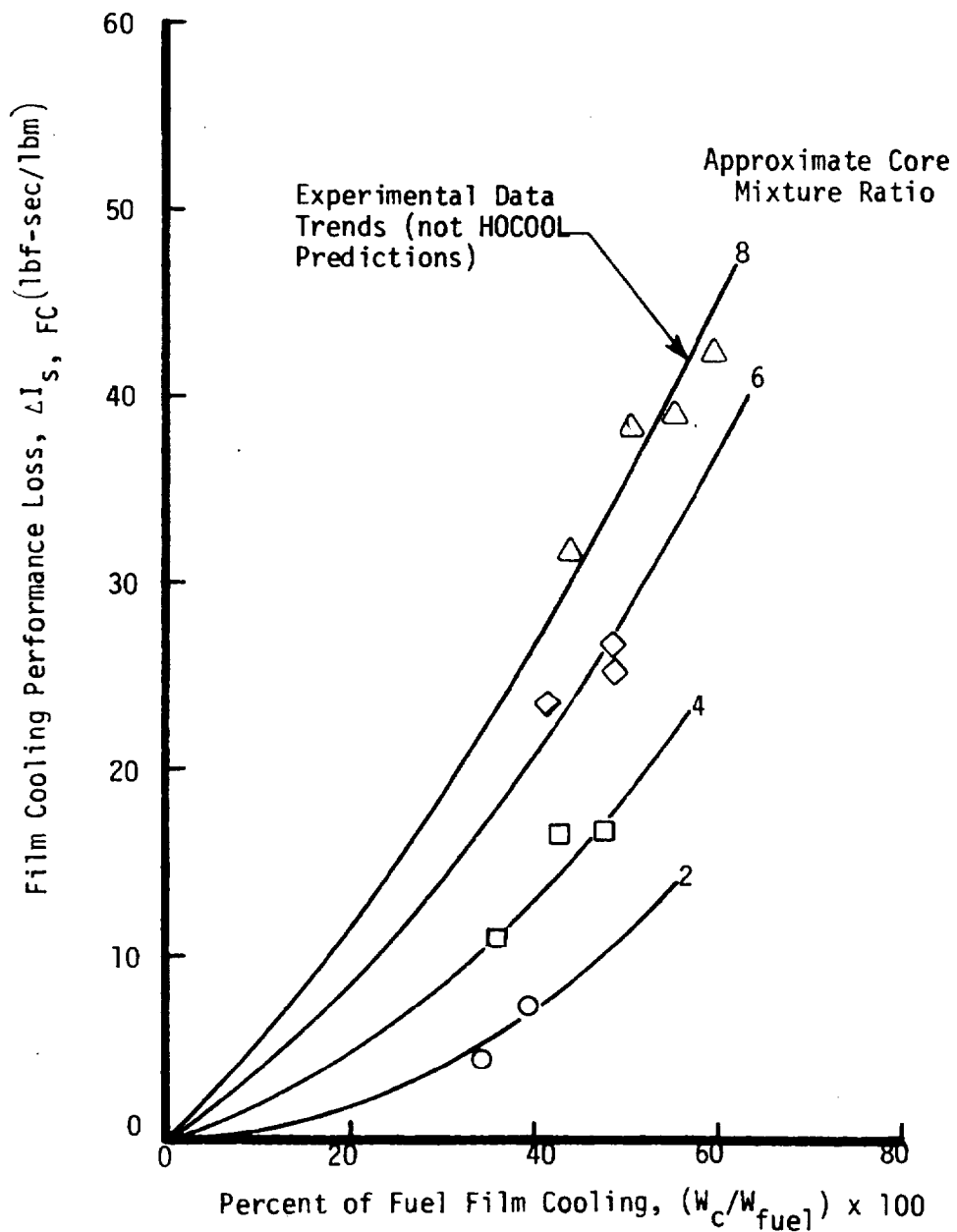


Figure 46. Film Cooling Performance Loss vs. Film Cooling Percentage

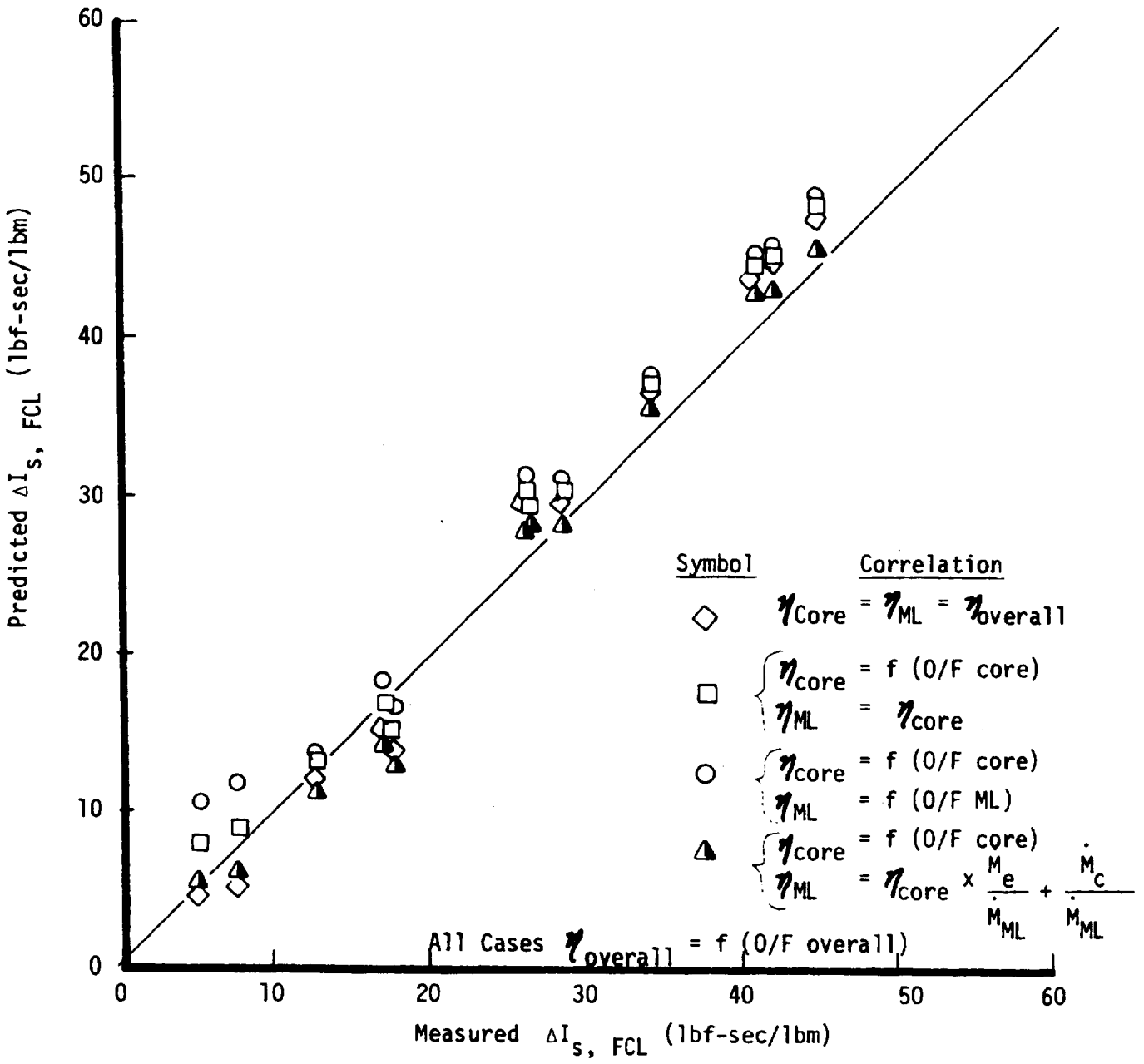


Figure 47. Correlation of Hydrogen Film Cooled Performance Loss Data

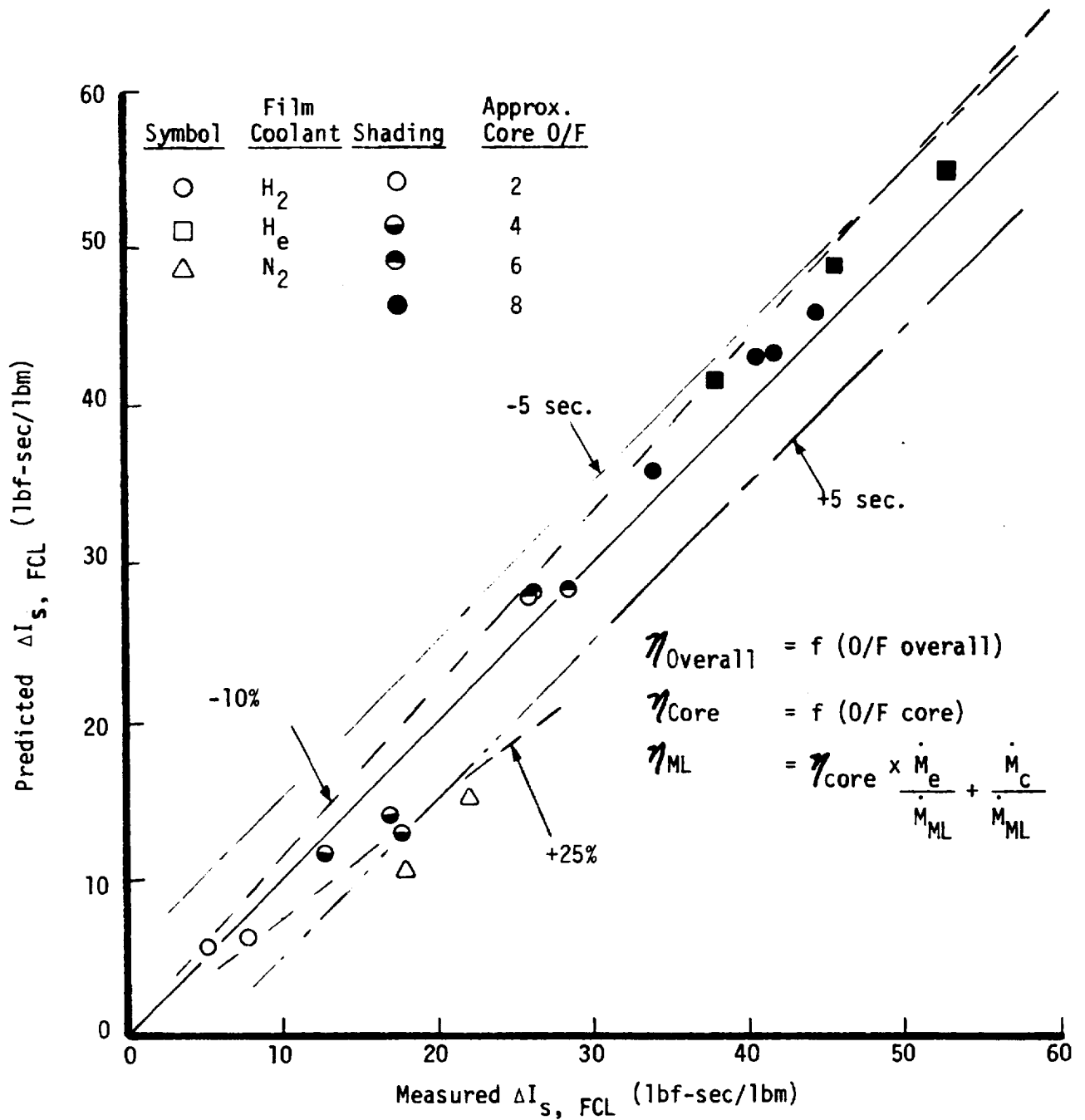


Figure 48. Comparison of Predicted and Measured Film Cooling Performance Loss Values

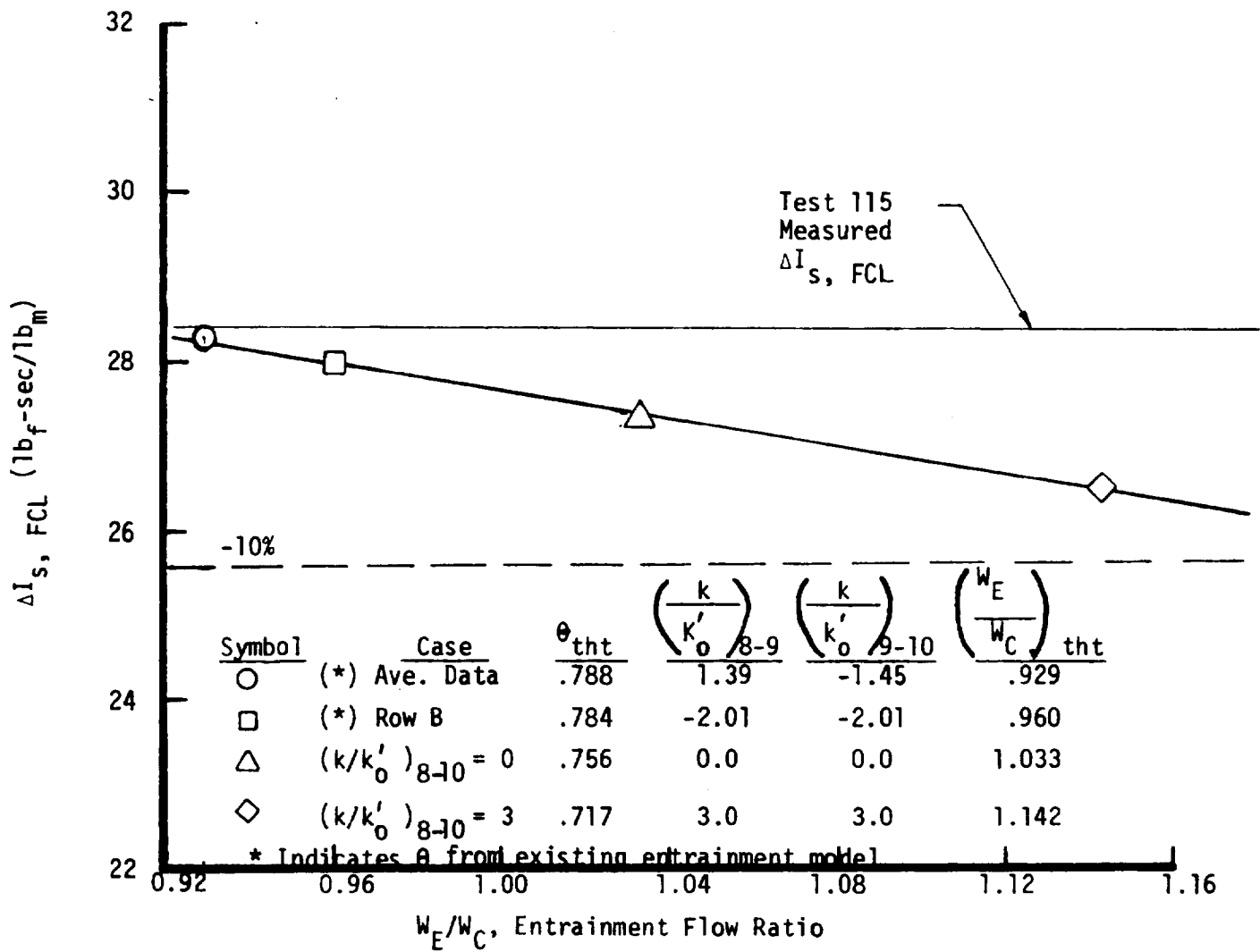


Figure 49. Effect of Shape Factor on Predicted Film Cooling Loss

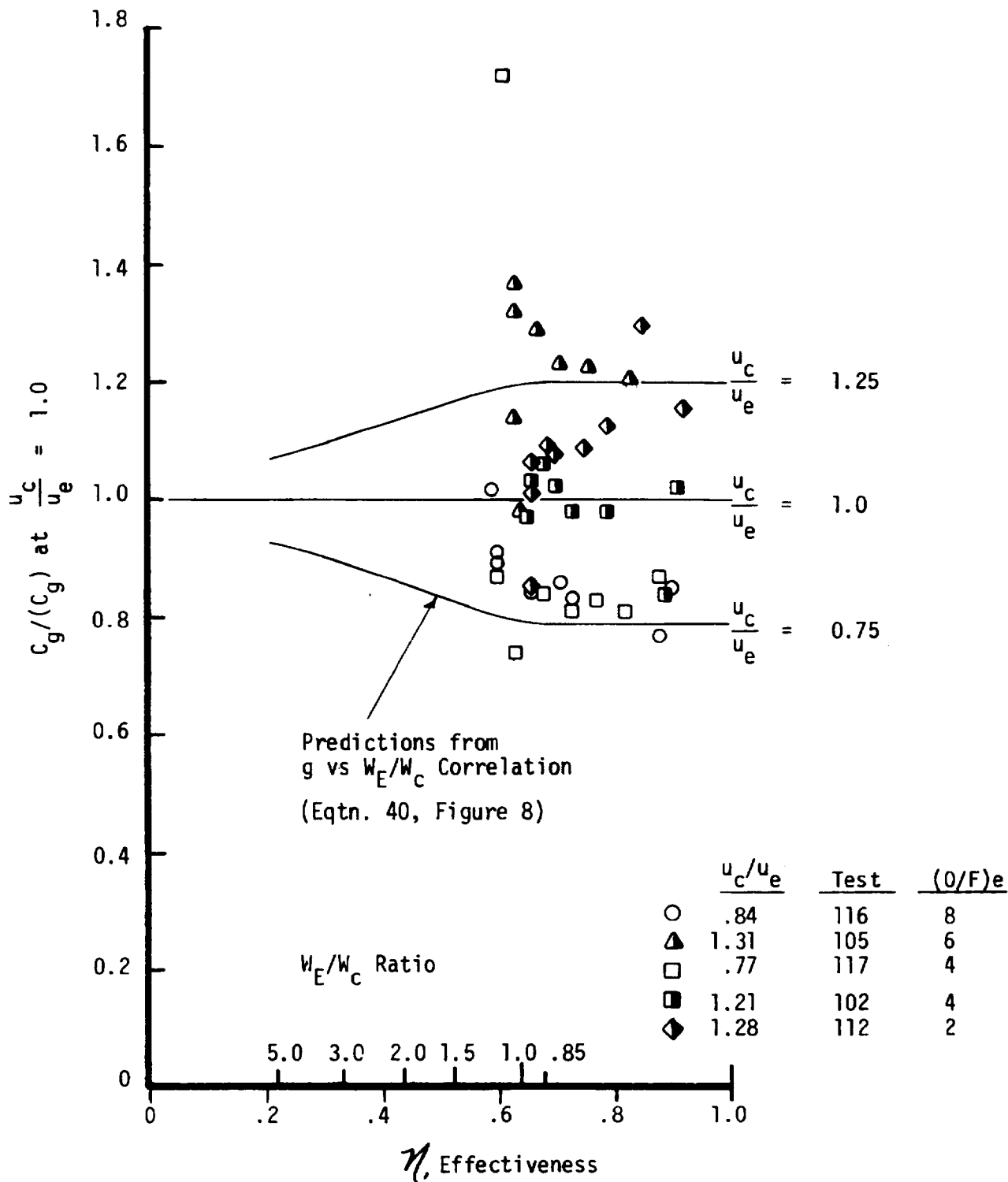


Figure 50. Comparison of Measured and Predicted Velocity Ratio and Effectiveness Effects on C_g

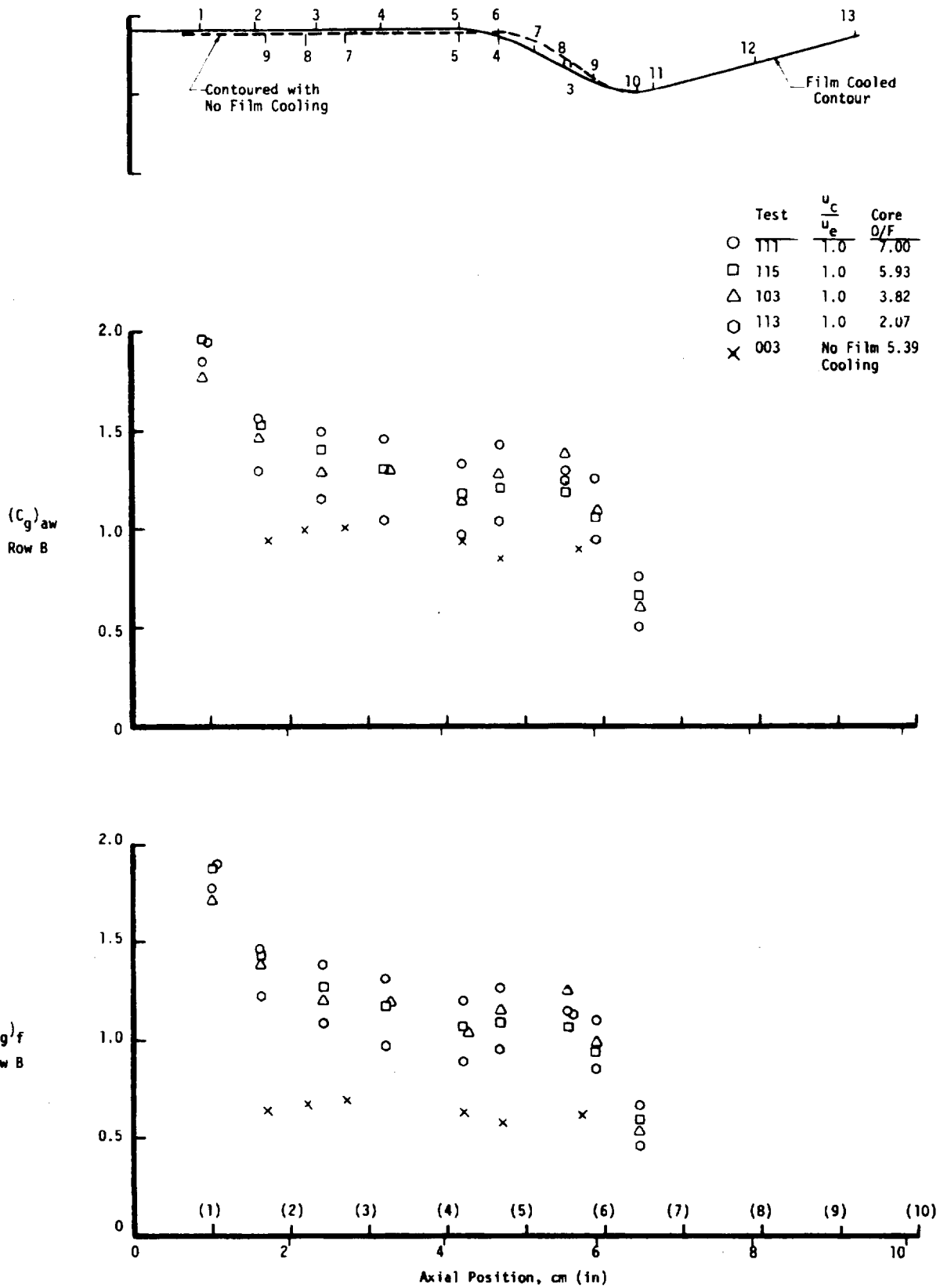


Figure 51. Row B Cg Profiles With and Without Film Cooling

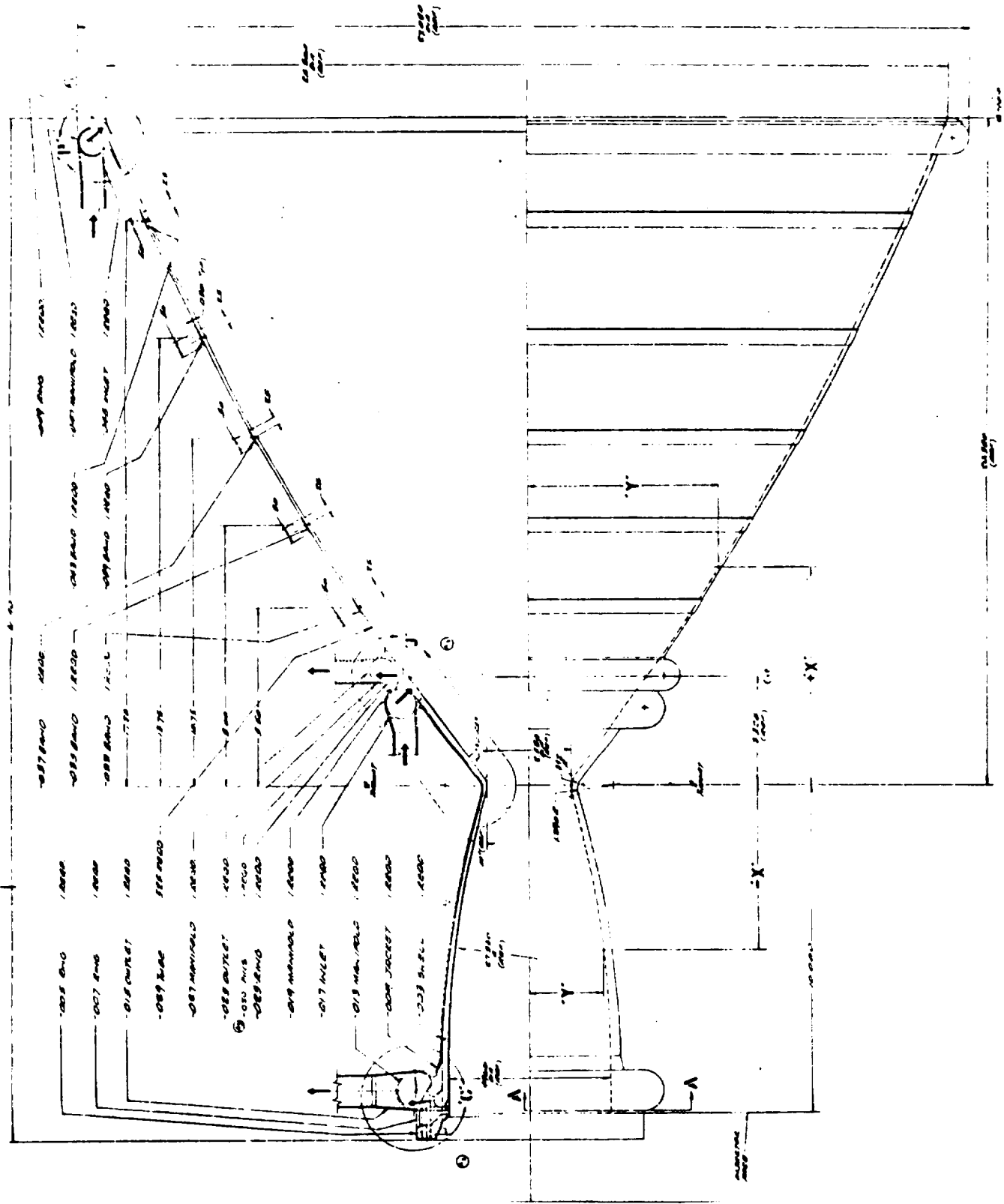


Figure 52. Proposed O_2/H_2 Thrust Chamber Design

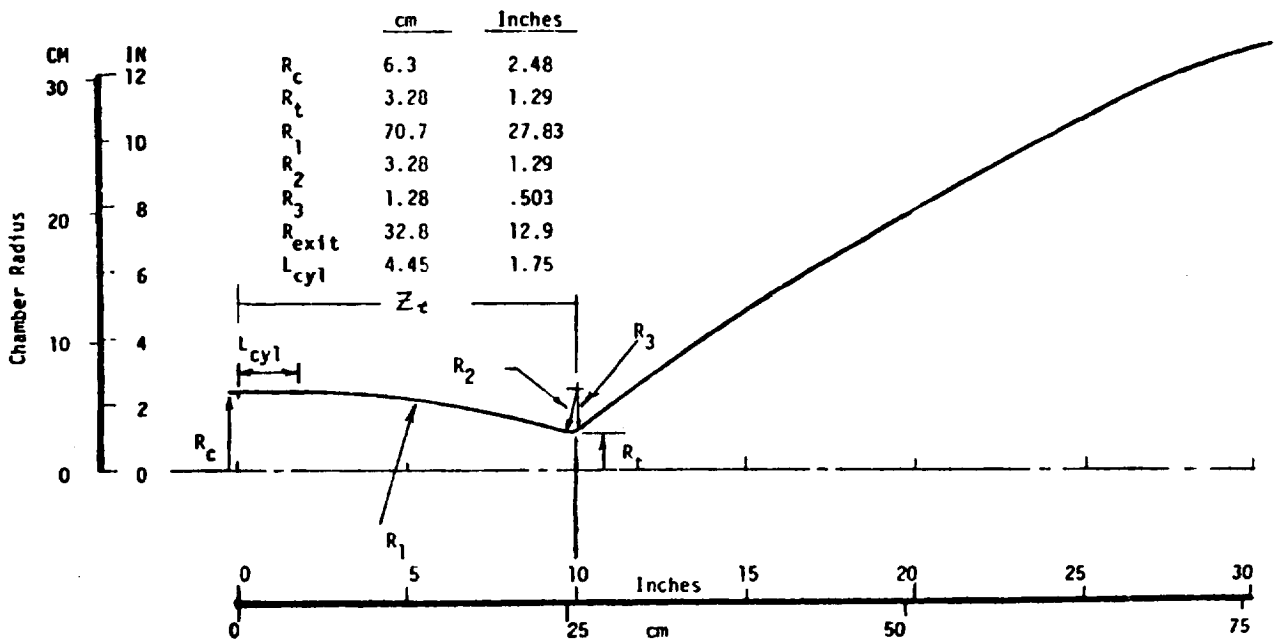
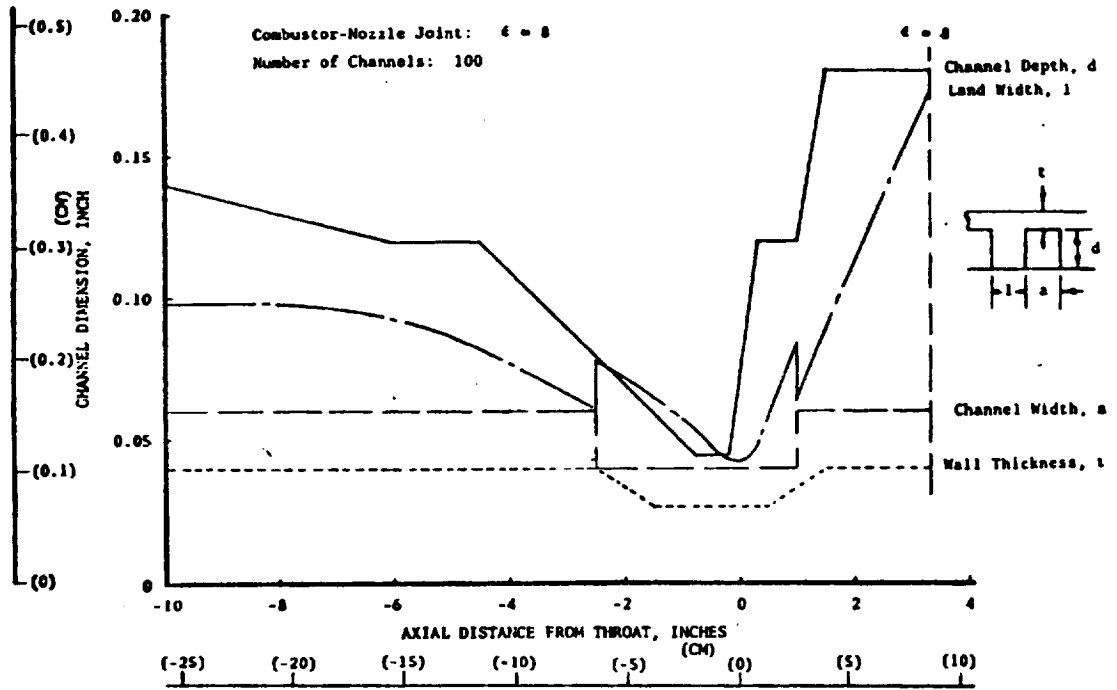


Figure 53. Coolant Passage Geometry and Chamber Contour

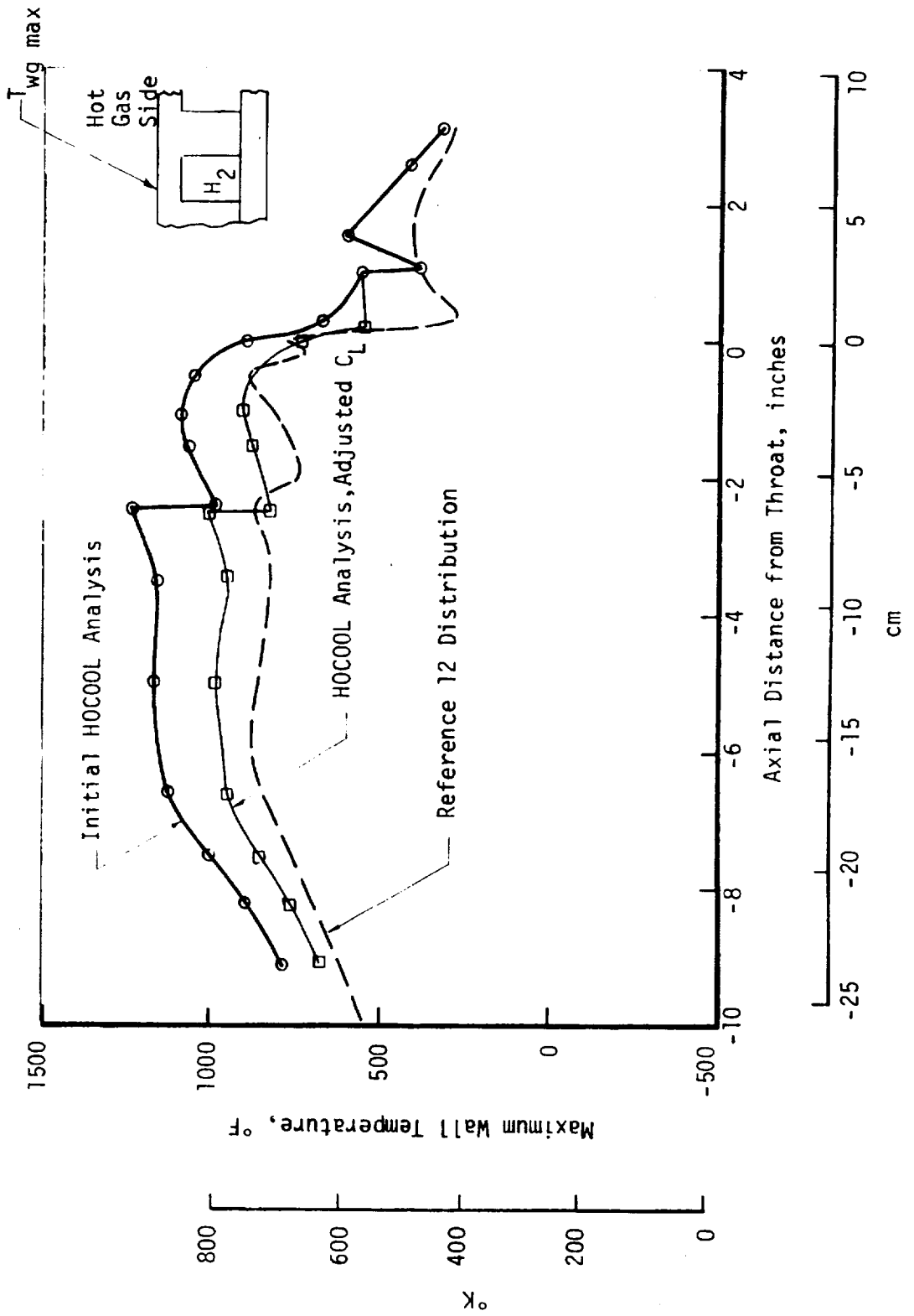


Figure 54. Combustor Wall Temperature Predictions Without Film Cooling

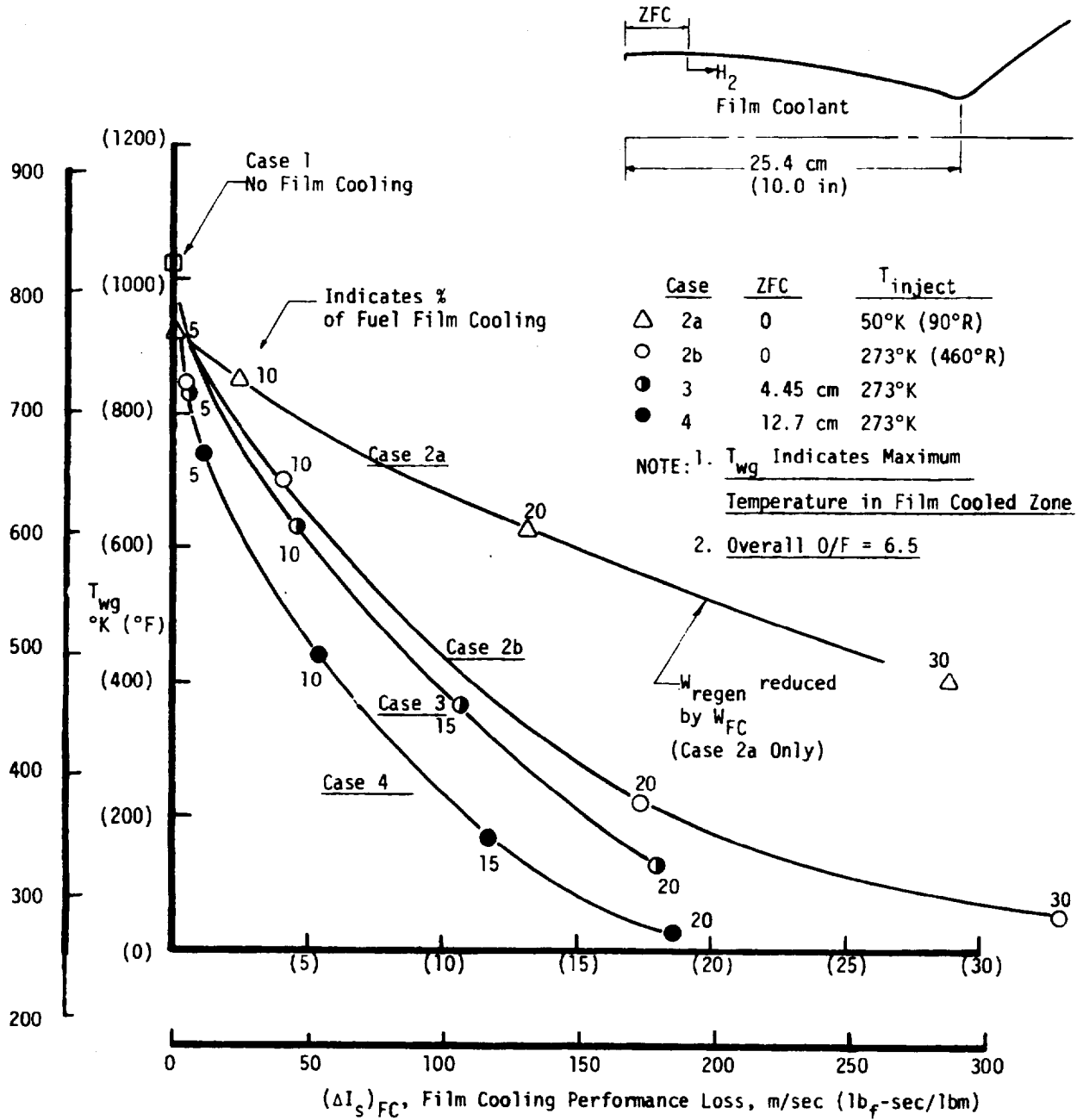


Figure 55. HOCOOL Predictions of Maximum Wall Temperature in the Film Cooled Region and Performance Loss

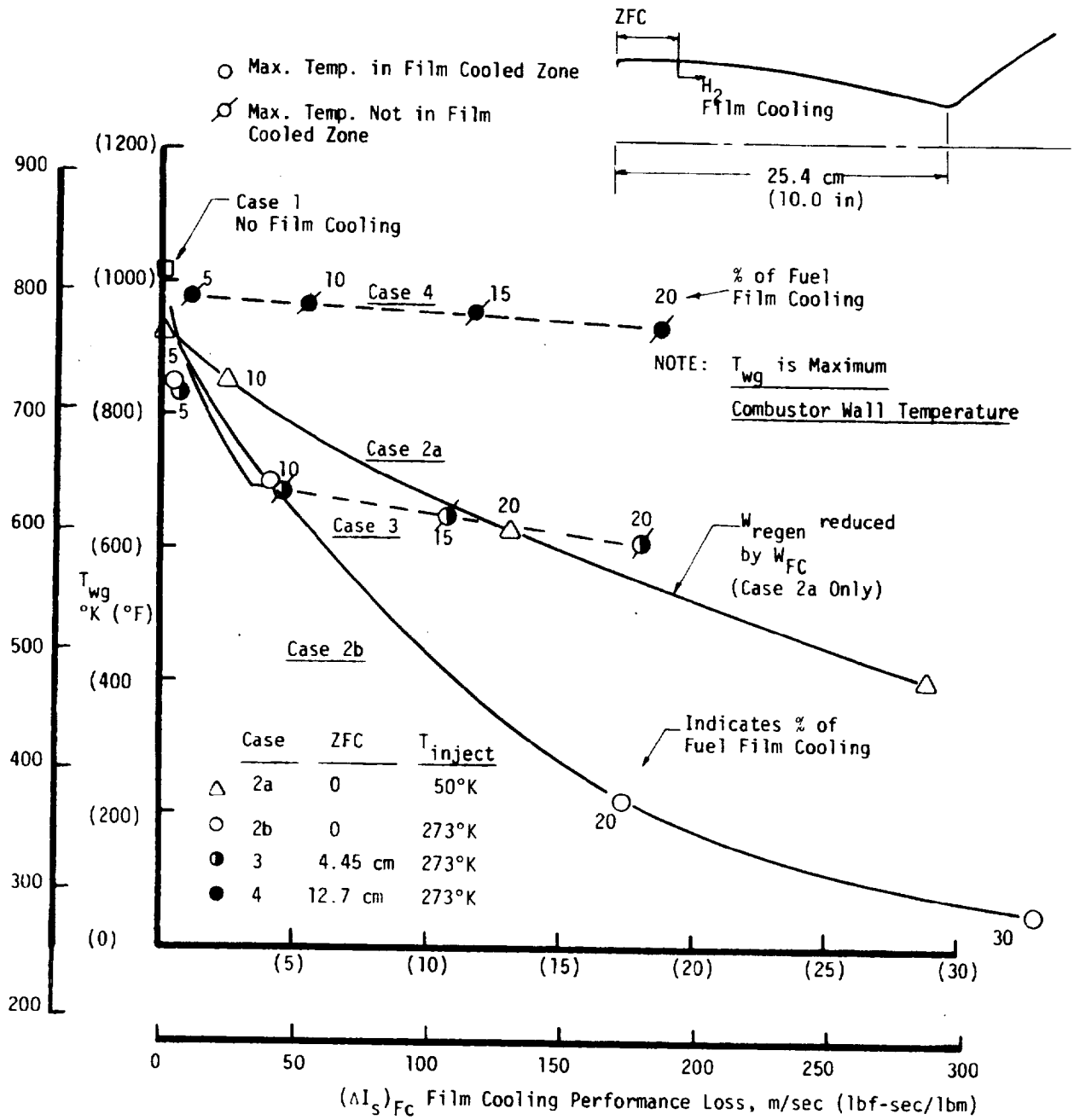


Figure 56. HOCOOL Predictions of Maximum Combustor Temperature and Film Cooling Performance Loss

APPENDIX A
NOMENCLATURE

English Letters

c	Mass fraction
C_g	Heat transfer correlation coefficient
C_p	Specific heat
$f(u_c/u_e)$	Velocity ratio correlating function (Figure 7)
g	velocity decay function (Equation 41)
G	Mass flux
h	Slot height
H	Static enthalpy
h_{ex}	External or ambient-side heat transfer coefficient
h_g	Gas-side heat transfer coefficient
H_o	Total enthalpy
H_{aw}	Adiabatic wall enthalpy
$I_{sp ML}$	Specific impulse of mixing layer stream tube
$I_{sp core}$	Specific impulse of core gas stream tube
$\Delta I_{sp FCL}$	Film cooling specific impulse loss
$I_{sp uncooled}$	Uncooled engine delivered specific impulse
$I_{sp cooled}$	Cooled engine delivered specific impulse
$I_{sp ODE}$	One dimensional equilibrium specific impulse
$\Sigma I_{sp losses}$	Summation of real engine performance losses excluding film cooling
k	Entrainment fraction
k_o	Entrainment fraction for plane, unaccelerated flow with continuous slot injection, defined by Equation 21
k_o'	Defined by Equation 44
k_m	Plane, unaccelerated flow entrainment fraction multiplier (Defined by Equations 48 and 56)
k_t	Entrainment fraction multiplier due to flow turning

Nomenclature (cont.)

English Letters

k_{lip}	Lip wake factor
k_f	Velocity ratio factor
k_∞	Asymptotic cylindrical section multiplier
MW	Molecular weight
m	Acceleration exponent
O/F	Mixture ratio, O_2/H_2
Pr	Prandtl number
Q/A	Nozzle wall heat flux
r	Local chamber or nozzle radius
R	Radius of curvature of nozzle wall
Re_c	Coolant Reynolds number based on slot height, $\rho_c u_c h/\mu_c$
Re_D	Nozzle Reynolds number in Equation 39
St	Stanton Number in Equation 39
s	Mixing layer thickness
t_{lip}	Slot lip thickness
T	Static temperature
T_o	Total temperature
T_{aw}	Adiabatic wall temperature
T_{wg}	Gas-side nozzle wall temperature
\bar{u}	Effective mixing layer velocity (Equation 7)
u	Axial velocity
u_c/u_e	Film coolant to core gas velocity ratio at the injection point
V (W_E/W_C)	Velocity mixing function (Equation 7A)
W	Total flow rate
W_{ML}	Mixing layer flow rate at the throat

Nomenclature (cont.)

English Letters

W_c	Film coolant flow rate
W_{core}	Core gas streamtube flow rate at the throat
W_E	Entrained flow rate
x	Contour distance from the film coolant injection point
\bar{X}	Contour integral defined by Eq. (28)
\bar{y}	Value of \bar{X} required to satisfy Eq. (27)

Greek Letters

α	Angle between the nozzle centerline and the wall tangent
γ	Mass fraction of the injected film coolant
η	Film cooling effectiveness, defined by Eq. (1)
ηI_{sp}	Performance efficiency factor, $I_{sp \text{ uncooled}}/I_{sp \text{ ODE}}$
θ	Enthalpy and mass fraction profile shape factor for the mixing layer
μ	Viscosity
ξ	Mixing layer area fraction
ρ	Density
ρ_c/ρ_e	Film coolant to core gas density ratio at the injection point
\emptyset	Ratio of 2D flow mass velocity to 1D flow mass velocity

Subscripts

@ O/F overall	Evaluated at engine overall mixture ratio
@ O/F core	Evaluated at core mixture ratio
@ O/F _{ML}	Evaluated at mixing layer mixture ratio
aw	Adiabatic wall condition
b	Bulk value for the mixing layer
c	Coolant at the injection point

Nomenclature (cont.)

Subscripts

Core	Evaluated for core mass at nozzle throat plane
e	Freestream or core
f	Average film temperature
ML	Evaluated for mixing layer mass at nozzle throat plane
o	Film coolant injection location (except H_o , T_o , k_o)
v	At the edge of the viscous sublayer
w	At the chamber wall

APPENDIX B
TABULATED FILM COOLING TEST DATA

The following pages contain output from the data reduction version of the ALRC entrainment film cooling model. Pertinent data parameters are listed for each of the film cooling tests. Most of the parameters listed are defined in Appendix D and Reference 5; however there are a few exceptions and they are defined below.

Wall Temp.	=	Adiabatic Wall Temperature
Temp.	=	Measured Wall Temperature
Core MR	=	Mixture Ratio of Core Gases
TF_c	=	Film Coolant Injection Temperature

TEST NO. 2486 - 12- 102 M2 FILM COOLANT O / F = 4.0 RUN 8

INJECTION CONDITIONS--ENTRAINMENT DATA MODE

VELOCITY RATIO	FILM COOLANT FLOW FR	FILM COOLANT AREA FR	SLOT HEIGHT	OVERALL MIXTURE RATIO	FUEL FLOW FRACTION	OXIDIZER FLOW FRACTION	COOLANT REYNOLDS NUMBER	$\frac{P_c}{P_e}$	$\frac{w}{15/64}$	Case MR	Temp °F
1.2069	.1561	.0654	.0595	2.0427	.4749	.0000	117047.	2.117	4.110	3.2.2	65.
MIXING PARAMETER# .5230-02											
SPECIAL DATA MODE OUTPUT											
AXIAL LENGTH	CONTOUR LENGTH	XBAR	DATA XBAR	ENTRAIN. MULT.	ETA	WALL TEMP	TEMP				
.9000	.9000	.9000	7.6388	7.8209	.9132	183.	180.0				
1.6000	1.6000	1.6000	11.9211	6.9747	.6423	314.	308.0				
2.4000	2.4000	2.4000	16.4090	5.6098	.7879	438.	428.0				
3.2000	3.2000	3.2000	21.9000	6.8638	.7324	552.	539.0				
4.2000	4.2000	4.2000	25.7421	3.8821	.6969	640.	623.0				
4.6700	4.6746	4.6732	27.7711	4.2039	.6807	685.	668.0				
5.1500	5.1920	5.1782	30.2935	4.9947	.6606	744.	728.0				
5.5250	5.6211	5.5807	31.0802	1.9543	.6544	760.	744.0				
5.9000	6.0503	5.9653	30.6568	-1.1010	.6577	746.	731.0				
6.4500	6.6245	6.4544	30.4312	-4.613	.6595	716.	699.0				
6.6600	6.8366	6.6334	30.6051	2.0895	.6566	719.	700.0				
7.9600	8.1812	7.8249	32.4136	1.3500	.6439	690.	670.0				
9.2600	9.5258	9.1083	36.0009	2.7951	.6187	724.	697.0				

TEST NO. 2486 - 12- 102 M2 FILM COOLANT O / F = 4.0 RUN D

INJECTION CONDITIONS--ENTRAINMENT DATA MODE

VELOCITY RATIO	FILM COOLANT FLOW FR	FILM COOLANT AREA FR	SLOT HEIGHT	OVERALL MIXTURE RATIO	FUEL FLOW FRACTION	OXIDIZER FLOW FRACTION	COOLANT REYNOLDS NUMBER	$\frac{P_c}{P_e}$	$\frac{w}{15/64}$	Case MR	Temp °F
1.2066	.1560	.0654	.0595	2.0433	.4749	.0000	117047.	2.117	4.110	3.2.2	65.
MIXING PARAMETER# .5228-02											
SPECIAL DATA MODE OUTPUT											
AXIAL LENGTH	CONTOUR LENGTH	XBAR	DATA XBAR	ENTRAIN. MULT.	ETA	WALL TEMP	TEMP				
.9000	.9000	.9000	6.7874	7.5415	.9170	176.	174.0				
1.6000	1.6000	1.6000	12.6345	8.3531	.8323	335.	329.0				
2.4000	2.4000	2.4000	17.3260	5.8644	.7779	457.	447.0				
3.2000	3.2000	3.2000	18.6693	1.6791	.7632	486.	474.0				
4.2000	4.2000	4.2000	22.3011	3.6318	.7287	561.	546.0				
4.6700	4.6746	4.6732	23.1512	1.7966	.7209	579.	565.0				
5.1500	5.1920	5.1782	23.1169	-0.0678	.7212	577.	565.0				
5.5250	5.6211	5.5807	24.4387	3.2835	.7091	603.	591.0				
5.9000	6.0503	5.9653	25.4232	2.5598	.7002	623.	611.0				
6.4500	6.6245	6.4544	26.1103	1.4047	.6940	617.	602.0				

REPRODUCIBILITY OF THE ORIGINAL PAGE IS POOR

TEST NO. 2K86 - 12- 103 M2 FILM COOLANT O / F = 4.0 ROM 8

INJECTION CONDITIONS--ENTRAINMENT DATA MODE

VELOCITY RATIO	FILM COOLANT FLOW FR	FILM COOLANT AREA FR	SLOT HEIGHT	OVERALL MIXTURE RATIO	FUEL FLOW FRACTION	OXIDIZER FLOW FRACTION	COOLANT REYNOLDS NUMBER
1.0186	.1335	.0654	.0595	2.1900	.4260	.0000	94241.
MIXING PARAMETERS .5084-02							
SPECIAL DATA MODE OUTPUT							
AXIAL LENGTH	CONTOUR LENGTH	XBAR	DATA XBAR	ENTRAIN. MULT.	ETA	WALL TEMP	TEMP
.9000	.9000	.9000	6.5614	7.2904	.9036	208.	205.0
1.6000	1.6000	1.6000	10.6346	5.8189	.8350	338.	332.0
2.4000	2.4000	2.4000	14.2291	4.4931	.7850	451.	441.0
3.2000	3.2000	3.2000	18.4242	5.2439	.7350	554.	540.0
4.2000	4.2000	4.2000	21.4565	3.0323	.7022	633.	615.0
4.6700	4.6743	4.6728	23.2943	3.8869	.6839	682.	664.0
5.1500	5.1682	5.1751	25.6340	4.6586	.6618	746.	729.0
5.5250	5.6162	5.5776	26.2590	1.5227	.6559	760.	744.0
5.9000	6.0443	5.9627	25.8926	-.9513	.6594	746.	731.0
6.4500	6.6239	6.4572	25.6688	-.4527	.6615	715.	698.0
6.8000	6.8360	6.6361	25.6242	-.6683	.6600	713.	695.0
9.2600	9.5252	9.1110	30.2364	1.7828	.6214	723.	694.0

W 3.86
Core MR 3.82
TFC 70.

TEST NO. 2K86 - 12- 103 M2 FILM COOLANT O / F = 4.0 ROM 0

INJECTION CONDITIONS--ENTRAINMENT DATA MODE

VELOCITY RATIO	FILM COOLANT FLOW FR	FILM COOLANT AREA FR	SLOT HEIGHT	OVERALL MIXTURE RATIO	FUEL FLOW FRACTION	OXIDIZER FLOW FRACTION	COOLANT REYNOLDS NUMBER
1.0186	.1335	.0654	.0595	2.1900	.4260	.0000	94241.
MIXING PARAMETERS .5084-02							
SPECIAL DATA MODE OUTPUT							
AXIAL LENGTH	CONTOUR LENGTH	XBAR	DATA XBAR	ENTRAIN. MULT.	ETA	WALL TEMP	TEMP
.9000	.9000	.9000	6.3936	7.1040	.9067	203.	200.0
1.6000	1.6000	1.6000	11.2055	6.8741	.8264	357.	350.0
2.4000	2.4000	2.4000	14.9109	4.6317	.7763	468.	463.0
3.2000	3.2000	3.2000	18.1332	1.5279	.7606	499.	487.0
4.2000	4.2000	4.2000	18.0164	2.6852	.7307	563.	548.0
4.6700	4.6743	4.6728	19.6829	1.8283	.7214	585.	570.0
5.1500	5.1682	5.1751	19.6793	-.0070	.7214	584.	571.0
5.5250	5.6162	5.5776	20.9069	3.0547	.7081	613.	600.0
5.9000	6.0443	5.9627	21.8496	2.4428	.6980	635.	623.0
6.4500	6.6239	6.4572	22.2392	.7679	.6939	624.	609.0

TEST NO. 105 T/C ROM B H2 FILM COOLANT D/F = 6.0

INJECTION CONDITIONS--ENTRAINMENT DATA MODE

VELOCITY RATIO	FILM COOLANT FLOW FR	FILM COOLANT AREA FR	SLOT HEIGHT	OVERALL MIXTURE RATIO	FUEL FLOW FRACTION	OXIDIZER FLOW FRACTION	COOLANT REYNOLDS NUMBER
1.3077	.1469	.0654	.0595	2.6590	.5375	.0000	110975.
MIXING PARAMETERS .5937-02							
SPECIAL DATA MODE OUTPUT							
AXIAL LENGTH	CONTOUR	XBAR	DATA XBAR	ENTRAIN. MULT.	ETA	WALL TEMP	TEMP
.9000	.9000	.9000	6.1780	6.8645	.9057	207.	205.0
1.6000	1.6000	1.6000	10.5689	6.2727	.8268	371.	364.0
2.4000	2.4000	2.4000	15.4603	6.1243	.7607	527.	516.0
3.2000	3.2000	3.2000	19.5313	5.0787	.7143	649.	633.0
4.2000	4.2000	4.2000	23.2990	3.7677	.6749	774.	758.0
4.6700	4.6746	4.6732	25.1828	3.0814	.6565	834.	812.0
5.1500	5.1920	5.1782	27.6825	4.9498	.6333	898.	877.0
5.5250	5.6211	5.5807	28.4370	1.8744	.6249	914.	893.0
5.9000	6.0503	5.9653	27.8873	-1.4295	.6315	896.	878.0
6.4500	6.6245	6.4544	26.4615	-2.9149	.6441	840.	819.0
6.6600	6.6366	6.6334	26.5238	.3480	.6435	836.	818.0

$\frac{\rho_c}{\rho_f}$ W Core MR Tfc
 1.88 4.131 5.75 61.

TEST NO. 105 T/C ROM D H2 FILM COOLANT D/F = 6.0

INJECTION CONDITIONS--ENTRAINMENT DATA MODE

VELOCITY RATIO	FILM COOLANT FLOW FR	FILM COOLANT AREA FR	SLOT HEIGHT	OVERALL MIXTURE RATIO	FUEL FLOW FRACTION	OXIDIZER FLOW FRACTION	COOLANT REYNOLDS NUMBER
1.3077	.1469	.0654	.0595	2.6590	.5375	.0000	110975.
MIXING PARAMETERS .5937-02							
SPECIAL DATA MODE OUTPUT							
AXIAL LENGTH	CONTOUR	XBAR	DATA XBAR	ENTRAIN. MULT.	ETA	WALL TEMP	TEMP
.9000	.9000	.9000	5.6027	6.2252	.9142	189.	184.0
1.6000	1.6000	1.6000	9.7237	5.8672	.8430	337.	331.0
2.4000	2.4000	2.4000	13.6591	4.9192	.7849	474.	463.0
3.2000	3.2000	3.2000	15.6136	2.6935	.7562	538.	522.0
4.2000	4.2000	4.2000	19.3121	3.4962	.7107	642.	620.0
4.6700	4.6746	4.6732	20.7252	2.9867	.7009	688.	666.0
5.1500	5.1920	5.1782	21.2290	.9976	.6953	703.	684.0
5.5250	5.6211	5.5807	22.1559	2.3025	.6861	732.	710.0
5.9000	6.0503	5.9653	22.4681	.8116	.6830	739.	728.0
6.4500	6.6245	6.4544	22.1950	-.5544	.6857	710.	688.0

TEST NO. 2MB6 - 12- 109 H2 FILM COOLANT O / F = 8.0

INJECTION CONDITIONS--ENTRAINMENT DATA MODE

VELOCITY RATIO	FILM COOLANT FLOW FR	FILM COOLANT AREA FR	SLOT WEIGHT	OVERALL MIXTURE RATIO	FUEL FLOW FRACTION	OXIDIZER FLOW FRACTION	COOLANT REYNOLDS NUMBER
1.5131	.1405	.0654	.0595	3.2306	.5986	.0000	120704.
MIXING PARAMETER = .7519-02							
SPECIAL DATA MODE OUTPUT							
AXIAL LENGTH	CONTOUR LENGTH	XBAR	DATA XBAR	ENTRAIN. MULT.	ETA	MALL TEMP	TEMP
.9000	.9000	.9000	4.1678	4.6309	.9170	206.	203.0
1.6000	1.6000	1.6000	7.5979	4.9002	.8358	383.	376.0
2.4000	2.4000	2.4000	11.3795	4.7270	.7644	555.	543.0
3.2000	3.2000	3.2000	14.8709	4.1142	.7135	700.	683.0
4.2000	4.2000	4.2000	18.2312	3.5603	.6645	863.	839.0
4.6700	4.6746	4.6732	19.6447	2.9874	.6461	917.	893.0
5.5250	5.6211	5.5807	21.7396	2.3083	.6215	994.	972.0
5.9000	6.0503	5.9653	21.2739	-1.2109	.6268	973.	954.0
6.4500	6.6245	6.4544	20.4510	-1.6822	.6361	924.	903.0

ROW B

P-PC JJ CORE NR TFC

154 470 1.117 72.9

BP 5

AXIAL LENGTH	CONTOUR LENGTH	XBAR	DATA XBAR	ENTRAIN. MULT.	ETA	MALL TEMP	TEMP
.9000	.9000	.9000	4.1500	4.6111	.9174	205.	202.0
1.6000	1.6000	1.6000	7.5838	5.0197	.8343	387.	380.0
2.4000	2.4000	2.4000	10.7644	3.6758	.7753	528.	517.0
3.2000	3.2000	3.2000	12.2234	1.8237	.7503	591.	578.0
4.2000	4.2000	4.2000	14.6249	2.6015	.7112	707.	689.0
5.1500	5.1920	5.1782	16.3270	1.5356	.6894	781.	764.0
5.9000	6.0503	5.9653	16.9806	.8304	.6808	808.	792.0
6.4500	6.6245	6.4584	16.3608	-1.2671	.6890	760.	743.0

ROW D

AXIAL LENGTH	CONTOUR LENGTH	XBAR	DATA XBAR	ENTRAIN. MULT.	ETA	MALL TEMP	TEMP
1.6000	1.6000	1.6000	7.7367	4.8354	.8327	391.	384.0
2.4000	2.4000	2.4000	10.2909	3.1927	.7838	508.	499.0
3.2000	3.2000	3.2000	13.3963	3.6818	.7326	641.	624.0

ROW F

AXIAL LENGTH	CONTOUR LENGTH	XBAR	DATA XBAR	ENTRAIN. MULT.	ETA	MALL TEMP	TEMP
1.6000	1.6000	1.6000	6.6809	4.1755	.8569	332.	326.0
2.4000	2.4000	2.4000	9.1411	3.0753	.8053	461.	452.0
3.2000	3.2000	3.2000	10.9792	2.2976	.7715	537.	526.0

ROW G

TEST NU. 2K86 - 12- 110 W2 FILM COOLANT O / F = 8.0

INJECTION CONDITIONS--ENTRAINMENT DATA MODE

VELOCITY RATIO	FILM COOLANT FLOW FR	FILM COOLANT AREA FR	SLOT WEIGHT	OVERALL MIXTURE RATIO	FUEL FLOW FRACTION	OXIDIZER FLOW FRACTION	COOLANT REYNOLDS NUMBER	ρ_c	$\frac{\rho_c}{\rho_c}$	W	Core MR	TFC
1.2967	.1235	.0654	.0595	3.4628	.5510	.0000	103330.	1.55		4.58	7.71	77.6
MIXING PARAMETER = .6141=02												
SPECIAL DATA MODE OUTPUT												
AXIAL LENGTH	CONTOUR LENGTH	XBAR	DATA XBAR	ENTRAIN. MULT.	ETA	WALL TEMP	TEMP					
.9000	.9000	.9000	4.7396	5.2662	.9089	225.	222.0					
1.6000	1.6000	1.6000	8.2849	5.0647	.8297	402.	394.0					
2.4000	2.4000	2.4000	12.1671	4.8778	.7605	567.	554.0					
3.2000	3.2000	3.2000	15.4265	4.0492	.7131	702.	684.0					
4.2000	4.2000	4.2000	18.9133	3.4869	.6670	856.	831.0					
4.6700	4.6700	4.6700	20.4715	3.2932	.6475	913.	887.0					
5.5250	5.5211	5.5807	22.7459	2.5061	.6218	993.	969.0					
5.9000	6.0503	5.9653	22.2172	-1.3747	.6275	971.	950.0					
6.4500	6.6245	6.4544	21.5037	-1.4588	.6353	927.	904.0					
ROM B												
AXIAL LENGTH	CONTOUR LENGTH	XBAR	DATA XBAR	ENTRAIN. MULT.	ETA	WALL TEMP	TEMP					
.9000	.9000	.9000	4.5837	5.0930	.9125	219.	215.0					
1.6000	1.6000	1.6000	8.1631	5.1134	.8322	396.	386.0					
2.4000	2.4000	2.4000	11.3191	3.9450	.7753	531.	519.0					
3.2000	3.2000	3.2000	12.8124	1.8667	.7508	592.	578.0					
4.2000	4.2000	4.2000	15.5028	2.6903	.7120	706.	686.0					
5.1500	5.1920	5.1782	17.1946	1.7296	.6886	785.	766.0					
5.9000	6.0503	5.9653	17.7669	.7270	.6814	806.	789.0					
6.4500	6.6245	6.4544	17.1607	-1.2394	.6891	761.	742.0					
7.9800	8.1812	7.8249	18.2669	.6072	.6751	754.	733.0					
ROM D												
AXIAL LENGTH	CONTOUR LENGTH	XBAR	DATA XBAR	ENTRAIN. MULT.	ETA	WALL TEMP	TEMP					
1.6000	1.6000	1.6000	6.4538	5.2837	.8266	410.	402.0					
2.4000	2.4000	2.4000	10.9694	3.1445	.7812	517.	507.0					
3.2000	3.2000	3.2000	14.0869	3.8968	.7324	644.	625.0					
ROM F												
AXIAL LENGTH	CONTOUR LENGTH	XBAR	DATA XBAR	ENTRAIN. MULT.	ETA	WALL TEMP	TEMP					
1.6000	1.6000	1.6000	7.2952	4.5595	.8511	349.	342.0					
2.4000	2.4000	2.4000	9.7361	3.0512	.8030	469.	458.0					
3.2000	3.2000	3.2000	12.2486	3.1407	.7595	570.	555.0					
ROM G												

TEST NO. 2444 - 12- 111 H2 FILM COOLANT O / F = 0.0

INJECTION CONDITIONS--ENTRAINMENT DATA MODE

VELOCITY RATIO 1.0727
 FILM COOLANT AREA FL 0.054
 SLUT HEIGHT 0.595
 OVERALL MIXTURE RATIO 3.9718
 FUEL FLOW FRACTION 0.5029
 OXIDIZER FLOW FRACTION 0.0000
 COOLANT REYNOLDS NUMBER 82554
 CORE MR 7.99
 W 4.46
 $\frac{\rho_c}{\rho_c}$ 1.50
 TFC 85.6

MIXING PARAMETERS
 SPECIAL DATA MODE OUTPUT
 .5599-02

AXIAL LENGTH	AXIAL LENGTH	COOLANT AREA FL	SLUT HEIGHT	OVERALL MIXTURE RATIO	FUEL FLOW FRACTION	OXIDIZER FLOW FRACTION	COOLANT REYNOLDS NUMBER
.9000	.9000	1.6000	7.7182	4.4636	.8195	.8970	257.
1.6000	1.6000	2.4000	10.0592	3.9263	.7561	439.	429.0
2.4000	2.4000	3.2000	13.5906	3.1643	.7140	589.	574.0
3.2000	3.2000	4.0000	15.2042	2.8735	.6988	659.	691.0
4.0000	4.0000	4.8000	17.0321	2.6912	.6500	791.	832.0
4.8000	4.8000	5.6000	19.0604	2.1697	.6230	917.	889.0
5.2500	5.2500	5.9653	19.3296	-7036	.6272	984.	973.0
5.9000	5.9000	6.4544	19.7274	-1.2307	.6349	940.	962.0
6.4500	6.4500						916.0

AXIAL LENGTH	AXIAL LENGTH	COOLANT AREA FL	SLUT HEIGHT	OVERALL MIXTURE RATIO	FUEL FLOW FRACTION	OXIDIZER FLOW FRACTION	COOLANT REYNOLDS NUMBER	W	Core MR	$\frac{\rho_c}{\rho_c}$	TFC
.9000	.9000	1.6000	7.7182	4.4636	.8195	.8970	257.				
1.6000	1.6000	2.4000	10.0592	3.9263	.7561	439.	429.0				
2.4000	2.4000	3.2000	13.5906	3.1643	.7140	589.	574.0				
3.2000	3.2000	4.0000	15.2042	2.8735	.6988	659.	691.0				
4.0000	4.0000	4.8000	17.0321	2.6912	.6500	791.	832.0				
4.8000	4.8000	5.6000	19.0604	2.1697	.6230	917.	889.0				
5.2500	5.2500	5.9653	19.3296	-7036	.6272	984.	973.0				
5.9000	5.9000	6.4544	19.7274	-1.2307	.6349	940.	962.0				
6.4500	6.4500						916.0				

AXIAL LENGTH	AXIAL LENGTH	COOLANT AREA FL	SLUT HEIGHT	OVERALL MIXTURE RATIO	FUEL FLOW FRACTION	OXIDIZER FLOW FRACTION	COOLANT REYNOLDS NUMBER	W	Core MR	$\frac{\rho_c}{\rho_c}$	TFC
.9000	.9000	1.6000	7.7182	4.4636	.8195	.8970	257.				
1.6000	1.6000	2.4000	10.0592	3.9263	.7561	439.	429.0				
2.4000	2.4000	3.2000	13.5906	3.1643	.7140	589.	574.0				
3.2000	3.2000	4.0000	15.2042	2.8735	.6988	659.	691.0				
4.0000	4.0000	4.8000	17.0321	2.6912	.6500	791.	832.0				
4.8000	4.8000	5.6000	19.0604	2.1697	.6230	917.	889.0				
5.2500	5.2500	5.9653	19.3296	-7036	.6272	984.	973.0				
5.9000	5.9000	6.4544	19.7274	-1.2307	.6349	940.	962.0				
6.4500	6.4500						916.0				

AXIAL LENGTH	AXIAL LENGTH	COOLANT AREA FL	SLUT HEIGHT	OVERALL MIXTURE RATIO	FUEL FLOW FRACTION	OXIDIZER FLOW FRACTION	COOLANT REYNOLDS NUMBER	W	Core MR	$\frac{\rho_c}{\rho_c}$	TFC
.9000	.9000	1.6000	7.7182	4.4636	.8195	.8970	257.				
1.6000	1.6000	2.4000	10.0592	3.9263	.7561	439.	429.0				
2.4000	2.4000	3.2000	13.5906	3.1643	.7140	589.	574.0				
3.2000	3.2000	4.0000	15.2042	2.8735	.6988	659.	691.0				
4.0000	4.0000	4.8000	17.0321	2.6912	.6500	791.	832.0				
4.8000	4.8000	5.6000	19.0604	2.1697	.6230	917.	889.0				
5.2500	5.2500	5.9653	19.3296	-7036	.6272	984.	973.0				
5.9000	5.9000	6.4544	19.7274	-1.2307	.6349	940.	962.0				
6.4500	6.4500						916.0				

TEST NO. 2K86 - 12- 112 H2 FILM COOLANT 0 / F = 2.0

INJECTION CONDITIONS--ENTRAINMENT DATA MODE

VELOCITY RATIO	FILM COOLANT FLOW FR	FILM COOLANT AREA FR	SLOT HEIGHT	OVERALL MIXTURE RATIO	FUEL FLOW FRACTION	OXIDIZER FLOW FRACTION	COOLANT REYNOLDS NUMBER	$\frac{\rho_c}{\rho_e}$	w	core MR	Tfc
1.2016	.1742	.0654	.0595	1.2530	.3926	.0000	130476.	2.35	4.07	2.06	50.7
MIXING PARAMETERS .5383-02											
SPECIAL DATA MODE OUTPUT											
AXIAL LENGTH	CONTOUR LENGTH	XBAR	DATA XBAR	ENTRAIN. MULT.	ETA	WALL TEMP	TEMP				
.9000	.9000	.9000	7.3035	8.1151	.9201	143.	141.0				
1.6000	1.6000	1.6000	12.9239	8.0290	.8464	250.	246.0				
2.4000	2.4000	2.4000	17.9843	6.3256	.7905	348.	341.0	ROM B			
3.2000	3.2000	3.2000	22.3402	5.4448	.7493	430.	420.0				
4.2000	4.2000	4.2000	26.2422	5.9020	.7010	512.	499.0				
4.6700	4.6746	4.6732	30.2926	4.3336	.6856	541.	528.0				
5.1500	5.1920	5.1782	30.8458	1.0954	.6817	548.	536.0				
5.5250	5.4211	5.5807	33.4530	6.4767	.6632	581.	569.0				
5.9000	6.0503	5.9653	33.3755	-.2014	.6637	576.	565.0				
6.4500	6.6245	6.4544	33.8411	.9519	.6605	558.	545.0				

AXIAL LENGTH	CONTOUR LENGTH	XBAR	DATA XBAR	ENTRAIN. MULT.	ETA	WALL TEMP	TEMP				
.9000	.9000	.9000	6.8032	7.5591	.9271	133.	132.0				
1.6000	1.6000	1.6000	14.0097	10.2950	.8327	273.	268.0				
2.4000	2.4000	2.4000	19.0706	6.3262	.7799	369.	361.0	ROM D			
3.2000	3.2000	3.2000	21.1289	2.5729	.7599	409.	400.0				
4.2000	4.2000	4.2000	26.7197	5.5908	.7134	490.	477.0				
5.1500	5.1920	5.1782	30.2375	3.5964	.6860	539.	528.0				
6.4500	6.6245	6.4544	33.2233	2.3395	.6648	549.	536.0				

AXIAL LENGTH	CONTOUR LENGTH	XBAR	DATA XBAR	ENTRAIN. MULT.	ETA	WALL TEMP	TEMP				
1.6000	1.6000	1.6000	12.4238	7.7649	.8527	240.	236.0				
2.4000	2.4000	2.4000	16.4555	5.0396	.8065	318.	312.0				
3.2000	3.2000	3.2000	21.0471	5.7395	.7607	408.	398.0	ROM F			

AXIAL LENGTH	CONTOUR LENGTH	XBAR	DATA XBAR	ENTRAIN. MULT.	ETA	WALL TEMP	TEMP				
1.6000	1.6000	1.6000	12.4418	7.7886	.8522	241.	237.0				
2.4000	2.4000	2.4000	16.6277	5.4575	.8026	326.	319.0				
3.2000	3.2000	3.2000	20.1115	4.1847	.7698	389.	380.0	ROM G			

TEST NU. 2K86 - 12- 113 M2 FILM COOLANT O / F = 2.0

INJECTION CONDITIONS--ENTRAINMENT DATA MODE

VELOCITY RATIO	FILM COOLANT FLOW FR	FILM COOLANT AREA FR	SLOT WEIGHT	OVERALL MIXTURE RATIO	FUEL FLOW FRACTION	OXIDIZER FLOW FRACTION	COOLANT REYNOLDS NUMBER	$\frac{\rho_c}{\rho_e}$	W	core MR	TEC
1.0103	.1454	.0654	.0595	1.3582	.3428	.0000	106073.	2.41	3.16	2.07	57.5
MIXING PARAMETERS											
SPECIAL DATA MODE OUTPUT											
AXIAL LENGTH	CONTOUR LENGTH	XBAR	DATA XBAR	ENTRAIN. MULT.	ETA	WALL TEMP	TEMP				
.9000	.9000	.9000	6.7219	7.4688	.9169	154.	152.0				
1.6000	1.6000	1.6000	11.6676	7.0652	.8440	261.	256.0				
2.4000	2.4000	2.4000	15.6675	5.0249	.7939	349.	341.0				
3.2000	3.2000	3.2000	18.9764	4.1111	.7574	421.	411.0				
4.2000	4.2000	4.2000	23.5984	4.6220	.7140	495.	482.0				
5.1500	5.1920	5.1782	25.6776	2.1257	.6948	529.	517.0				
5.5250	5.6211	5.5807	28.3214	6.5677	.6732	567.	554.0				
5.9000	6.0503	5.9653	28.3698	.1256	.6726	568.	553.0				
6.4500	6.6245	6.4544	28.6512	.5753	.6705	548.	531.0				
AXIAL LENGTH	CONTOUR LENGTH	XBAR	DATA XBAR	ENTRAIN. MULT.	ETA	WALL TEMP	TEMP				
.9000	.9000	.9000	6.6653	7.4281	.9174	153.	151.0				
1.6000	1.6000	1.6000	12.9586	6.9620	.8264	290.	285.0				
2.4000	2.4000	2.4000	17.1068	5.1852	.7780	379.	371.0				
3.2000	3.2000	3.2000	18.7412	2.0430	.7600	416.	406.0				
4.2000	4.2000	4.2000	23.2125	4.4713	.7176	489.	476.0				
5.1500	5.1920	5.1782	24.7504	1.5723	.7033	513.	502.0				
6.4500	6.6245	6.4544	27.6187	2.2474	.6789	527.	515.0				
AXIAL LENGTH	CONTOUR LENGTH	XBAR	DATA XBAR	ENTRAIN. MULT.	ETA	WALL TEMP	TEMP				
1.6000	1.6000	1.6000	11.2252	7.0157	.8503	251.	255.0				
2.4000	2.4000	2.4000	14.1770	3.6898	.8119	316.	315.0				
3.2000	3.2000	3.2000	17.5692	4.2402	.7729	309.	305.0				
AXIAL LENGTH	CONTOUR LENGTH	XBAR	DATA XBAR	ENTRAIN. MULT.	ETA	WALL TEMP	TEMP				
1.6000	1.6000	1.6000	11.6824	7.3015	.8438	261.	257.0				
2.4000	2.4000	2.4000	15.6341	4.9396	.7945	347.	340.0				
3.2000	3.2000	3.2000	18.4501	3.5201	.7632	409.	399.0				

TEST NO. 2M66 - 12- 114 1/2 FILM COOLANT D / F = 6.0 RUM B

INJECTION CONDITIONS--ENTRAINMENT DATA GUIDE

VELOCITY RATIO .6373 .0919 .0654 .0595 3.6124 .4237 .0000 66250. 1.73 6.27 24.
 MIXING PARAMETERS .0276=02
 SPECIAL DATA MODE OUTPUT
 AXIAL LENGTH 1.6000 2.4000 3.2000 4.2000 5.1920 5.9250 6.4500
 COOLANT FLOW FR 1.6000 2.4000 3.2000 4.2000 5.1920 5.9250 6.4500
 FILM AREA FR 1.6000 2.4000 3.2000 4.2000 5.1920 5.9250 6.4500
 SLUIT HEIGHT 4.0596 6.5106 8.9283 10.7473 13.0085 15.4601 18.5687
 OVERALL MIXTURE RATIO 4.4085 3.5300 3.0221 2.2737 2.2612 2.5268 2.7043
 FUEL FLOW FRACTION .8851 .6104 .7511 .7133 .6698 .6268 .6095
 UXTIOIZER FLOW FRACTION 273. 445. 581. 684. 630. 952. 1005.
 COOLANT REYNOLDS NUMBER 268.0 434.0 563.0 661.0 797.0 919.0 974.0
 RUM B 4.03 6.27 24.
 Core No. TFC

ROW B

ROW D

ROW F

ROW G

TEST NU. 2486 - 12- 115 M2 FILM COOLANT O / F = 6.0

INJECTION CONDITIONS--ENTRAINMENT DATA MODE

VELOCITY RATIO	FILM COOLANT FLOW FR	FILM COOLANT AREA FR	SLOT HEIGHT	OVERALL MIXTURE RATIO	FUEL FLOW FRACTION	OXIDIZER FLOW FRACTION	COOLANT REYNOLDS NUMBER	$\frac{\rho_c}{\rho_a}$	W	Core MR	TFC
1.0722	.1188	.0654	.0595	3.0663	.4829	.0000	87270.	1.80	4.08	5.93	77.6
MIXING PARAMETERS -5373-02											
SPECIAL DATA MODE OUTPUT											
AXIAL LENGTH	CONTOUR LENGTH	XBAR	DATA XBAR	ENTRAIN. MULT.	ETA	MALL TEMP	TEMP				
.9000	.9000	.9000	5.5393	6.1547	.9013	234.	230.0				
1.6000	1.6000	1.6000	9.2917	5.3606	.8257	397.	389.0				
2.4000	2.4000	2.4000	13.0490	4.7216	.7643	538.	525.0	ROM 8			
3.2000	3.2000	3.2000	16.2012	3.9153	.7216	648.	630.0				
4.2000	4.2000	4.2000	19.9127	3.7114	.6755	794.	769.0				
5.1500	5.1920	5.1782	22.3203	2.4614	.6478	876.	852.0				
5.5250	5.6211	5.5807	23.8090	3.6982	.6319	918.	896.0				
5.9000	6.0503	5.9653	23.1832	-1.6270	.6382	897.	877.0				
6.4500	6.6245	6.4544	22.0546	-2.3070	.6509	841.	820.0				

AXIAL LENGTH	CONTOUR LENGTH	XBAR	DATA XBAR	ENTRAIN. MULT.	ETA	MALL TEMP	TEMP				
.9000	.9000	.9000	5.6220	6.4669	.8952	245.	241.0				
1.6000	1.6000	1.6000	9.5861	5.3772	.8207	410.	402.0				
2.4000	2.4000	2.4000	13.7542	5.2102	.7540	563.	550.0	ROM D			
3.2000	3.2000	3.2000	15.1735	1.7741	.7352	611.	595.0				
4.2000	4.2000	4.2000	17.5824	2.4089	.7035	701.	680.0				
5.1500	5.1920	5.1782	19.5656	2.0275	.6795	779.	760.0				
5.9000	6.0503	5.9653	20.8938	1.6674	.6642	826.	808.0				
6.4500	6.6245	6.4544	20.6088	-1.5827	.6675	795.	778.0				

AXIAL LENGTH	CONTOUR LENGTH	XBAR	DATA XBAR	ENTRAIN. MULT.	ETA	MALL TEMP	TEMP				
1.6000	1.6000	1.6000	9.5333	5.9583	.8216	408.	399.0				
2.4000	2.4000	2.4000	11.7811	2.8098	.7844	493.	481.0	ROM F			
3.2000	3.2000	3.2000	15.0270	4.0573	.7371	605.	589.0				
4.2000	4.2000	4.2000	19.1637	4.1368	.6841	764.	740.0				

AXIAL LENGTH	CONTOUR LENGTH	XBAR	DATA XBAR	ENTRAIN. MULT.	ETA	MALL TEMP	TEMP				
1.6000	1.6000	1.6000	9.4290	5.8931	.8233	403.	402.0				
2.4000	2.4000	2.4000	12.6256	3.9958	.7712	522.	520.0				
3.2000	3.2000	3.2000	15.2285	3.2536	.7345	612.	609.0	ROM G			
4.2000	4.2000	4.2000	18.3424	3.1139	.6936	732.	727.0				

TEST NO. 2KPB - 12- 116 H2 FILM COOLANT O / F = 8.0

INJECTION CONDITIONS--ENTRAINMENT DATA MODE

VELOCITY RATIO	FILM COOLANT FLOW FR	FILM COOLANT AREA FR	SLOT HEIGHT	OVERALL MIXTURE RATIO	FUEL FLOW FRACTION	OXIDIZER FLOW FRACTION	COOLANT REYNOLDS NUMBER
.8372	.0817	.0654	.0595	4.3058	.4335	.0000	59755.
MIXING PARAMETERS .6565-02							
SPECIAL DATA MODE OUTPUT							
AXIAL LENGTH	CONTOUR LENGTH	XBAR	DATA XBAR	ENTRAIN. MULT.	ETA	WALL TEMP	TEMP
.9000	.9000	.9000	3.5421	3.9356	.8792	302.	296.0
1.6000	1.6000	1.6000	5.7069	3.0926	.8033	484.	472.0
2.4000	2.4000	2.4000	7.8200	2.6415	.7430	629.	611.0
3.2000	3.2000	3.2000	9.3094	1.8617	.7060	740.	717.0
4.2000	4.2000	4.2000	11.3603	2.0709	.6594	891.	859.0
5.1500	5.1920	5.1782	13.6515	2.3219	.6136	1037.	1003.0
5.5250	5.6211	5.5807	14.5955	2.3451	.5959	1102.	1070.0
5.9000	6.0503	5.9653	14.5541	-.1076	.5967	1096.	1069.0
6.4500	6.6245	6.4544	15.0293	.9715	.5882	1110.	1079.0

AXIAL LENGTH	CONTOUR LENGTH	XBAR	DATA XBAR	ENTRAIN. MULT.	ETA	WALL TEMP	TEMP
.9000	.9000	.9000	3.2451	3.6057	.8909	278.	272.0
1.6000	1.6000	1.6000	5.6949	3.4997	.8037	483.	472.0
2.4000	2.4000	2.4000	7.5141	2.2740	.7506	608.	592.0
3.2000	3.2000	3.2000	8.2989	.9810	.7310	663.	643.0
4.2000	4.2000	4.2000	9.5062	1.2073	.7011	757.	731.0
5.1500	5.1920	5.1782	10.7079	1.2285	.6741	850.	826.0
5.9000	6.0503	5.9653	11.3640	.8355	.6594	844.	864.0
6.4500	6.6245	6.4544	11.2094	-.3101-	.6032	856.	835.0

W Core MR 4.22 7.60 95

ROM B

ROM D

ROM F

ROM G

TEST NO. 2440 - 12- 117 H2 FILM COOLANT O / F = 4.0

INJECTION CONDITIONS--ENTRAINMENT DATA MODE

VELOCITY RATIO	FILM COOLANT FLOW FR	FILM COOLANT AREA FR	SLUT HEIGHT	OVERALL MIXTURE RATIO	FUEL FLOW FRACTION	OXIDIZER FLOW FRACTION	COOLANT REYNOLDS NUMBER	$\frac{P_c}{P_e}$	W	core MR	TFC
.7000	.1004	.0054	.0595	2.5087	.3582	.0000	66745.	2.08	3.76	4.00	84.

MIXING PARAMETERS
SPECIAL DATA MODE OUTPUT

AXIAL LENGTH	COOLANT LENGTH	FILM LENGTH	SLUT HEIGHT	ENTRAIN. MULT.	ETA	MALL TEMP	ETA	MALL TEMP
.9000	.9000	.9000	4.1103	4.5737	.8930	241.		237.0
1.6000	1.6000	1.6000	6.2472	3.6150	.6215	365.		376.0
2.4000	2.4000	2.4000	8.4012	2.8176	.7688	500.		487.0
3.2000	3.2000	3.2000	11.0769	2.7195	.7254	595.		578.0
4.2000	4.2000	4.2000	13.6446	2.5717	.6787	719.		695.0
5.1920	5.1920	5.1742	16.0192	3.0370	.6306	862.		837.0
5.5250	5.6211	5.5037	18.5131	4.7048	.6032	931.		908.0
5.9000	6.0503	5.8653	18.1232	-1.0139	.6088	912.		892.0
6.4500	6.6245	6.4333	19.1521	2.1035	.5940	929.		905.0

AXIAL LENGTH	COOLANT LENGTH	FILM LENGTH	SLUT HEIGHT	ENTRAIN. MULT.	ETA	MALL TEMP	ETA	MALL TEMP
.9000	.9000	.9000	4.0450	4.5389	.8946	239.		235.0
1.6000	1.6000	1.6000	7.6471	4.5172	.8070	419.		409.0
2.4000	2.4000	2.4000	9.6510	3.0050	.7526	534.		520.0
3.2000	3.2000	3.2000	10.4106	1.4607	.7303	584.		567.0
4.2000	4.2000	4.2000	12.7393	1.9197	.6439	676.		654.0
5.1920	5.1920	5.1742	14.1601	1.4526	.6702	743.		724.0
5.9000	6.0503	5.8653	16.2347	2.6420	.6361	841.		823.0
6.4500	6.6245	6.4333	18.3578	1.3578	.6265	841.		820.0

AXIAL LENGTH	COOLANT LENGTH	FILM LENGTH	SLUT HEIGHT	ENTRAIN. MULT.	ETA	MALL TEMP	ETA	MALL TEMP
1.6000	1.6000	1.6000	6.7265	4.2031	.8190	389.		380.0
2.4000	2.4000	2.4000	8.3712	2.0559	.7607	477.		464.0
3.2000	3.2000	3.2000	10.6409	2.4371	.7337	576.		559.0
4.2000	4.2000	4.2000	13.2343	2.5434	.6850	699.		676.0

AXIAL LENGTH	COOLANT LENGTH	FILM LENGTH	SLUT HEIGHT	ENTRAIN. MULT.	ETA	MALL TEMP	ETA	MALL TEMP
1.6000	1.6000	1.6000	6.7363	4.2114	.8193	390.		381.0
2.4000	2.4000	2.4000	8.4090	2.7010	.7688	500.		487.0
3.2000	3.2000	3.2000	11.2220	2.9038	.7226	602.		584.0
4.2000	4.2000	4.2000	13.4112	2.6892	.6743	732.		707.0

TEST NO. 2K86 - 12- 119 Mt FILM COOLANT O / F = 8.0

INJECTION CONDITIONS--ENTRAINMENT DATA MODE

VELOCITY RATIO	FILM COOLANT FLOW FR	FILM COOLANT AREA FR	SLUT HEIGHT	OVERALL MIXTURE RATIO	FUEL FLOW FRACTION	OXIDIZER FLOW FRACTION	COOLANT REYNOLDS NUMBER
1.0184	.1745	.0654	.0595	2.7192	.6492	.0000	69767.
MIXING PARAMETER = .5227=02							
SPECIAL DATA MODE OUTPUT							
AXIAL LENGTH	CONTOUR LENGTH	XBAR	DATA XBAR	ENTRAIN. MULT.	ETA	WALL TEMP	TEMP
.9000	.9000	.9000	4.3691	4.8546	.9658	256.	251.0
1.6000	1.6000	1.6000	7.1184	3.9276	.9257	454.	442.0
2.4000	2.4000	2.4000	10.1458	3.7843	.8861	660.	640.0
3.2000	3.2000	3.2000	12.5248	2.9737	.8563	821.	793.0
4.0000	4.0000	4.0000	15.9998	3.4750	.8166	1046.	1008.0
4.6700	4.6746	4.6732	17.1198	2.3672	.8051	1112.	1068.0
5.1500	5.1920	5.1782	17.2395	.2371	.8039	1117.	1076.0
5.5250	5.6211	5.5807	18.4111	2.9104	.7920	1181.	1142.0
5.9000	6.0503	5.9653	18.2530	.4109	.7936	1166.	1132.0
6.4500	6.6245	6.4544	17.9777	8.5629	.7964	1110.	1098.0

AXIAL LENGTH	CONTOUR LENGTH	XBAR	DATA XBAR	ENTRAIN. MULT.	ETA	WALL TEMP	TEMP
.9000	.9000	.9000	4.0743	4.5270	.9703	235.	230.0
1.6000	1.6000	1.6000	7.0753	4.2871	.9263	451.	440.0
2.4000	2.4000	2.4000	9.8390	3.4546	.8401	639.	620.0
3.2000	3.2000	3.2000	11.2570	1.7726	.8719	736.	712.0
4.0000	4.2000	4.2000	13.3739	2.1169	.8460	878.	845.0
4.6700	4.6746	4.6732	14.5325	2.4487	.8318	957.	922.0
5.1500	5.1920	5.1782	15.6155	2.1446	.8205	1021.	987.0
5.5250	5.6211	5.5807	15.8780	.6520	.8178	1030.	997.0
5.9000	6.0503	5.9653	15.7462	.2128	.8187	1019.	989.0
6.4500	6.6245	6.4544	15.3974	.8152	.8227	957.	926.0

AXIAL LENGTH	CONTOUR LENGTH	XBAR	DATA XBAR	ENTRAIN. MULT.	ETA	WALL TEMP	TEMP
2.4000	2.4000	2.4000	9.2229	3.8429	.8981	596.	579.0
3.2000	3.2000	3.2000	11.6446	3.0271	.8671	762.	736.0
4.2000	4.2000	4.2000	15.0335	3.3889	.8265	986.	950.0

AXIAL LENGTH	CONTOUR LENGTH	XBAR	DATA XBAR	ENTRAIN. MULT.	ETA	WALL TEMP	TEMP
2.4000	2.4000	2.4000	9.3620	3.9008	.8963	606.	588.0
3.2000	3.2000	3.2000	11.6021	2.8002	.8676	759.	733.0
4.2000	4.2000	4.2000	14.3508	2.7487	.8341	945.	907.0

TEST NO. 2486 - 12-120 HE FILM COOLANT O / F = 8.0

INJECTION CONDITIONS--ENTRAINMENT DATA MODE

VELOCITY RATIO	FILM COOLANT FLOW FR	FILM COOLANT AREA FR	SLOT HEIGHT	OVERALL MIXTURE RATIO	FUEL FLOW FRACTION	OXIDIZER FLOW FRACTION	COOLANT REYNOLDS NUMBER
.8211	.1447	.0654	.0595	3.0681	.5886	.0000	53637.
MIXING PARAMETERS .6167-02							
SPECIAL DATA MODE OUTPUT							
AXIAL LENGTH	CONTOUR LENGTH	XBAR	DATA XBAR	ENTRAIN. MULT.	ETA	MALL TEMP	TEMP
.9000	.9000	.9000	3.3208	3.6898	.9578	311.	303.0
1.6000	1.6000	1.6000	5.4124	2.9880	.9141	528.	512.0
2.4000	2.4000	2.4000	7.5032	2.6136	.8738	738.	713.0
3.2000	3.2000	3.2000	9.1951	2.1148	.8430	906.	871.0
4.2000	4.2000	4.2000	11.7275	2.5324	.8024	1137.	1085.0
4.6700	4.6746	4.6732	12.7374	2.1344	.7874	1225.	1169.0
5.1500	5.1920	5.1782	13.0977	.7134	.7623	1254.	1199.0
5.5250	5.6211	5.5807	13.9982	2.2371	.7696	1324.	1271.0
5.9000	6.0503	5.9653	13.6427	-1.7943	.7739	1292.	1249.0
6.4500	6.6245	6.4544	14.2797	1.2000	.7657	1303.	1255.0

ROW B

$\frac{P_c}{P_e}$ 2.15
W 4.66
Core MR 7.46
TFC 113.

AXIAL LENGTH	CONTOUR LENGTH	XBAR	DATA XBAR	ENTRAIN. MULT.	ETA	MALL TEMP	TEMP
.9000	.9000	.9000	3.1004	3.4449	.9627	287.	280.0
1.6000	1.6000	1.6000	5.3508	3.2148	.9153	522.	507.0
2.4000	2.4000	2.4000	7.2640	2.3915	.8783	714.	691.0
3.2000	3.2000	3.2000	8.2785	1.2681	.8597	814.	784.0
4.2000	4.2000	4.2000	9.7797	1.5011	.8325	965.	923.0
4.6700	4.6746	4.6732	10.7673	2.0874	.8171	1053.	1007.0
5.1500	5.1920	5.1782	11.5235	1.4973	.8055	1117.	1074.0
5.5250	5.6211	5.5807	11.6258	.7509	.8010	1137.	1095.0
5.9000	6.0503	5.9653	11.5863	-1.6226	.8046	1110.	1073.0
6.4500	6.6245	6.4544	11.2765	-1.6334	.8093	1045.	1008.0

ROW D

AXIAL LENGTH	CONTOUR LENGTH	XBAR	DATA XBAR	ENTRAIN. MULT.	ETA	MALL TEMP	TEMP
2.4000	2.4000	2.4000	6.1303	2.5543	.9002	599.	579.0
3.2000	3.2000	3.2000	7.7802	2.0624	.8686	765.	736.0
4.2000	4.2000	4.2000	10.0920	2.3118	.8274	994.	950.0

ROW F

AXIAL LENGTH	CONTOUR LENGTH	XBAR	DATA XBAR	ENTRAIN. MULT.	ETA	MALL TEMP	TEMP
2.4000	2.4000	2.4000	6.9572	2.6988	.8842	883.	860.0
3.2000	3.2000	3.2000	8.6092	2.0649	.8537	847.	814.0
4.2000	4.2000	4.2000	10.7559	2.1466	.8172	1052.	1003.0

ROW G

MIXING PARAMETER= .5524-02
SPECIAL DATA MODE OUTPUT

VELOCITY RATIO	FILM COOLANT FLOW FR	FILM COOLANT AREA FR	SLOT HEIGHT	OVERALL MIXTURE RATIO	FUEL FLOW FRACTION	OXIDIZER FLOW FRACTION	COOLANT REYNOLDS NUMBER	$\frac{\rho_c}{\rho_f}$	W	Core MR	TFL
1.2462	.2098	.0654	.0595	2.3327	.6991	.0000	68944.	3.04	5.14	7.75	24.1
ENTRAINMENT DATA MODE											
AXIAL LENGTH	CONTOUR LENGTH	XBAR	DATA XBAR	ENTRAIN. MULT.	ETA	WALL TEMP	TEMP				
.9000	.9000	.9000	4.8173	5.3525	.9707	218.	214.0				
1.6000	1.6000	1.6000	7.7606	4.2048	.9383	397.	387.0				
2.4000	2.4000	2.4000	11.2164	4.3197	.8957	595.	578.0				
3.2000	3.2000	3.2000	14.1015	3.6064	.8650	759.	735.0				
4.0000	4.2000	4.2000	18.1722	4.0707	.8287	985.	949.0				
4.6700	4.6746	4.6732	19.3621	2.5147	.8156	1043.	1006.0				
5.1500	5.1920	5.1782	19.2441	2.2335	.8156	1036.	1001.0				
5.5250	5.6211	5.5807	20.7879	3.8352	.8025	1105.	1072.0				
5.9000	6.0503	5.9653	20.5725	5.5601	.8043	1089.	1059.0				
6.4500	6.6245	6.4544	20.6144	8.0855	.8040	1052.	1019.0				
ENTRAINMENT DATA MODE											
AXIAL LENGTH	CONTOUR LENGTH	XBAR	DATA XBAR	ENTRAIN. MULT.	ETA	WALL TEMP	TEMP				
.9000	.9000	.9000	4.5479	5.0532	.9741	202.	198.0				
1.6000	1.6000	1.6000	7.8260	4.6830	.9335	401.	391.0				
2.4000	2.4000	2.4000	11.0771	4.0638	.8972	587.	571.0				
3.2000	3.2000	3.2000	12.7406	2.0795	.8791	683.	662.0				
4.0000	4.2000	4.2000	15.4775	2.7368	.8510	836.	807.0				
4.6700	4.6746	4.6732	16.7551	2.7002	.8380	909.	878.0				
5.1500	5.1920	5.1782	17.7931	2.0555	.8280	964.	935.0				
5.5250	5.6211	5.5807	18.1842	9.716	.8246	977.	948.0				
5.9000	6.0503	5.9653	18.2787	2.456	.8238	976.	949.0				
6.4500	6.6245	6.4544	18.0210	5.5268	.8260	925.	895.0				
ENTRAINMENT DATA MODE											
AXIAL LENGTH	CONTOUR LENGTH	XBAR	DATA XBAR	ENTRAIN. MULT.	ETA	WALL TEMP	TEMP				
2.4000	2.4000	2.4000	10.6830	4.4513	.9015	564.	547.0				
3.2000	3.2000	3.2000	12.6991	2.5201	.8796	680.	659.0				
4.2000	4.2000	4.2000	16.3049	3.6058	.8426	883.	852.0				
ENTRAINMENT DATA MODE											
AXIAL LENGTH	CONTOUR LENGTH	XBAR	DATA XBAR	ENTRAIN. MULT.	ETA	WALL TEMP	TEMP				
2.4000	2.4000	2.4000	10.5249	4.3854	.9032	555.	540.0				
3.2000	3.2000	3.2000	13.2092	3.3554	.8741	709.	687.0				
4.2000	4.2000	4.2000	16.6726	3.4634	.8388	904.	871.0				

REPRODUCIBILITY OF THE ORIGINAL PAGE IS POOR

TEST NO. 2K86 - 12- 123 N2 FILM COOLANT O / F = 2.0

INJECTION CONDITIONS--ENTRAINMENT DATA MODE

VELOCITY RATIO .4225
 FILM COOLANT FLOW FR AREA FR
 FILM COOLANT FLOW FR AREA FR
 SLOT HEIGHT
 OVERALL MIXTURE RATIO
 FUEL FLOW FRACTION
 OXIDIZER FLOW FRACTION
 COOLANT REYNOLDS NUMBER
 .3162
 .4225
 .0654
 .0595
 .6436
 .6986
 .0000
 .0000
 .22961.
 33.11
 5.93
 5.93
 W Core MR
 TFC
 61.4

AXIAL LENGTH	CONTOUR LENGTH	XBAR	DATA XBAR	ENTRAIN. MULT.	ETA	WALL TEMP	COOLANT REYNOLDS NUMBER
.9000	.9000	.9000	9.5411	10.3790	.9953	126.	125.0
1.6000	1.6000	1.6000	10.9341	2.2757	.9889	229.	226.0
2.4000	2.4000	2.4000	13.6001	3.3325	.9781	392.	381.0
3.2000	3.2000	3.2000	17.1880	4.4049	.9641	588.	568.0
4.0000	4.2000	4.2000	21.3248	4.1368	.9482	789.	749.0
4.8700	4.6746	4.6732	24.0800	5.8232	.9363	901.	860.0
5.1500	5.1920	5.1762	27.2331	6.2435	.9269	1012.	967.0
5.5250	5.6211	5.5807	31.1088	9.6183	.9140	1086.	1046.0
5.9000	6.0503	5.9653	33.4212	6.0230	.9065	1106.	1071.0
6.4500	6.6245	6.4544	54.8982	43.9075	.8412	1259.	1210.0

AXIAL LENGTH	CONTOUR LENGTH	XBAR	DATA XBAR	ENTRAIN. MULT.	ETA	WALL TEMP	COOLANT REYNOLDS NUMBER
.9000	.9000	.9000	9.2503	10.2781	.9957	120.	119.0
1.6000	1.6000	1.6000	11.1657	2.7363	.9979	244.	240.0
2.4000	2.4000	2.4000	14.3768	4.0138	.9751	436.	423.0
3.2000	3.2000	3.2000	17.3609	3.7301	.9634	597.	573.0
4.0000	4.2000	4.2000	21.9645	4.6037	.9459	816.	777.0
4.8700	4.6746	4.6732	23.6244	3.5081	.9399	883.	843.0
5.1500	5.1920	5.1762	24.0935	.9289	.9382	890.	857.0
5.5250	5.6211	5.5807	28.4231	10.7557	.9228	1001.	965.0
5.9000	6.0503	5.9653	32.5639	10.7666	.9093	1081.	1048.0
6.4500	6.6245	6.4544	52.4021	40.5573	.8484	1202.	1157.0

AXIAL LENGTH	CONTOUR LENGTH	XBAR	DATA XBAR	ENTRAIN. MULT.	ETA	WALL TEMP	COOLANT REYNOLDS NUMBER
2.4000	2.4000	2.4000	12.9218	5.3841	.9808	352.	342.0
3.2000	3.2000	3.2000	16.5848	4.5787	.9664	556.	539.0
4.2000	4.2000	4.2000	21.0363	4.4514	.9493	776.	739.0

AXIAL LENGTH	CONTOUR LENGTH	XBAR	DATA XBAR	ENTRAIN. MULT.	ETA	WALL TEMP	COOLANT REYNOLDS NUMBER
2.4000	2.4000	2.4000	13.9920	5.8300	.9766	415.	402.0
3.2000	3.2000	3.2000	18.1490	5.1968	.9604	637.	611.0
4.2000	4.2000	4.2000	24.0118	5.8624	.9385	902.	856.0

TEST NO. 2K86 - 12- 124 N2 FILM COOLANT U / F = 2.0 ROW B

INJECTION CONDITIONS--ENTRAINMENT DATA MIXED

VELOCITY RATIO	FILM COOLANT FLOW FM	FILM COOLANT AREA FR	SLOT HEIGHT	OVERALL MIXTURE RATIO	FUEL FLOW FRACTION	OXIDIZER FLOW FRACTION	COOLANT REYNOLDS NUMBER
.2674	.3791	.0654	.0595	.7183	.6514	.0000	190059.
MIXING PARAMETERS .5491=02							
SPECIAL DATA MIXED OUTPUT							
AXIAL LENGTH	COOLANT LENGTH	XBAR	DATA XBAR	ENTRAIN. MULT.	ETA	WALL TEMP	TEMP
.9000	.9000	.9000	0.8410	7.6011	.9451	138.	136.0
1.6000	1.6000	1.6000	8.1433	1.8605	.9878	253.	246.0
2.4000	2.4000	2.4000	10.5620	3.0234	.9744	449.	431.0
3.2000	3.2000	3.2000	13.9862	4.2602	.9560	693.	659.0
4.2000	4.2000	4.2000	18.0998	4.1136	.9351	938.	885.0
4.6700	4.6746	4.6732	20.9775	6.0418	.9210	1081.	1022.0
5.1500	5.1920	5.1782	24.6121	7.1971	.9046	1223.	1197.0
5.5250	5.6211	5.5807	29.7419	12.7437	.8816	1354.	1297.0
5.9000	6.0503	5.9653	34.1082	11.3529	.8632	1432.	1381.0
6.4500	6.6245	6.4544	56.8778	46.5501	.7823	1636.	1563.0
6.6600	6.8366	6.8334	66.8538	55.7446	.7533	1718.	1629.0
7.9600	8.1812	7.8249	142.2518	63.2650	.6097	1785.	1673.0

U) $\frac{P_c}{P_c}$ 32.53 5.67 0.05 7.0.

TEST NO. 2K86 - 12- 124 N2 FILM COOLANT U / F = 2.0 ROW D

INJECTION CONDITIONS--ENTRAINMENT DATA MIXED

VELOCITY RATIO	FILM COOLANT FLOW FM	FILM COOLANT AREA FR	SLOT HEIGHT	OVERALL MIXTURE RATIO	FUEL FLOW FRACTION	OXIDIZER FLOW FRACTION	COOLANT REYNOLDS NUMBER
.2674	.3791	.0654	.0595	.7183	.6514	.0000	190059.
MIXING PARAMETERS .5491=02							
SPECIAL DATA MIXED OUTPUT							
AXIAL LENGTH	COOLANT LENGTH	XBAR	DATA XBAR	ENTRAIN. MULT.	ETA	WALL TEMP	TEMP
.9000	.9000	.9000	0.8461	7.6068	.9450	136.	136.0
1.6000	1.6000	1.6000	8.6168	2.5295	.9852	293.	284.0
2.4000	2.4000	2.4000	12.0466	4.2872	.9684	559.	537.0
3.2000	3.2000	3.2000	15.4205	4.2174	.9485	785.	748.0
4.2000	4.2000	4.2000	20.4159	4.9954	.9236	1059.	1000.0
4.6700	4.6746	4.6732	22.5559	4.5224	.9138	1151.	1040.0
5.1500	5.1920	5.1782	23.2436	1.4606	.9105	1169.	1118.0
5.5250	5.6211	5.5807	29.5745	15.6031	.8824	1348.	1293.0
5.9000	6.0503	5.9653	35.6063	15.6836	.8570	1479.	1427.0
6.4500	6.6245	6.4544	55.9169	41.5229	.7852	1620.	1552.0
6.6600	6.8366	6.8334	54.8352	21.4451	.7735	1609.	1533.0
7.9600	8.1812	7.8249	134.4541	62.6278	.6205	1738.	1631.0

APPENDIX C
TEST COMPONENTS AND COLD FLOW DATA

I FILM COOLING TEST ASSEMBLY

The film cooling test assembly is shown schematically on Figure 1 and as an assembly drawing in Figure C1. The following test components were designed and fabricated in this program: film cooled chamber, film coolant injector, and water cooled cylinder. These components are described in Sections II, III, and IV. Section III also contains cold flow data for the film coolant injector. Core injector cold flow data are presented in Section V.

II FILM COOLED CHAMBER

The film cooled chamber design is shown on Figure C2. This chamber was designed to be assembled with the core injector residual from the APS Program and the film coolant injector. The chamber was designed with variable cylinder length so as to provide flexibility during testing. The 4.0 inch cylindrical length design was fabricated and tested. Two thermocouples for measuring film coolant injection temperature were installed on the chamber ID as shown on Figure C3.

Stainless steel was chosen as the wall material for the film cooled thrust chamber. Hoop stress requirements dictated the .045 inch minimum wall thickness indicated on Figure C2. Thinner walls would be allowable for higher strength steels; however, wall conduction analyses indicated no advantage of thinner walls whereas the fabrication would be significantly more difficult.

Chamber wall thickness is important from the standpoint of data reduction because measured wall temperatures differ from the desired adiabatic wall temperatures due to external heat losses and axial wall conduction. A two-dimensional conduction analysis of the chamber wall in the cylindrical section was run using the ANSYS computer program in order to evaluate the

II Film Cooled Chamber (cont.)

effect of wall thickness on axial conduction error and the magnitude of ($T_{aw} - T_{wall}$ measured). An injection velocity ratio of 0.75 with a core mixture ratio of 8.0 was selected to maximize the axial temperature gradient. Each wall thickness case was run two ways; with the external surface insulated, and with a heat loss coefficient of 0.5×10^{-4} Btu/in²-sec-°F. This is a typical loss coefficient measured during previous testing. The resultant differences between the adiabatic wall temperature (976°F in this case) and the external surface temperature at the end of the cylindrical section were as follows:

<u>Wall Thickness, in.</u>	<u>$T_{aw} - T_{measured}$, °F</u>		
	<u>(1)</u> Axial Conduction Error	<u>(2)</u> Error with External Losses and Axial Conduction	<u>External Heat Loss Error</u>
0	0	25	25
.025	3	34.5	31.5
.050	6	44	38

(1) Perfectly insulated wall assumed

(2) Includes axial conduction and external loss effects

The insulated wall results show that the axial conduction effects are small since only a 6°F error is introduced for a .050 inch wall thickness. The results obtained assuming external losses show that the external loss error is a function of wall thickness. Since the axial effects were so small, they were neglected and the external loss error was calculated using a one-dimensional model.

III FILM COOLANT INJECTOR

The film coolant injector design is shown on Figure C4. This design was based upon the film coolant injectors fabricated and tested on the two previous NASA Lewis film cooling programs conducted at ALRC. A hydraulics analysis of the design yielded the predicted pressure drop characteristic shown on Figure C5, and indicated flow circumferential uniformity within $\pm 5\%$.

Heat transfer analyses of the film coolant injector were performed to obtain estimates of (1) the temperature of the injector lip which separates the film coolant and core gases upstream of the injection point, (2) the gas-side temperature of the injector forward end flange, and (3) the film coolant bulk temperature rise. The heat transfer analysis results are summarized below.

LIP TEMPERATURE AND BULK TEMPERATURE RISE

<u>Film Coolant</u>	<u>Core O/F</u>	<u>U_c/U_e</u>	<u>$T_{lip}, ^\circ F$</u>	<u>Film Coolant $\Delta T_{Bulk}, ^\circ F$</u>
H ₂	2	0.75	945	-
H ₂	4	0.75	1250	44
H ₂	6	1.25	1045	-
H ₂	6	0.75	1290	-
H ₂	8	0.75	1270	48
H _e	8	0.75	1440	60
N ₂	2	0.3	1615	-
N ₂	2	0.2	1850	70

Maximum Forward Flange Temperature = 1190°F
(for maximum thickness = .085")

Two cold flow tests were conducted to measure orifice-to-orifice mass flow distribution of the gaseous film coolant injector. Gaseous nitrogen was flowed to ambient back-pressure at flowrates that established Mach

III Film Coolant Injector (cont.)

number similarity between the cold flows and hydrogen-cooled hot fire tests at 300 psia chamber pressure. A photograph of the test setup is shown as Figure C6. The film coolant ring was bolted to a steel mounting assembly. A lathe-type spindle was mounted on the same assembly in a manner resulting in centerline alignment between the film coolant ring and the spindle. A total pressure probe (i.e., pitot tube) was attached to the spindle allowing circumferential and radial indexing of the probe. The probe measured the dynamic head at the centerline of all 60 orifices during a test. The orifice numbering system used in presentation of the flow test results is shown on Figure C7.

Figure C8 shows the flow distributions calculated for the two film coolant ring cold flow tests. The results of the two tests both indicate ± 4 percent orifice-to-orifice coolant flowrate distribution. These results agree well with the analytical prediction of ± 5 percent distribution allowing for manufacturing tolerances. Measured flowrates and pressure drops for each test are all indicated on the figure. Flow stagnation points would be expected to occur 90° from the ring inlets and the high orifice flows at 90° and 270° in the plots indicate this effect.

On Figure C5, the predicted coolant ring pressure-drop characteristic is compared with the measured data. The nitrogen flowrate was converted to an equivalent hydrogen flow rate with the following equation (based on Mach number similarity).

$$(W)_{N_2} = (W)_{H_2} (P_{amb}/P_c)^{1/2} (MW \text{ of } N_2 / MW \text{ of } H_2)$$

The agreement between measured and predicted ΔP is satisfactory and probably within the accuracy of the manifold mercury manometer measurement.

The effect of ribs on orifice velocity distribution was investigated in a short cold flow test conducted with a single orifice (Orifice #1). Total pressure was measured at the orifice centerline and over the orifice rib at

III Film Coolant Injector (cont.)

two axial planes. The first axial station was at the face plane and the second one-half inch downstream. The results are summarized on Figure C9. At the injection point the measured rib velocity was significantly less than the orifice centerline velocity, as would be expected. At one-half inch from the injection point the rib velocity is 90 percent of the centerline value, indicating rapid diffusion. The data indicates rib effects could be expected to be minimal at axial distances greater than approximately one inch. This test was conducted with unconstrained free jet orifice flow. The expected effect of a chamber wall would be more rapid attainment of a uniform velocity profile.

IV REGENERATIVELY COOLED CYLINDER

The design for the water cooled cylinder which separated the propellant injector and the film coolant injector is shown on Figure C10. Cooling of the channel walls was accomplished with water flowing in 60 milled channels which are nominally 3/32 inch wide by .075 inch deep. The design water cooling conditions were: 10 lb/sec flow rate at 500 psia total inlet manifold pressure. A regenerative cooling analysis produced the axial distributions of coolant bulk temperature, gas-side wall temperature, gas-side heat flux, and burnout safety factor which are plotted on Figure C11. The gas-side heat flux data of Reference 4 were utilized in performing the analysis.

V INJECTOR CORE DISTRIBUTION TEST

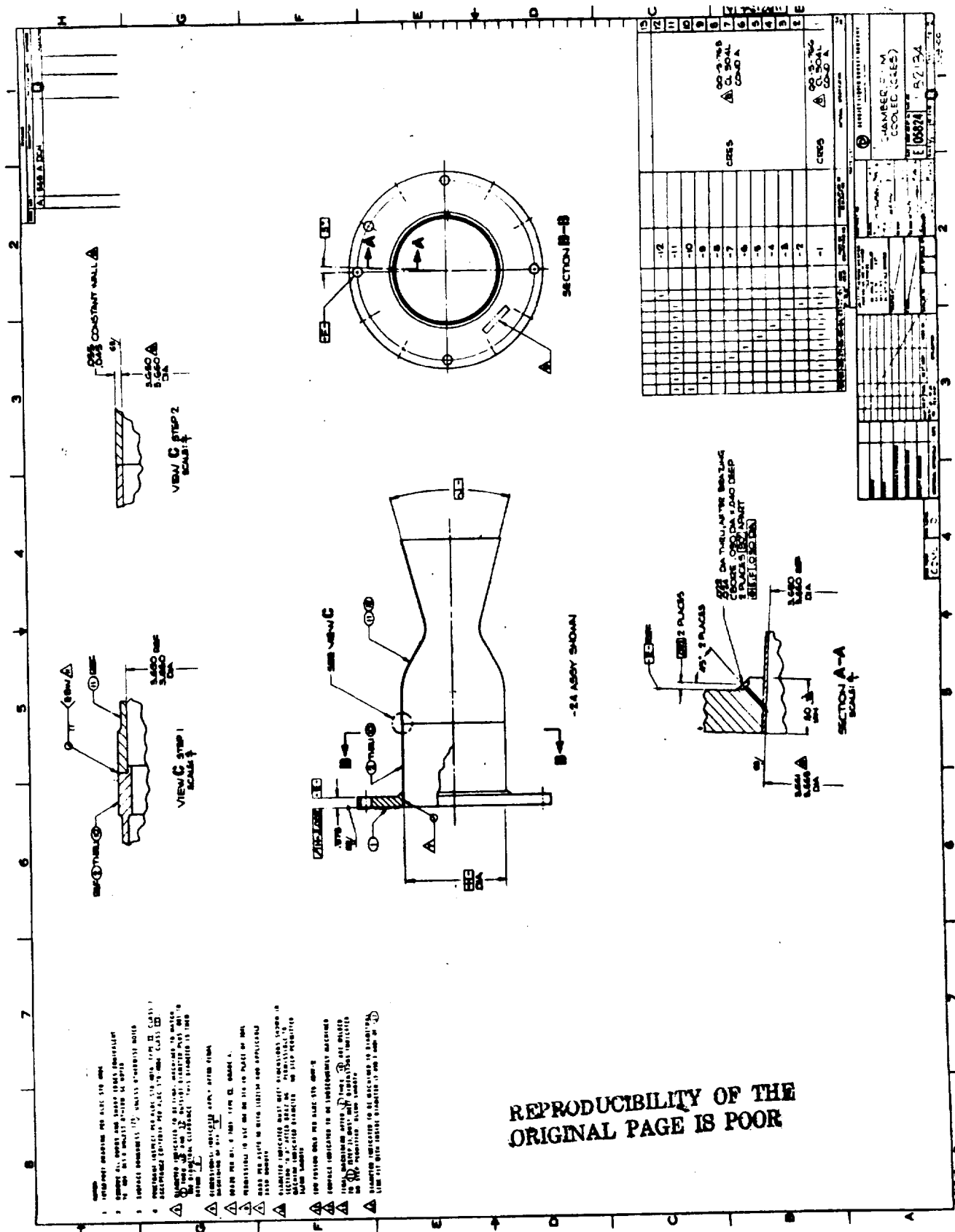
A GN_2 cold flow distribution test was also conducted for each propellant circuit of the premix triplet injector. The flow of each element in the outer injector row (36 out of 72 total elements) was sampled with a plastic tube connected to a float type rotameter. The oxidizer and fuel circuits were both flowed at GN_2 flowrates of 0.12 lbm/sec, corresponding to oxygen and hydrogen hot fire flowrates of 2.67 and .67 lbm/sec, respectively. These flowrates are consistent with a nominal operating condition of 4:1 mixture ratio and 300 psia chamber pressure.

V Injector Core Distribution Test (cont.)

The two test results are summarized on Figure C12. The element numbering system utilized is indicated on the figure. Both circuits have elements that deviate up to 8 percent from a nominal single element flow-rate. At a total injection mixture ratio of 4:1 the element-to-element mixture ratio varies from 3.6 to 4.4:1. This corresponds to a + 10% range in outer row mixture ratio for all core mixture ratios.

VI COPPER HEAT SINK THRUST CHAMBER

The copper heat sink thrust chamber used in the no-film-cooling tests consisted of the heat sink chamber and L* section shown on Figure C-13. These components were residual from Contract NAS 3-14379 (Reference 4).



REPRODUCIBILITY OF THE ORIGINAL PAGE IS POOR

Figure C2. Film Cooled Chamber Design, P/N 1182134 (Sheet 1 of 2)

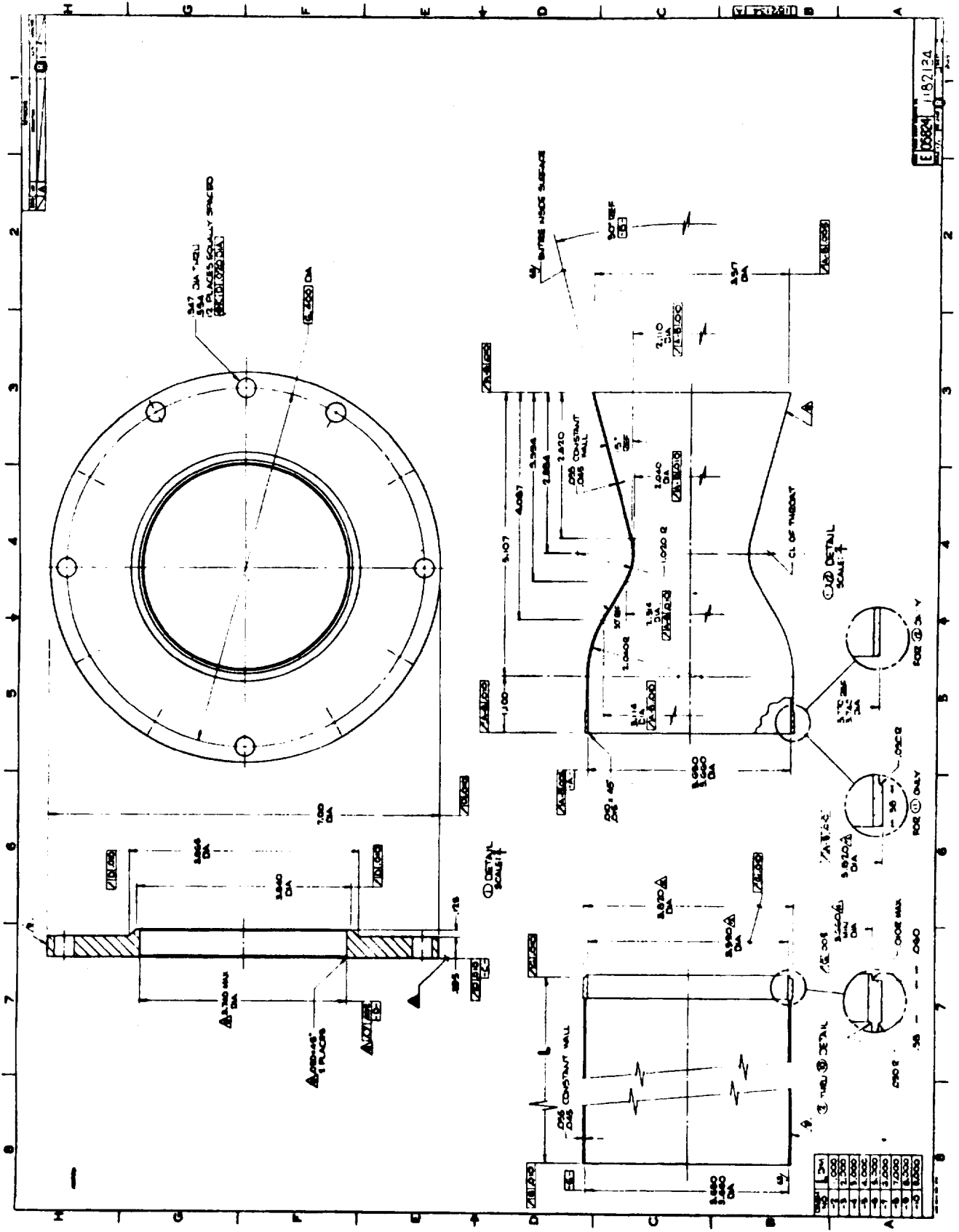


Figure C2. Film Cooled Chamber Design, P/N 1182134 (Sheet 2 of 2)

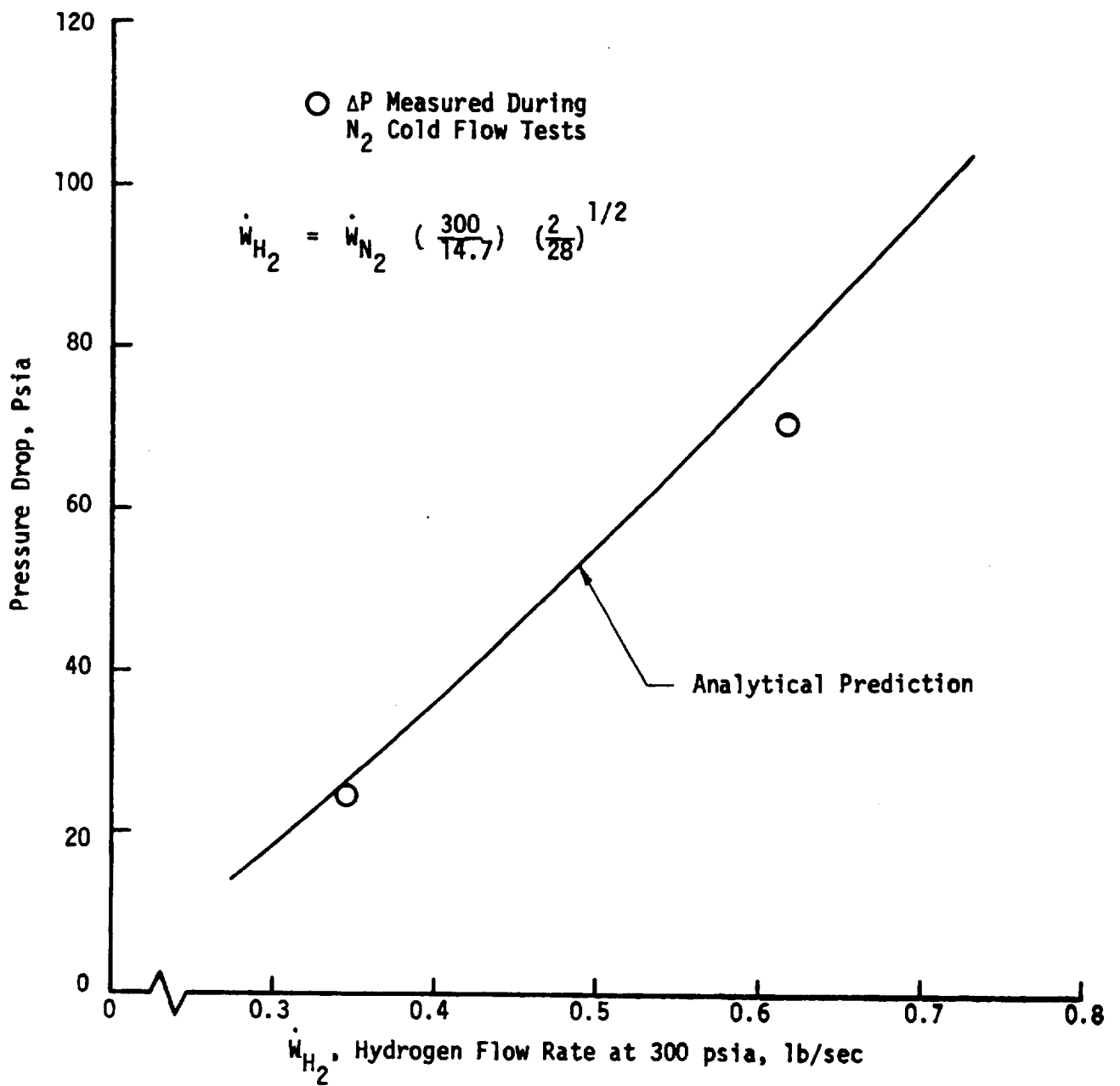


Figure C5. Pressure Drop Across the Film Coolant Injector

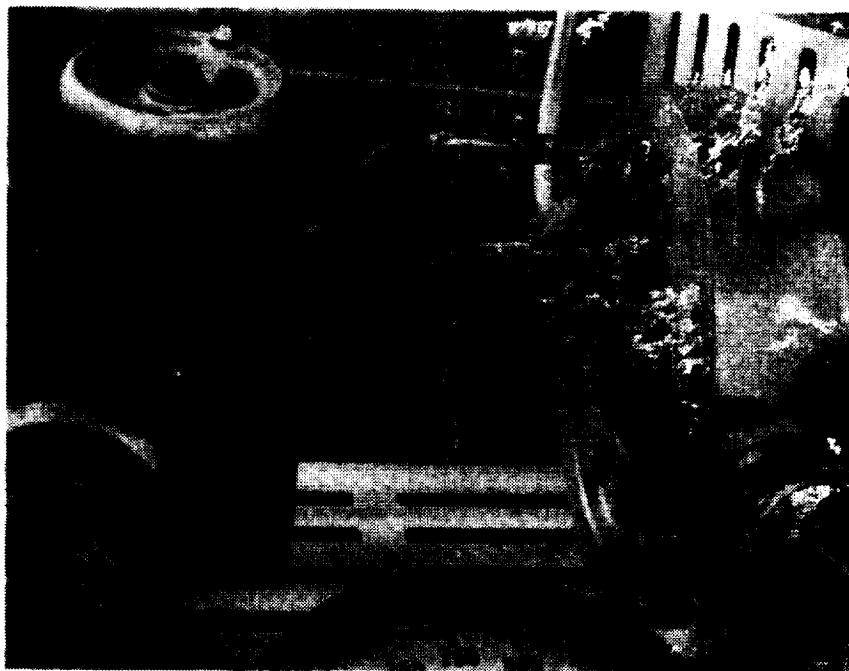


Figure C6. Film Coolant Injector Cold Flow Test Setup

REPRODUCIBILITY OF THE
ORIGINAL PAGE IS POOR

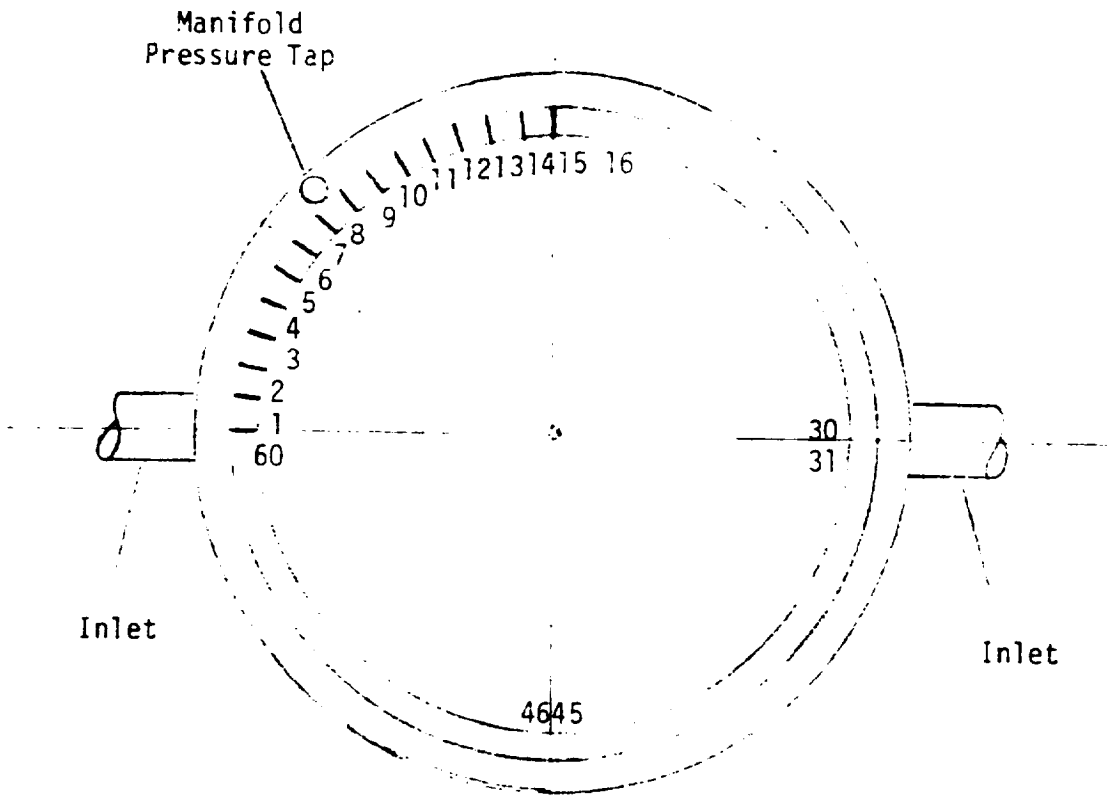
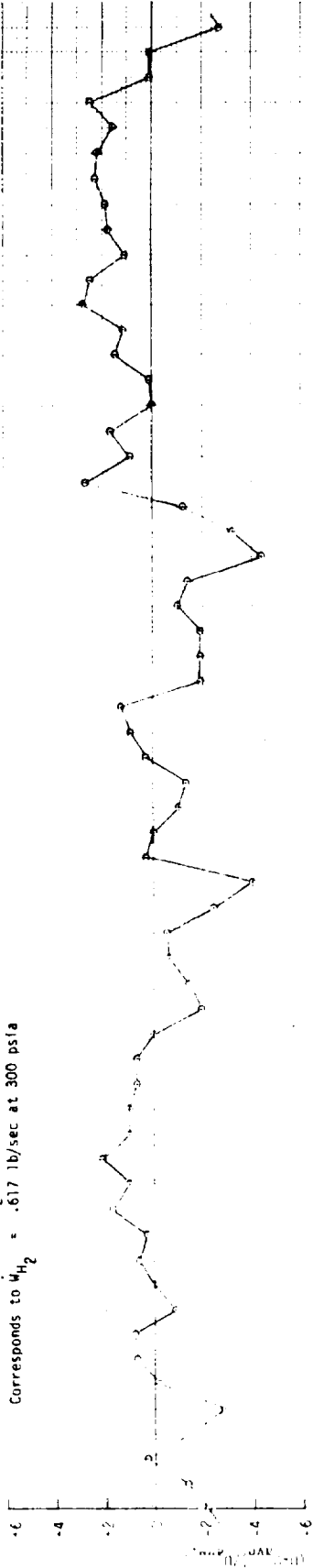


Figure C7. Film Coolant Injector Orifice Nomenclature

COLD FLOW TEST RESULTS FOR THE FILM COOLANT INJECTOR

High Flow Condition: $\dot{M}_{N_2} = .113 \text{ lb/sec}$
 Corresponds to $\dot{M}_{H_2} = .617 \text{ lb/sec at 300 psia}$



C-16

Low Flow Condition: $\dot{M}_{N_2} = .063 \text{ lb/sec}$
 Corresponds to $\dot{M}_{H_2} = .346 \text{ lb/sec at 300 psia}$

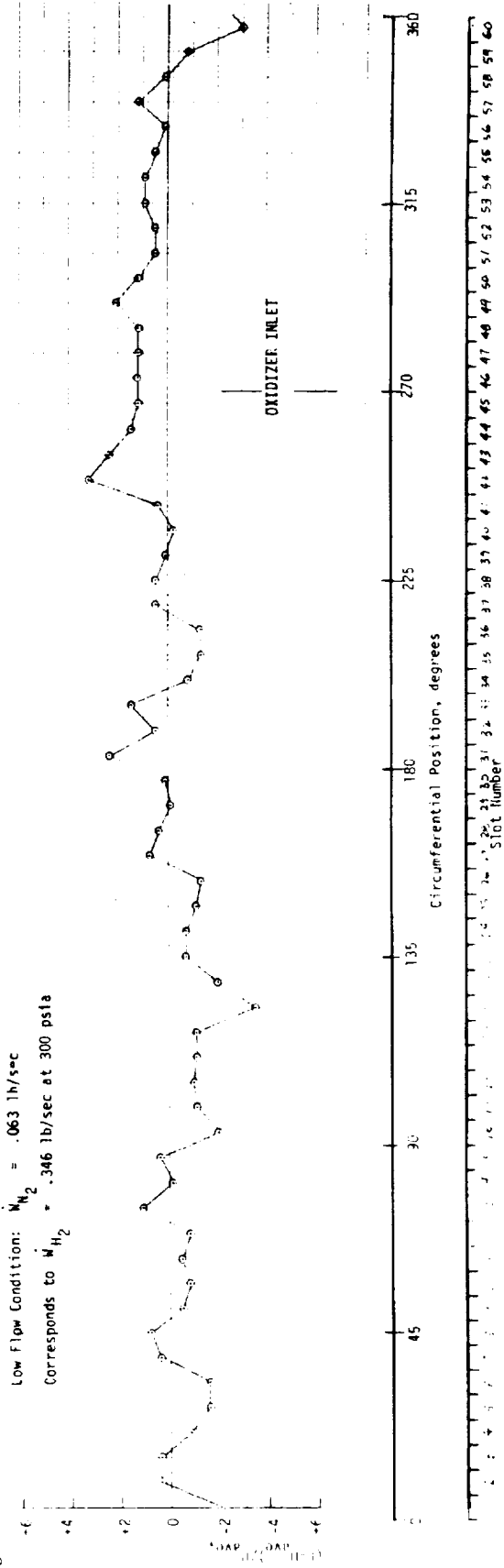


Figure C8. Cold Flow Test Results for the Film Coolant Injector

Figure C8. Cold Flow Test Results for the Film Coolant Injector

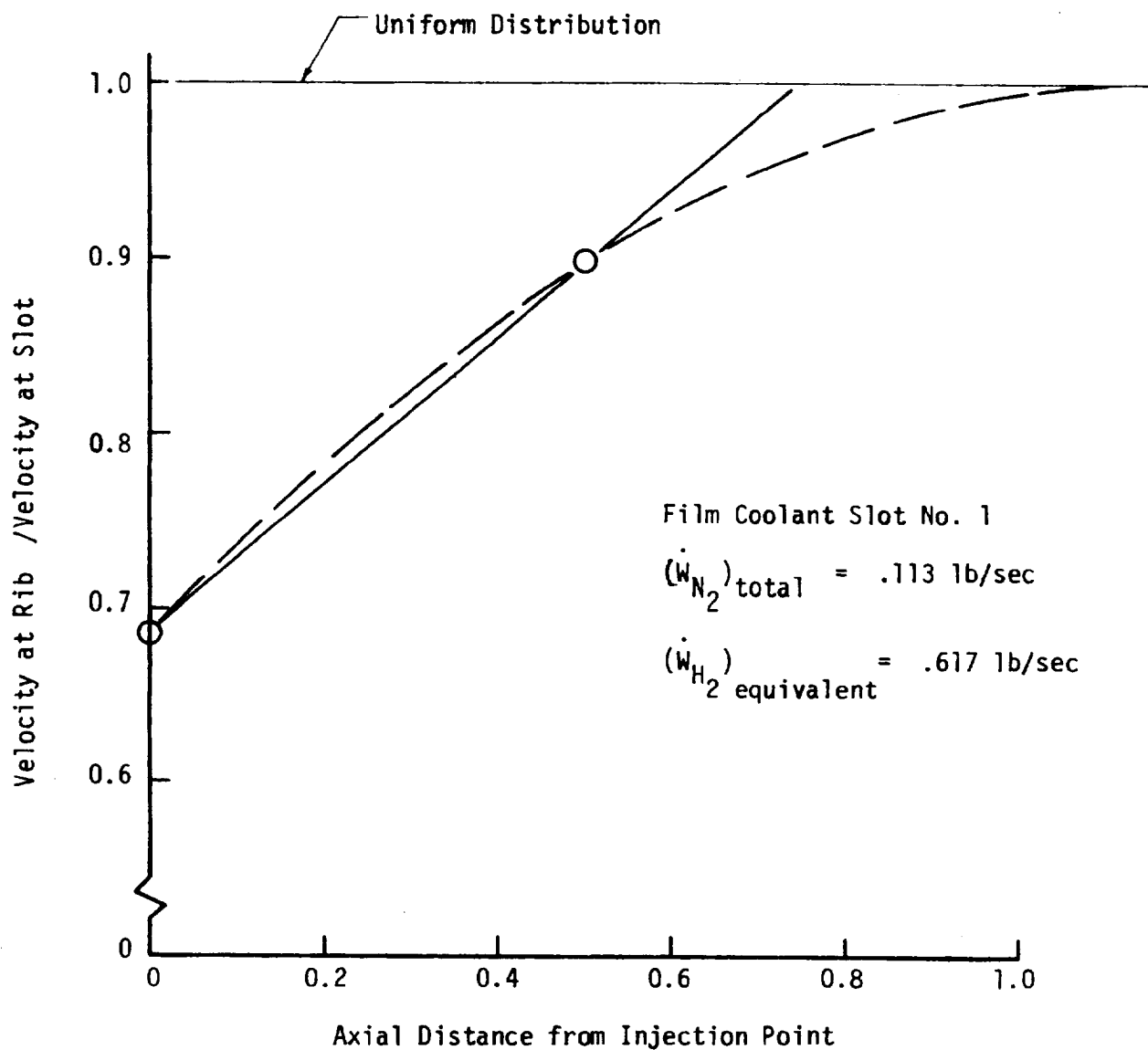


Figure C9. Comparison of Rib and Orifice Centerline Velocity Measurements

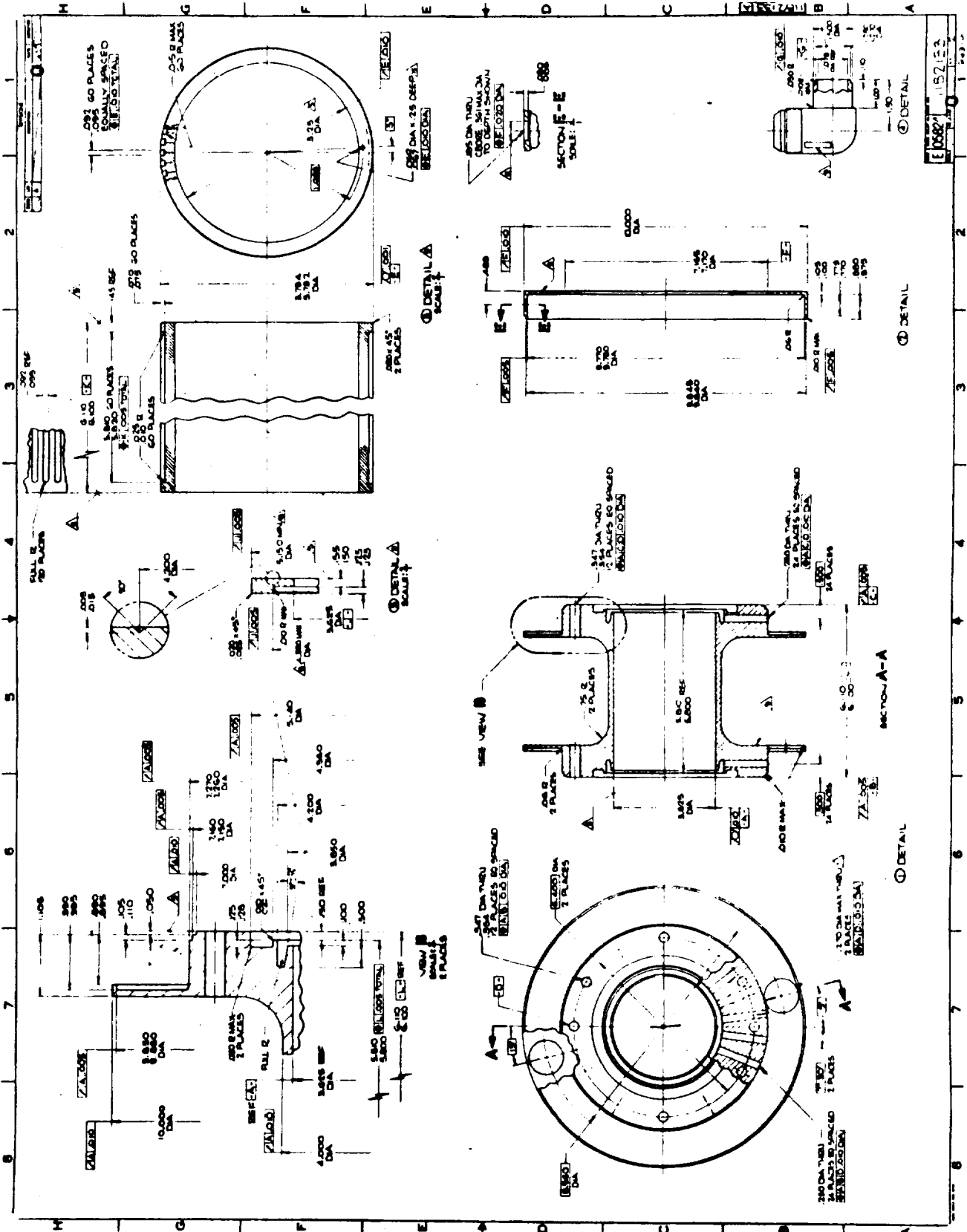


Figure C10. Water Cooled Cylinder Design, P/N 1182133 (Sheet 2 of 2)

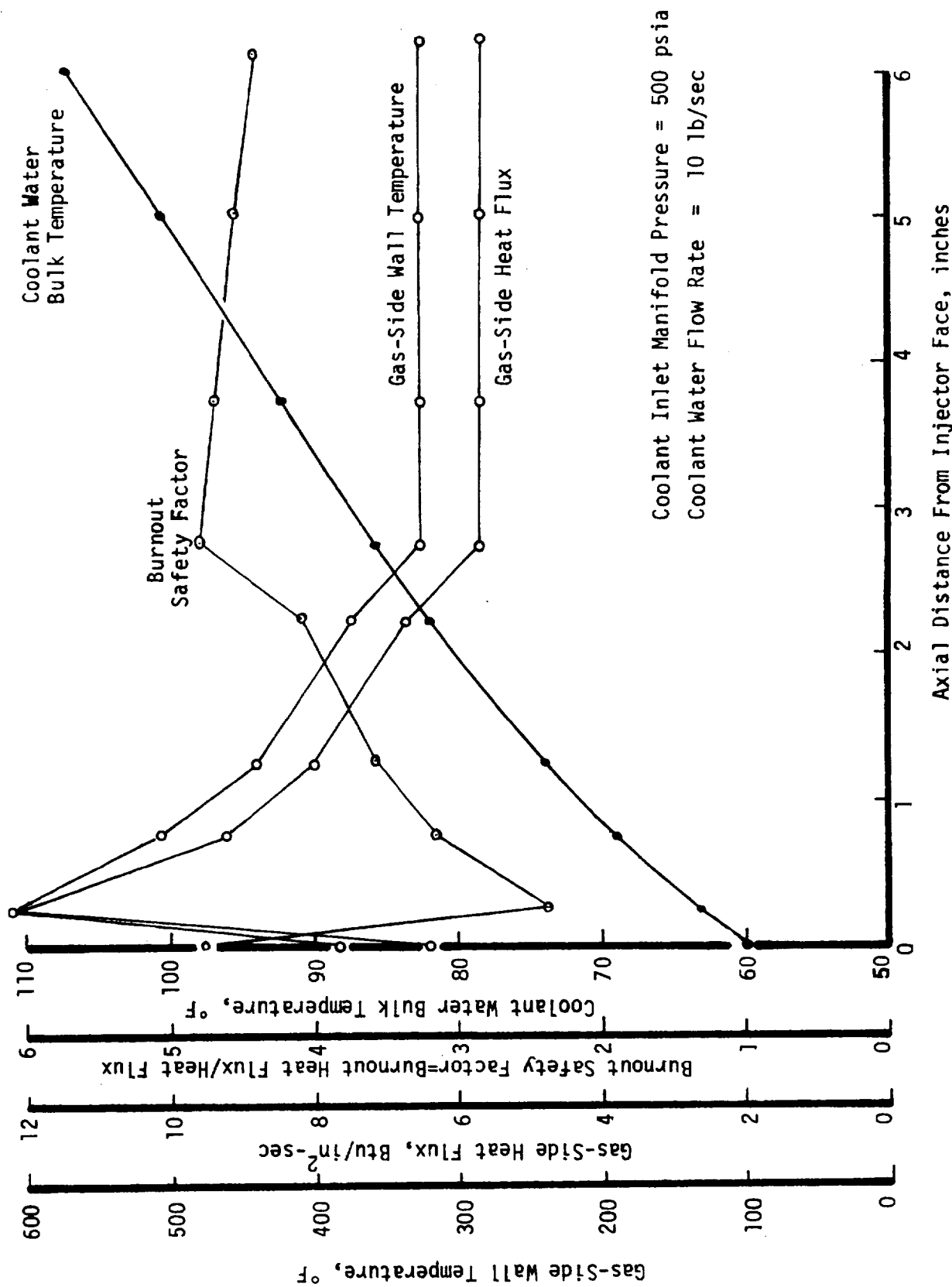


Figure C11. Regenerative Cooling Analysis Results for the Water Cooled Cylinder

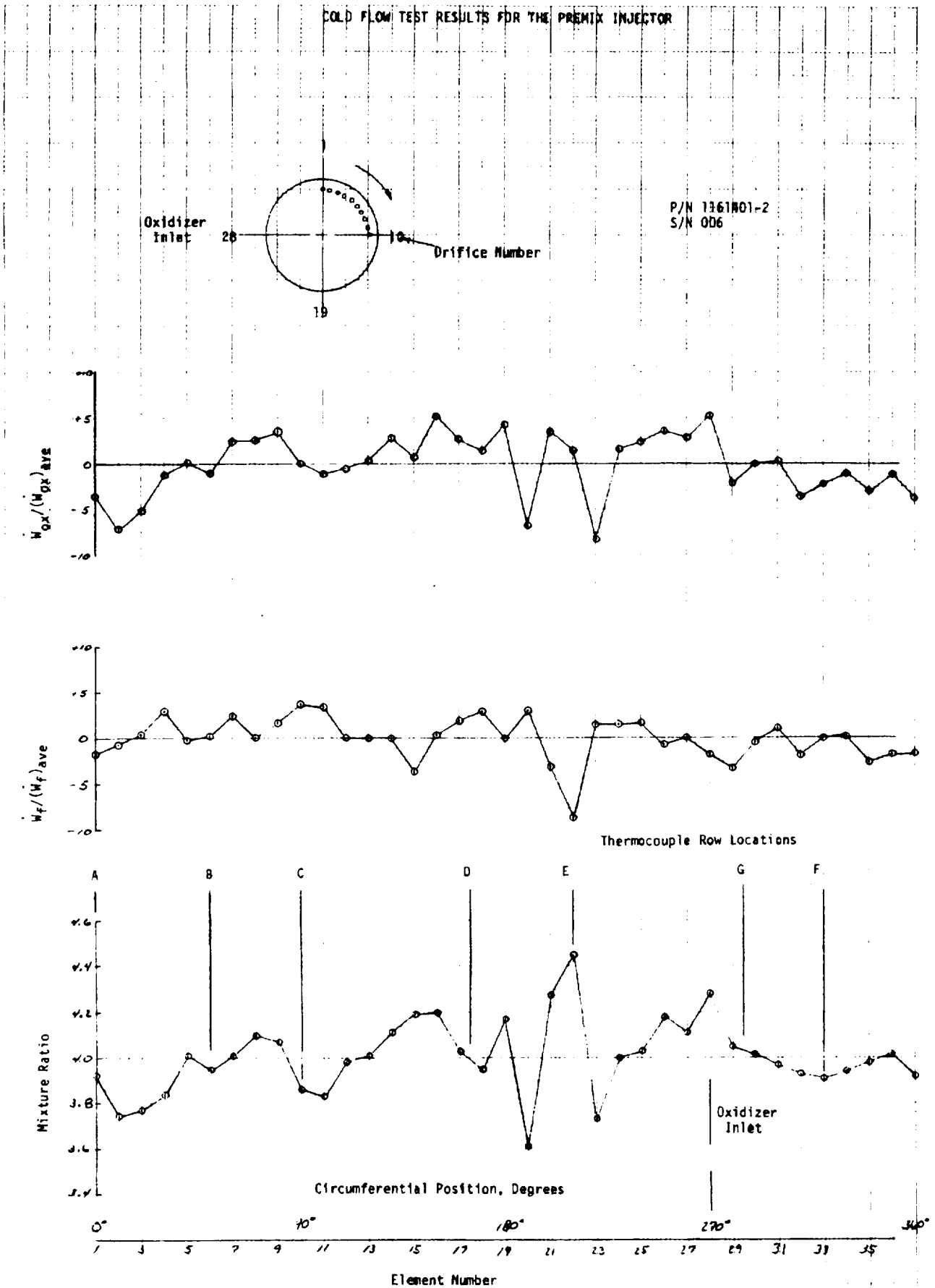


Figure C12. Cold Flow Test Results for the Premix Injector

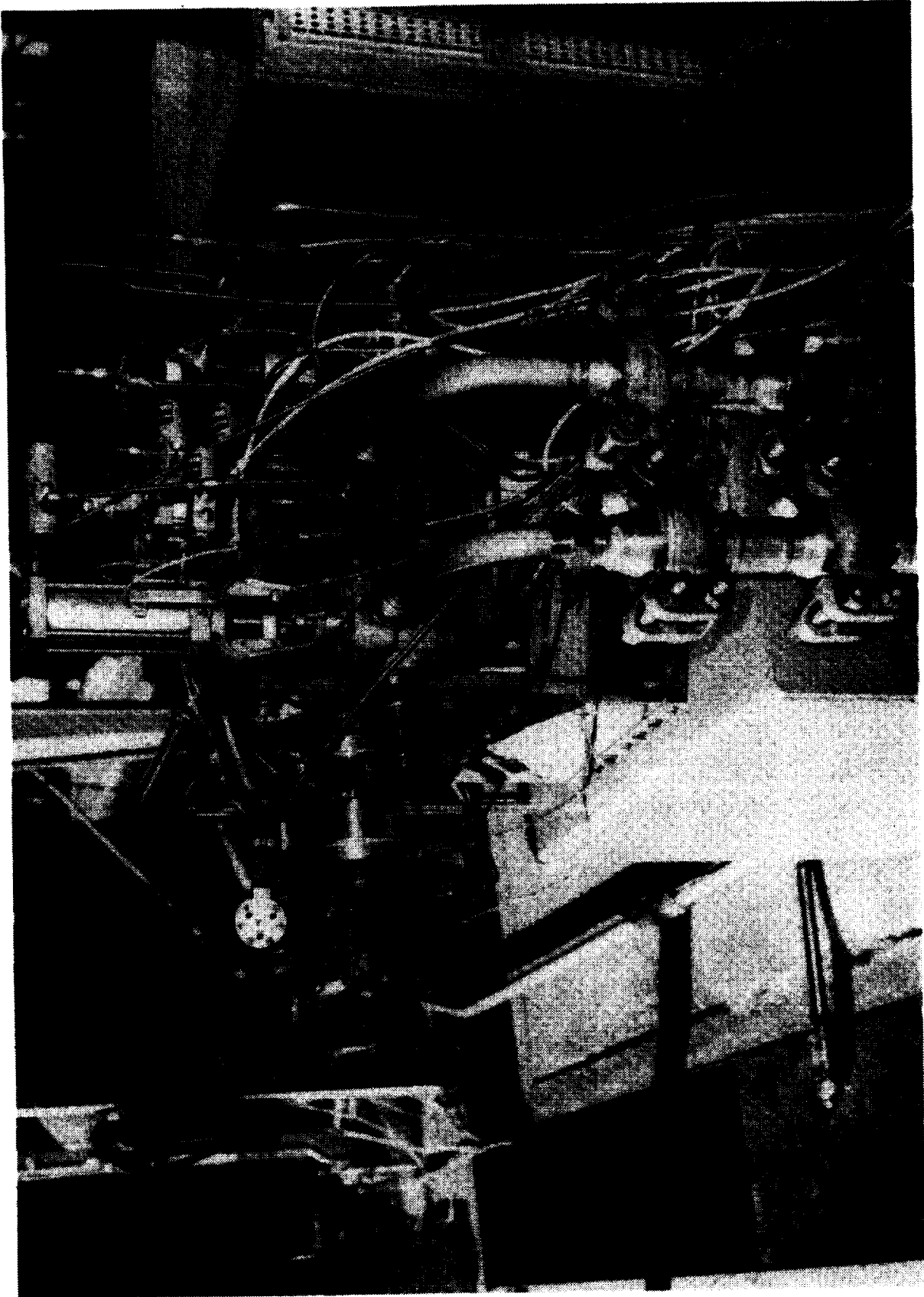


Figure C14. Copper Heat Sink Chamber Installed on Test Stand

